GOLD DISTRIBUTION AT THE E26 PORPHYRY COPPER-GOLD DEPOSIT, GOONUMBLA N.S.W

BY

Michael John House

A thesis submitted as a partial fulfilment of the requirements of the Master of Economic Geology Degree.

University of Tasmania

December, 1994.

Declaration

This thesis contains no material which has been accepted for a degree or diploma by the University or any other institution, except by way of background information and duly acknowledged in the thesis, and contains no material previously published or written by another person except where due acknowledgment is given.

Michael House.

ABSTRACT

The E26 porphyry copper-gold deposit is the largest of several copper-gold deposits discovered to date in the Goonumbla region of central west N.S.W. Cu and Au mineralisation occurs in areas of strong pervasive potassic alteration and quartz veining, associated with a small pipe-like quartz monzonite porphyry (QMP1). The mineralisation occurs both within the porphyry and the covolcanic late Ordovician trachyte-latite lavas and volcanic breccias that it has intruded. The deposit is bounded at depth and to the east by a biotite quartz monzonite, while to the immediate north, is another younger QMP (QMP2) which has stoped out the Cu-Au mineralisation. Several other QMP's occur to the northwest and at deeper levels in the E26 deposit.

Copper mineralisation occurs principally as bornite with lesser chalcopyrite and chalcocite-digentite. Two bornite phases have been identified based on colour and mineral associations. Gold occurs principally as fine inclusions in bornite. The sulphides are zoned from a bornite-rich core, through a chalcopyrite zone to an outer pyrite halo associated with propylitic alteration. A weak base metal/gold association occurs in thin structurally controlled zones of quartz-sericite-pyrite alteration, away from the main E26 mineralisation. Within E26 itself, the bulk of the Au is confined to the central and deeper parts of the system and immediately around QMP1. Cu however, continues to shallower depths and laterally further away from QMP1. This pattern is reflected in the Cu/Au ratios, and has led to the definition of two distinct vertical domains within the higher grade areas of E26. The upper domain is characterised by high copper grades but low gold grades; the lower domain contains similar copper grades but much higher gold grades.

Sulphide composition, timing and alteration are similar within the Cu/Au domains defined. A geochemical model developed shows that the Cu/Au relationships observed at E26 can be explained by coprecipitation of Cu and Au, but at different rates due to differing changes in saturation levels between the two metals. Deposition of both metals from chloride complexes in high temperature, saline fluids was in response to a decrease in T, and changes in fO_2 and pH associated with hematisation of secondary magnetite associated with earlier biotite (potassic) alteration. The deposits at E22, E27 and E31N do not show the same degree of magnetite destruction as E26 and E48, are more deeply eroded, and therefore not as enriched in copper.

TABLE OF CONTENTS

FIGURES

TABLES

APPENDICES

ACKNOWLEDGMENTS

This work, and part of the Masters course work, has been supported by Northparkes Mines for which I am thankful.

My supervisor, Dr David Cooke has provided invaluable guidance and help. I am particularly grateful for his hurried reading of drafts of this work, his constructive comments, organising probe work and providing reference material.

I acknowledge and greatly appreciate the assistance of the following people:

Dr Paul Heithersay for spending time to discuss aspects of this work and providing information and reference material.

R Nagorcka, J Schumacher, L Vink and S Dunn, for helping with some of the diagram preparation and colour photocopying.

Kim Bischoff for proof reading an early draft of part of this thesis.

Mike Hannington of North Exploration for gathering the magnetic susceptibility data for E26.

Dr Geoff Clarke of the University of Sydney for allowing me use of his microscope for photomicrography.

North Exploration, Parkes, for use of their petrological microscope.

Most importantly, thankyou to my wife Judith for her support and encouragement, help with typing, diagram preparation, data entry and validation; and covering for me in many things domestically, particularly during the last couple of months of thesis preparation. And finally to my son Timothy, who learnt to sleep through the night at a very early age.

1. INTRODUCTION

Porphyry-related Cu/Au mineralisation occurs near Goonumbla approximately 28km northwest of Parkes in central west New South Wales (Figure 1.1). The Endeavour 26 deposit (E26, formerly Endeavour 26 North) is the largest of several porphyry-related Cu-Au deposits discovered in the region to date.

1.1 AIMS

This study focuses on the distribution and controls of Au mineralisation at E26. To do this, it is necessary to update the current geological knowledge of the deposit. The large E26 assay database that has been compiled over 15 years of drilling is used to establish the Au distribution, which is compared to the known geology, alteration, mineralisation and distribution of other metals (eg. Cu, Ag). Petrographic and electron microprobe studies are used to help establish the chemistry, timing and evolution of the mineralising system. A comparison of Au and Cu distributions with the other deposits in the area (E22, E27, E31N & E48) is also provided.

1.2 EXPLORATION AND MINING HISTORY

Disseminated Cu mineralisation associated with potassic alteration was intersected in the Goonumbla district by 1km spaced scout auger holes in 1976 (Jones 1985). Further drilling outlined the Endeavour 22 (E22) deposit, and with it, the recognition of a major new porphyry Cu-Au province. Subsequent drilling also led to the discovery of other major mineralised centres, including E26, E27, E31N and, more recently, E48.

In November 1992, the board of North Broken Hill Peko Ltd. approved the development of the Northparkes project to mine and process Cu and Au ore from the E26, E22 and E27 deposits (Figure 1.2). Project development would start with open cut mining and processing of oxide Au and oxide Cu-Au ore from the E22 and E27 deposits, before proceeding onto sulphide Cu-Au ore from the open cuts at E22 and E27 and underground mine at E26. The recent approval of an expansion plan will allow 5M tonnes of sulphide ore to be treated per year, of which 3.9M tonnes will be mined from E26. Total capital

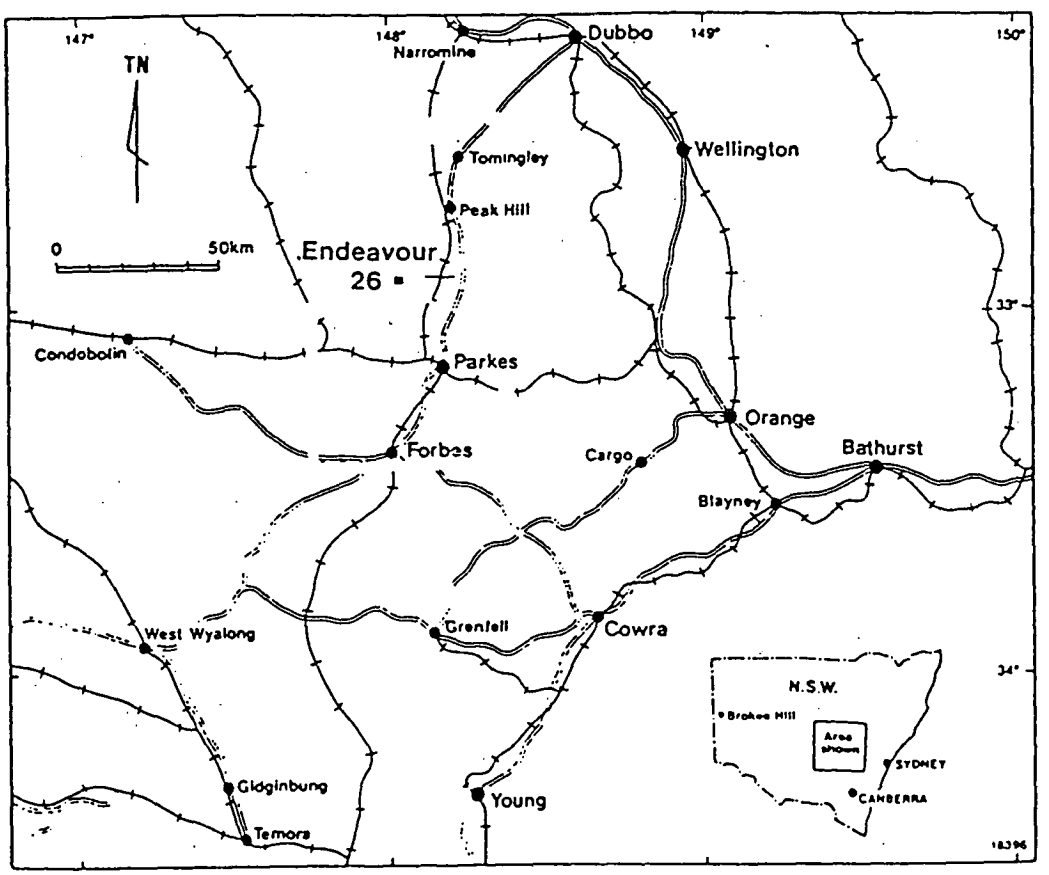

Figure 1.1 Locality map of the Endeavour 26 deposit (From Heithersay, 1991).

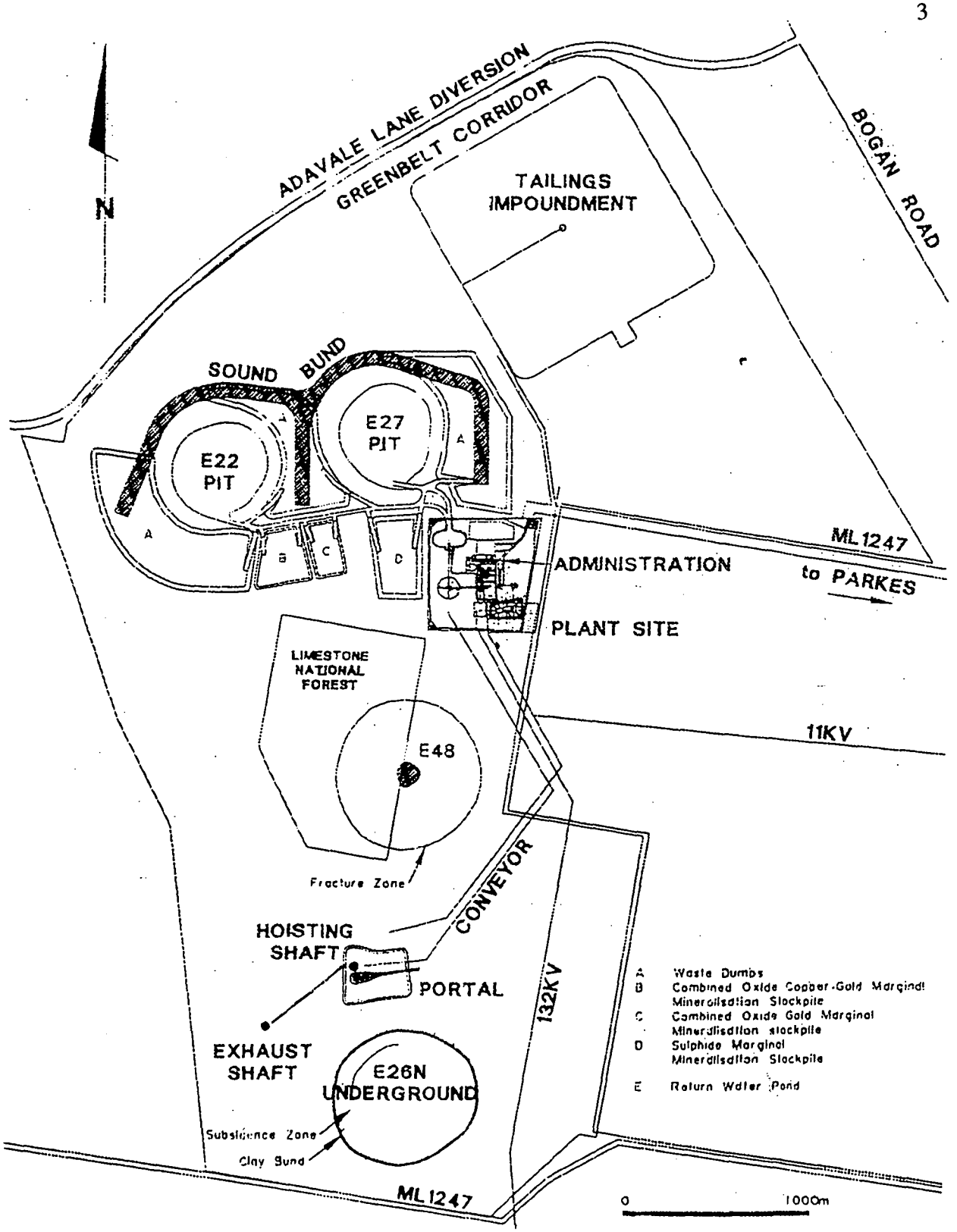

Figure 1.2 General arrangement of Northparkes Mines.

expenditure is estimated at $255 million. A mine life of up to 20 years is expected with the first gold pour having already occurred in May 1994. Resource and reserve estimates as at December 1993 are given in Table 1.1. E26 contains approximately 70% of the Cu resource and 50% of the Au resource at Northparkes.

1.3 PREVIOUS WORK

The first, detailed published account of the Goonumbla deposits is by Jones (1985). This summarises much of Geopeko's work in the area, giving a description of the regional geology and a detailed account of the three main Goonumbla deposits (E22, E27 and E26). A detailed description of E26 is described in Heithersay (1986), and in his PhD thesis (Heithersay, 1991). An update on the three main deposits is given in Heithersay et al. (1990). Recent Honours theses include Squires (1992) on E27, Hall (1993) on the Goonumbla Volcanics, and Wolfe (1994) on E48. Numerous, unpublished Geopeko reports on the Goonumbla region, and the mineralised centres, have also been written.

1.4 DATA COLLECTION AND HANDLING METHODS

Because elemental assays are used extensively in this study, a brief description of sampling and assaying procedures, and data storage and manipulation is given.

1.4.1 Grid

All data is stored and handled in the standard ISG 55/3 grid co-ordinate system. The vertical grid is calculated by adding 10 000 to the Australian Standard Datum. The land surface is approximately 10280mRL - i.e. 280m above sea level plus 10 000m. The mineralisation at E26 is reasonably well defined to 9400mRL, i.e. 880m below the topographic surface.

1.4.2 Drilling Methods

As outcrop is poor to non existent, nearly all assay data and geological information has been obtained from drill core. Minor assay and additional geological information has been obtained from exposures in the E26 ramp development. Typical drilling techniques

1.0 Identified Mineral Resources

Mineralisation Type	Deposit	Nominal Cutoff Grad	December 1993 Tonnes	Grade copper %	Grade gold g/t	June 1992 Tonnes	Grade copper %	Grade gold g/t
1.1 Measured Resource								
Oxide Gold								
	E22	0.75gAu/t	586,000	–	1.6	586,000	–	1.6
	E27	0.75gAu/t	1,314,000	–	1.9	1,314,000	–	1.9
	Total		1,900,000		1.8	1,900,000		1.8
Oxide Copper-Gold								
	E22	1.0%eCu	764,000	1.0	0.9	764,000	1.0	0.9
	E27	1.0%eCu	2,598,000	0.9	1.0	2,598,000	0.9	1.0
	Total		3,362,000	0.9	1.0	3,362,000	0.9	1.0
1.2 Indicated Resource								
Sulphide Copper-Gold								
	E22	0.6%eCu	18,153,000	0.7	0.6	18,153,000	0.7	0.6
	E27	0.6%eCu	13,696,000	0.7	0.7	13,696,000	0.7	0.7
	E26N (above 9450m	1.2%eCu	38,533,000	1.8	0.6	38,533,000	1.8	0.6
	E48 (10200-9800mR	1.2%eCu	8,000,000	1.4	0.6			
	Total		78,382,000	1.3	0.6	70,382,000	1.3	0.6
1.3 Inferred Resource								
Sulphide Copper-Gold								
	E26N (below 9600m	1.2%eCu	3,000,000	1.4	0.5	3,000,000	1.4	0.5
	E48 (9800-9400mRL	1.2%eCu	10,900,000	1.0	0.7			
	Total		13,900,000	1.1	0.7	3,000,000	1.4	0.5

2.0 Ore Reserves

Ore Type	Mine	Nominal Cutoff Grad	June 1993 Tonnes	Grade copper %	Grade gold g/t	June 1992 Tonnes	Grade copper %	Grade gold g/t
2.1 Proved Reserve								
Oxide Gold								
	E22 Open Pit	0.75gAu/t	500,000	–	1.7			
	E27 Open Pit	0.75gAu/t	1,180,000	–	2.1			
	Total		1,680,000		2.0	1,580,000	–	2.0
Oxide Copper-Gold								
	E22 Open Pit	1.5%eCu	380,000	1.2	1.1			
	E27 Open Pit	1.5%eCu	1,280,000	1.1	1.4			
	Total		1,660,000	1.1	1.3	1,660,000	1.1	1.4
2.2 Probable Reserve								
Sulphide Copper-Gold								
	E22 Open Pit	0.6%eCu	11,160,000	0.7	0.6			
	E27 Open Pit	0.6%eCu	10,648,000	0.7	0.8			
	E26N Underground	1.2%eCu	42,350,000	1.6	0.6			
	Subtotal O/Pit		21,808,000	0.7	0.7	32,800,000	0.9	0.5
	Subtotal U/G		42,350,000	1.6	0.6			
	Total		64,158,000	1.3	0.6			

Table 1.1 Northparkes Mines, Mineral Resources and Ore Reserves at 31 December 1993.

AREA	N/S	VERTICAL
Main above 9700mRL	60 m	60-100 m
Main below 9700mRL	80 m	100-150 m
North above 9700mRL	100 m	130 m
North below 9700mRL	No drilling	

Table 1.2 Average drilling densities at E26

involved precollars of 4" to 6" rotary blade RC aircore in the weathered zone, 4.5" reverse circulation percussion in the hard oxide zone and HQ, NQ and (especially with earlier exploration drilling) BQ diamond core in the primary zone. Directional drilling with wedging of daughter holes was used during the 1991 drilling program. Most drillholes are drilled from east to west, only a few have been drilled in other directions. Drilling densities vary for different regions of the deposit, and are given in Table 1.2.

1.4.3 Sample Preparation and Assaying Methods

All holes are sampled on a 1m interval. Half core samples are prepared for assay by crushing, disc pulverising, and ring grinding. Sample splitting between processes gives a final 50-70g sub-sample. All Cu and Ag assays have been by AAS, differing only in digestion reagents and sample mass. Some caution should be given to the Ag assays as many samples are near the detection limit. No drillholes after E26P79 (drilled in 1984) have been assayed for Ag. Prior to 1985, most Au assays were by AAS with an aqua regia digest. Any Au analysis greater than 0.5g/t was routinely checked by classical (gravimetric) or AAS finish fire assay. Since 1985, all Au assays have been by fire assay.

1.4.4 Geotechnical & Magnetic Data Collection

Interval and oriented geotechnical data has been collected from drillcore. Interval data is collected for each 3m core interval, and includes RQD, core recovery and fracture counts. Of interest for this study is the number of weakly healed and strongly healed fractures per 3m interval. Weakly healed fractures are defined as those containing vein fill that can be scratched with a knife, and at E26, mostly correspond to gypsum or anhydrite veins. Strongly healed fractures are those containing vein fill that cannot be scratched with a knife - typically quartz.

Magnetic susceptibilities of drillcore using hand held magnetometer readings, forms the basis for the analysis of magnetite. It is assumed that most of the magnetic response is due to the presence of magnetite, as no other magnetic phases such as pyrrhotite

occur at E26. With this consideration a conversion factor of 3.47 can be used to approximate magnetite content from susceptibility units (cgs) (M Hannington, pers. com., 1994).

1.4.5 Data Storage and Handling

Assay data is stored as DATAMINE desurveyed drill hole files. The E26 database contains approximately 36 000 Cu, 36 000 Au and 21 000 Ag assays. Geotechnical interval, magnetic susceptibility and lithology data is also stored as DATAMINE desurveyed files. These desurveyed files can be plotted in section or plan, viewed graphically in two or three dimensions, or used for statistical and geostatistical analysis.

Plotting and viewing of data allows grade and geology outlines or contours to be interpreted. These contours of Au and Cu grade, and outlines of geology, have been digitised into DATAMINE and wireframed using the datamine graphical interface, GUIDE, to give a three dimensional image.

2. REGIONAL GEOLOGY

2.1 REGIONAL TECTONICS

The Cu-Au deposits of the Goonumbla region are hosted by a belt of Ordovician volcanics in the Paleozoic Lachlan Fold Belt (LFB) of Eastern Australia. The LFB has been divided into four structural belts by Glenn (1992). The Eastern Belt in which the Northparkes deposits occur, contains six separate belts of Ordovician Volcanics and arc-derived volcaniclastics (Figure 2.1). The volcanics are mainly shoshonitic in composition and Late Ordovician in age (Wyborn, 1992).

Most workers have suggested that the shoshonitic volcanics are related to Ordovician island arc volcanism associated with a west-dipping subduction zone to the east. Several tectonic models have been put forward for the Ordovician of the LFB, including:

i) single meridional island arc complex and marginal sea to the west (e.g. Oversby, 1971)

ii) extensional splitting of a single meridional arc (Molong Rise) by eastward migration of the subduction zone (e.g. Scheibner, 1973)

iii) extensional splitting of a single meridional arc by left-lateral strike-slip movement associated with the subduction of an oblique SE-trending spreading ridge (e.g. Packham, 1987)

iv) a single NW-trending arc characterised by a discontinuous arcuate line of volcanoes, rather than a single volcanic arc (e.g. Cas et al., 1980).

Glenn (1992) poses the following as problems with the simple island arc interpretation:

i) the extreme width of the Ordovician volcanics

ii) lack of volcanic detritus in coeval turbidites

iii) recognition that volcanism was coeval with two major periods of quiescence during clastic sedimentation.

Wyborn (1992) suggested that subduction-related magmatism is absent in the Ordovician of Central New South Wales. Instead, the source of the high-K Ordovician shoshonites was a metasomatised lithospheric mantle. Mantle metasomatism could have been induced during thermal perturbation, lithospheric delamination or pressure reduction

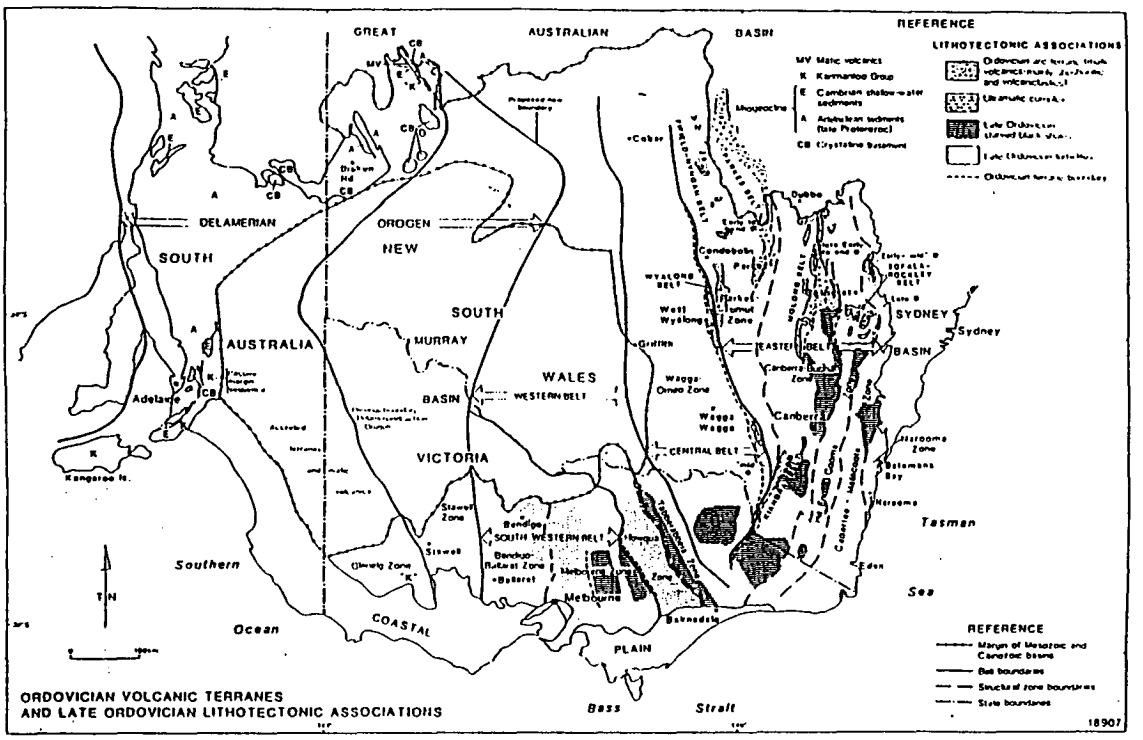

Figure 2.1 Ordovician volcanic terranes of the Lachlan Fold Belt (From Glenn, 1992).

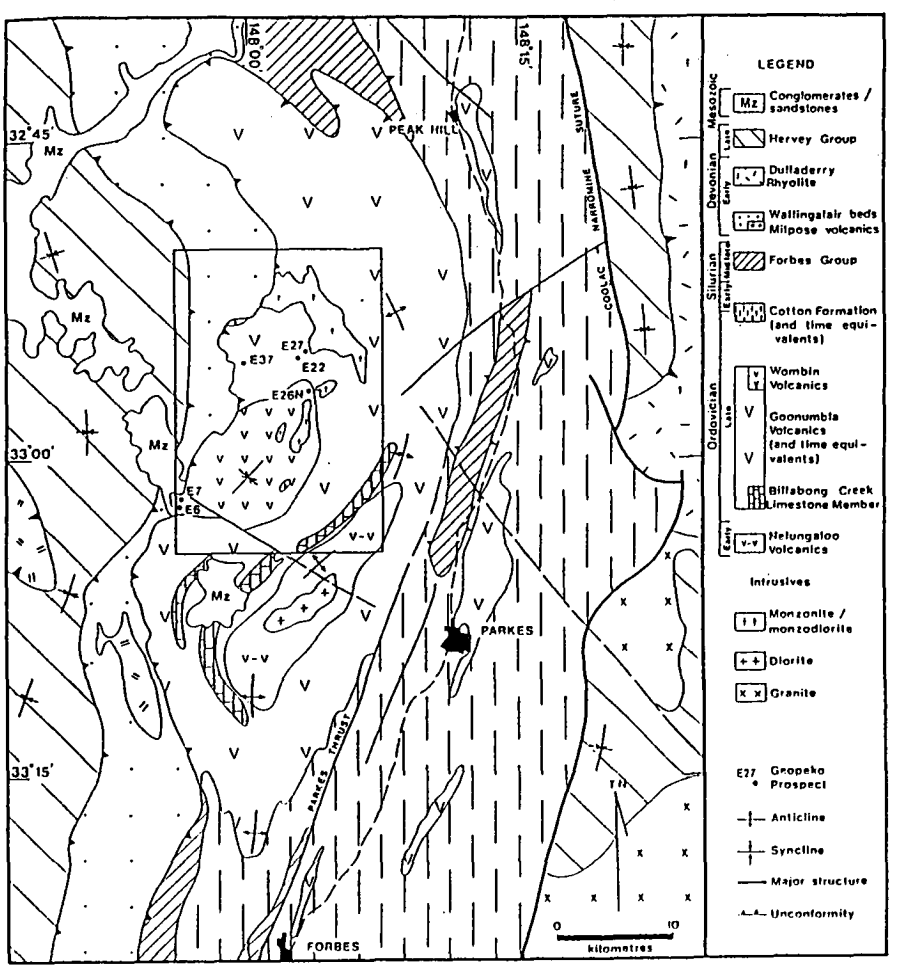

Figure 2.2 Geology of the Goonumbla area (From Heithersay et al., 1990).

associated with a rearrangement of plate geometry (Wyborn, 1994). The importance of this process in relation to the formation of porphyry Cu-Au deposits will be discussed in the next chapter.

2.2 GEOLOGY OF THE GOONUMBLA AREA

The Goonumbla Volcanic Complex (GVC) (Figure 2.2) is part of the Bogan Gate Synclinorial Zone of Scheibner (1973). The Late Ordovician Goonumbla Volcanics (approximately 440Ma; Perkins et al., 1990) were erupted from shallow water to partly emergent(?) volcanic centres, and show a broad range in composition from shoshonite through latite to trachyte (Heithersay, 1991). Minor volcaniclastic rocks and limestones are interdigitated with the volcanics on the flanks of these centres. A pronounced circular feature approximately 22km in diameter can be seen in magnetic and gravity images of the Goonumbla region and is interpreted by Jones (1985) to be a collapsed caldera formed by explosive mechanisms. More recent work by Hall (1993) suggests that the caldera formed by block subsidence and downsagging. The lack of pyroclastic deposits in the area suggests that effusive rather than explosive mechanisms were important in caldera formation, supporting Hall's (1993) model. The Wombin Volcanics of Jones (1985) are now considered part of the Goonumbla Volcanics (Hall, 1993).

The thickness of individual flows in the Goonumbla Volcanics range from metres to tens of metres. Hall (1993) has documented several lava varieties, including:

i) subaerial, porphyritic, blocky lavas

ii) sparsely porphyritic, diffusely flow banded lavas

iii) sparsely porphyritic hyaloclastite lavas

iv) flow-layered lava sequences characterised by angular phenocrysts.

Occurrences of latite lavas within latite debris have been interpreted by Hall (1993) to be a megaclast breccia facies derived from a volcanic debris avalanche. Recent mapping in the E26 decline and hoisting shaft supports this interpretation, recognising variably sized clasts of fine aphanitic orange-pink latite set in a polymictic matrix containing crystal debris and lithic fragments of flow banded lavas, coherent latite lavas and felsic to mafic porphyritic lavas and/or subvolcanic intrusives. The latite clasts vary from 0.1m to 50m in diameter. Clast boundaries can be sharp and well defined, or irregular and

marked by increased internal fracturing on the margin of the clast. This increased fracturing results in a jigsaw-fit texture which is increasingly matrix-supported away from the parent clast.

Coeval monzonite porphyries have intruded the volcanics within the GVC. The monzonite porphyries are transitional to monzodiorite, diorite and gabbro, and are interpreted by Jones (1985) to form a large truncated ring dyke. The Endeavour 31 stock which crops out in the northeast corner of the GVC is a porphyritic mafic monzonite stock distinguished by biotite and lesser hornblende phenocrysts, and is 1.5km by 1km in plan dimension at the surface (Heithersay, 1991; Figure 2.2). The E31 stock is interpreted to be the parent for the mineralised porphyritic pipes such as at E26, E28 and E48 which occur around its margins (Heithersay, 1991). These quartz monzonite porphyries (QMP) crosscut the E31 stock, and represent late-stage focused release of magma and volatiles which had collected on the shoulders of the stock (Heithersay, 1991). Subvolcanic emplacement of the intrusives is suggested by their fine grained nature, breccia pipes, and pebble dykes (Heithersay, 1994). The deposits show varying degrees of preservation. At E26, mineralisation contracts quickly near the base of oxidation, suggesting that a full profile of a porphyry system is preserved. The deposits at E22 and E27, however contain high grade mineralisation to the base of oxidation and are capped by a residual oxide gold deposit, suggesting that these deposits are eroded, with only the middle and deeper parts of the system preserved. Late, post-mineralisation quartz monzonite dykes, locally termed zero porphyries, crosscut the mineralisation. These are subvertical and tend to follow structural trends.

A large complex Cu anomaly ranging from 1000ppm to >4000ppm blankets the E31 stock (Heithersay, 1991). Local highs are associated with the quartz monzonite porphyries. The QMP's disrupt an annular Zn geochemical pattern centred on the E31 stock. It appears that these Cu and Zn halos are associated with the E31 stock and have been overprinted by the quartz monzonite porphyries (Heithersay, 1991).

The volcanics at E22, E26, E27 and E48 dip gently to the southeast, and lie on the western limb of Jones' (1985) Milpose Syncline. The vertical to sub-vertical attitude of the quartz monzonite pipes suggests little post-mineralising deformation (Jones, 1985).

Few major faults or shears have been mapped, although lineaments have been defined from aerial magnetics, along which many of the major deposits lie, suggesting some structural control to QMP emplacement. The E48 and E28 deposits are intersected by a major shallow east dipping fault known as the Altona Thrust. Small shears, faults and post-mineralisation dykes tend to be subvertical to steeply dipping with strikes of NW-SE and NNE-SSW.

3. PORPHYRY COPPER-GOLD DEPOSITS

3.1 INTRODUCTION

A brief overview of porphyry Cu-Au deposits from around the world provides a comparative basis for this study of E26. Salient comparative aspects are the geometry and size of the porphyritic stocks, the distribution of mineralisation, alteration (particularly K-feldspar-biotite-magnetite) and stockwork quartz veining, and the associations of bornite-Au, and distal Pb-Zn-Ag-Au. It is important to note that the majority of porphyry Cu-Au deposits do not fit the classic porphyry Cu deposit model of Lowell and Guilbert (1970). The 'type' models for porphyry Cu-Au deposits are taken from deposits in the South west Pacific (eg. Sillitoe and Gappe, 1984; Sillitoe, 1990; Figure 3.1).

Au-rich porphyry deposits were classified by Sillitoe (1979) as those deposits with >0.4g/t Au. Given that the reported resource grade of a deposit is an economic rather than natural indication of the mineralised system, the validity of such a definition must be questioned. Despite E26 containing the same amount of Au as E22 and E27 combined, Sillitoe (1990) excluded E26 but included E22 and E27 in his Au-rich porphyry category. This was because of the low cut-off grade used to report the E26 deposit by Jones (1985) which Sillitoe (1990) used as a source. Similarly, Bingham Canyon, with a Au production in excess of 15 million ounces, but at a grade of only 0.2g/t Au, would not be classified as a Cu-Au porphyry based on Sillitoe's criteria. Based on the current resources (using a higher cut-off grade), E26 would be included in Sillitoe's (1990) classification.

The principal porphyry Cu-Au deposits of the world occur in the circum-Pacific region. The deposits are confined mostly to the Philippines, Indonesia, New Guinea and British Columbia. The porphyry Cu deposits of the western U.S.A. and South America tend to be Au-poor, although there are numerous exceptions. While there is still considerable debate on the influence of tectonics on metallogenesis and on the metal components of porphyry systems, Jones and Thompson (1991) note that Au-enriched deposits tend to be emplaced in island arc and oceanic crust settings. Major element and isotopic

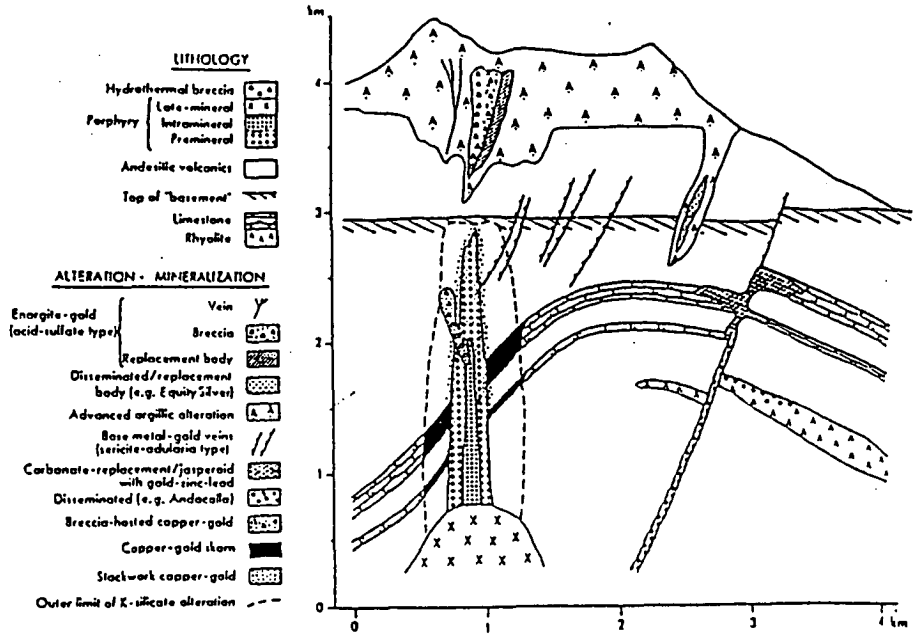

Figure 3.1 Distribution of styles of Au and Ag mineralisation around porphyry deposits (From Sillitoe, 1989).

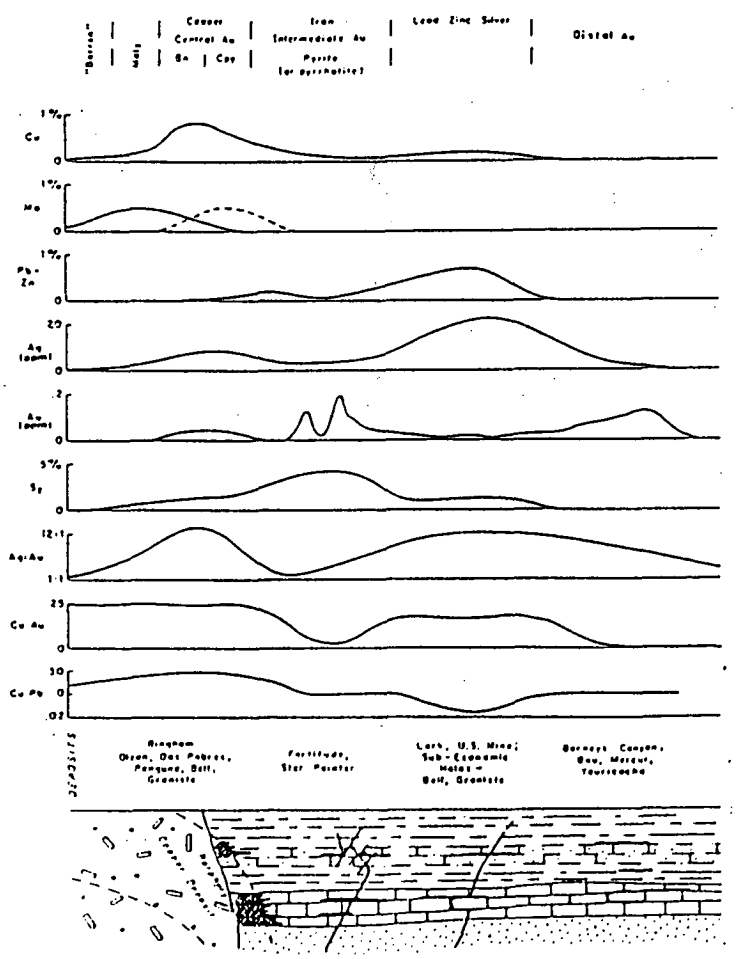

Figure 3.2 Metal zonation around gold-enriched porphyry copper systems (From Jones 1992).

compositions require that the magmas that generate porphyry Cu-Au deposits contain a mantle-rich source. Mantle metasomatism could be the result of a thermal perturbation, lithospheric delamination or pressure reduction due to plate rearrangements (Wyborn, 1994). Solomon (1990) presented a model in which metasomatism and the generation of gold enriched magma occurs during an arc reversal, such as the Philippines. Au-poor and Mo-enriched porphyry systems tend to occur in thick continental arc settings with magmas derived from partial melting of continental crust. Recent discoveries of porphyry Au deposits in Chile (eg. Marte) demonstrates that there are exceptions to this association (Sillitoe, 1990).

3.2 CHARACTERISTICS

3.2.1 Geometry and Composition

Porphyry Cu-Au deposits are characteristically related to shallowly emplaced stocks that have intruded coeval volcanic sequences. The stocks are commonly pipe-like in structure, having a small plan area but extenuated vertical extent. Mineralisation can occur both within the intrusive stock and surrounding volcanics. Of the Philippine deposits, over half are less than 0.5km^2 in plan at surface (Sillitoe and Gappe, 1984). Vertical extents of 700-1100m and a widening with depth is typical for many of the Philippine stocks (Sillitoe and Gappe, 1984). At Batu Hijau in Indonesia, the mineralising tonalite stock is 500m in diameter at 600m depth and tapers upward (Meldrum et al., 1994). The main Grasberg Intrusive at Grasberg, Irian Jaya, is a subcircular stock 300m in diameter that extends for at least 1500m vertically (Kavalieris, 1994).

The stocks and host volcanics range in composition from low-K calc-alkaline through high-K calc-alkaline to potassic-alkaline (Sillitoe, 1990). Most of the stocks in the Philippines (Sillitoe and Gappe, 1984) and at Panguna (Clark, 1990) have diorite to quartz diorite compositions. Other compositions are also important: tonalites occur at Batu Hijau (Meldrum et al., 1994); monzonites and quartz monzonites occur at Grasberg (MacDonald and Arnold, 1994); while deposits in British Columbia are hosted by silica-saturated to undersaturated alkalic monzonite-syenite stocks (Thompson, 1994).

3.2.2 Alteration and Mineralisation

Five distinctive types of alteration are recognised in Au-rich porphyry deposits:- K-silicate (potassic); propylitic; intermediate argillic; sericitic (phyllic); and advanced argillic (Sillitoe, 1990). Cu and Au mineralisation is nearly always associated with potassic alteration. This alteration is characterised by biotite ± K-felspar. Magnetite is a common accessary phase, comprising up to 8vol% at Santo Tomas II (Sillitoe and Gappe, 1984) and up to 15wt% at Grasberg where it is associated with auriferous quartz-magnetite-biotite-sulphide veins (MacDonald and Arnold, 1994). The Au-magnetite relationship is a common and important association in Philippine deposits (Sillitoe and Gappe, 1984). However, as Titley (1990) has cautioned, K-silicate related magnetite alteration can also occur in systems where little or no Au occurs.

Stockwork quartz veining is intimately associated with mineralisation in potassically altered zones, comprising up to 25% of the rock volume in some deposits (Sillitoe and Gappe, 1984). Dense quartz stockworks can coalesce to give massive bodies of mineralised quartz. The main sulphide phases are chalcopyrite and bornite, with lesser pyrite. Au and Cu grades generally correlate closely. Au or electrum occurs as fine inclusions in Cu sulphides. In pyrite-poor deposits there is a strong bornite-Au association (eg San Antonio and Santo Tomas II; Sillitoe and Gappe, 1984). Chalcopyrite is more abundant than bornite at many deposits (eg. Grasberg and Panguna). Some deposits show vertical Cu/Au zonation (eg. Batu Hijau, where Au content increases at a greater rate than Cu with depth, Meldrum et al., 1994), and vertical Cu sulphide zonation (eg. Grasberg, where bornite increases with depth in the Dalam stage, MacDonald and Arnold, 1994).

The other alteration types in Philippine porphyries (SCC, sericitic, advanced argillic, propylitic) vary in their occurrence and intensity and typically have overprinted potassic alteration. A summary of the typical mineral assemblages for each alteration type is given in Table 3.1. Of interest, anhydrite (and/or gypsum) occurs in nearly all Philippine deposits in all alteration types including potassic (Sillitoe and Gappe, 1984). Most Philippine deposits are also encircled by well-developed pyrite halos.

K-Silicate	*SCC*	*Sericitic*	*Advanced Argillic*	*Propylitic*
Biotite	Sericite	Quartz	Alunite	Chlorite
K-feldspar	Clay	Sericite	Kaolinite	Epidote
Albite	Chlorite	Pyrite	Dickite	Calcite
Magnetite	Quartz		Chalcedony	
Quartz	Anhydrite		Pyrophyllite	
Amphibole	Calcite		Sericite	
Anhydrite	(Hematite)		Pyrite	
(Chlorite)	(Pyrite)			
(Epidote)				

Table 3.1 - Typical alteration assemblages - Philippine porphyry copper deposits (Compiled from Sillitoe and Gappe, 1984)

3.2.3 Fluid Chemistry

Fluid inclusion and isotope studies have shown that Cu and Au were transported in high temperature (400-700°C) saline (>20wt% NaCl) hydrothermal brines, released during second boiling from a crystallising magma (Sillitoe, 1990). At these conditions, Au and Cu are likely to be transported as chloride complexes. Pb, Zn and Ag however, are highly soluble under these conditions, and will be transported through the main mineralised environment, and precipitated on the peripheries of the porphyry system (Cooke, pers. comm., 1994). While Au is probably transported as a chloride complex in the hotter porphyry fluids, in more distal cooler fluids, bisulphide is a more efficient ligand for Au transport. The significance of remobilisation and redeposition of Au late in the cooling history of the porphyry system is still a matter of some debate.

3.3 METAL ZONATION

A model of metal zonation around porphyry systems proposed by Sillitoe (1989) is shown in Figure 3.1. Gold occurs in the central quartz-vein stockwork associated with K-silicate alteration. Gold can also occur with Ag in distal settings where it is most likely precipitated from later, cooler (meteoric?) fluids. Jones (1992) notes that Au can occur in the pyrite halo of a porphyry system in shear zones, quartz-sericite-pyrite stockworks and distal skarns. Distal Au may also partly overlap with a Pb-Zn-Ag zone (Figure 3.2). In shallow crustal settings (<1km), epithermal Au deposits may occur in association with porphyry mineralisation.

4. GEOLOGY OF E26

4.1 INTRODUCTION

Significant increases in collected data and data display methods has occurred in the last four years including:

i) drilling in 1991

ii) site drilling in 1993

iii) underground development mapping in 1993 and 1994

iv) fully computerised database

v) 3-dimensional graphical viewing of data.

This review of the geology of E26 is intended to build on the work of Heithersay (1991) using this new information and computer-assisted analysis of it, and is based on the Geopeko drill logs, re-examination of drill core, and mapping of underground exposures. A plan of the current underground development and the orebody location is given in Figure 4.1.

Cu-Au mineralisation at E26 occurs in stockwork quartz veins and disseminations associated with potassic alteration which is intimately associated spatially and temporally with small finger-like quartz monzonite porphyries that have intruded the Goonumbla Volcanics. Mineralisation is concentrically zoned around the intrusive stocks and extends for at least 1 000m vertically. The dominant sulphide phase is bornite, and Au occurs principally as small inclusions in bornite. The mineralisation halo thins upwards to 50m x 50m below the base of surface oxidation, and as a result, only a small part of the system has suffered supergene alteration. Due to the lack of erosion/weathering and the low Au contents of the upper areas, no oxide Au enrichment (as seen at E22 and E27) occurs. A small zone of oxide Cu mineralisation occurs immediately above the base of oxidation. Chalcocite, malachite and atacamite are the main copper minerals in this zone.

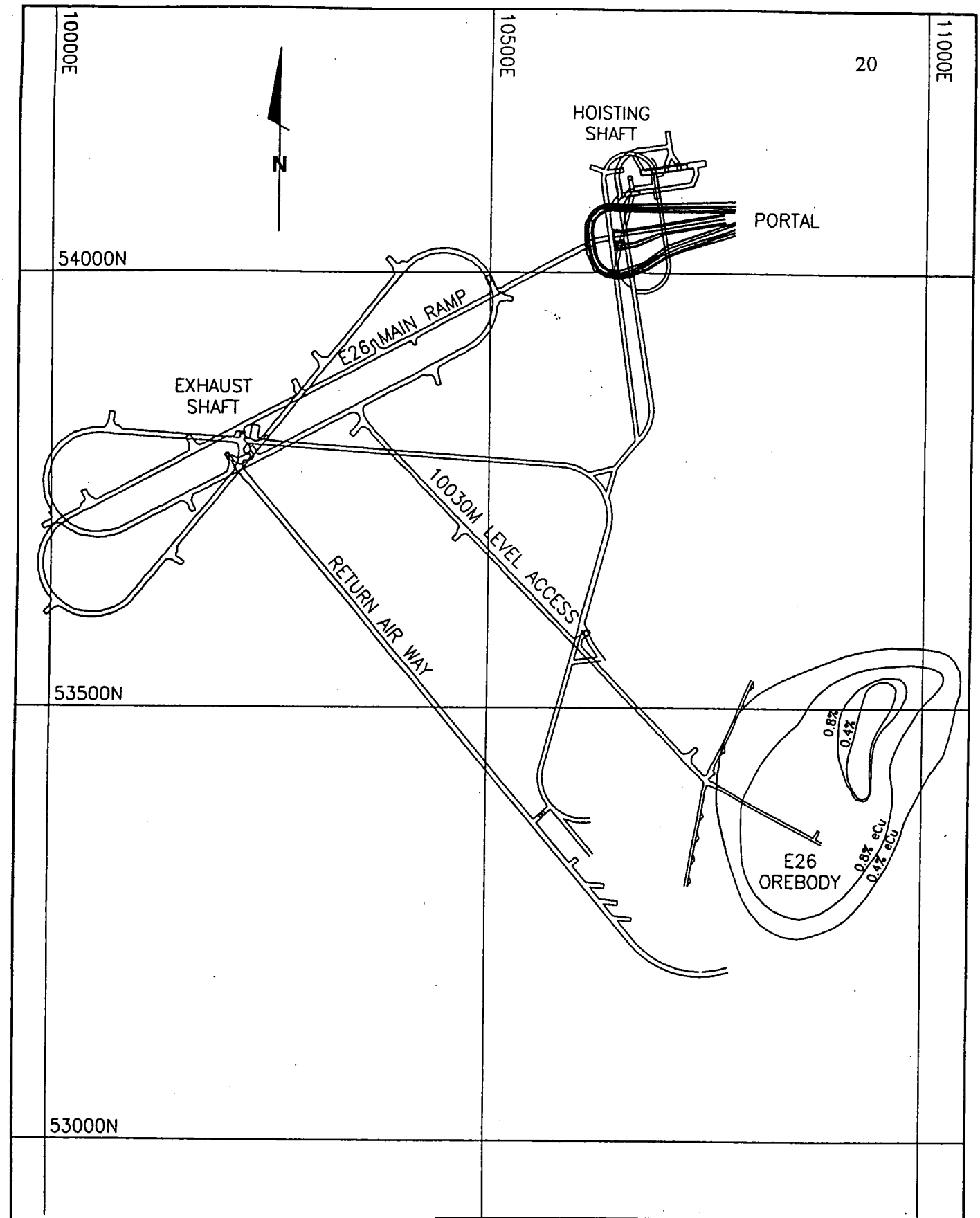

NORTHPARKES

NORTHPARKES MINES

A Division of North Mining Limited (ACN 000 081 434) as agent for and manager of the Northparkes Joint Venture

Scale 1:6000

0 250m

Date:	14/12/94
Drawn:	R.M.N.
Author:	M.J.H.
Checked:	
Revision:	

E26
STAGE 1
RAMP DEVELOPMENT

Figure 4.1

Integrated survey grid zone 55/3 is shown.

4.2 INTRUSIONS

4.2.1 Biotite Quartz Monzonite (E31 stock)

To the immediate east and beneath the E26 deposit is the E31 stock (Figure 4.2), locally termed a biotite quartz monzonite. Monzodiorites, monzonites and syenites were intersected in the outer 350m of the E31 stock in hole E26D46 indicating that stock is a composite body, containing considerable intrusive activity in the outer margins (Heithersay, 1991).

4.2.2 QMP1

Two main quartz monzonite porphyry (QMP) intrusions were described at E26 by Heithersay (1991; Figures 4.2 and 4.3). Most of the Cu and Au mineralisation is associated with QMP1. This intrusion is oval in plan view with dimensions of approximately 20m by 70m, and a vertical extent of at least 600m. QMP1, was previously known as the 'mosaic porphyry' and is characterised by K-feldspar and plagioclase phenocrysts set in a fine K-feldspar and quartz groundmass (Heithersay, 1991). Intense potassic alteration, stockwork quartz veining, and Cu mineralisation are common. The porphyry can contain angular to rounded fragments of quartz monzonite porphyry, biotite monzonite, quartz veins and sulphide clots in a porphyritic monzonite matrix (Figure 4.4). These fragments (xenoliths?) suggest that the porphyry intruded in several episodes, each episode marked by brecciation of the pre-existing phases. A lower grade (<2.0% eCu) core marked by a more massive finer grained monzonite and by the lack of stockwork quartz veining occurs in the porphyry, particularly at depth. Cu mineralisation is most abundant (>2% Cu) on the margins of QMP1 and in the immediately adjacent volcanics. The simple boundaries of the QMPs shown on the geological interpretations (Figures 4.2 and 4.3) do not accurately reflect the complex and jagged margins that will only be fully understood when underground exposures become available.

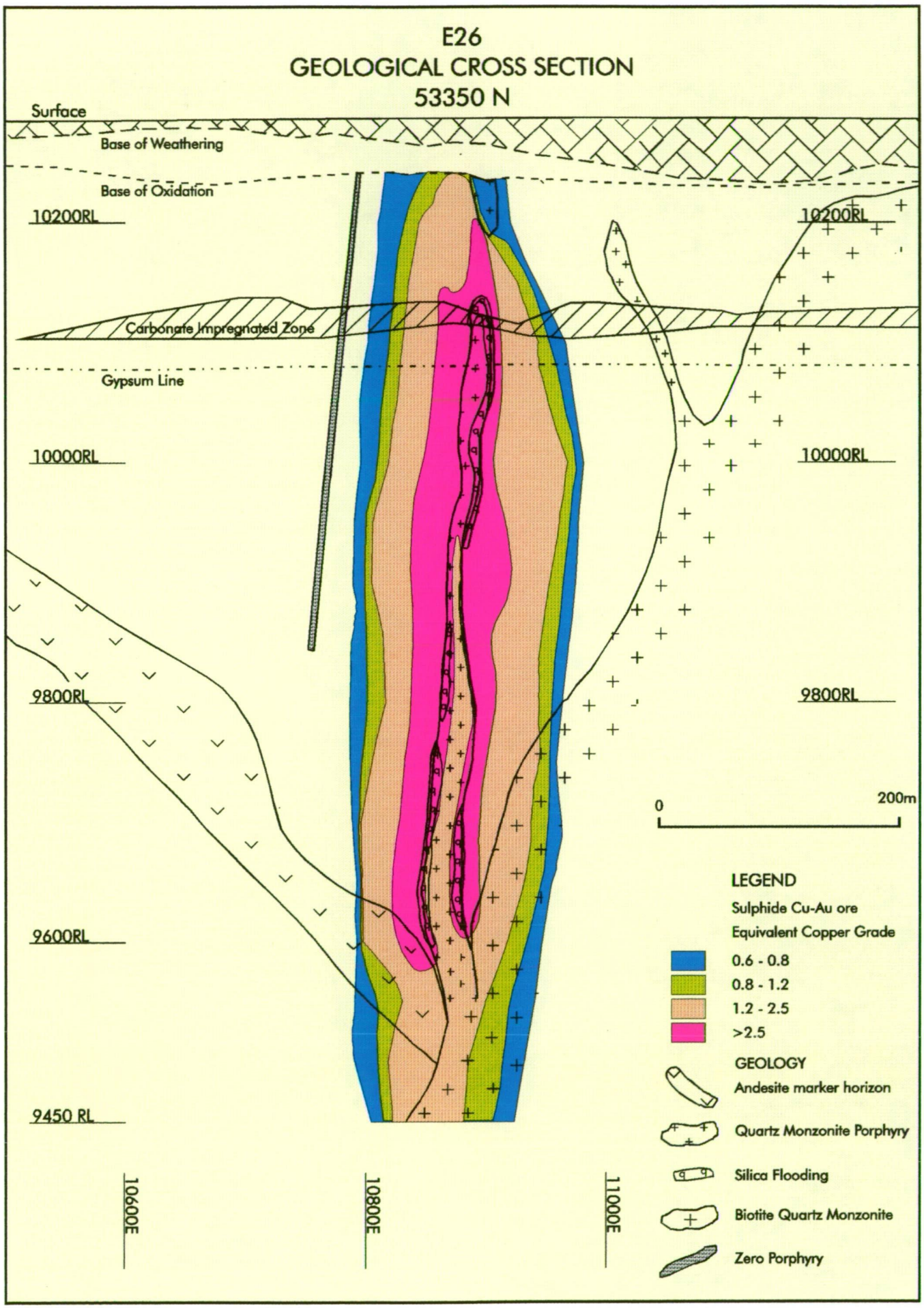

Figure 4.2 Geological cross-section of E26 - 53350N.

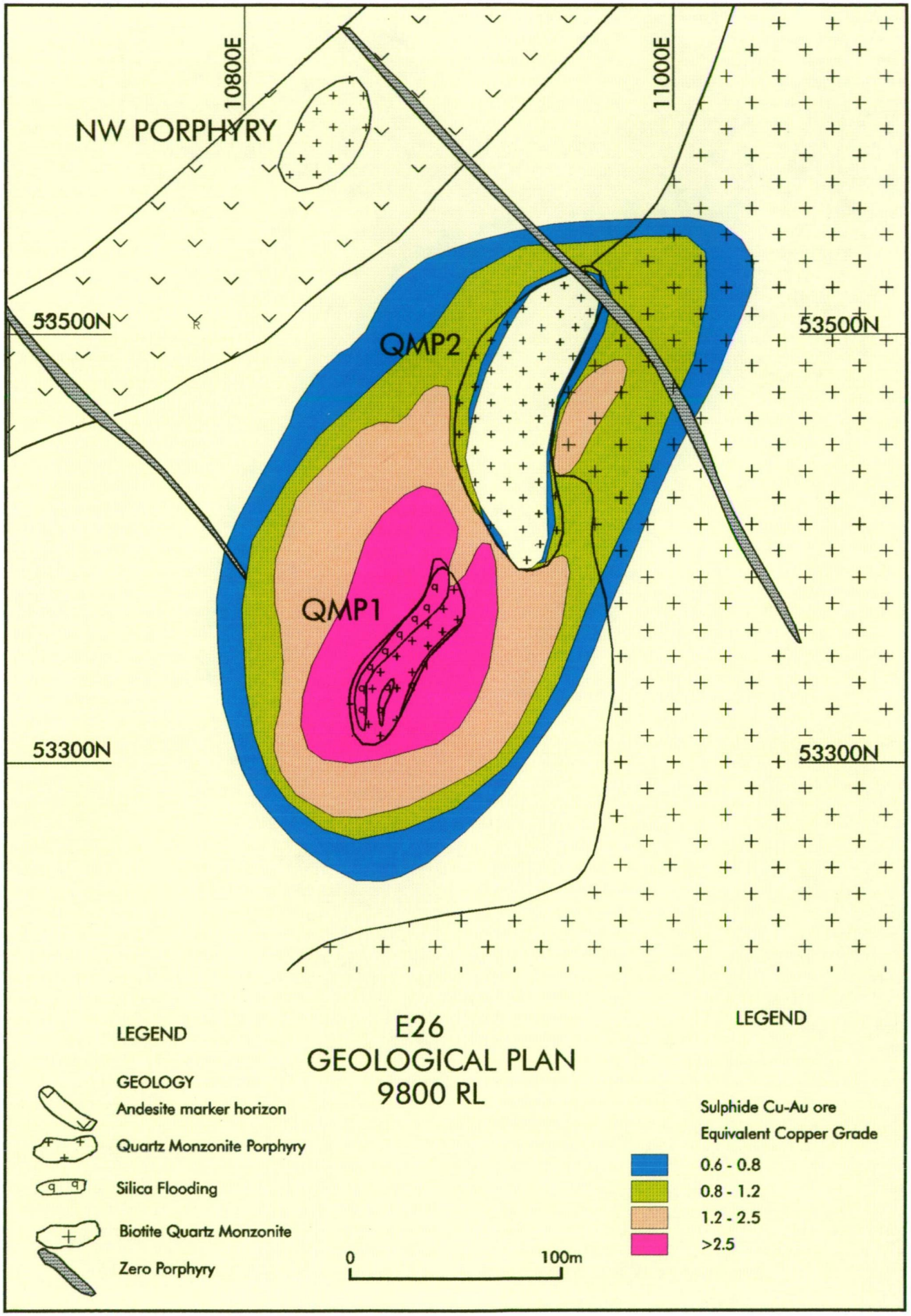

Figure 4.3 Geological plan of E26 - 9800mRL.

Figure 4.4 Fragments (xenoliths?) within QMP1 (Hole E26D126W2, 550m).

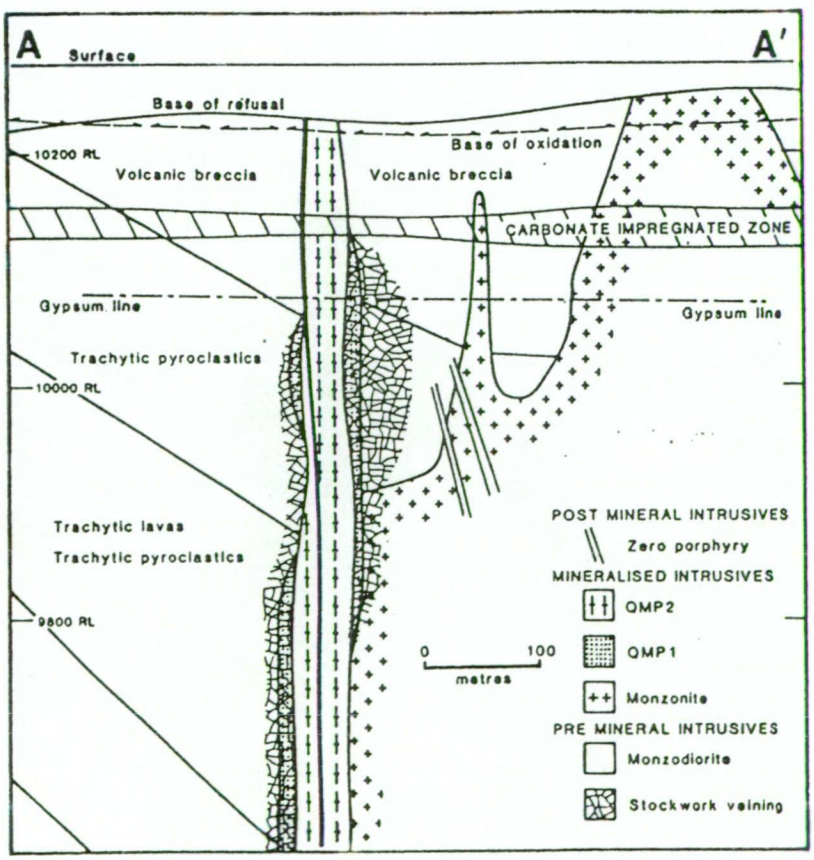

Figure 4.5 Geological cross-section of E26 - 53450N (From Heithersay, 1991).

4.2.3 QMP2

The second main quartz monzonite porphyry (QMP2) occurs to the north of QMP1 and is thought to partly intrude QMP1 and its associated mineralisation (Heithersay, 1991). QMP2 (also known as the 'square' porphyry) reaches maximum dimensions of 40m by 130m in plan, with a vertical extent of at least 700m (Figure 4.5). The porphyry contains pale euhedral square to rectangular zoned and/or twinned plagioclase phenocrysts, euhedral rectangular deep red-brown Fe-oxide-stained K-feldspar phenocrysts and minor partially altered biotite and hornblende phenocrysts set in a fine grained K-feldspar-quartz groundmass (Heithersay, 1991). The core of QMP2 is particularly lower grade (<0.4% Cu) than its margins. The weak mineralised envelope that surrounds QMP2 is interpreted to be the remnants of pre-existing QMP1-associated mineralisation (Heithersay, 1991).

4.2.4 Deep Porphyritic Intrusions

The relatively simple intrusive sequence of QMP1 and QMP2 becomes more complex below approximately 9650mRL (Figure 4.6). This complexity, highlighted by drilling in 1991, is still not well understood due to the sparse drillhole spacing. Below 9650mRL, numerous small quartz monzonite porphyry stocks have characteristics of both QMP1 and QMP2. These intrusions occur within and on the immediate edge of the biotite quartz monzonite. There is no well-defined high grade Cu zone associated with QMP1, which appears to die out within the biotite quartz monzonite. Instead, the mineralised centre occurs approximately 100m north and is focused on another QMP1-type porphyry. Stockwork quartz veining occurs in and around this porphyry which contains xenoliths of biotite quartz monzonite. Several small, low grade QMP2-type stocks occur to the east and north of the mineralised porphyry and clearly postdate stockwork quartz veining. A QMP2-type 'square' porphyry intercepted in drillhole E26D130W3 immediately adjacent and to the west of the mineralised QMP1-type porphyry, contains moderate stockwork quartz veining and mineralisation, suggesting it may predate or be contemporaneous with mineralised QMP1-type porphyry. Stockwork quartz veining is intense within the biotite quartz monzonite and volcanics surrounding the QMP1-type porphyry (eg. drillhole E26D132W2). A three dimensional model of the intrusive geology was made in DATAMINE, and shown in Figure 4.7.

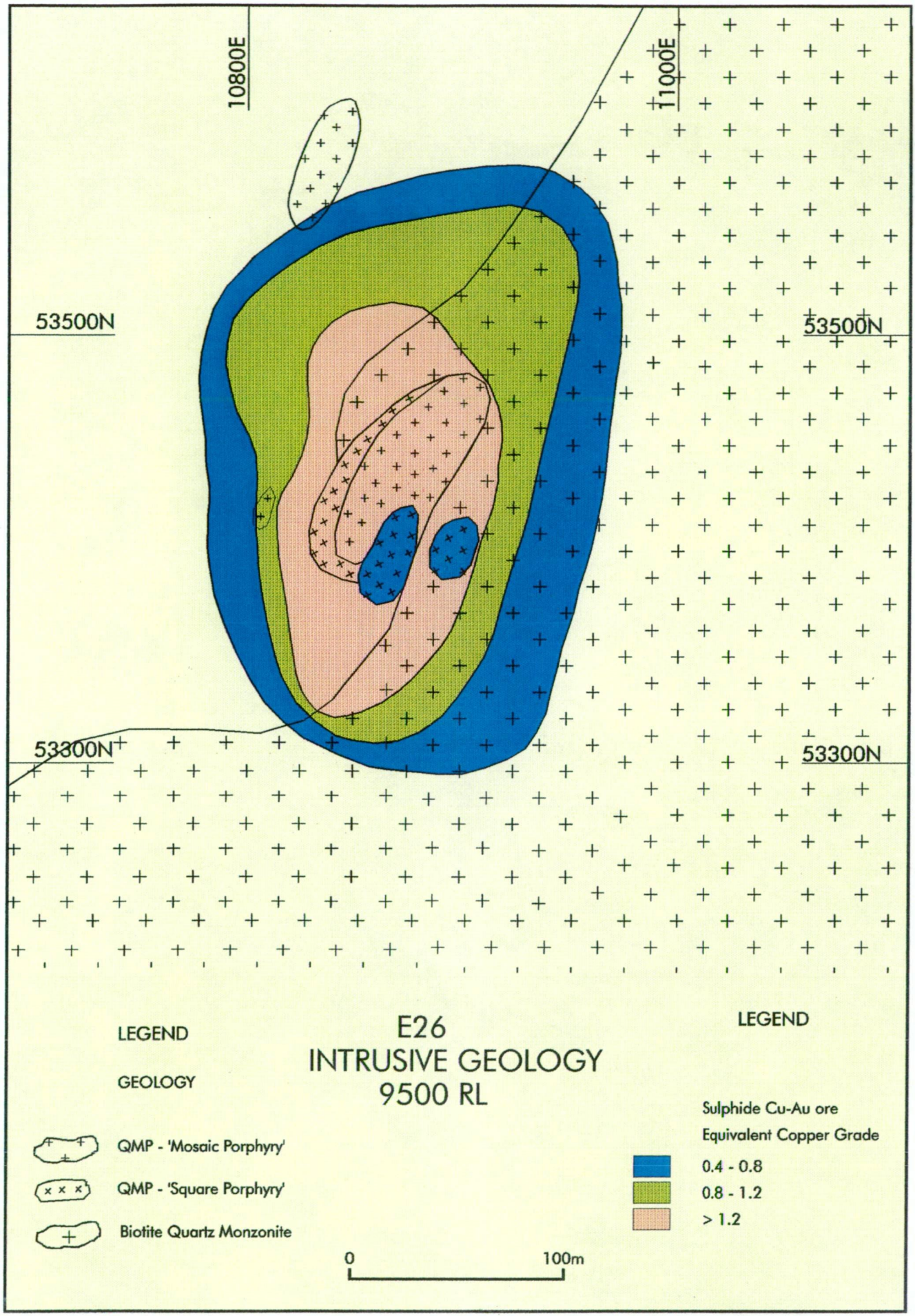

Figure 4.6 Geological plan of E26 - 9500mRL.

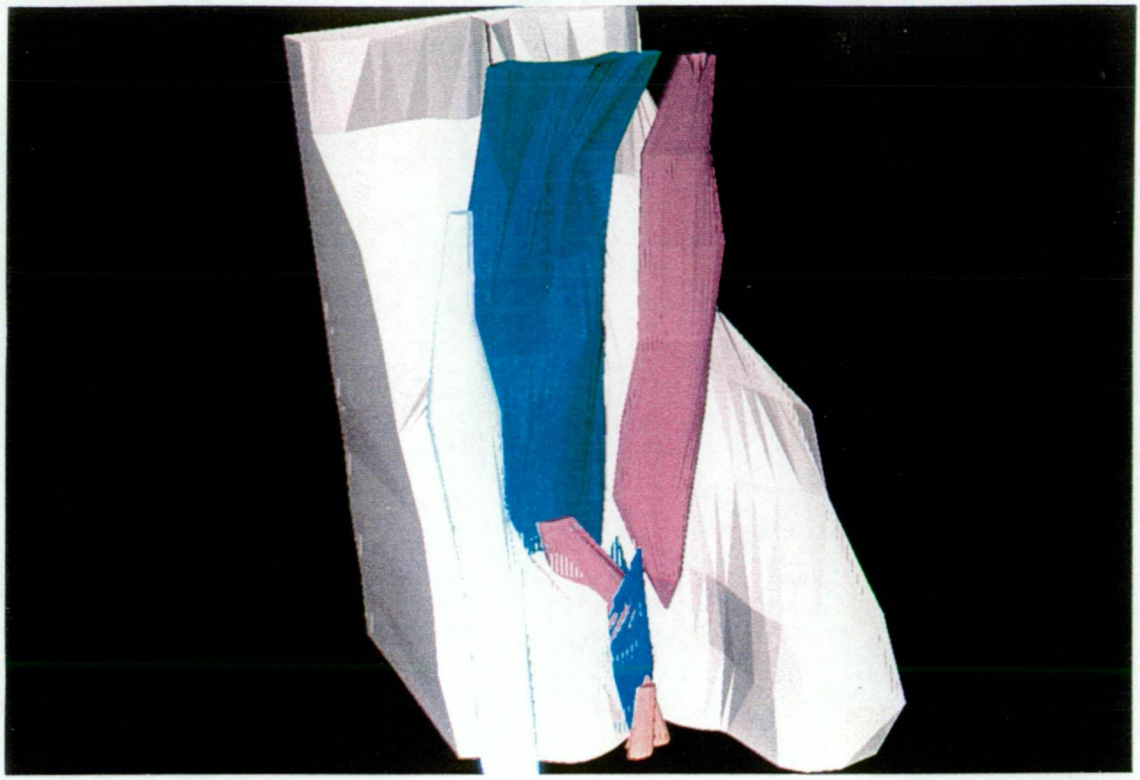

Figure 4.7 Wireframe model of the intrusive geology at E26 - looking to the Southeast. The light brown at rear is the BQM; the purple at right is QMP1; the green is QMP2; the grey is the Northwest Porphyry; while at the base are numerous small porphyries.

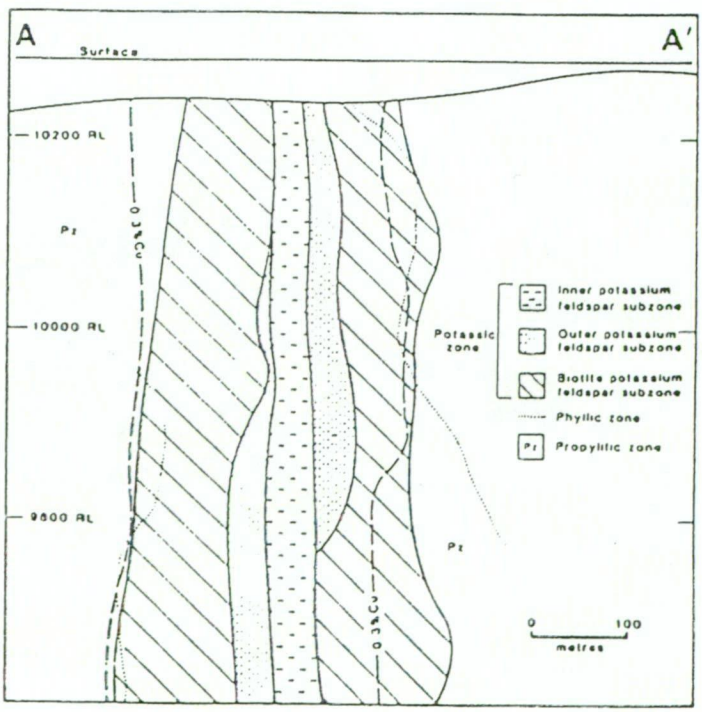

Figure 4.8 Alteration zones at E26 - 53450N (From Heithersay, 1991).

4.2.5 Other Porphyries

To the northwest of the main QMP's at E26 is a smaller satellite quartz monzonite porphyry. Locally termed the 'northwest porphyry' it appears be 20-30m across and 500m in vertical extent. Mineralisation associated with the northwest porphyry is weakly developed and discontinuous.

A quartz monzonite porphyry protruding from the upper regions of the E31 stock into the surrounding volcanics on section 53350N is weakly mineralised. The porphyry contains abundant plagioclase phenocrysts and chloritised mafic phenocrysts set in a fine grained K-feldspar-rich groundmass. Quartz and magnetite blebs are common. Potassic alteration is only weakly developed, with minor quartz veining and weak phyllic alteration. Weak anomalous Cu mineralisation (up to 0.8% Cu) is associated with this porphyry.

A later stage of barren porphyry dykes crosscut the E26 mineralising system. Locally termed 'zero porphyries', the dykes are up to 10m thick and trend NW, subparallel to quartz-sericite-pyrite shears. Pebble dykes, which are strongly healed breccias up to 2m thick, have a similar orientation.

4.3 ALTERATION

Heithersay (1991) gives a detailed description of the alteration types, zonation and paragenesis at E26. All of the economic mineralisation is associated with potassic alteration. The earliest stages of potassic alteration include pervasive and fracture-controlled biotite alteration with minor alkali-feldspar and magnetite (Heithersay, 1991). This is overprinted by several generations of pervasive and vein controlled K-feldspar and quartz alteration, with associated sericite, anhydrite, biotite, albite, hematite, calcite, rutile ± apatite, ± sphene ± fluorite. Hematite occurs as fine dustings in K-feldspar, and as a replacement phase of early magnetite.

Three subzones of potassic alteration have been defined by Heithersay (1991;Figure 4.8). An inner subzone of K-feldspar occurs in QMP2 and is associated with minor veining and mineralisation. An outer subzone of K- feldspar alteration occurs in QMP1, the

volcanics and the biotite quartz monzonite. The outer subzone is characterised by intense, texturally destructive alteration and intense quartz stockwork veining and related sulphide mineralisation. The outer K-feldspar subzone has overprinted a biotite K-feldspar subzone, remnants of which are preserved outside the K-feldspar subzones.

Outside the potassic alteration zone (approximately 150-200m from the QMP stocks) is a large envelope of propylitic alteration. This alteration style is characterised by epidote, chlorite, carbonate and pyrite. Propylitic alteration in the E26 ramp development comprises:- fracture controlled epidote and chlorite; selective replacement of phenocrysts by epidote and carbonate; and disseminated and fracture controlled pyrite. Locally, pyrite can comprise up to 5% of the rock volume in propylitically altered samples. Propylitic alteration is moderate to strong in the lower E26 ramp access, even though it is ≈500m from the QMP's, possibly indicating that this alteration style is associated with the E31 stock.

Structurally controlled quartz-sericite-pyrite alteration crosscuts propylitic alteration in the E26 ramp development and are locally termed 'qsp shears'. Quartz and pyrite veins are typically associated with the shears, and carbonate and lesser sphalerite, galena and chalcopyrite may also occur in these zones (Figure 4.9). Strong pervasive sericite alteration haloes up to 2m wide surround the shear zones. The qsp shears strike WNW and dip steeply to the north. Due to the absence of definitive markers and intensity of sericitic alteration, no sense of movement has been demonstrated on the shear zones, although shearing is indicated by the pervasive foliation and occasional puggy infill. As with the propylitic alteration, the distal location of this alteration style from the E26 quartz monzonite porphyries, may indicate a relationship to a larger system, such as the E31 stock. Similar qsp faults crosscut E48 and alternatively may relate to a regional structural system.

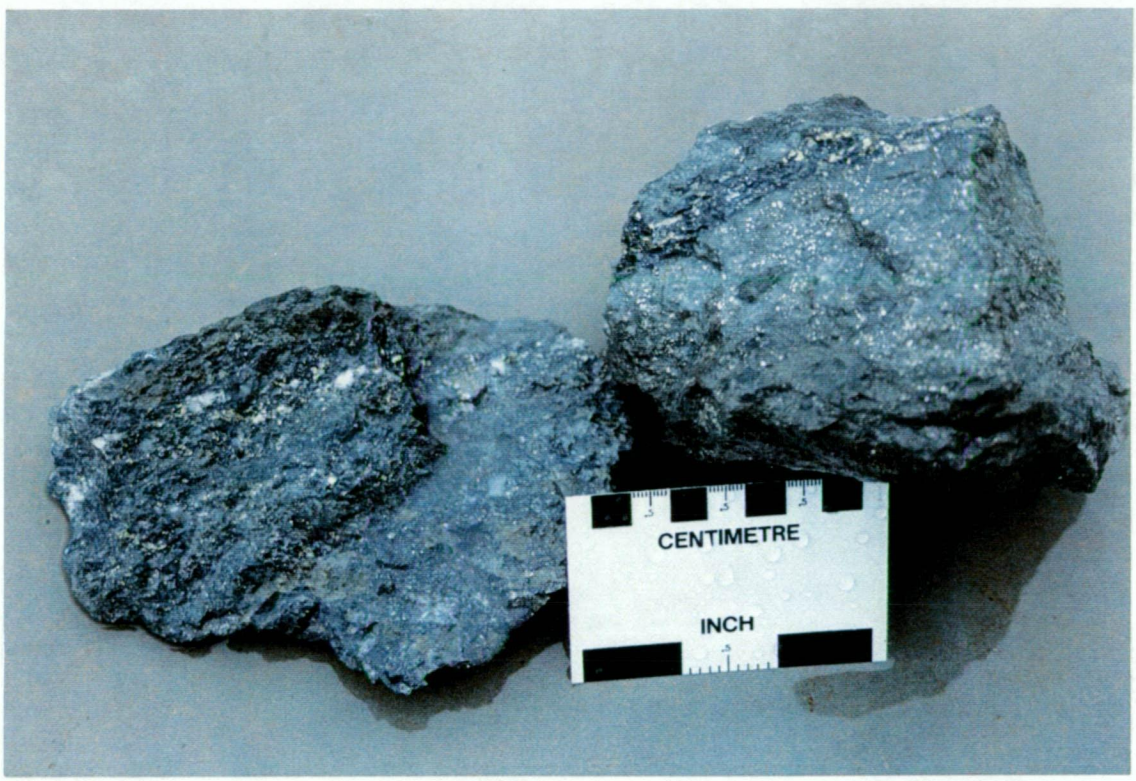

Figure 4.9 Mineralisation associated with structurally controlled qsp alteration from the E26 ramp - the bands at the top of each piece are galena, sphalerite, chalcopyrite and carbonate.

4.4 VEINING

4.4.1 Stockwork Quartz Veining

Stockwork quartz veining is localised around QMP1 (Figure 4.10). Measurements from drillcore suggest two principal vein sets, one striking to the NNE and dipping steeply to the west and east, the other to the NW with a steep northeasterly dip. In areas of intermediate Cu grade, the veins are typically sheeted. In higher grade areas, complex conjugate and splayed veins are dominant. A vertical zonation is apparent in the number of quartz veins per interval (Figure 4.11), with the greatest concentration of quartz veins occurring at 9700-9800mRL, decreasing abruptly below this level. Above 9800mRL, veining decreases irregularly, with local maxima at 9950mRL and 10150mRL.

The stockwork veins locally coalesce to form massive quartz veins and intense wall rock silicification up to 7m thick and 60m long. The silica zones are confined to the margins of QMP1 and the adjacent volcanics, are discontinuous vertically and are restricted to between 9600mRL and 10170mRL. The silica zone is very strongly developed in the carapace of QMP1, between 10100mRL and 10170mRL. Intensely sericitised QMP and wallrock rock fragments are often found within the silica zone (Figure 4.12). In contrast to QMP1, quartz veining is absent to weakly developed in QMP2. With depth, the core of QMP1 is also only weakly veined.

The vertical and horizontal zonation of quartz vein counts per 3m interval is summarised in Table 4.1. The number of quartz veins increases with increasing Cu mineralisation. Unfortunately, information on vein thicknesses is not available. This is clearly an important consideration in areas of massive quartz veining, where high grades are correlated with the thickness of veining rather than the number of veins.

4.4.2 Gypsum/Anhydrite veins

Gypsum and anhydrite veining at E26 postdates quartz stockwork veining and Cu mineralisation. The vein frequencies are strongly zoned vertically, decreasing in abundance with depth (Table 4.1). At about 10000mRL, gypsum veins comprise approximately 2-3% of the rock volume, decreasing to less than 0.25% below 9800mRL.

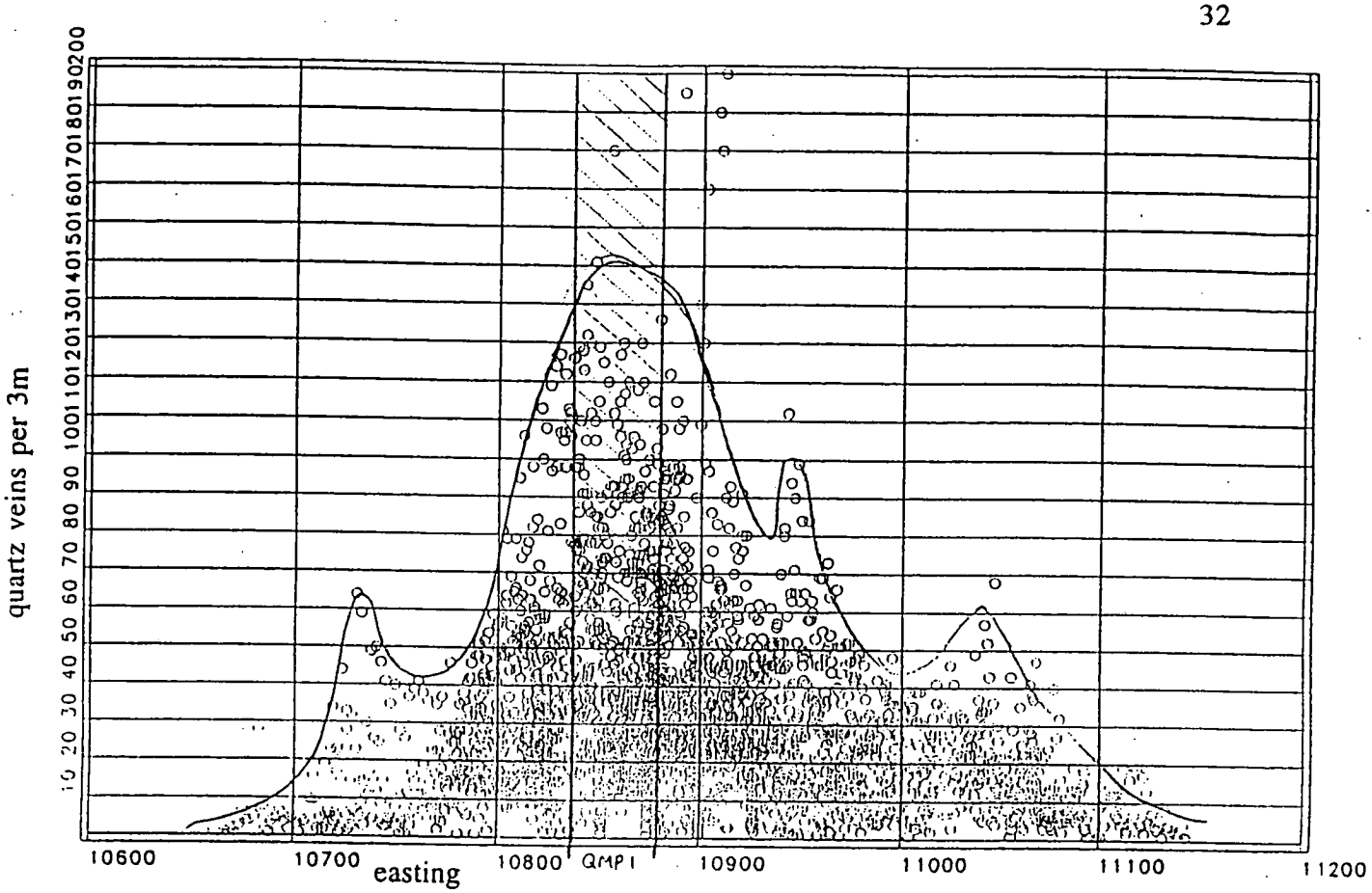

Figure 4.10 Variation in the number of quartz veins per 3m interval with easting.

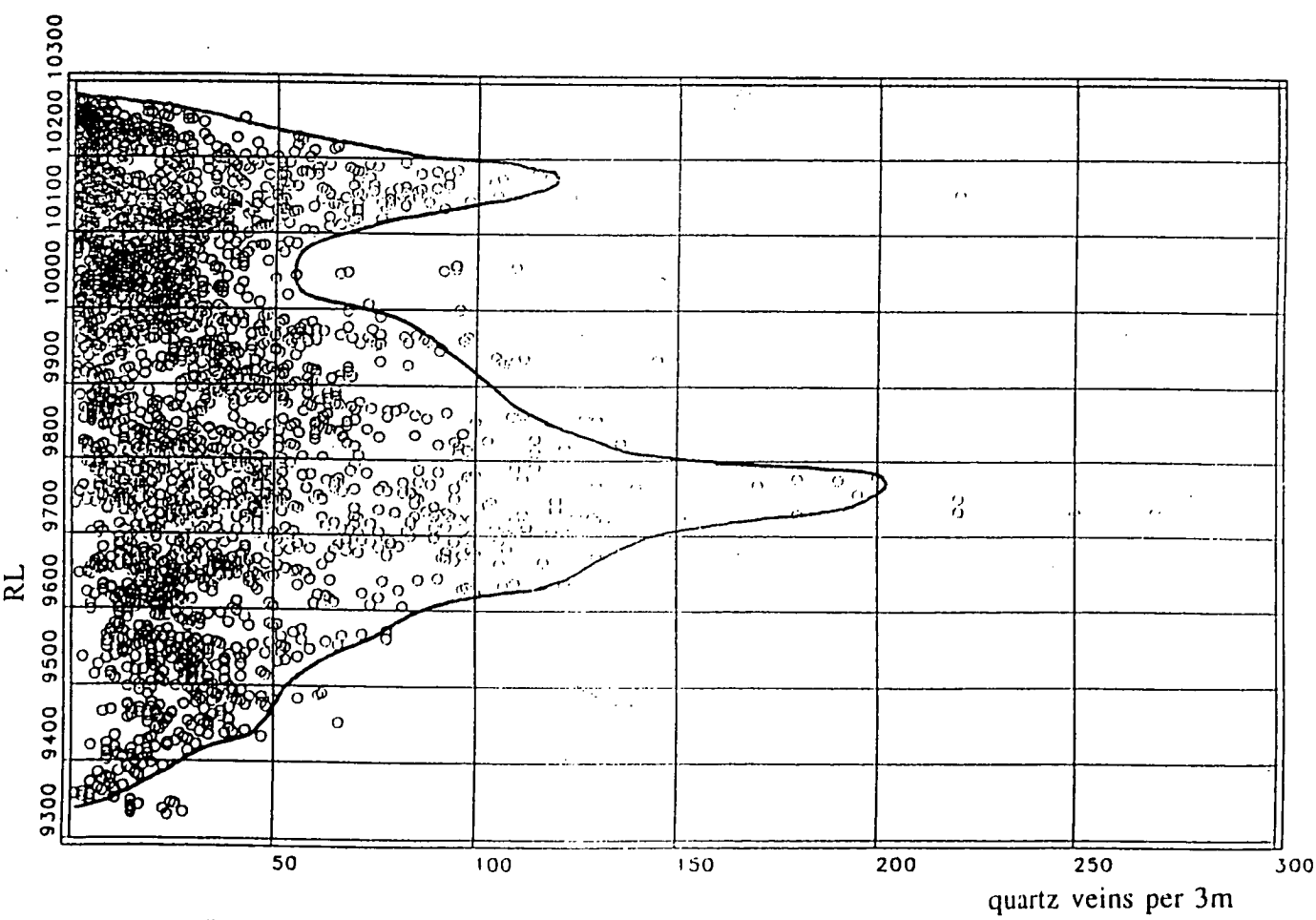

Figure 4.11 Variation in the number of quartz veins per 3m interval with depth.

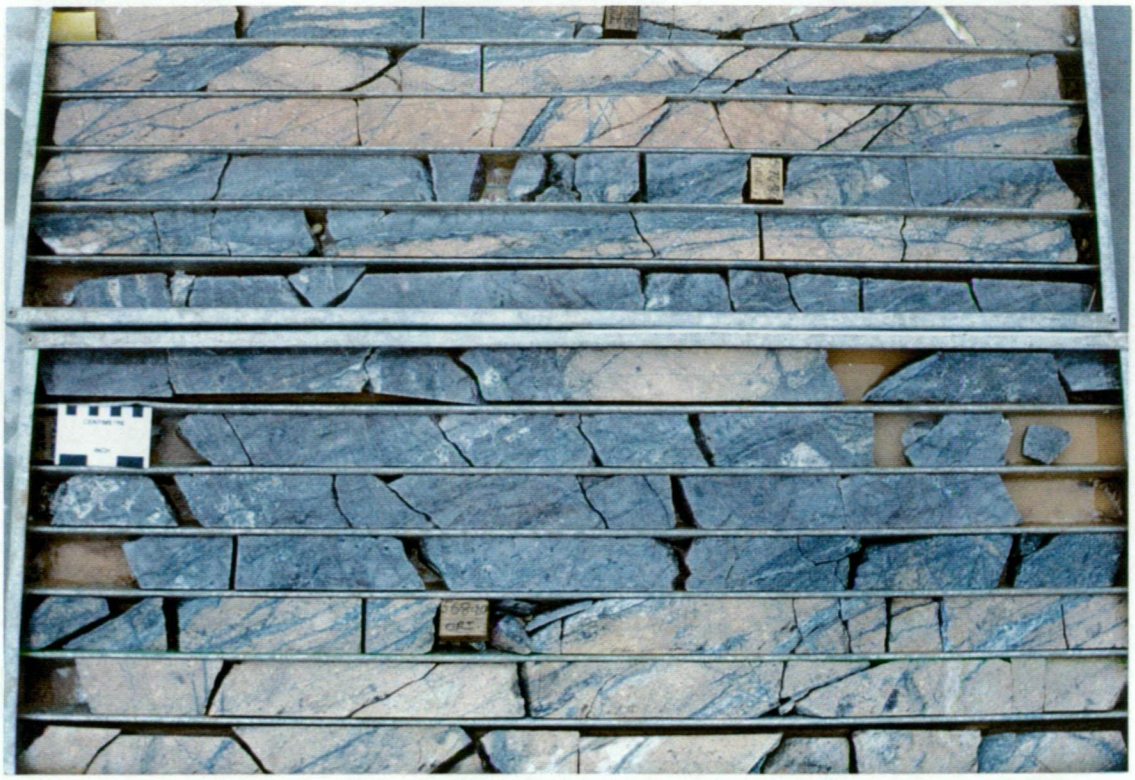

Figure 4.12 (a) Silica flooding at E26 - Hole E26D126W2, 570m .

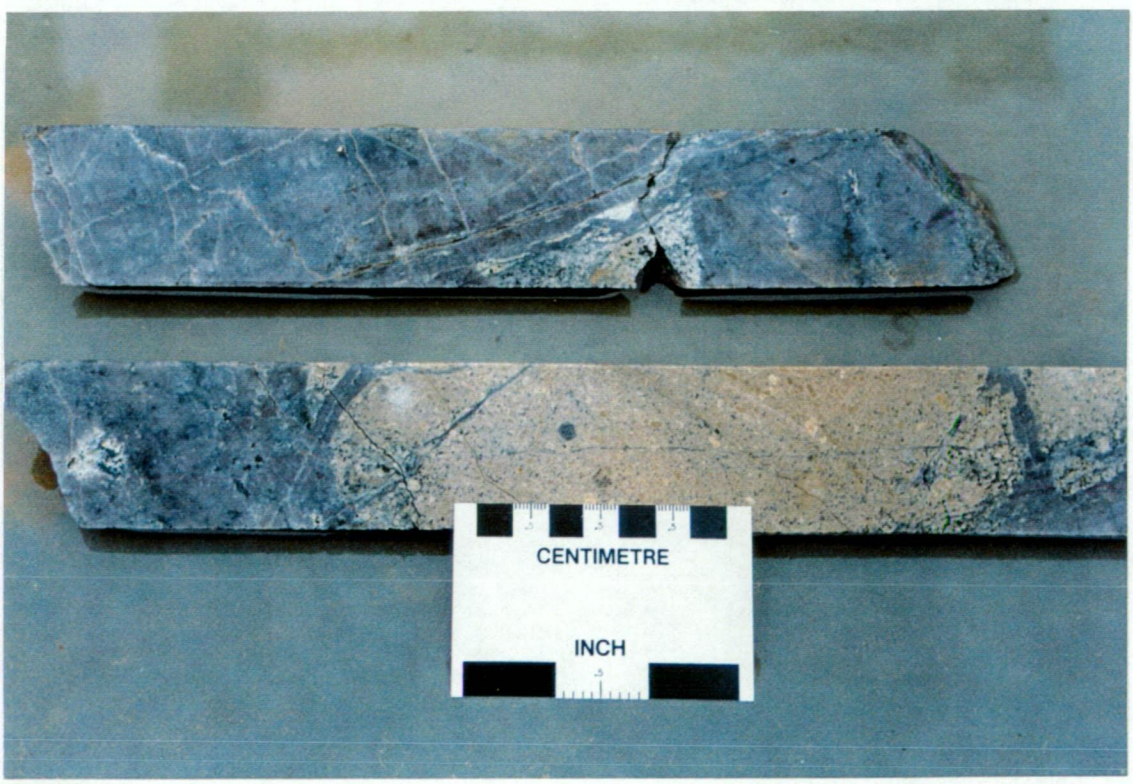

Figure 4.12 (b) Close up of the contact between silica flooded zone and QMP1.

	>2.0% Cu	1.0-2.0% Cu	0.5-1.0% Cu	<0.5% Cu
10080-BOX				
No. Samples	132	332	513	1987
Av. No. Quartz veins/3m	53	38	17	7
Av. No. Gypsum/anhydrite veins/3m	14	16	20	21
9950-10080				
No. Samples	116	169	308	1156
Av. No. Quartz veins/3m	43	37	26	12
Av. No. Gypsum/anhydrite veins/3m	28	29	35	36
9800-9950				
No. Samples	161	237	370	859
Av. No. Quartz veins/3m	65	52	41	21
Av. No. Gypsum/anhydrite veins/3m	14	22	20	19
9600-9800				
No. Samples	166	352	364	838
Av. No. Quartz veins/3m	93	53	40	32
Av. No. Gypsum/anhydrite veins/3m	19	24	20	16
<9600				
No. Samples	14	195	225	187
Av. No. Quartz veins/3m	64	34	29	21
Av. No. Gypsum/anhydrite veins/3m	53	31	21	14
Total				
No. Samples	589	1285	1780	5027
Av. No. Quartz veins/3m	66	44	30	15
Av. No. Gypsum/anhydrite veins/3m	19	23	22	23

Table 4.1 Vein counts showing zonation with Cu grade and depth

The veins extend 300m to the west and north from the centre of the orebody on the 10030m Level Access. Vein frequencies lessen within the higher grade core of E26. Underground exposures in the access drive shows the veins to be stockwork in nature, with steep to shallow-dipping sets of varying directions, though diamond drilling suggests that the veins are dominantly shallowly dipping within the orebody. Some of the veins are composite with anhydrite in the core and gypsum on the margins. Anhydrite increases with depth at the expense of gypsum.

Above 10080mRL (locally termed the 'Gypsum Line') the gypsum veins have been leached out, leaving open fractures. Approximately 20m above the Gypsum Line, a 10-25m thick zone of highly fractured rock has been re-cemented by carbonate (Carbonate Impregnate Zone).

4.5 MINERALISATION

Copper mineralisation occurs mainly as bornite, with lesser chalcopyrite and chalcocite, and minor tetrahedrite and covellite. The Cu sulphides occur as grains and clots within quartz veins, and as disseminations in the vein wall rocks. Many of the disseminated grains lie along thin fractures and hence are really fracture controlled rather than truly disseminated. As discussed above, there is a strong correlation between quartz vein densities and grade, with the highest grades associated with high quartz vein density, particularly in the silica zone. Pyrite is absent from the bornite-rich areas.

Sulphides are zoned laterally from the centre of mineralisation (Figures 4.13 and 4.14). The central portions are bornite-rich with minor chalcopyrite, zoning outward through equal proportions of bornite+chalcopyrite, to a chalcopyrite-rich zone 50-100m out from the core. Pyrite increases outward at the expense of bornite. Beyond the chalcopyrite zone at approximately 300m, pyrite is the main sulphide, and Cu-sulphides are minor to absent.

Au occurs principally within bornite as free Au, and occasionally as tellurides. The nature of the gold distribution is discussed in detail below.

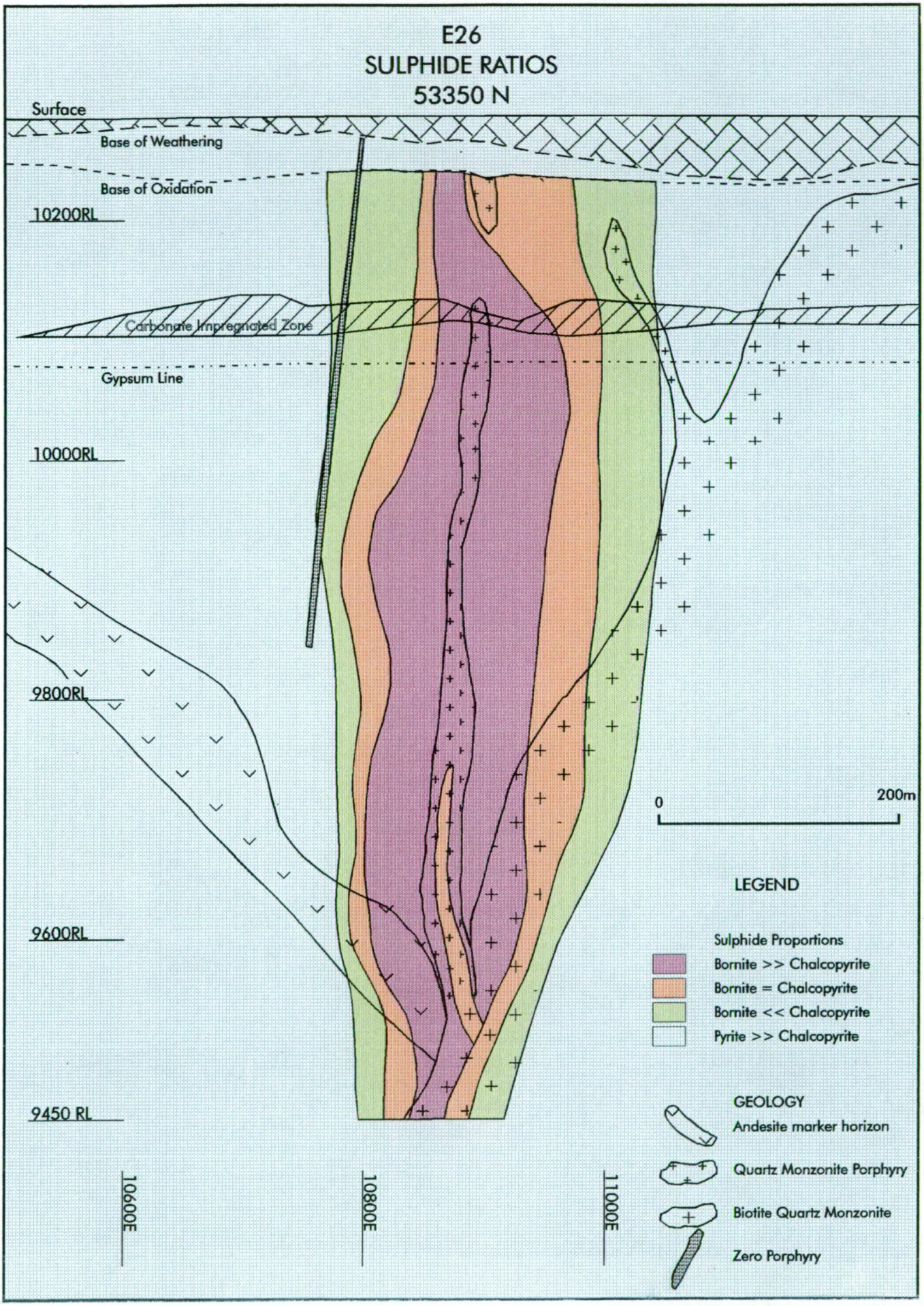

Figure 4.13 Cross-section at 53350N, showing the zonation in sulphide species.

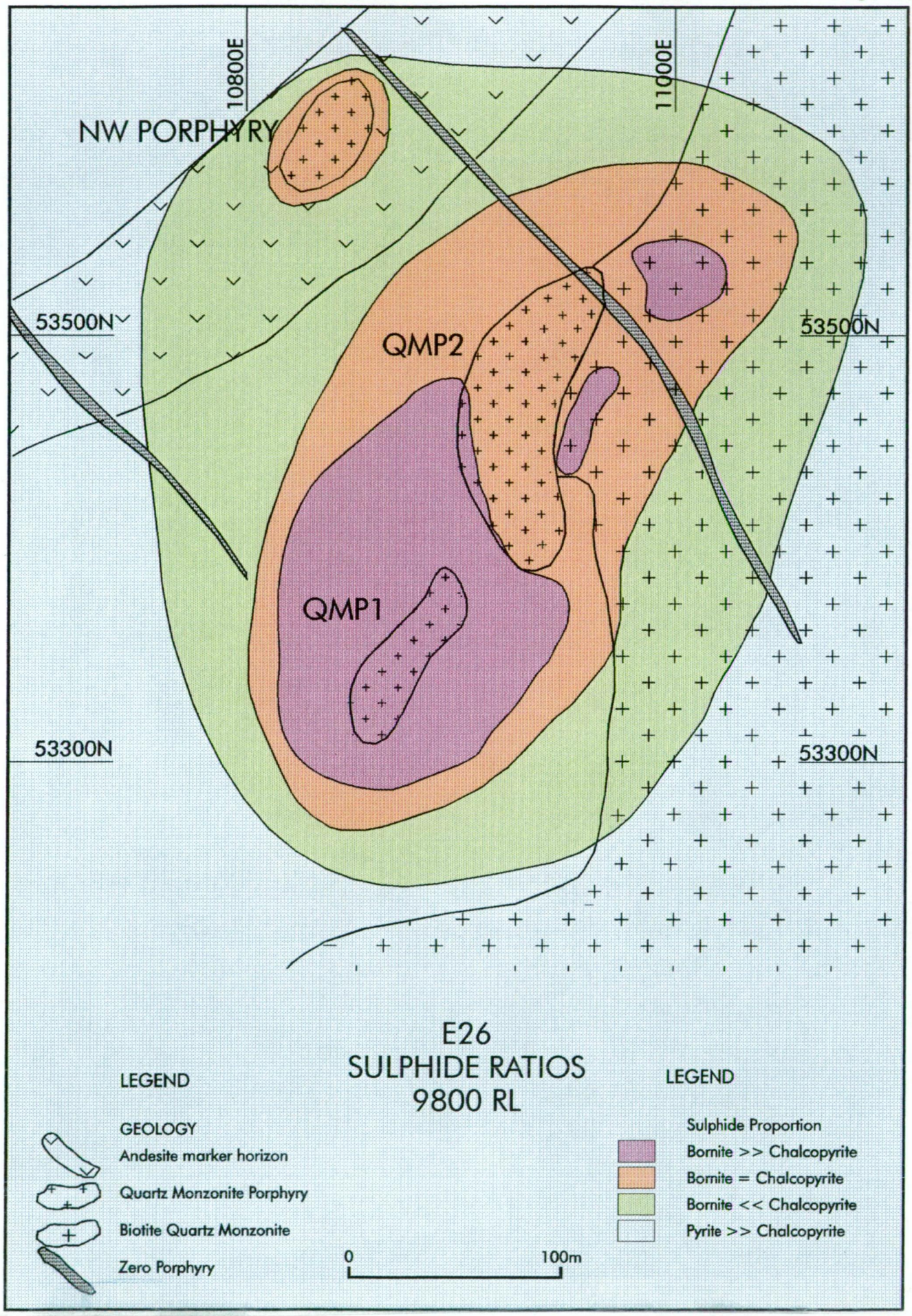

Figure 4.14 Plan at 9800mRL, showing the zonation in sulphide species.

5. METAL ZONATION AT E26

5.1 SPATIAL DISTRIBUTION OF GOLD.

5.1.1 Introduction

The spatial distribution of Au has been investigated through plotting and on-screen graphical representation of Au assays. The highest Au grades at E26 show a strong association with potassic alteration, Cu mineralisation and stockwork quartz veining. A weak distal association with minor Pb and Zn mineralisation along thin structurally controlled quartz-sericite-pyrite alteration zones has also been recognised in the E26 ramp access.

5.1.2 Summary Statistics

The Au assays at E26 show a positively skewed log normal distribution (Figure 5.1) with a mean of 0.16g/t. The change in slope of the log-probability plot at approximately 1g/t Au suggests that high grade Au occurrences form a different population group from the majority of the mineralisation, which is uniformly low grade. The highest Au assay (10.5g/t) occurs in QMP1 on the margin with the silica zone at 9940mRL. Only about 3% of the Au samples are above 1g/t, while 50% are below 0.02g/t. For comparison, Cu has a negatively skewed log normal distribution and mean of 0.71% (Figure 5.2), with 50% of the assays below 0.35% and 20% greater than 1% Cu. This is a direct manifestation of the tightly constrained Au distribution around QMP1 and will be discussed in more detail below.

5.1.3 Geometry and Spatial Distribution

Using 0.5g/t as an arbitrary cut-off, the zone of Au mineralisation at E26 is 100m long, 60m wide and 500m in vertical extent (Figures 5.3 & 5.4). Higher grades, particularly greater than 2.0g/t Au, are considerably more restricted and discontinuous. Cu mineralisation at a 0.5% cut-off is up to 400m long, 200m wide and >1000m in vertical

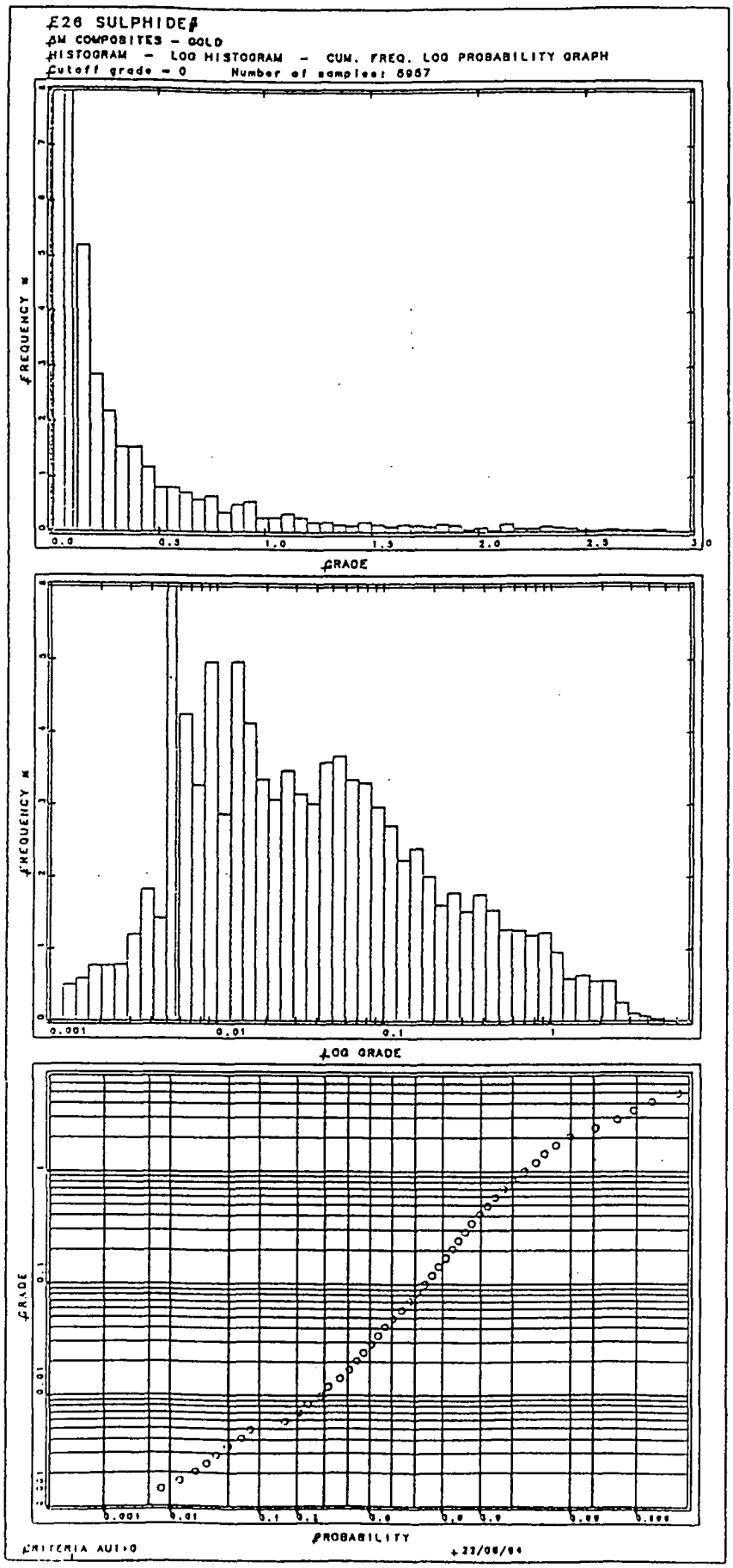

Figure 5.1 Frequency histograms and log probability plot of Au assays. The top chart is a frequency histogram of Au within defined grade bins. The middle chart is a log frequency histogram of the same data. The lower chart is a log-probability plot of the same data.

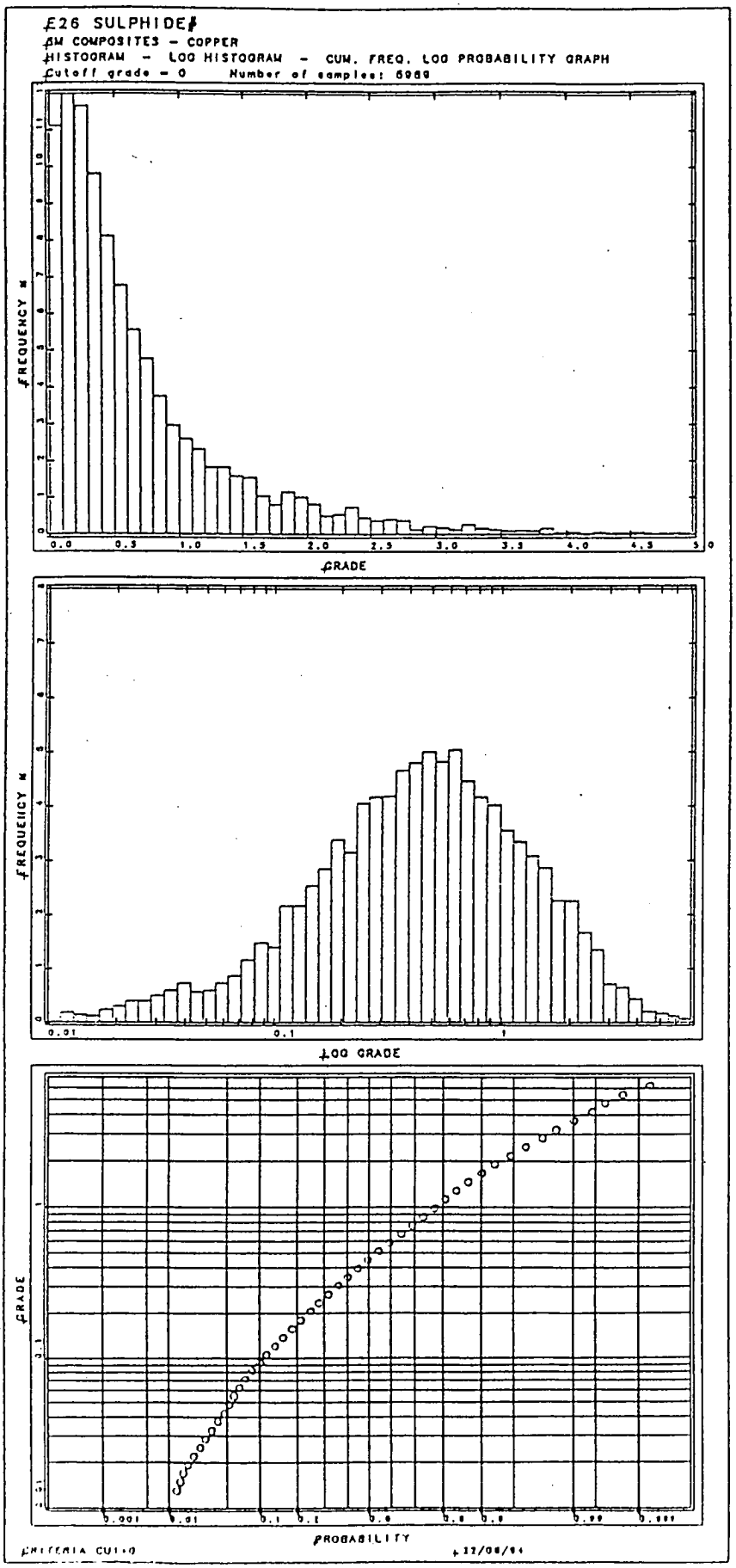

Figure 5.2 Frequency histograms and log probability plot of Cu assays.

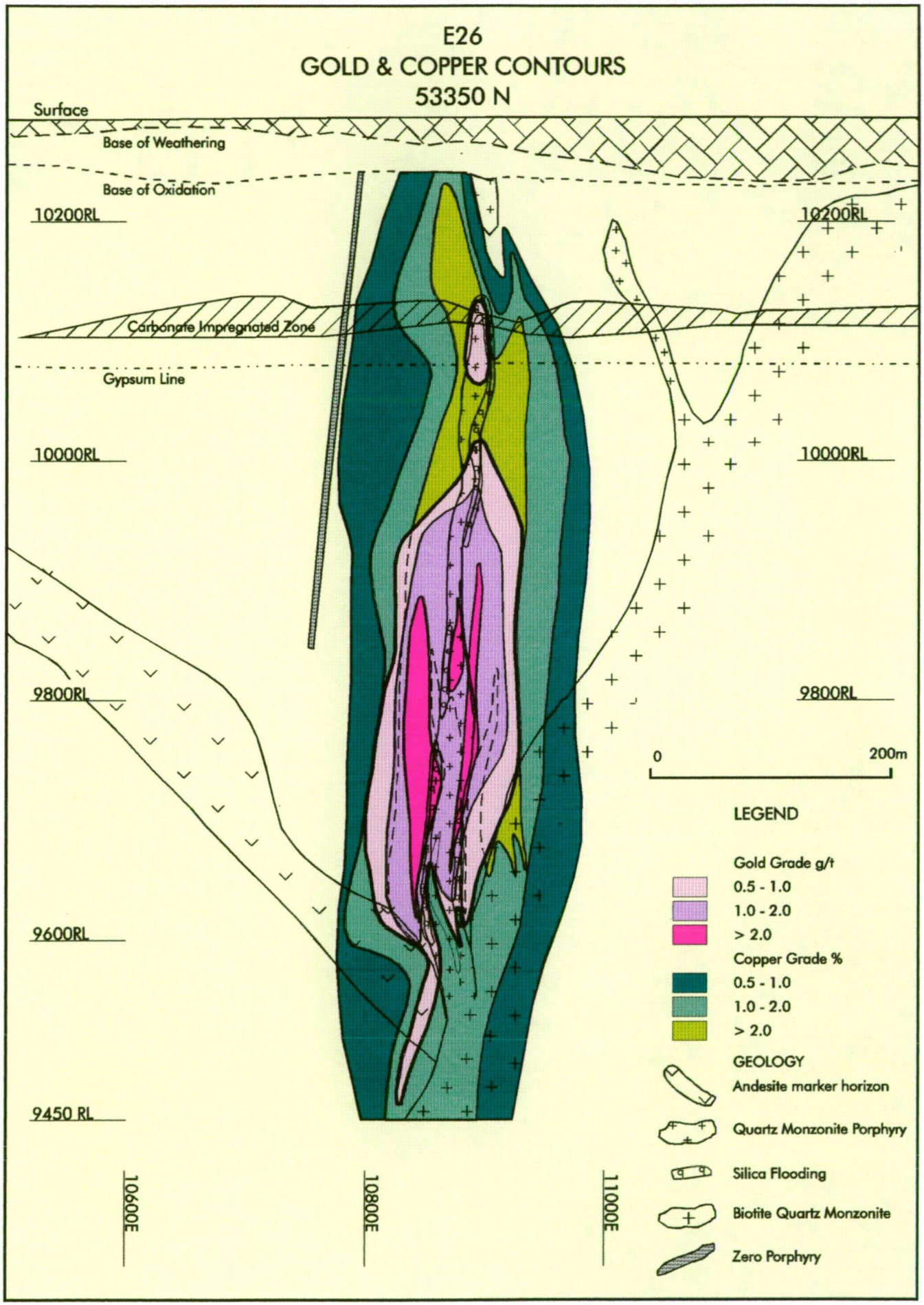

Figure 5.3 Cross-section of Au and Cu distribution at E26 - 53350N.

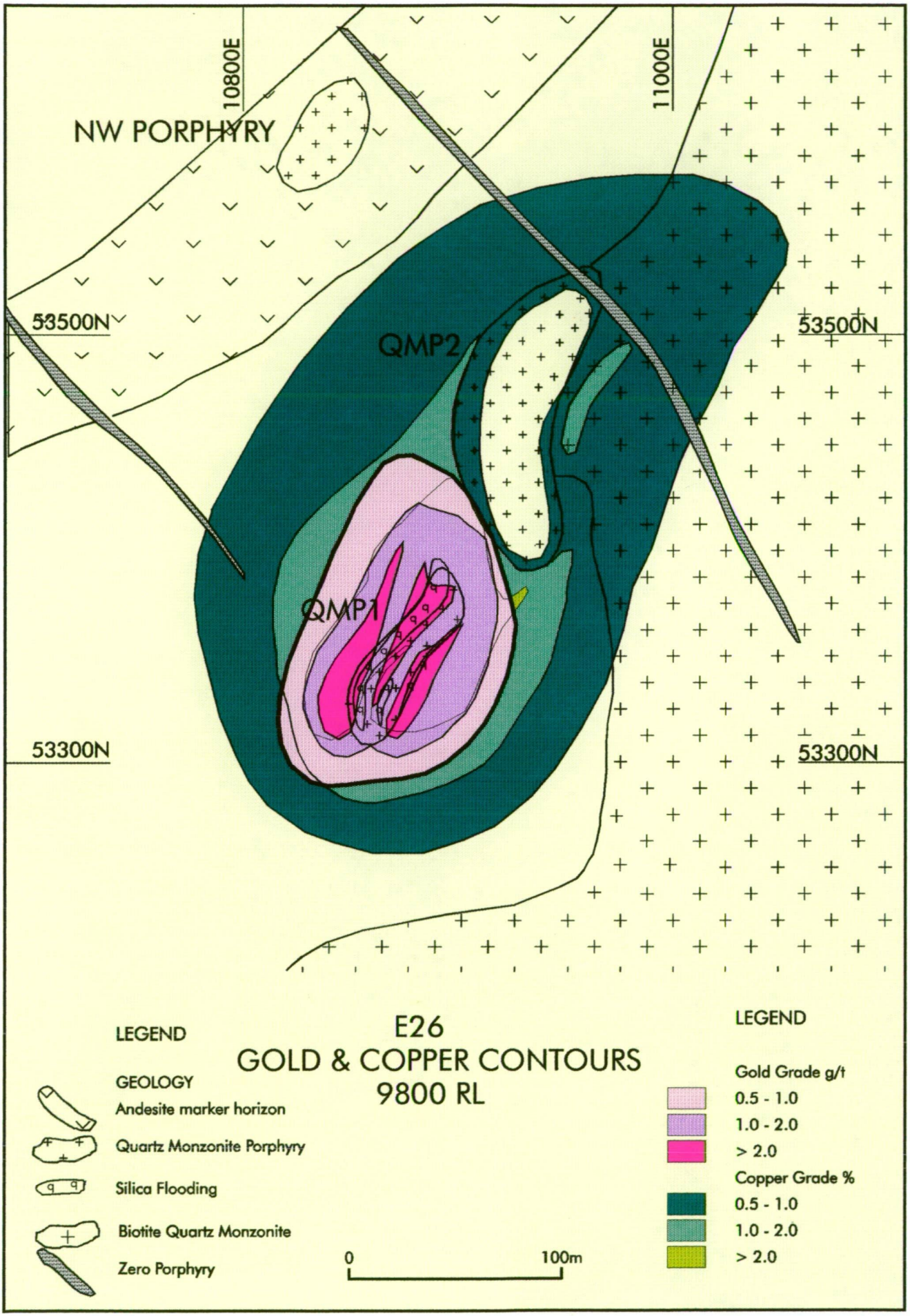

Figure 5.4 Plan of the Au and Cu distribution at E26 - 9800mRL.

extent (Figures 5.3 and 5.4). At a 2% cutoff, Cu forms a coherent zone 50m x 90m x 800m (Figure 5.3). Despite these differences, the aspect ratios (i.e. width/height) of equivalent (Au g/t = Cu %) grade areas are identical for higher grades. The aspect ratio for the area defined for Au g/t >0.5 and Cu % >0.5 is 0.12 and 0.20 respectively. For Au g/t >2.0 and Cu % >2.0, the aspect ratio is 0.06 for both. Au is concentrically distributed about QMP1 (Figure 5.3) as is the bulk of Cu mineralisation. Significant (>0.5g/t) Au grades do not occur with Cu mineralisation around QMP2. The core of QMP2 is anomalously low in both Au and Cu (Figure 5.4).

In cross-section, a vertical zonation in Au distribution is also apparent (Figure 5.5). The highest Au grades are between 9630mRL and 9950mRL (Figures 5.3 and 5.5). Above 9950mRL Au grades decrease abruptly. A slight increase in Au grades between 10100mRL and 10180mRL corresponds to a zone of significant Cu enrichment (compare Figures 5.5 and 5.6) but does not reach the high Au grades obtained below 9950mRL (Figure 5.5). A local high above 10230mRL is related to oxide mineralisation to the south of the main E26 orebody.

Cu grades also show a vertical zonation, though somewhat different from Au (Figure 5.6). The highest Cu grades occur near the top of the deposit between 10100mRL and 10200mRL. The value of maximum Cu grades decreases with depth. As for Au, a zone of depletion occurs between 9950mRL and 10100mRL. High Cu grades between 10230mRL and 10260mRL relates to the supergene chalcocite blanket.

5.1.4 Au and Cu Resource

Cu and Au grades at E26 have been block modelled using the inverse distance squared method (House and Bischoff, 1994). Metal content and resource grade above a 0.8% eCu cut off (equivalent copper unit, defined as eCu% = Cu% + k*Au g/t, where 'k' takes into consideration gold price, recoveries, etc., and approximates 0.5) by 40m vertical slices is shown in Figures 5.7 and 5.8. There is one clear maximum for Au with respect to contained metal and average grade, which occurs at 9750-9950mRL. Cu shows a more complex pattern, with the maximum value for contained metal occurring at approximately 9900mRL, with local maxima at 9650mRL and 10100mRL. Average

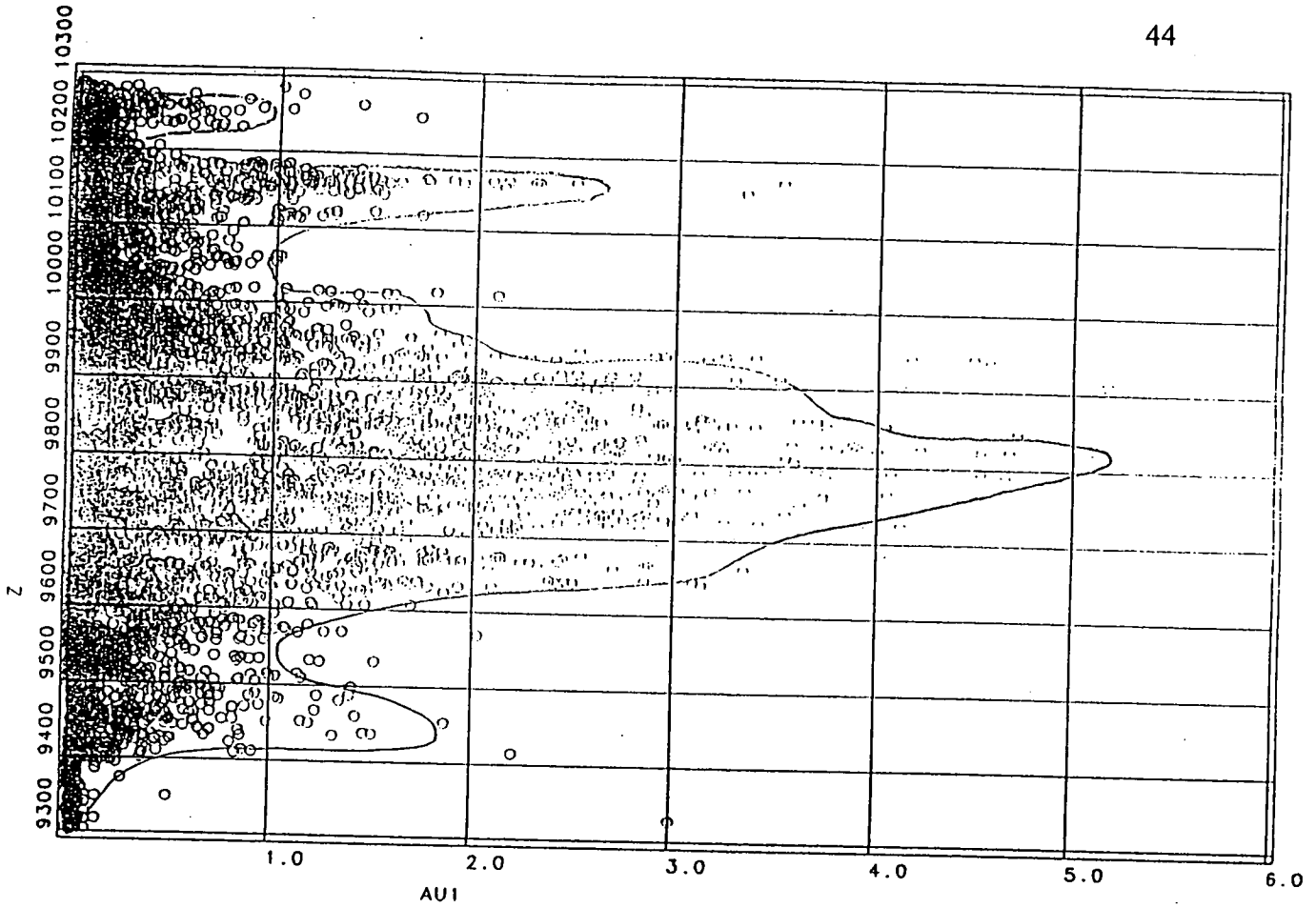

Figure 5.5 Vertical zonation of Au grade.

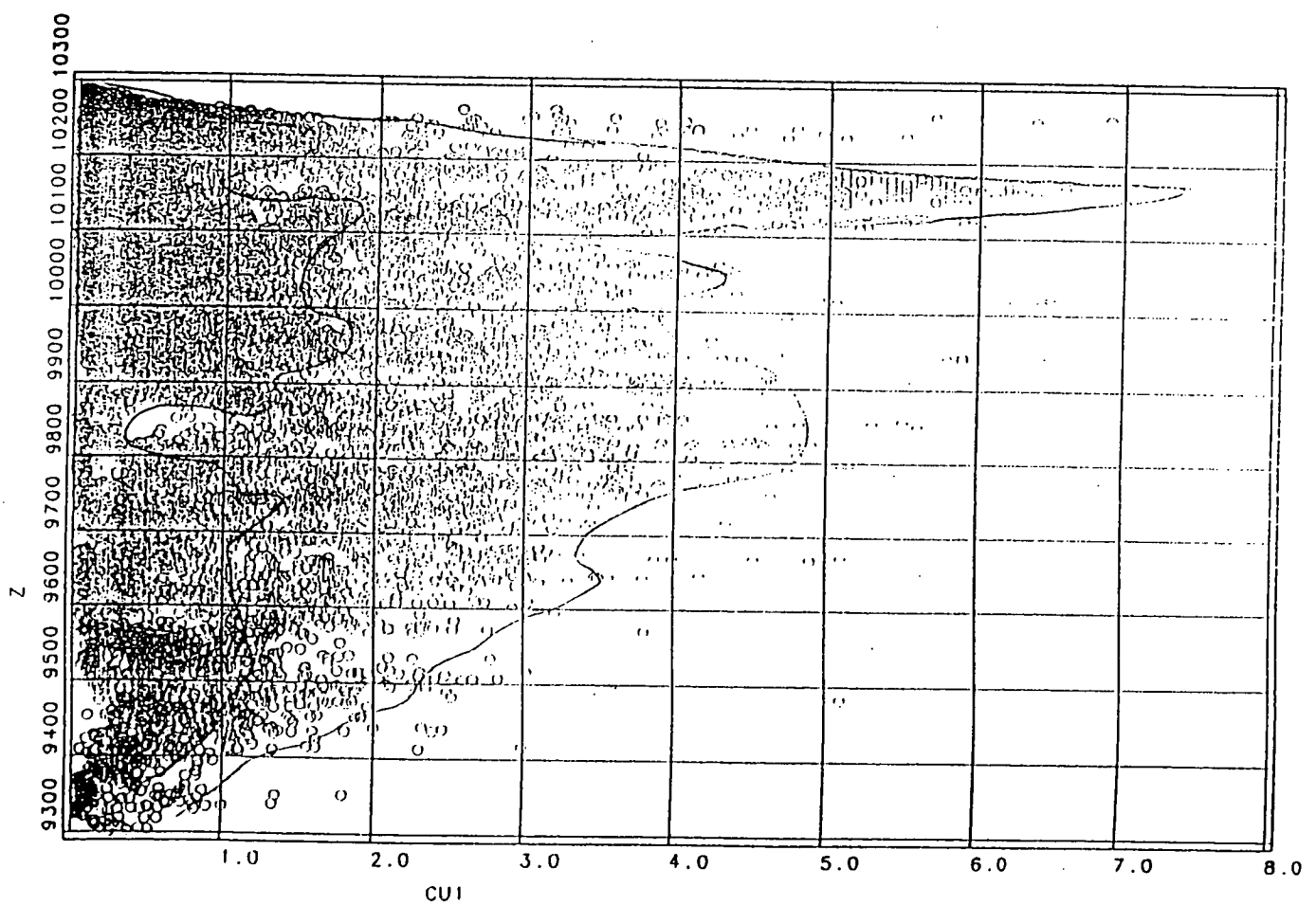

Figure 5.6 Vertical zonation of Cu grade.

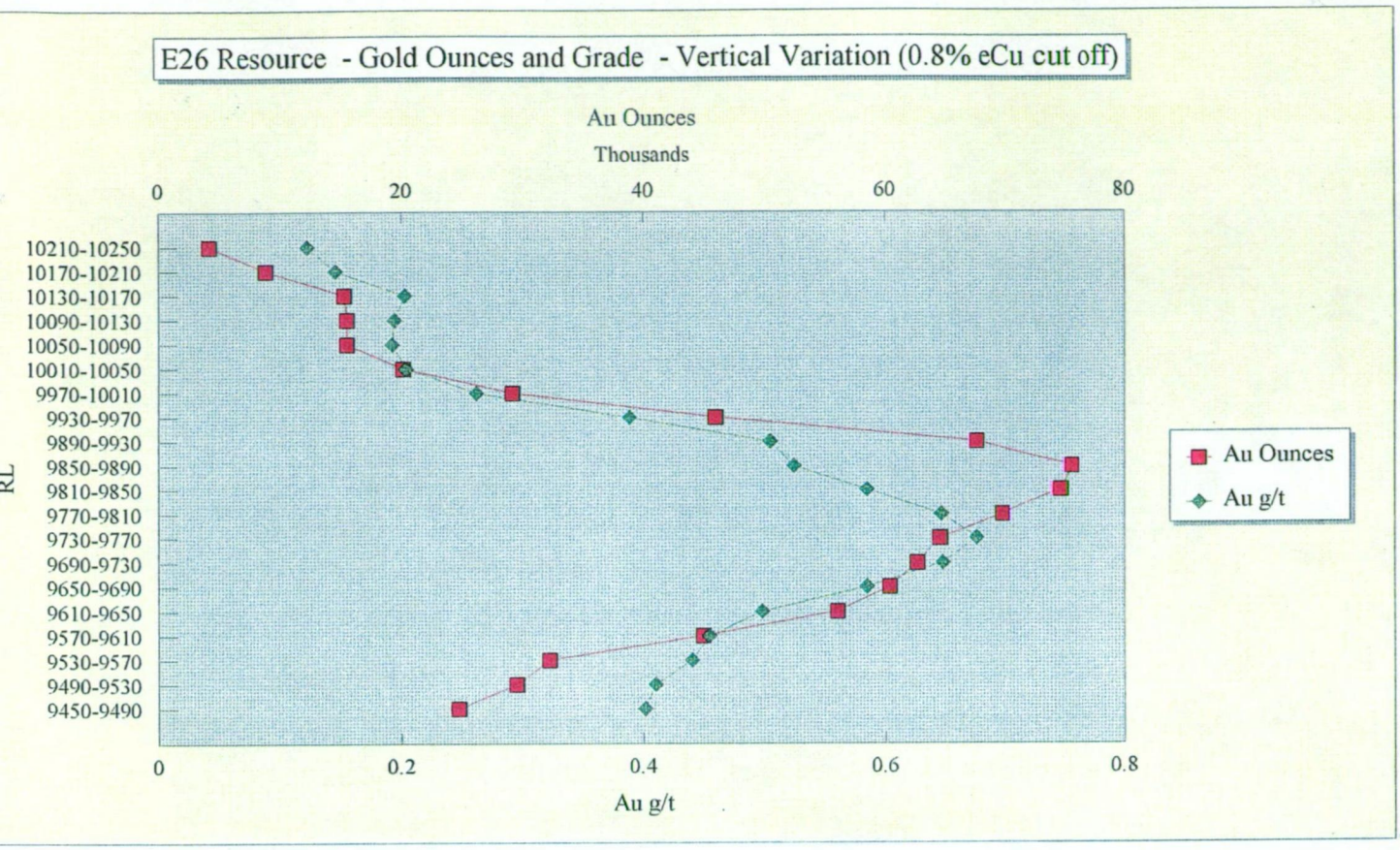

Figure 5.7 Vertical variation in the gold resource at E26

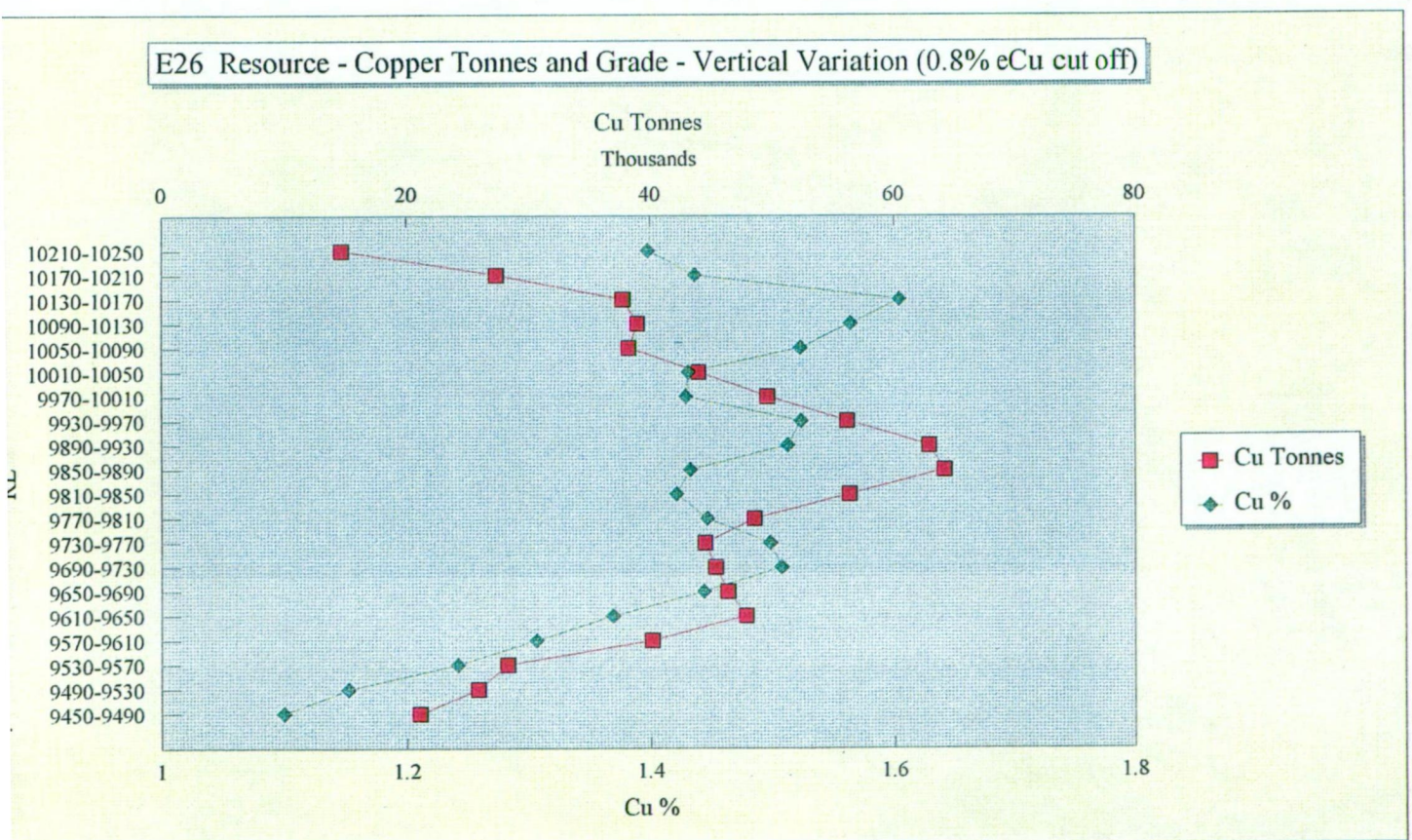

Figure 5.8 Vertical variation in the copper resource at E26.

Cu grade maxima occur at 10150mRL, 9950mRL and 9700mRL, with the 10150mRL peak being the highest. In comparison with Figure 5.6, although the highest Cu assays are in the vicinity of 10150mRL, the highest metal content is approximately 300m lower. However, the highest Au assays correspond closely to the highest Au metal content (approximately 9850mRL; compare Figures 5.5 and 5.7). Approximately 30% of the total copper resource at E26 (>0.8% eCu) lies above 9950mRL, compared to only 10% of the total gold resource.

5.2 PERIPHERAL GOLD

An outer Au association has been defined from mapping of the E26 decline access. Weak Au grades are associated with some structurally controlled quartz-sericite-pyrite (qsp) alteration zones described earlier. Au is associated with sphalerite, galena and lesser chalcopyrite, which are largely confined to the shear zones. Selective replacement of clasts in the volcanic mass flow deposit by carbonate and sphalerite away from the shears has been observed. Au assays of up to 1.6g/t over 0.5m and 0.9g/t over 1m have been obtained from wall chip sampling of these zones. Interestingly, qsp shears in the orebody do not show any Au enrichment.

5.3 CU/AU RATIOS

Scatter plots of Cu and Au and Cu/Au ratios are useful for defining population domains which can be used to define and map spatial domains. The Cu/Au ratio is defined in terms of Cu(%)/Au(g/t).

The scatter plot of Cu versus Au (Figure 5.9) allows the interpretation of five population groupings. Domains 1 (coloured purple) and 2 (blue) contain the bulk of low grade Au samples. Domain 2 is essentially the low grade tail of Domain 3 (green). Domain 3 shows a steady increase in Au with increasing Cu. Domain 4 (red) also shows increasing Au with increasing Cu but at lower Cu/Au ratios. Domain 5 (orange) contains samples that are low in Cu but relatively high in Au.

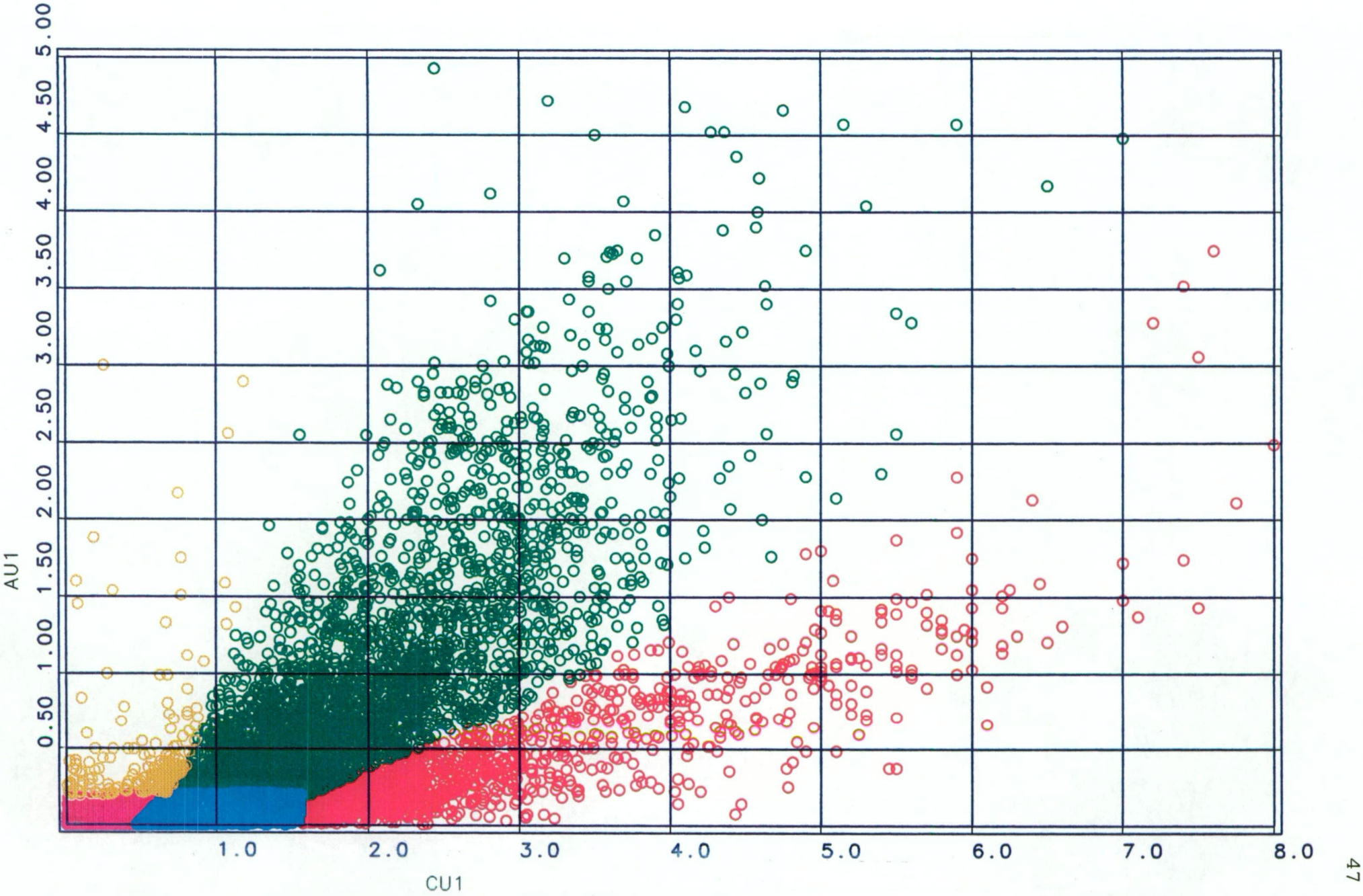

Figure 5.9 Bivariate scatterplot of Au grade versus Cu grade.

The Cu/Au ratio is a broad log normal distribution with values ranging from 0.01 to 600 and a mean of 22 (Figure 5.10). The plot of Cu/Au ratio versus Au grade (Figure 5.11) contains the same data points colour coded by domains as defined in Figure 5.9. Cu/Au ratios for Domains 1 and 2 display large variations even though the Au grade is low (<0.25g/t). Domain 3 shows a strong relationship between Cu/Au ratios and Au content; as the Au grade increases, the Cu/Au ratio approaches unity. Domain 4 shows a similar trend of decreasing Cu/Au ratio with increasing Au grade. However, unlike Domain 3, the Cu/Au ratio plateaus well above one. Domain 5 shows a Cu/Au ratio tending to below one with higher Au grades.

Cu/Au ratios at E26 are strongly zoned horizontally and vertically, increasing concentrically away from QMP1. The plan section through the orebody at 9800mRL (Figure 5.12) and the scatterplot of Cu/Au versus easting (Figure 5.13) illustrates the strong horizontal zonation of Cu/Au ratios, while Figure 5.14 illustrates the vertical zonation in Cu/Au ratios. Cu/Au ratios only approach unity between 9600-9950mRL, and are tightly constrained about QMP1 (Figure 5.14).

The five domains of Cu/Au ratio defined in Figures 5.9 and 5.11 are well defined spatially and show little overlap (Figure 5.15 and 5.16). The higher grade core (i.e. >1.2% eCu) is contained within Domains 3 and 4 (Figure 5.15). The two domains are clearly separate from the each other. Domain 3 occurs below 9950-10000mRL and is localised around QMP1. Domain 4 lies above Domain 3, and also occurs in association with mineralisation (>1.2% eCu) to the east of QMP2 (i.e. 'northeast extension'). Domain 2 encloses Domains 3 and 4 (out to approximately the 0.4% eCu outline) and is itself enclosed by Domain 1 (Figure 5.15). Domain 5 shows no strong spatial controls.

Sample data from within Domains 3 and 4 are given in Table 5.1. The differences between the two domains are highlighted in the high grade core. For a constant Cu grade (e.g. 4.0% Cu), Au grades in Domain 3 are similar, but are significantly lower in Domain 4 (<1.5g/t).

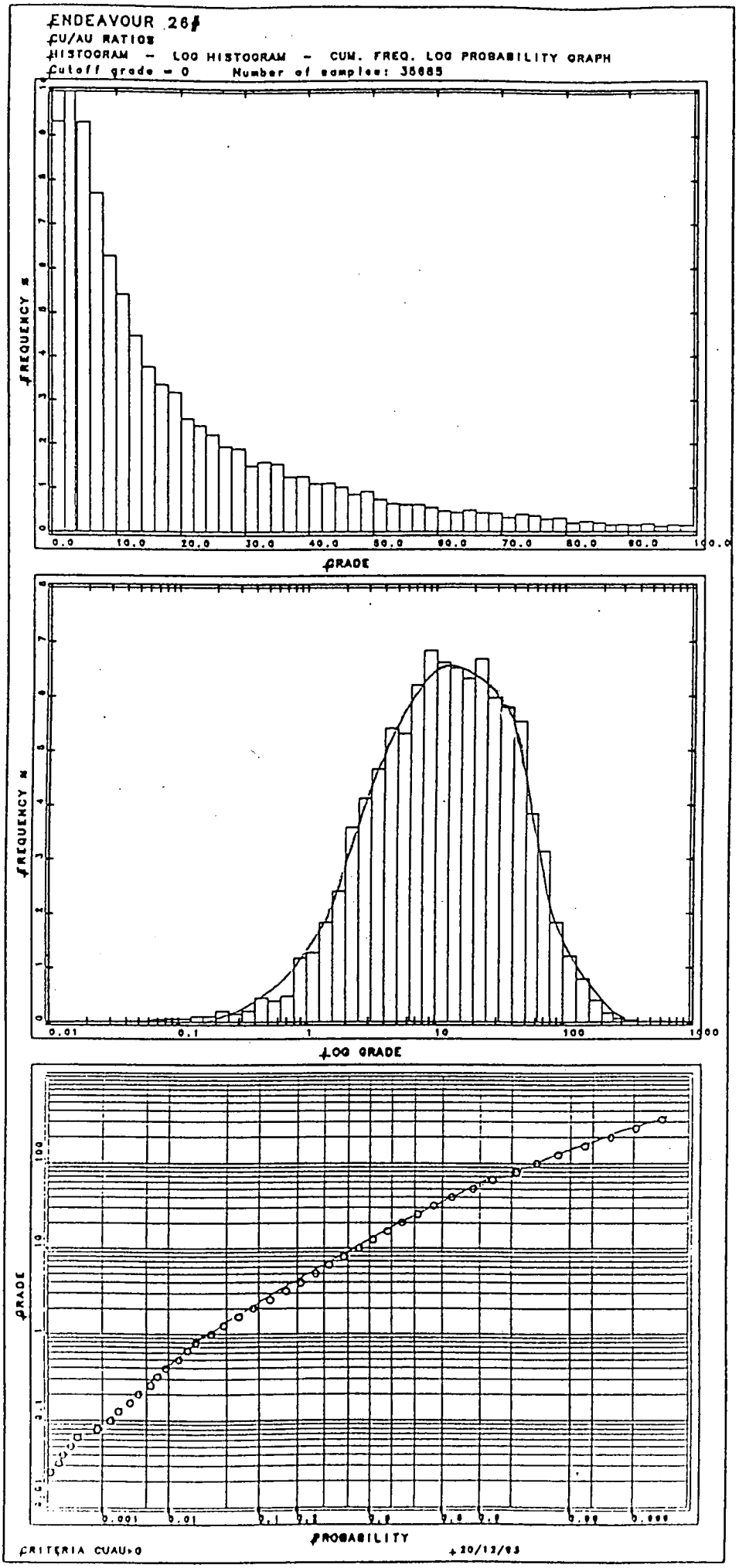

Figure 5.10 Frequency histograms and log probability plots of Cu/Au ratio.

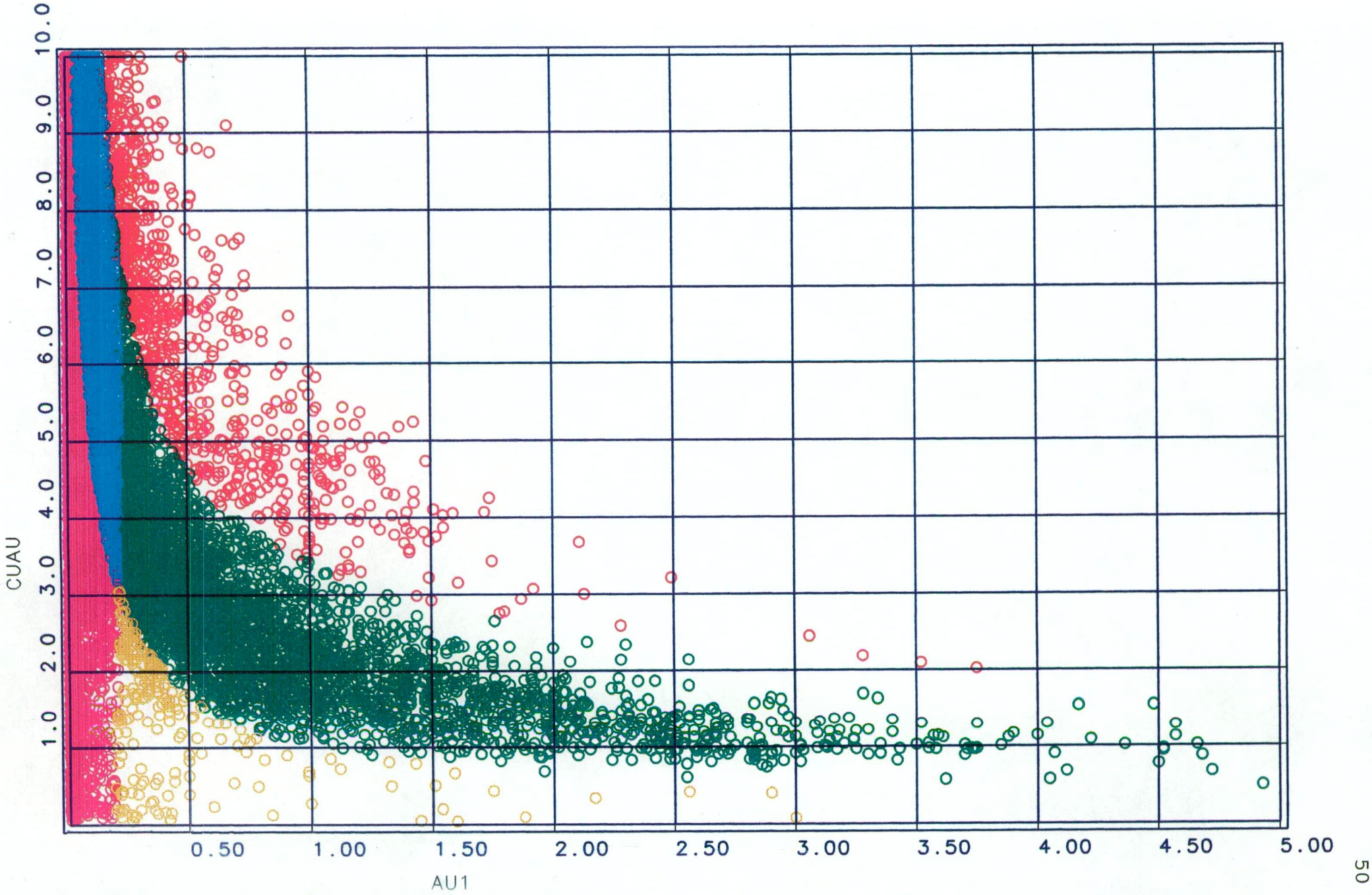

Figure 5.11 Bivariate scatterplot of Cu/Au ratio versus Au grade.

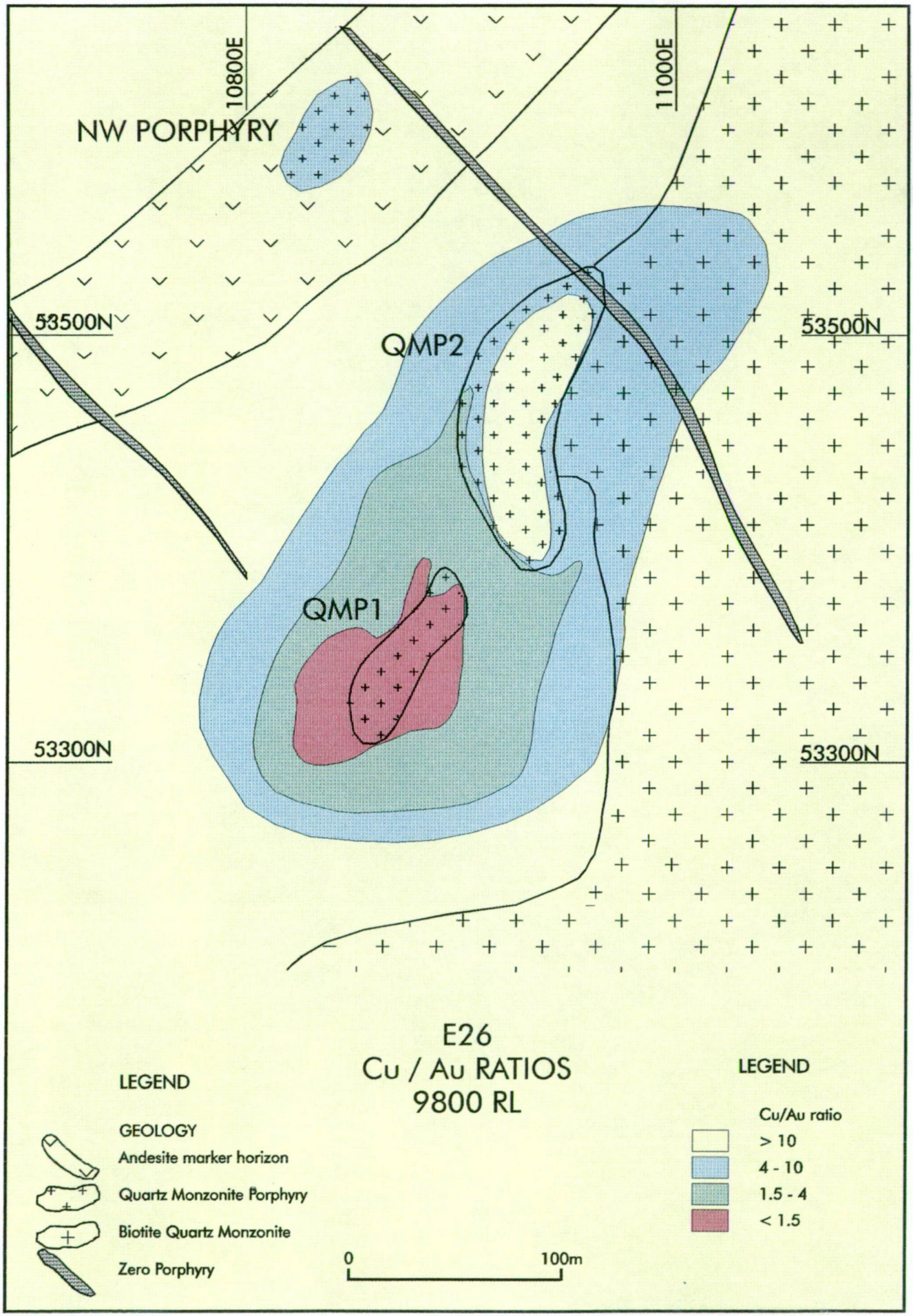

Figure 5.12 Plan at 9800mRL, showing lateral zonation in Cu/Au ratios.

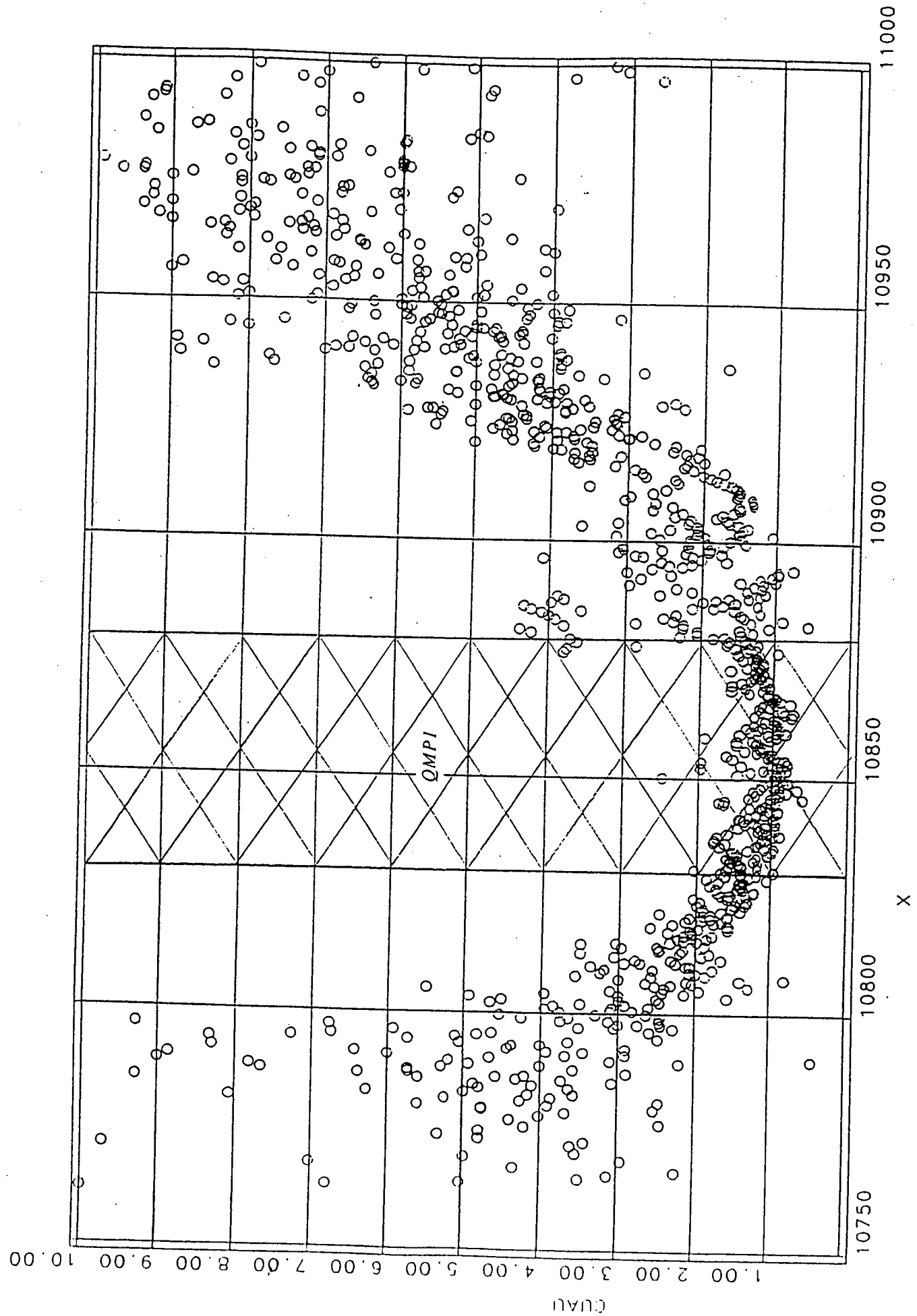

Figure 5.13 Scatterplot of Cu/Au ratios with easting.

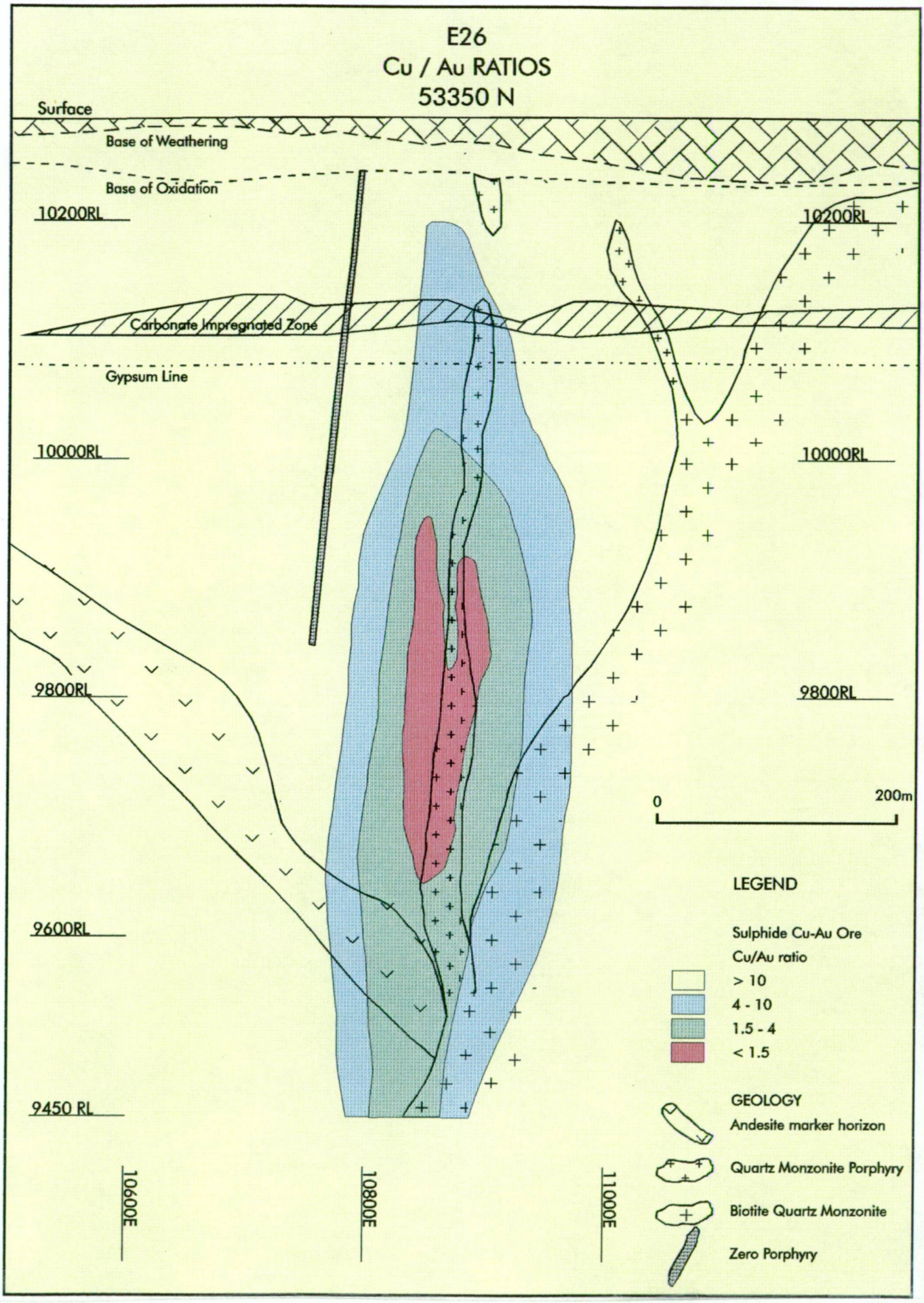

Figure 5.14 Cross-section at 53350N, showing vertical zonation in Cu/Au ratios.

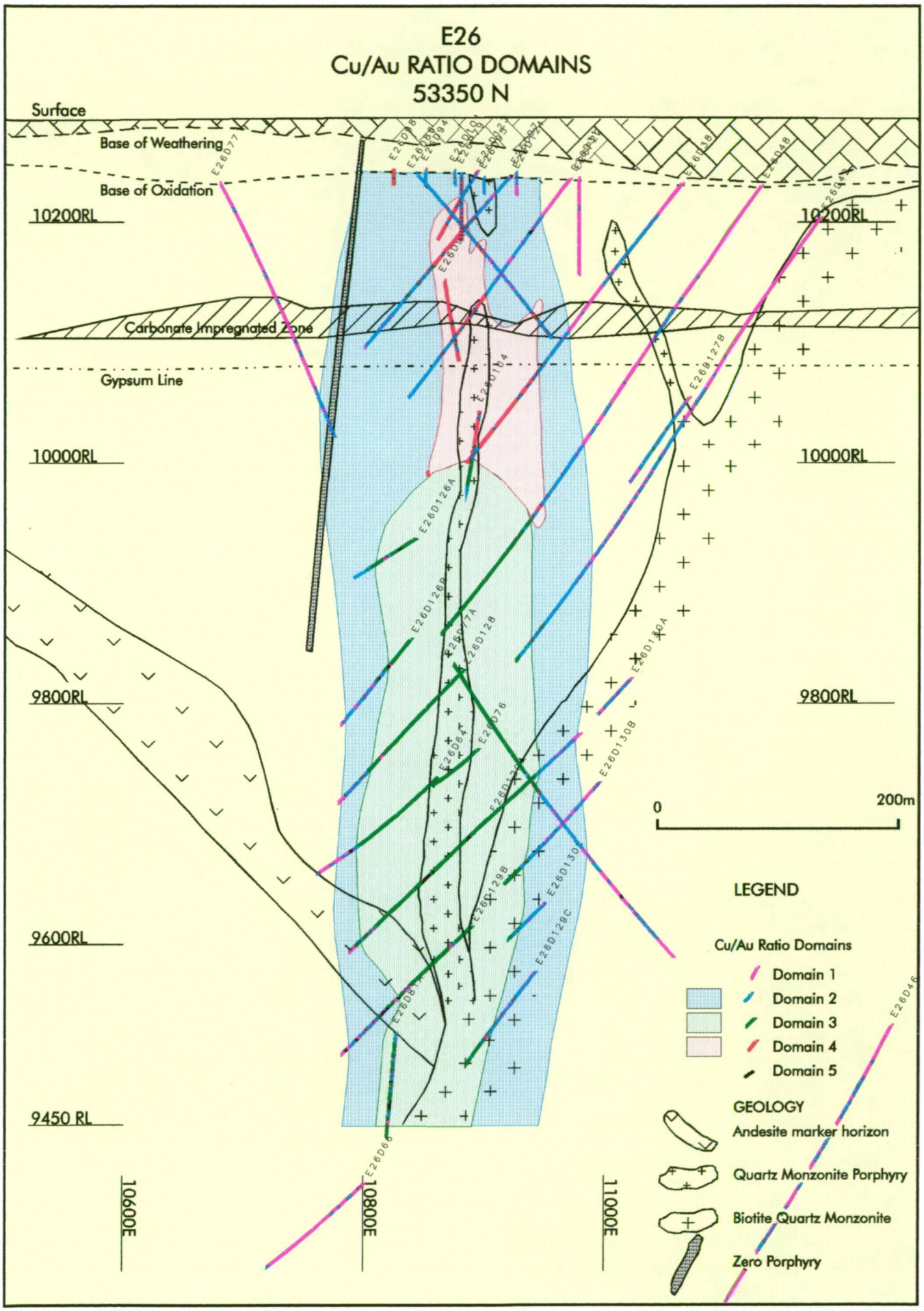

Figure 5.15 Cross-section at 53350N, showing Cu/Au ratio domains.

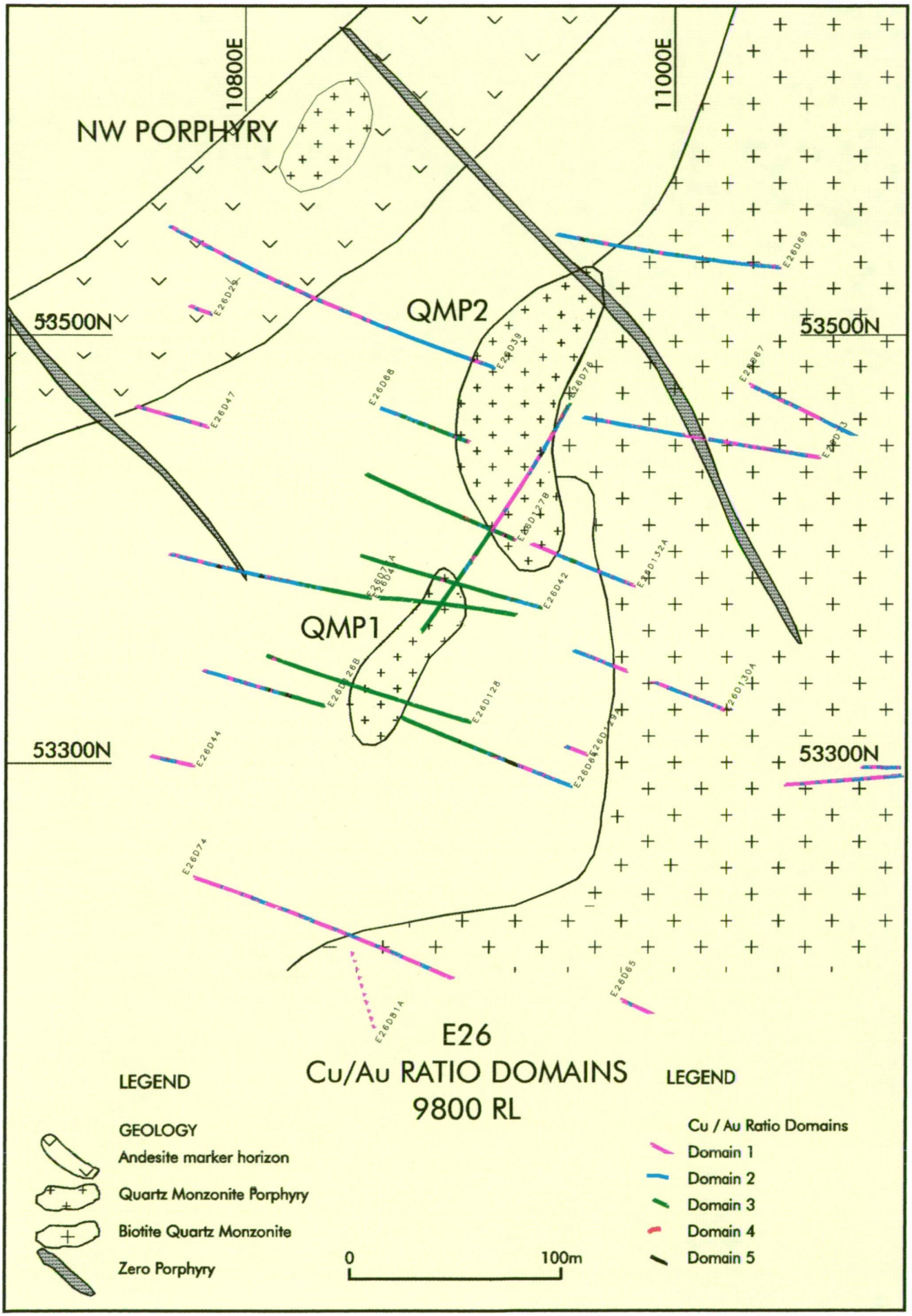

Figure 5.16 Plan at 9800mRL, showing Cu/Au ratio domains.

		No. Samples	Av. Cu %	Av. Au g/t
TOTAL	Domain4	759	2.86	0.50
	Domain3	3649	1.79	0.84
Cu > 1.5%	Domain4	742	2.89	0.50
	Domain3	2101	2.26	1.17
Cu > 2.5%	Domain4	372	3.78	0.72
	Domain3	623	3.09	1.92
Cu > 3.5%	Domain4	188	4.64	0.94
	Domain3	118	3.94	2.74
Cu > 4.5%	Domain4	95	5.30	1.11
	Domain3	16	4.81	3.57

Table 5.1 Comparison of Cu and Au assays within Cu/Au domains

5.4 SILVER DISTRIBUTION

Silver is also part of the mineralised system at E26, and its distribution will be briefly examined, particularly its metal ratios with Au and Cu. This analysis of Ag grades and distribution is based on assay data obtained from a range of assaying methods that have varied detection limits. The detection limits are relatively high with respect to the population data, which introduces bias and inaccuracies, particularly at lower assays. These biases are apparent in the histograms and probability plots (Figure 5.17) and data below about 1g/t (which comprises 70% of the Ag data) therefore should not be taken as accurate.

Removing the assay bias shows the Ag distribution to be log normal (Figure 5.17). The highest grade is 116g/t from an anomalously Ag-enriched zone in the biotite quartz monzonite that was intercepted by hole E26D46 at depths of 900-1000m. The origin of this anomalous zone, which is two orders of magnitude greater than the mean E26 Ag value (1.13g/t) is not known.

Ag is concentrically zoned about QMP1 (Figure 5.18) with the highest grades occurring in and immediately around the porphyry. A coherent zone of >5g/t Ag occurs in QMP1 and the adjacent volcanics to the east between 9700mRL and 10000mRL (Figure 5.18). Grades between 5 and 1g/t Ag form a broad coherent zone that encloses QMP1 and QMP2, whereas Ag grades are below 1g/t in QMP2.

5.5 AG/AU AND AG/CU RATIOS

Ag/Au and Ag/Cu ratios are defined as Ag(g/t)/Au(g/t) and Ag(g/t)/Cu(%) respectively. The scatterplot of Ag versus Au grades (Figure 5.19) shows poor correlation between the two. Some of the highest Ag grades are accompanied by low Au grades. The frequency histograms (Figure 5.20) show a broad log normal distribution with a mean of approximately 50. A spatial zonality is observed with a zone of Ag/Au below 10 tightly constrained about QMP1 (Figure 5.21) indicating that Au is enriched relative to Ag in the core of the system.

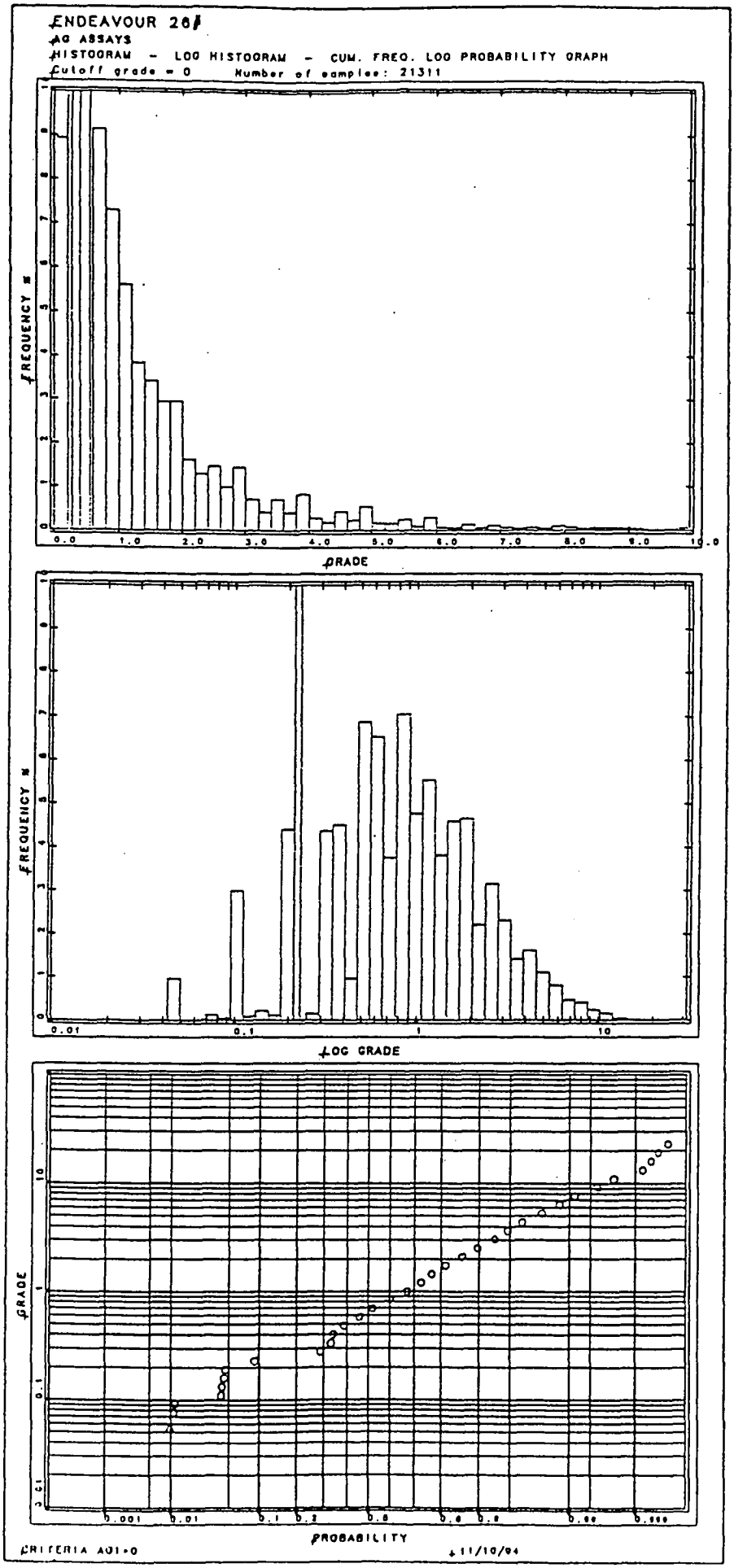

Figure 5.17 Frequency histograms and log probability plot for Ag grade.

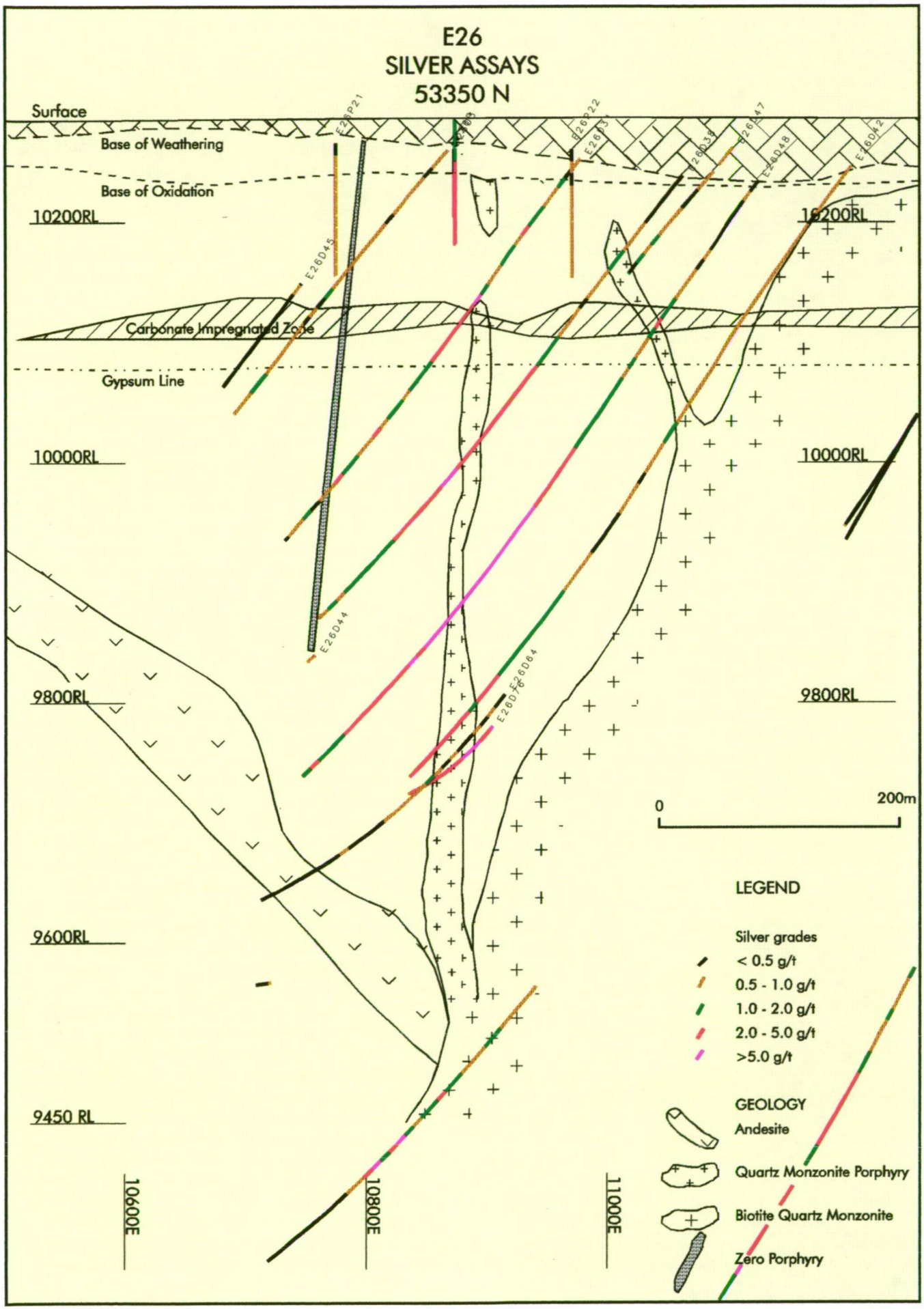

Figure 5.18 Cross-section at 53350N, showing silver grades.

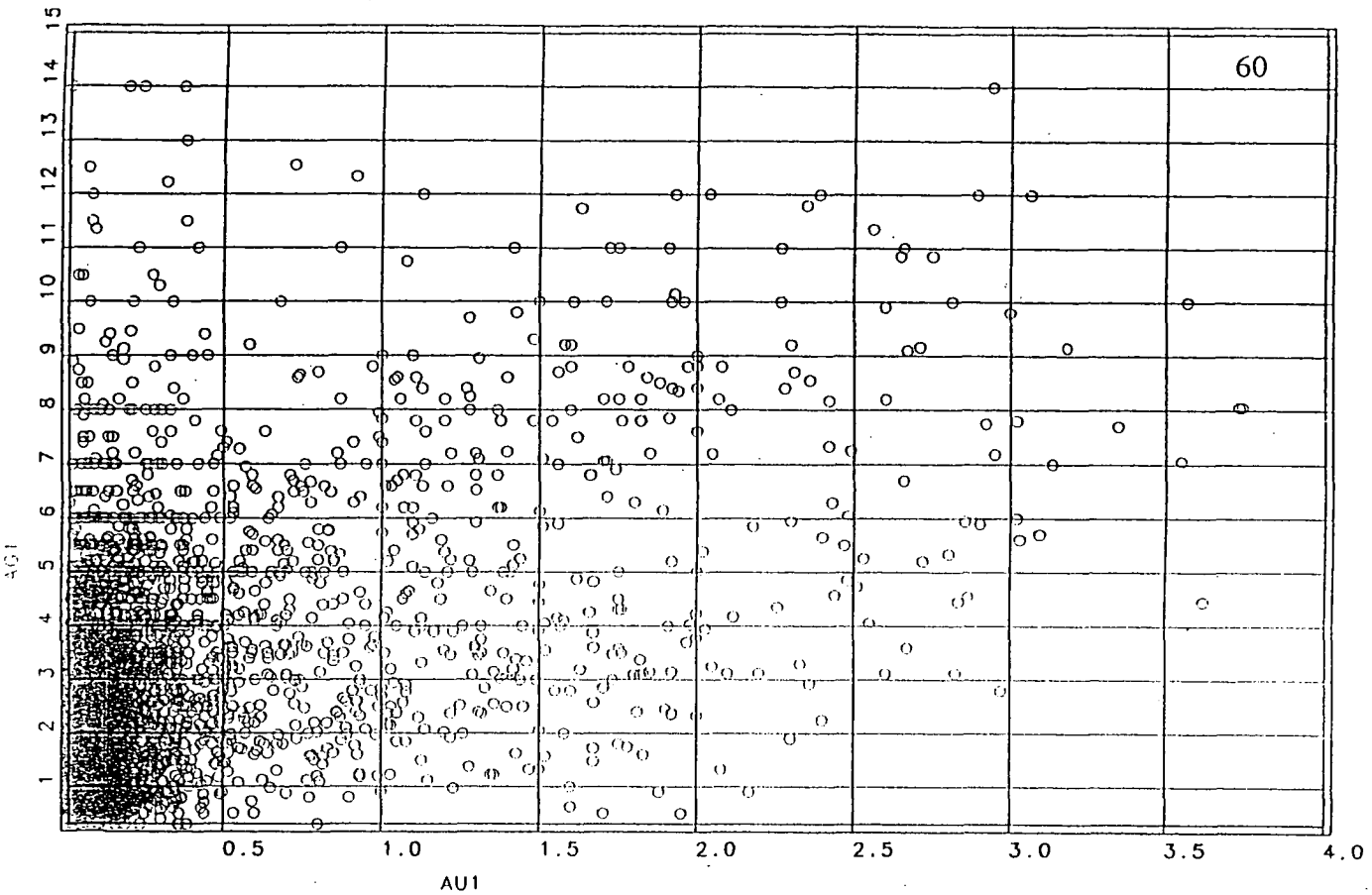

Figure 5.19 Bivariate scatterplot of Au grades versus Ag grades.

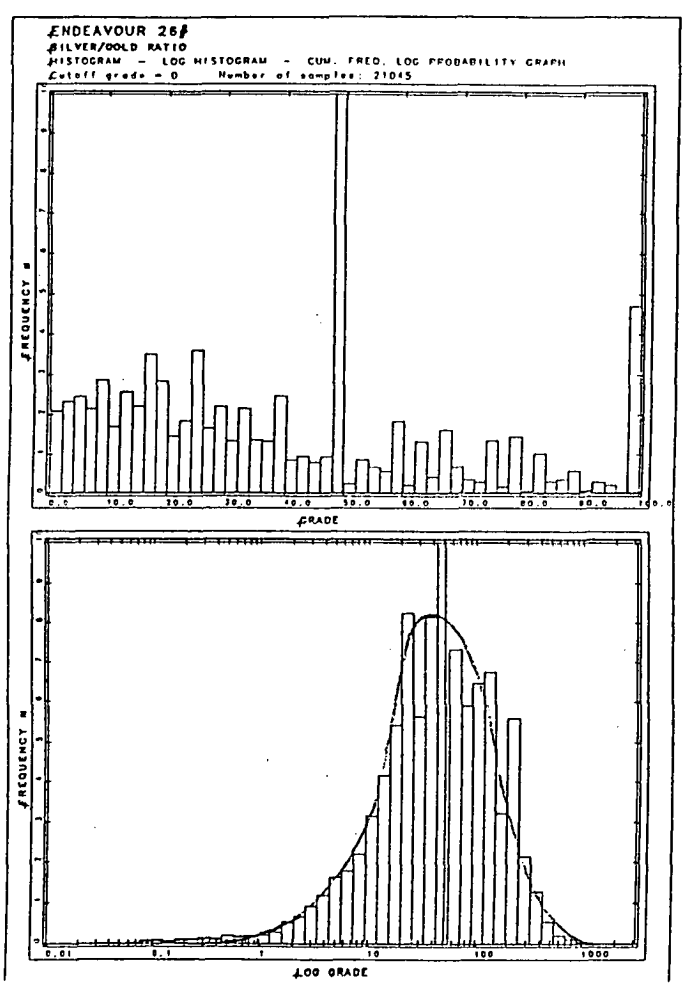

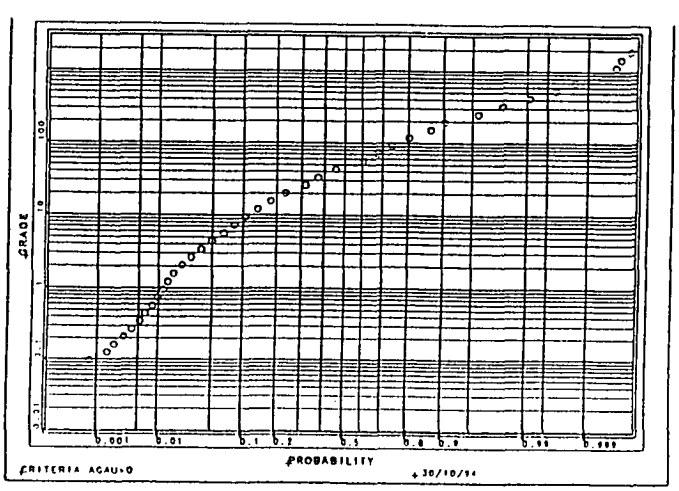

Figure 5.20 Frequency histograms and log probability plot for Ag/Au ratio.

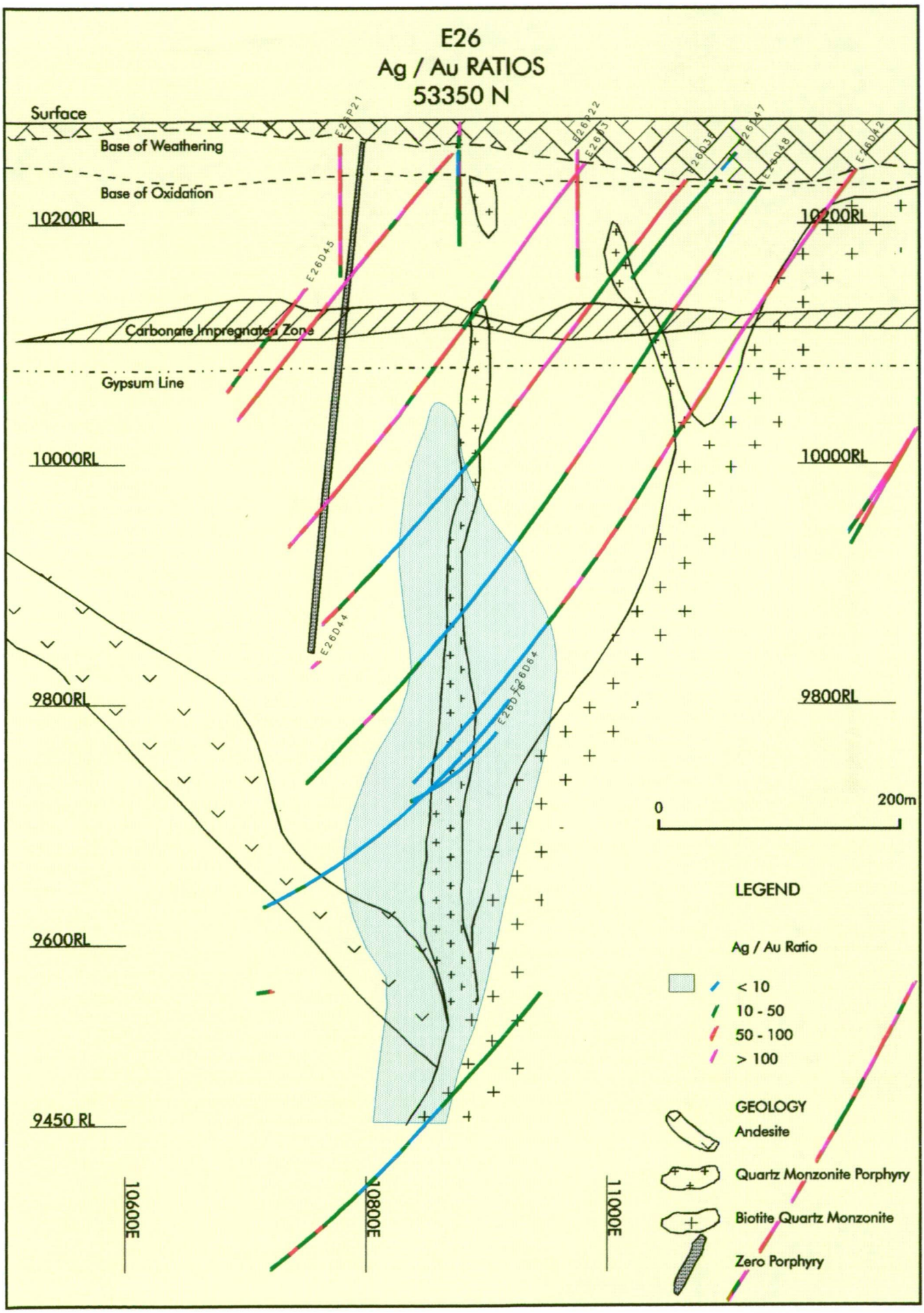

Figure 5.21 Cross-section at 53350N, showing the spatial zonation of Ag/Au ratios.

For Ag versus Cu a more coherent trend is apparent (Figure 5.22). The frequency histogram shows a tight log normal distribution in the Ag/Cu ratio (Figure 5.23). The Ag/Cu relationship is uniform spatially with no strong zonality.

5.6 OTHER METALS

Limited data is available for molybdenum, lead and zinc. Molybdenum assays vary from 0.5-250ppm with a mean of 7ppm. Highest assays (>20ppm) tend to associated with the main mineralised area. Pb and Zn data is available from peripheral near-surface drilling. Pb and Zn assays are uniformly below 1 000ppm with means of 90ppm and 280ppm respectively. Wall chip sampling along the E26 ramp development >600m to the north west of E26 has yielded assays of up to 4.6% Zn, 0.26% Pb, 0.79% Cu, 34g/t Ag and 0.90g/t Au over 1m in structurally controlled quartz-sericite-pyrite-carbonate alteration zones.

5.7 SUMMARY OF GOLD DISTRIBUTION

Au and Cu at E26 are localised around QMP1. Although most Au occurs below 9950mRL, high grade Cu continues up to the base of oxidation at approximately 10240mRL (i.e. >300m above the high grade Au zone). This vertical zonation is apparent in the analysis of Cu/Au ratios, which has defined two domains in the main zone of mineralisation. The upper zone (Domain 4) corresponds to a zone of relative Au depletion with respect to Cu. The lower zone (Domain 3) has Cu/Au ratios that tend towards unity with increasing grade. The highest Au grades (>2.0g/t) are concentrated on the eastern and western margins of QMP1 and in the immediately adjacent volcanics. The zone of enriched Cu and moderately enriched Au between 10100mRL and 10200mRL is related to quartz flooding in the carapace of QMP1. The analysis of Ag/Au ratios shows a dispersion of Ag away from the main Au zone, suggesting greater solubility of Ag.

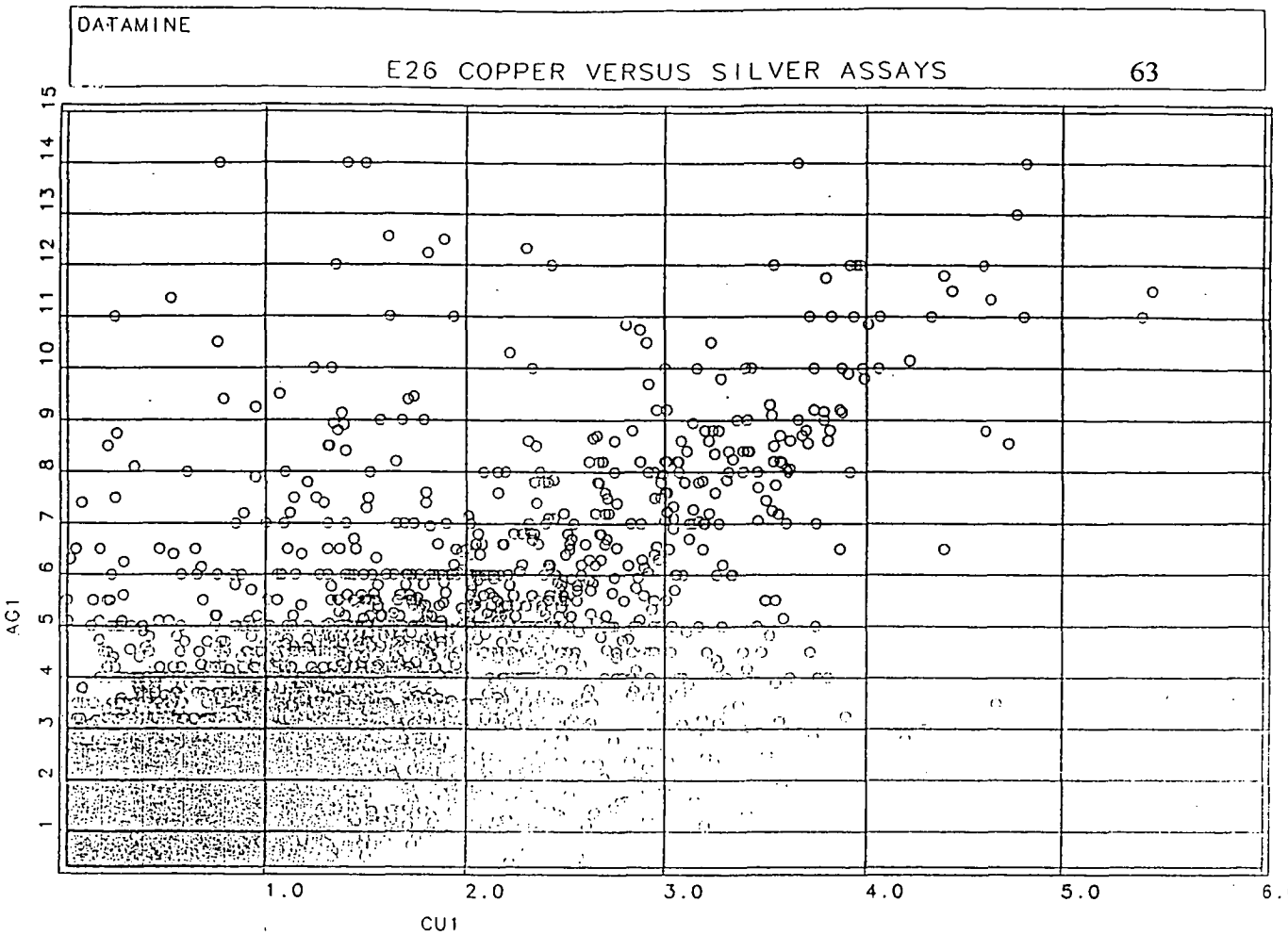

Figure 5.22 Bivariate scatterplot of Ag grade versus Cu grade.

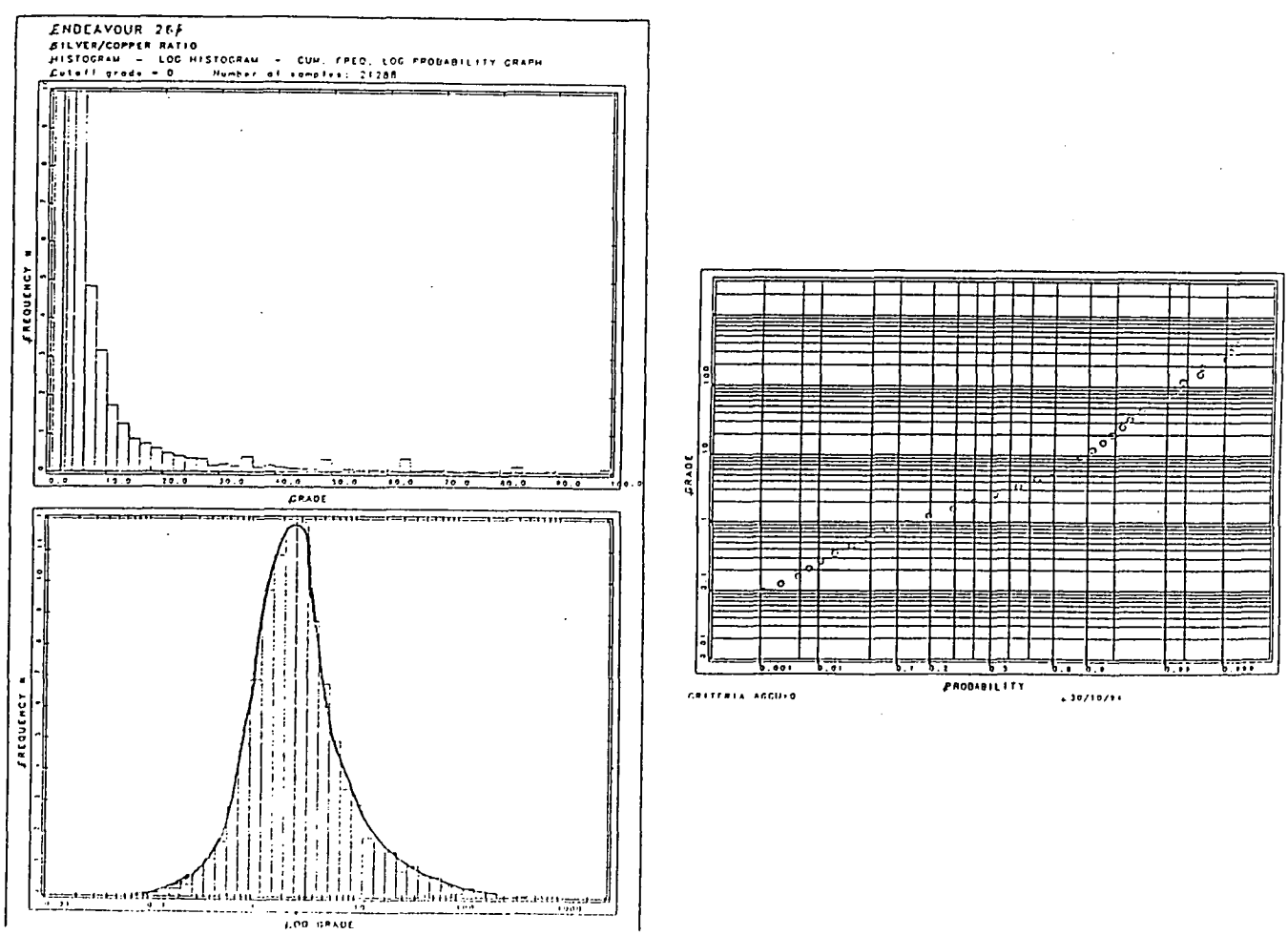

Figure 5.23 Frequency histograms and log probability plot for Ag/Cu ratio.

6. MINERALISATION AND ALTERATION PETROGRAPHY

6.1 INTRODUCTION

Twelve polished thin sections were prepared from drillcore. These samples were selected on the basis of the Cu/Au domains defined in Chapter 5, specifically to investigate the textural relationships that may explain the dramatic Au variations with depth. Detailed descriptions are given in Appendix 1.

6.2 ALTERATION AND VEINING PARAGENESIS

From a detailed examination of veins and vein envelopes in drill core, Heithersay (1991) has defined 11 stages of veining and alteration at E26 (Figure 6.1). Stages 1-3 represents veins and alteration assemblages that were the precursors to the main mineralising stages in QMP1. Biotite and magnetite alteration and veining occurred during Stage 3 associated with anhydrite and alkali feldspar. Stage 3 was overprinted by Stage 4 veinlets (quartz-K-feldspar-albite) with associated sulphides and hematisation of magnetite. This stage of veining is interpreted by Heithersay (1991) as the peak depositional stage for sulphides. Stage 5 is composed of multistage stockwork quartz veins and associated sulphides. Stage 6 breccias and vein dykes pre- and post-dates emplacement of QMP2. Stage 7 and 8 vein and veinlets (dominantly quartz) are confined to QMP2. Sulphide mineralisation is comprised mainly of chalcopyrite, with lesser bornite. Quartz-sericite alteration (usually structurally and fracture controlled) containing pyrite ± chalcopyrite is classified as Stage 9. Stages 10 and 11 gypsum and anhydrite veins overprint all other stages at E26. Sulphur isotope and fluid inclusion studies by Heithersay (1991) demonstrate high temperature and high salinity fluid conditions during formation of Stages 3 to 6 (peak hydrothermal conditions) related to the emplacement of QMP1 and QMP2. Decreasing temperatures and a waning of the hydrothermal system is recorded by Stages 7 to 11.

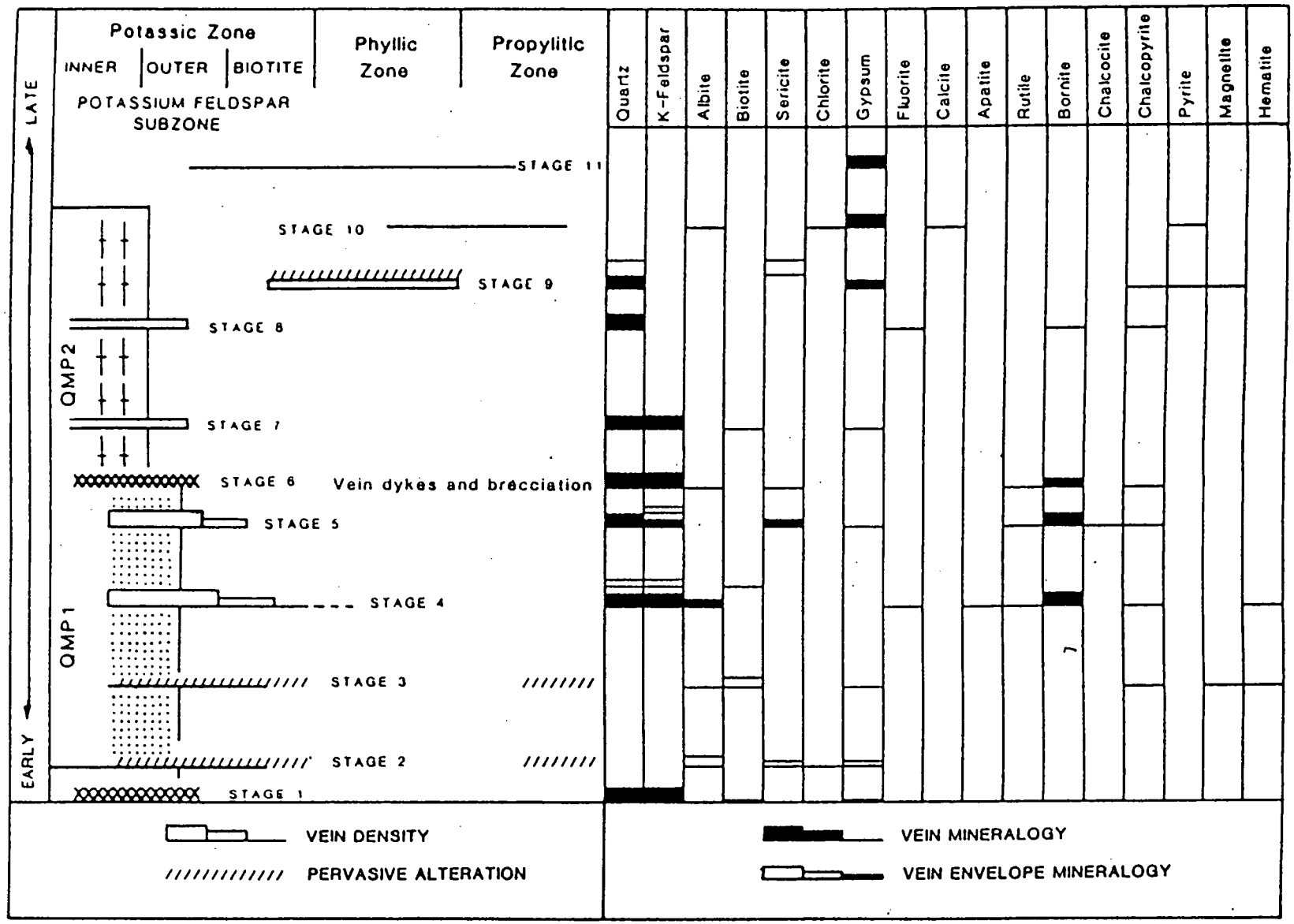

Figure 6.1 Alteration and veining paragenesis at E26 (From Heithersay, 1991).

As this work has focused on Au mineralisation, only samples from within and around QMP1 have been examined. Stages 1-2 and 6-8 of Heithersay's (1991) paragenetic sequence have therefore not been examined.

6.3 CU-BEARING SULPHIDE PHASES

6.3.1 Stages 4 & 5 Cu-bearing Sulphides

Bornite is the principal Cu-bearing sulphide at E26, with lesser chalcopyrite, chalcocite, and minor tetrahedrite and covellite. Bornite occurs in quartz veins and as disseminations in the potasically-altered wallrocks, associated with Stages 4 and 5 of Heithersay's (1991) paragenetic sequence. Bornite grains are generally ≤1mm in size, but can range up to >5mm. Bornite crystals in quartz veins tend to have smooth, well-defined margins and infill cavities between growth-zoned or massive quartz crystals (Figure 6.2). In contrast, bornite grains occurring as disseminations in the groundmass typically have an irregular and pitted outline; and may contain small acicular and bladed grains of sericite in intensely sericitised zones (Figure 6.3).

Two distinct bornite phases have been recognised based on colour when viewed under reflected light; orange-brown, and mauve varieties (Figure 6.4). Both phases occur within Stage 5 quartz veins and as disseminations in the potassically-altered groundmass. Orange-brown bornite is typically the most abundant variety. Chalcopyrite tends to be associated with the orange-brown bornite, while chalcocite tends to be associated with mauve bornite. In sample 128591.5, the orange-brown variety clearly predates the mauve variety (Figure 6.5). This is the only sample to provide a clear timing relationship between the two bornite varieties, as mutual contacts are extremely rare.

Both chalcopyrite and chalcocite can occur as discrete grains in contact with bornite, or as complex intergrowths with bornite (Figures 6.6 and 6.7). The exact timing relationships between bornite and chalcopyrite are also often hard to discern in many samples, as contradictory replacement textures are observed (Figure 6.8). These relationships suggest coprecipitation of chalcopyrite and chalcocite with the orange-brown and mauve bornites respectively.

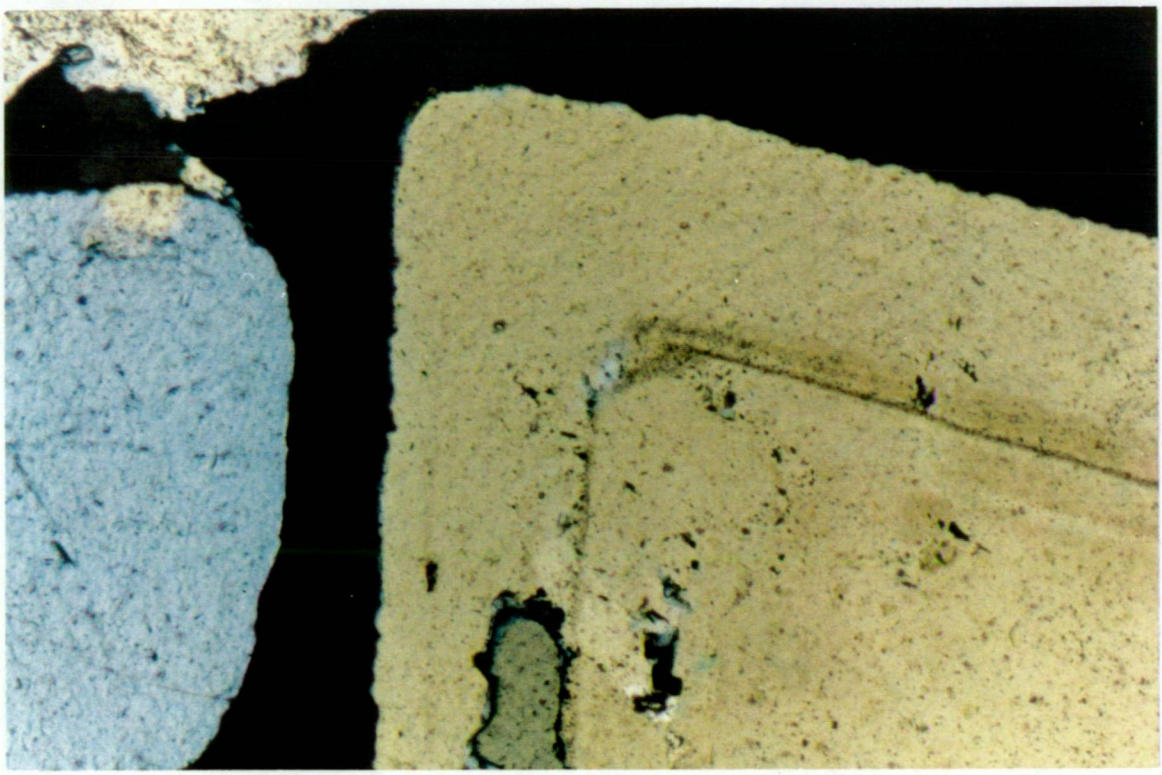

Figure 6.2 Growth zoned quartz crystal surrounded by interstitial bornite in a stage 5 quartz vein. Black is bornite. (sample 126W2571.4 transmitted light, crossed polars. Field of View 2.2mm).

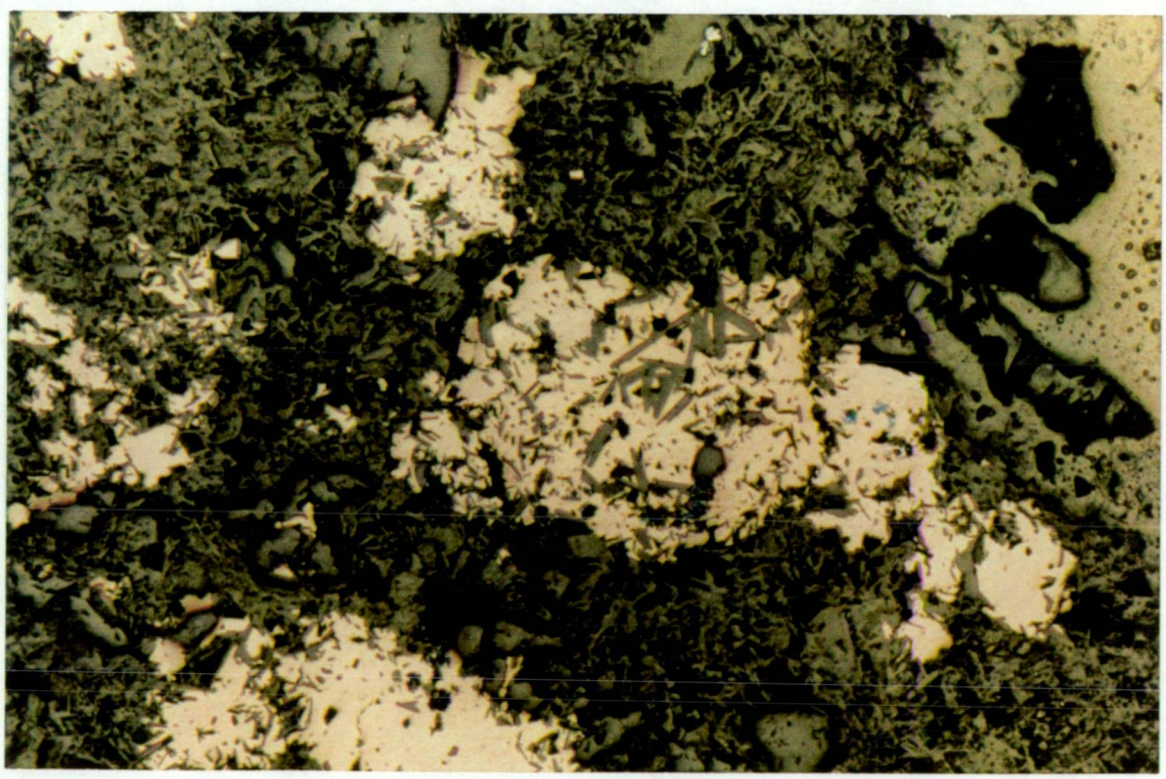

Figure 6.3 Disseminated bornite with small acicular and bladed grains of sericite, in strongly sericitised area within silica flooded zone. (Sample 126W2571.4, Reflected light FOV=2.2mm).

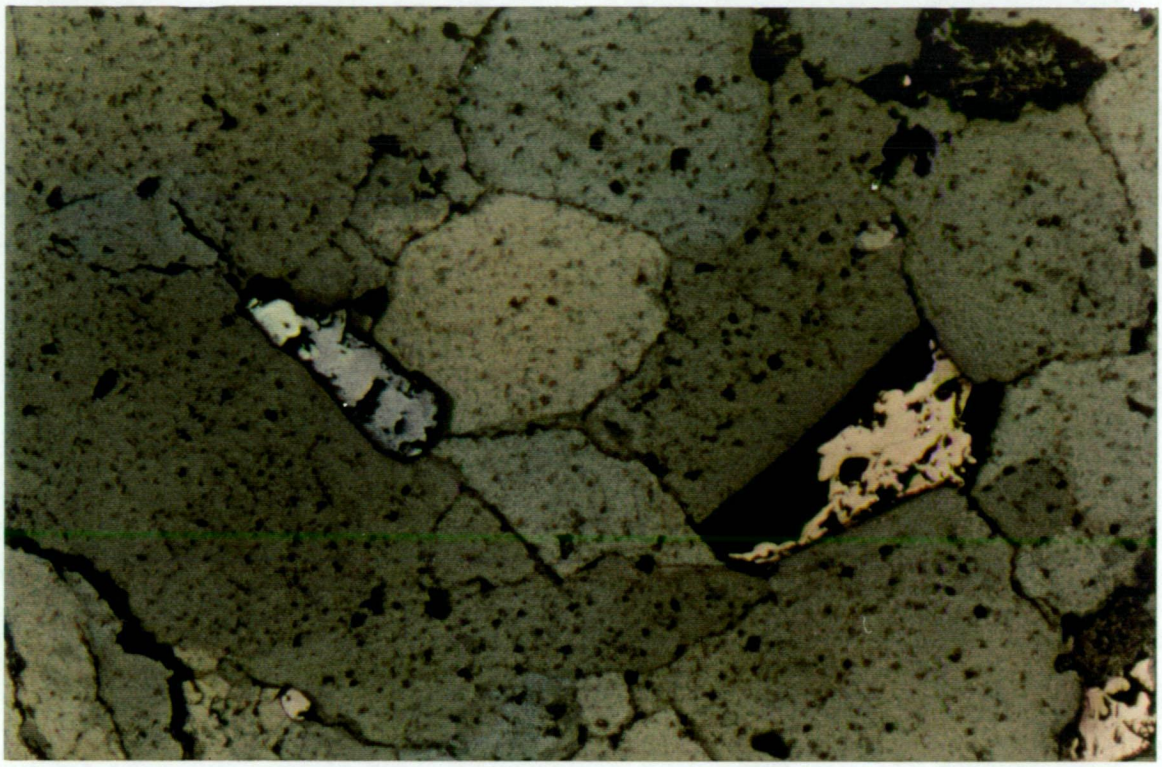

Figure 6.4 Two bornite phases in a stage 5 quartz vein: orange-brown bornite; and mauve bornite with light-grey chalcocite (sample 126W2571.4, Reflected light, FOV=2.2mm).

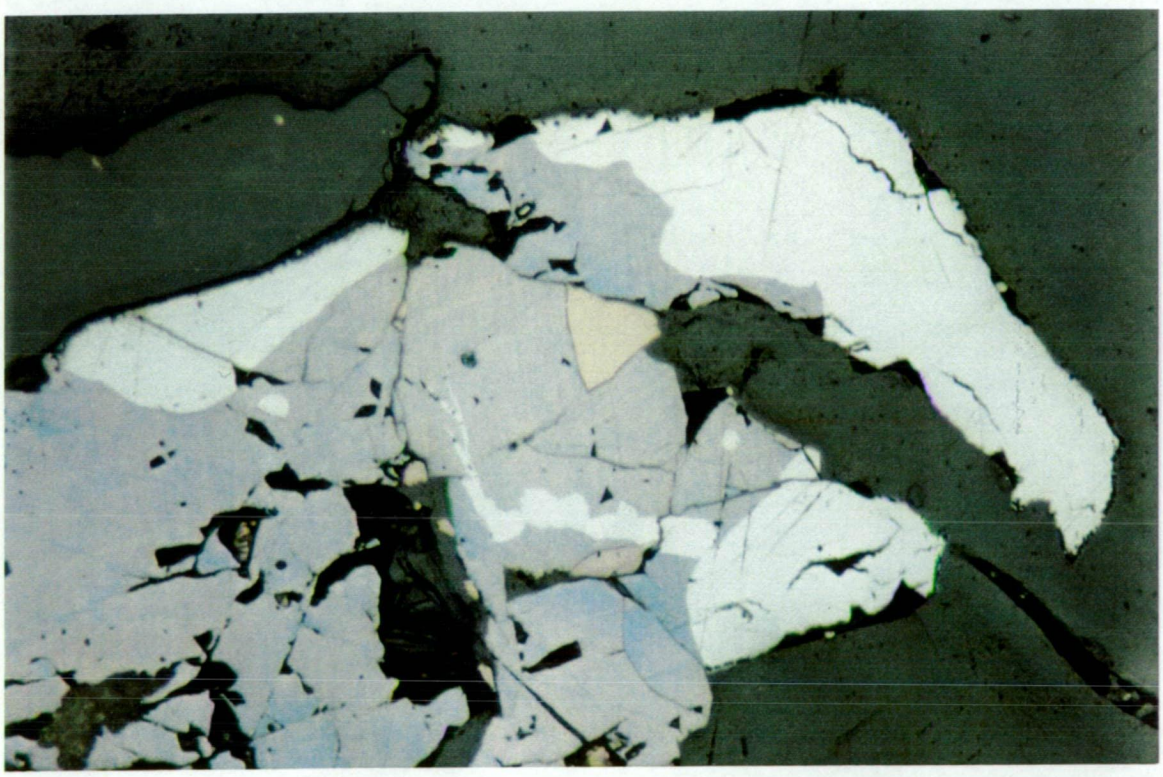

Figure 6.5 Two bornite phases in a stage 5 quartz vein. The orange brown phase predates the encompassing mauve phase which contains intergrown chalcocite (light grey). (Sample 128591.5, Reflected light, FOV=0.7mm).

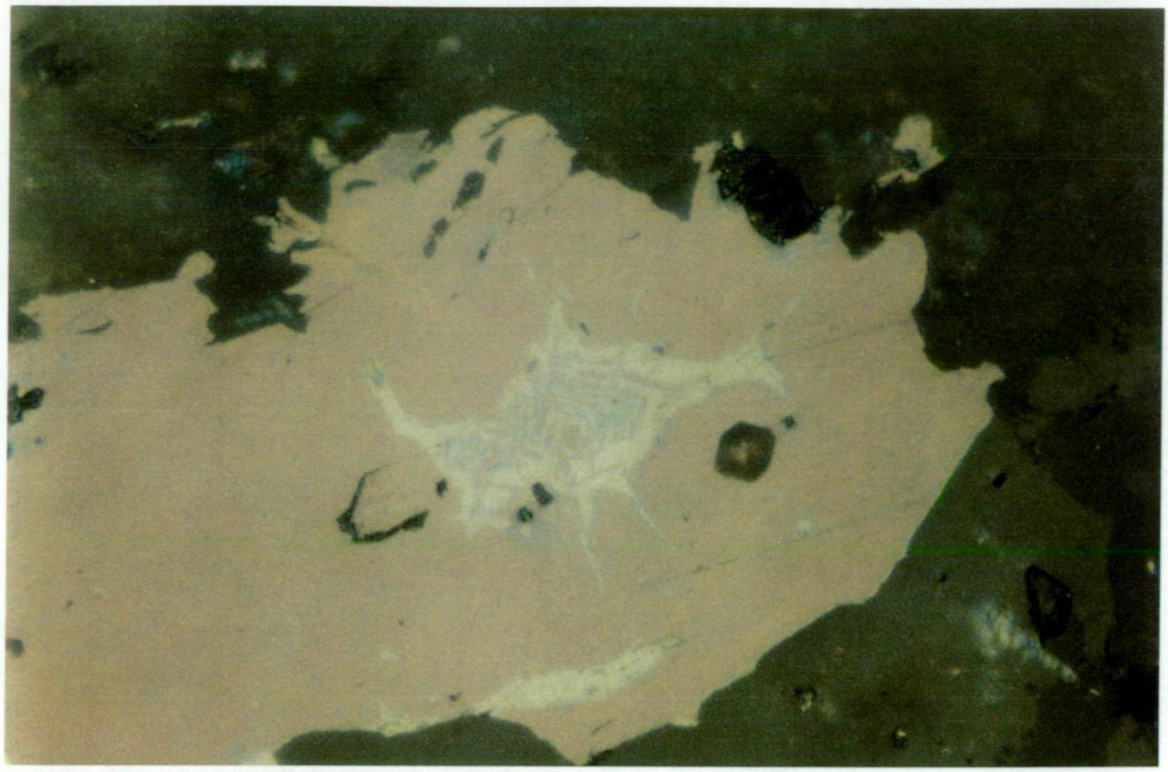

Figure 6.6 Complex intergrowth of bornite and chalcopyrite in stage 5 quartz vein (Sample 128591.5, Reflected light, FOV=0.25mm).

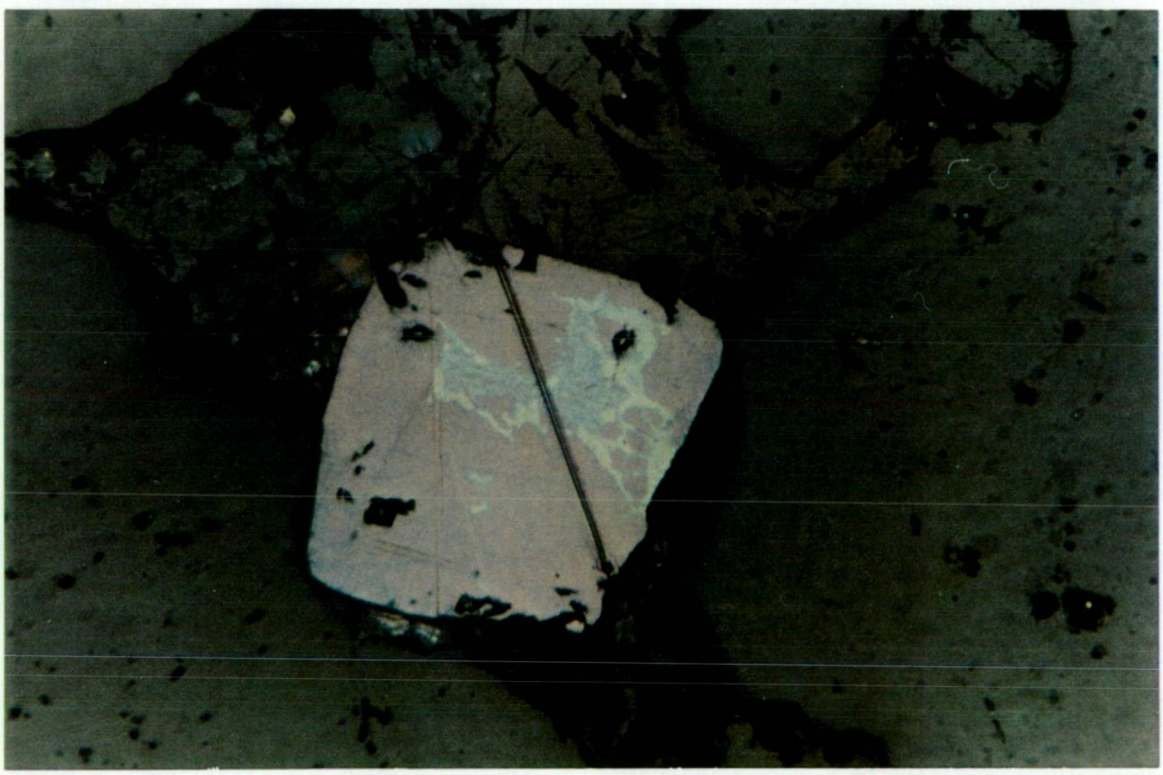

Figure 6.7 Complex intergrowth of mauve bornite and chalcocite (light grey) in stage 5 quartz vein. (Sample 39503, Reflected light, FOV=0.7mm).

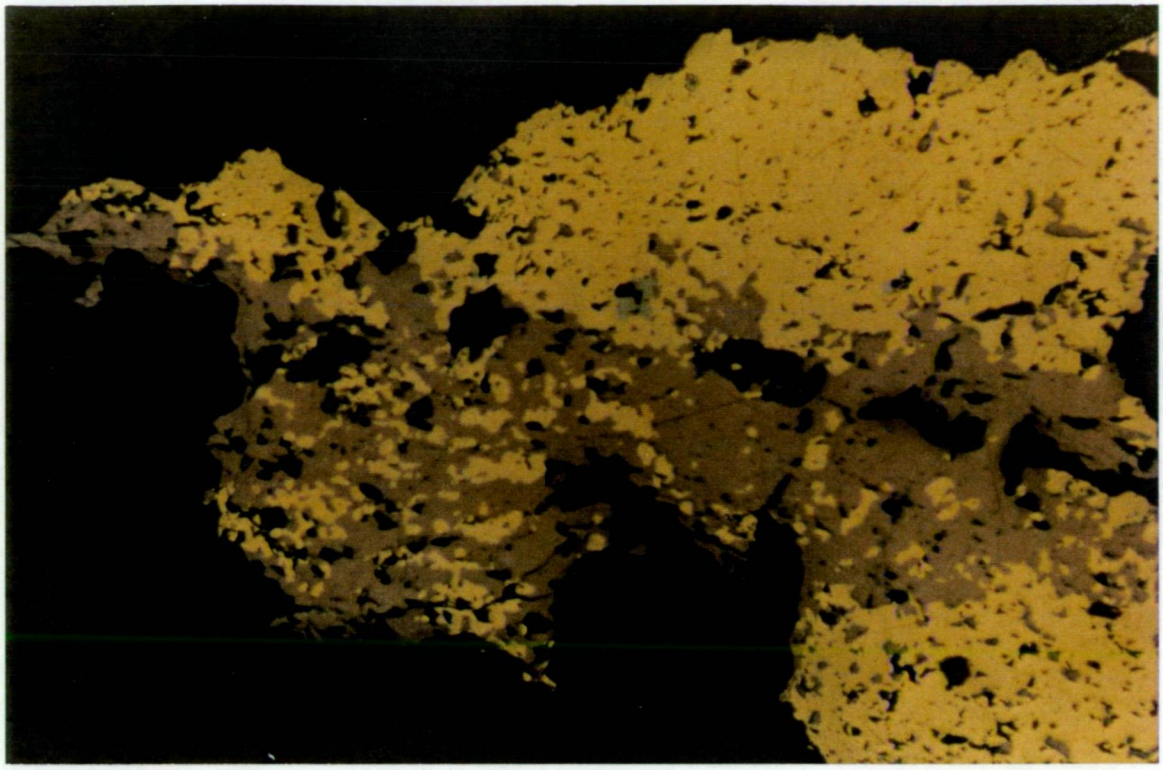

Figure 6.8 Composite grain containing chalcopyrite (yellow) and bornite (brown) that appear to have precipitated at the same time within a stage 5 quartz vein. Small light grey area just above centre is tetrahedrite (Sample 91175.4, Reflected light, FOV=2.2mm).

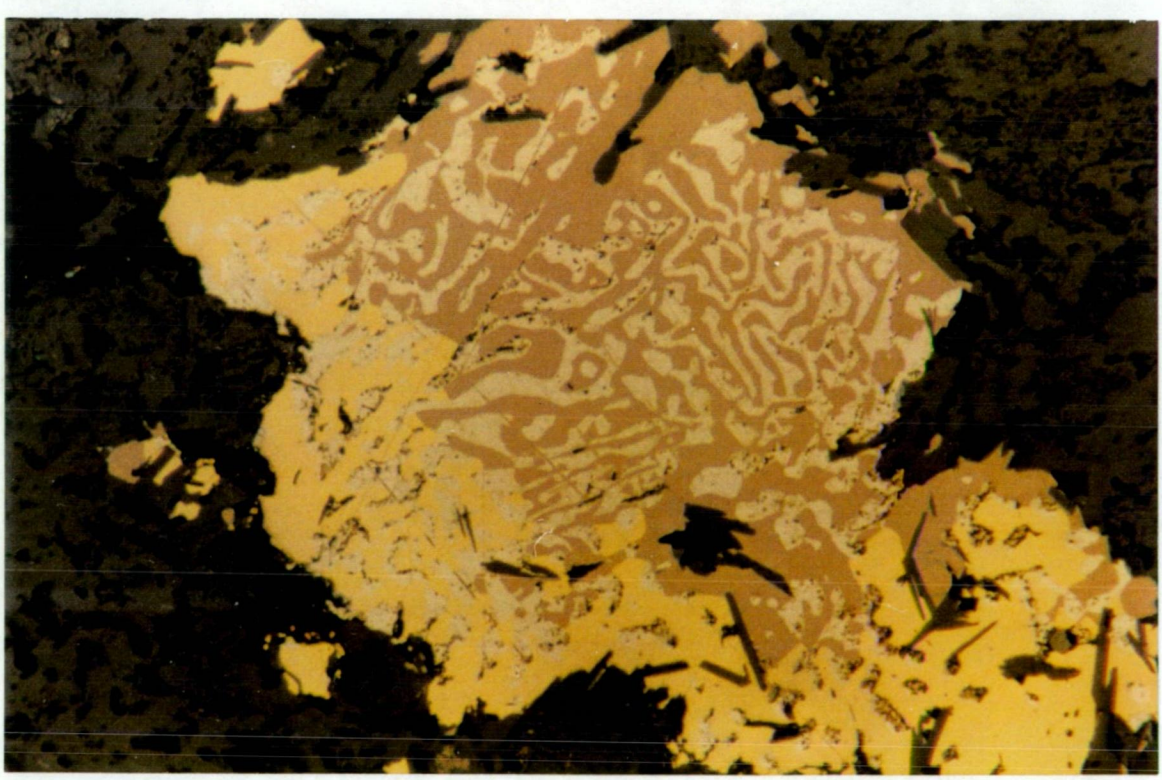

Figure 6.9 Myrmekitic intergrowth of bornite (brown) and tetrahedrite (grey). The chalcopyrite (yellow) appears to be replacing bornite. The grain is disseminated in stage 4 K-feldspar alteration which has a sericite overprint associated with stage 5. Note also inclusions of sericite needles in the sulphides. (Sample 91175.4, Reflected light, FOV=0.7mm)

Myrmekitic intergrowths of zincian (Appendix 2) tetrahedrite with bornite are present in a sample 91175.4 (Figure 6.9). In this sample, chalcopyrite appears to be replacing bornite. This sample also contains a coarse (2cm) Cu-sulphide aggregate of bornite, chalcopyrite and tetrahedrite in a Stage 5 quartz vein.

Rutile occurs as small inclusions in bornite (Figure 6.10). These inclusions range in size from 5 micron to 200 microns and are usually globular in shape.

6.3.2 Gold

Au occurs as <25 micron inclusions within bornite, typically associated with a fracture within bornite, and near the bornite grain edge (Figure 6.11). Some grains have also been observed in the silicate groundmass next to a bornite grain, but most occurrences are in coarse bornite grains hosted by Stage 5 quartz veins. Small Au grains have also been noted within chalcocite (Anon. Petrological report for Geopeko). Selenides and tellurides have been reported as small white inclusions within bornite (Anon. Petrological work for Geopeko). These were identified by scanning electron microscopy (SEM) as clausthalite (PbSe), calavarite ($AuTe_2$) and hessite (Ag_2Te). It is thought that a mineral optically similar to galena occurring within a bornite grain in sample 75153.3 is clausthalite (Figure 6.12).

6.3.3 Post Stage 5 Cu-bearing Phases.

Although veins associated with stages 6-8 of Heithersay's (1991) paragenetic sequence were not examined as part of this work, some of the replacement phases observed are thought to be related to these events. Chalcopyrite can occur as discrete grains unrelated to bornite in Stages 4 and 5 veins and alteration, or as a replacement phase after bornite. The most easily recognised replacement forms are as a rim around bornite, fine needles and fracture-fillings within bornite (Figure 6.13). The chalcopyrite 'needle' replacement is characterised by needles up to 50 microns long, that typically emanate from a chalcopyrite-filled fracture or replacement rim. In sample 126571.4 a chalcopyrite vein encloses shattered pyrite grains (Figure 6.14). This is probably a late stage vein (Stage 7 or 8) which cuts pre-existing mineralisation and quartz veins.

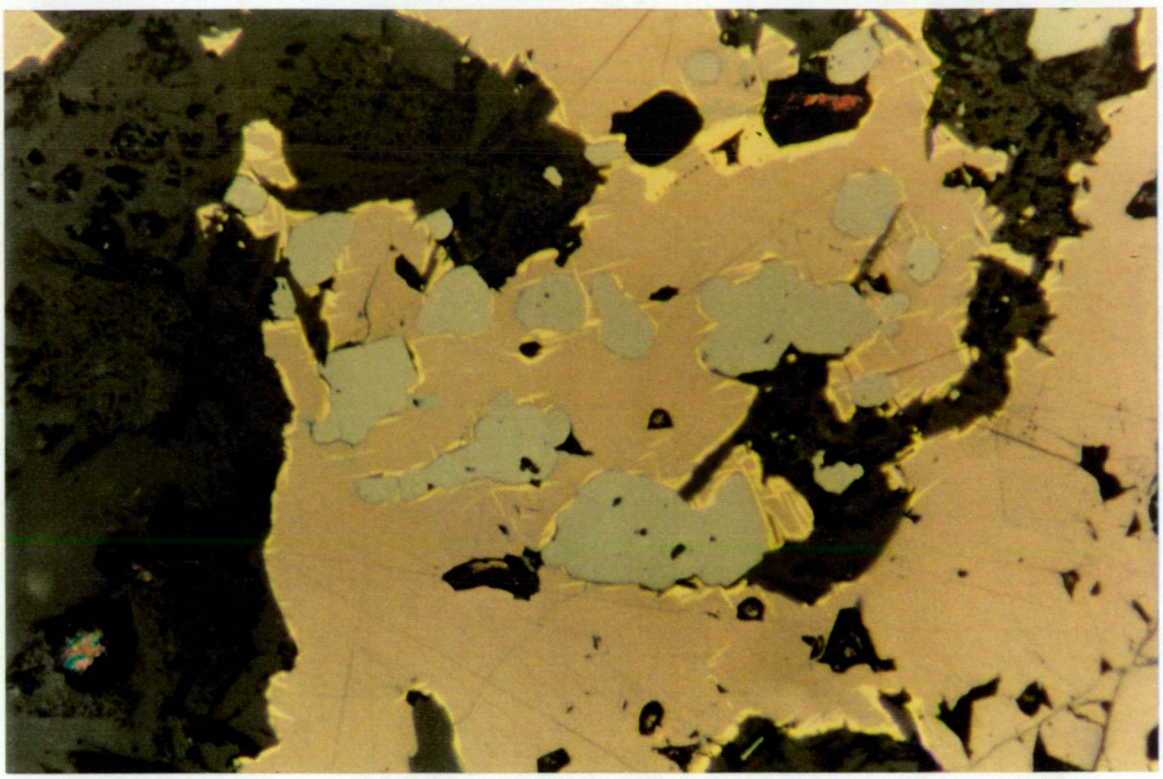

Figure 6.10 Globular rutile grains (grey) in bornite, disseminated within stage 4 K-feldspar altered ground mass. Note also replacement of bornite by chalcopyrite (yellow). (Sample 123138.3, Reflected light, FOV=0.7mm)

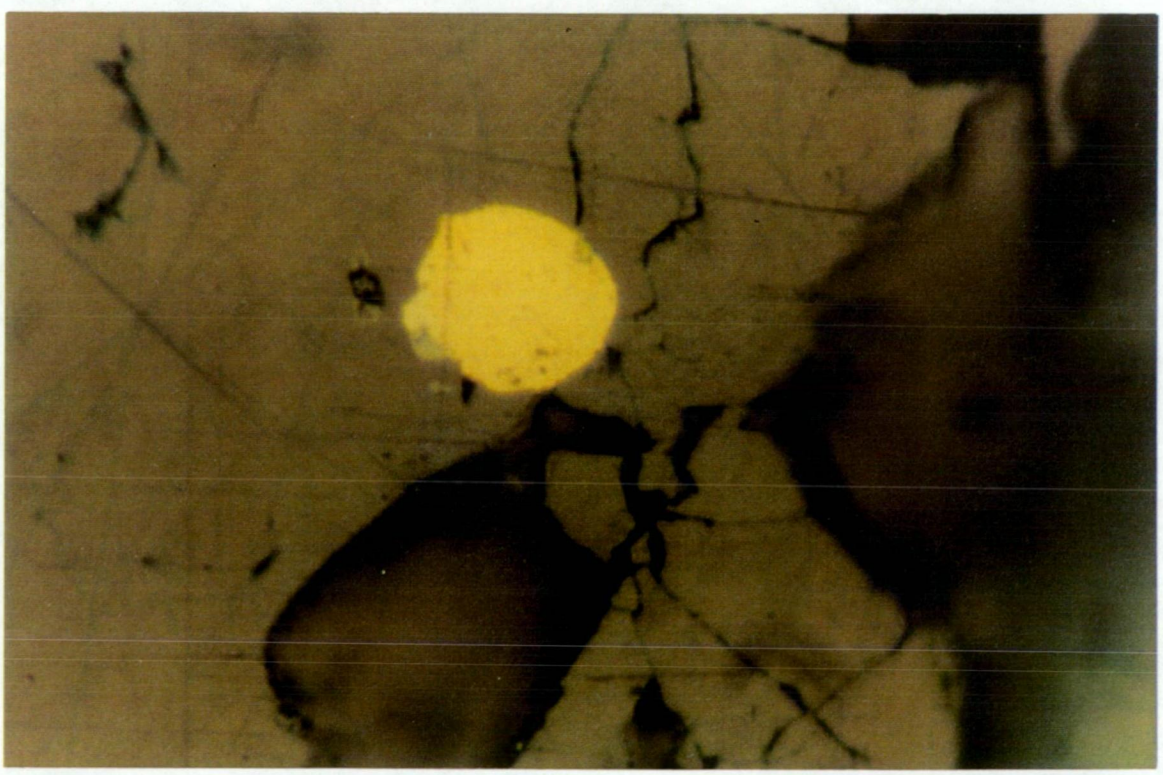

Figure 6.11 Gold inclusion in bornite within a stage 5 quartz vein (Sample 126W2513.4, Reflected light, FOV=0.13mm).

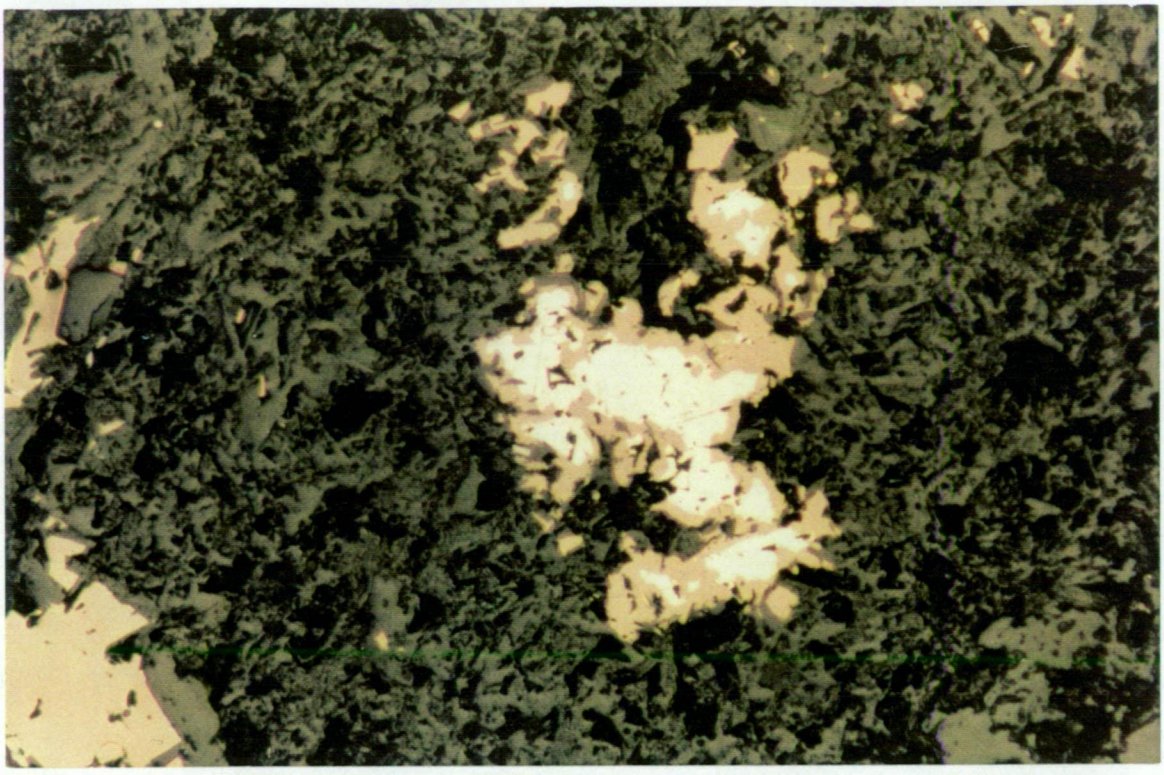

Figure 6.12 Disseminated bornite grain in sericitised groundmass adjacent to stage 5 quartz vein, with core of ?clausthalite - bright cream colour - optically similar to galena. (Sample 75153.3, Reflected light, FOV=1.2mm)

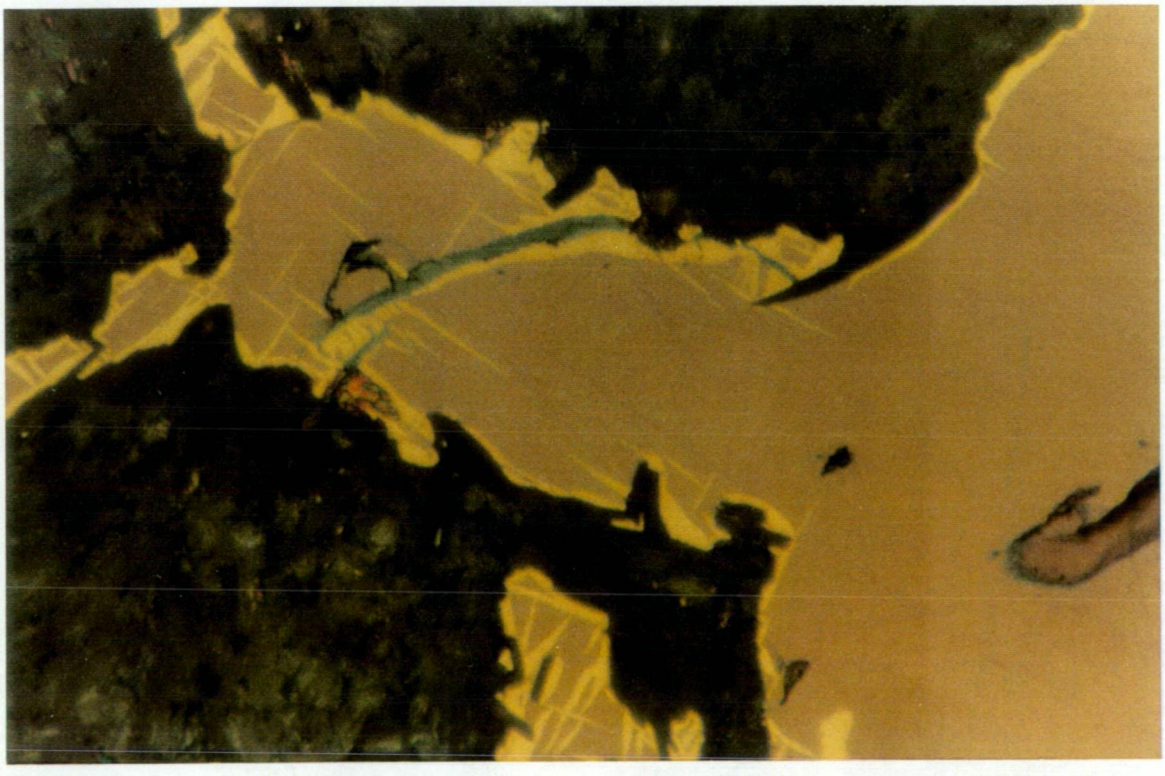

Figure 6.13 Chalcopyrite replacing bornite disseminated in K-feldspar altered groundmass. Replacement is along the grain rim, along fractures within the grain, and as small ?crystallographically controlled needles. Blue/grey mineral along fracture is covellite. (Sample 123138.3, Reflected light, FOV=0.25mm).

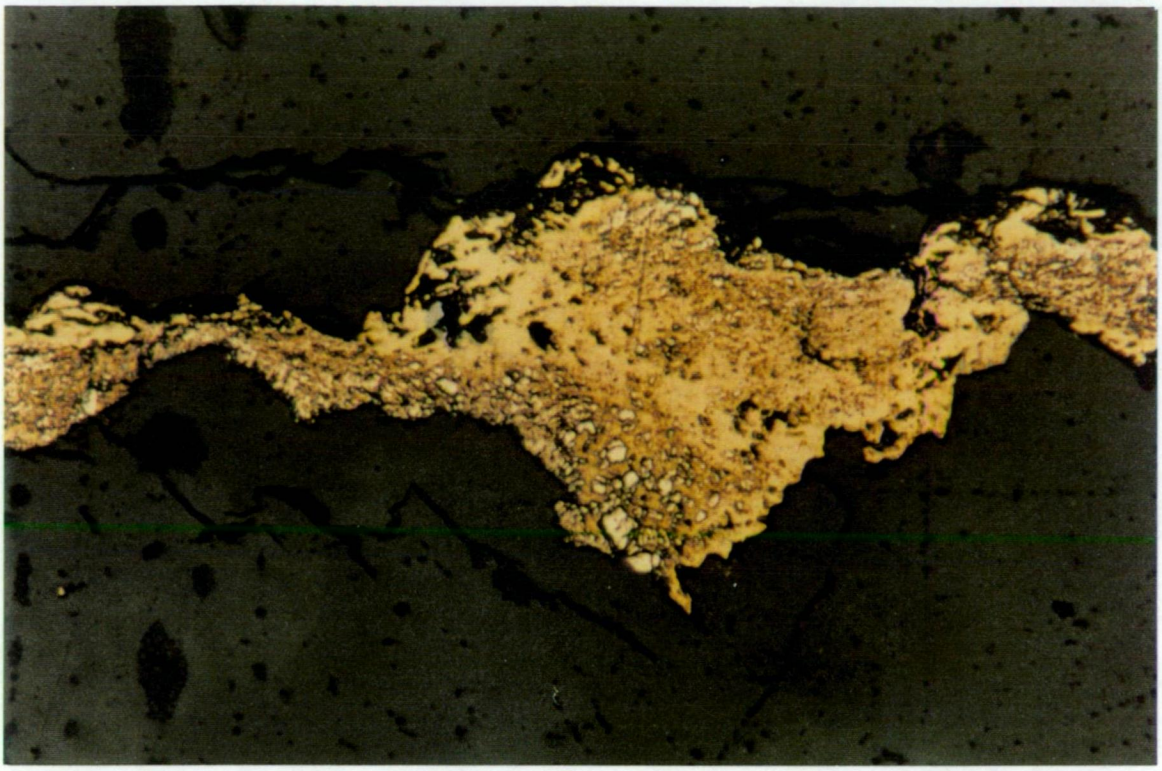

Figure 6.14 Chalcopyrite veinlet (yellow, stage 7 or 8) containing shattered grains of pyrite (pale white-yellow).Same veinlet crosscuts stage 5 quartz veins and causes replacement of bornite by chalcopyrite (Sample 75153.3, Reflected light FOV=0.7mm)

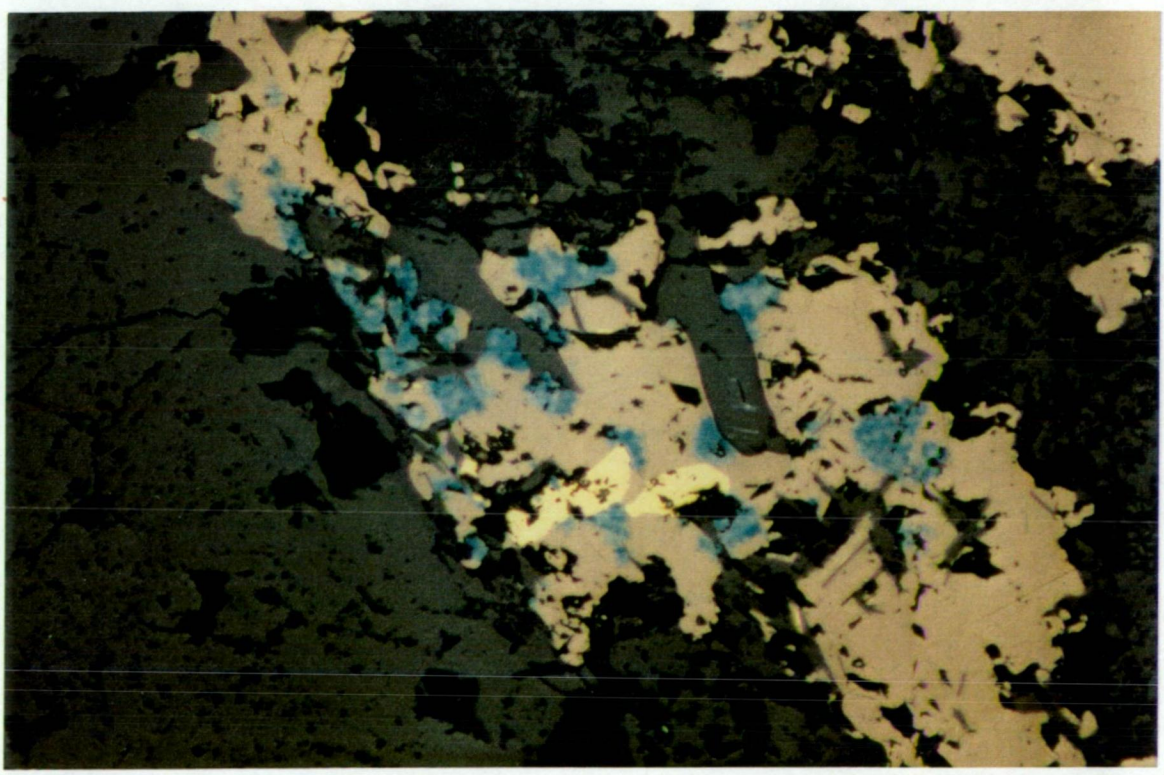

Figure 6.15 Replacement of bornite by covellite (blue), giving a 'diseased' texture. Chalcopyrite (pale yellow) also occurs within bornite but is not replaced by covellite. (Sample 123138.3, Reflected light, FOV=1.2mm).

Covellite is another common phase that has replaced bornite. The principal style is as a 'disease' replacement texture, where aggregates of fine radiating covellite needles occur within bornite typically near grain margins or fracture fillings (Figure 6.15). Fracture-related replacement is less common and postdates chalcopyrite replacement. In some of the samples, covellite has replaced chalcocite, but covellite has not replaced chalcopyrite in any of the samples studied. Chalcocite has replaced bornite in one sample studied (12382.8), where it occurs as a thin rim around bornite (Figure 6.16).

6.4 SILICATE AND OXIDE ALTERATION PHASES

6.4.1 Stage 3 Alteration

Stage 3 pervasive biotite/magnetite/albite/feldspar alteration is partially to completely overprinted by pervasive K-spar/quartz/sericite/hematite alteration. The Stage 3 pervasive biotite alteration has an erratic distribution which imparts a mottled appearance to the rock. Biotite alteration may be associated with albite and white K-feldpsar (which is not dusted by hematite). Coarser grained clusters of biotite also occur. Some areas of biotite alteration appear to be related to partial albitisation of plagioclase phenocrysts (Figure 6.17).

Magnetite occurs in Stage 3 alteration as grains in association with biotite or as discrete veins. In most of the samples studied, magnetite is absent due to its destruction by Stages 4 and 5 veins and pervasive potassic alteration. Where it has been observed in the polished sections, magnetite is commonly disseminated as euhedral crystals in biotite alteration, and is replaced to varying degrees by hematite and bornite. Magnetite veins are often observed in the lower grade areas on the western side of the orebody, but are rare in the main ore zone. Hole E26D126W2 is somewhat anomalous in this regard, as it contains magnetite veins in an area of strong copper and gold mineralisation. The veins contain coarse magnetite grains up to 3mm across which have been fractured and partially replaced by hematite along cleavage planes (Figure 6.18). Bornite and chalcopyrite commonly occur as partial replacements of magnetite, always in association with hematite (Figure 6.19). Unlike hematite, there is no strong crystallographic control on sulphide replacement of magnetite. Chalcopyrite may have been precipitated as a

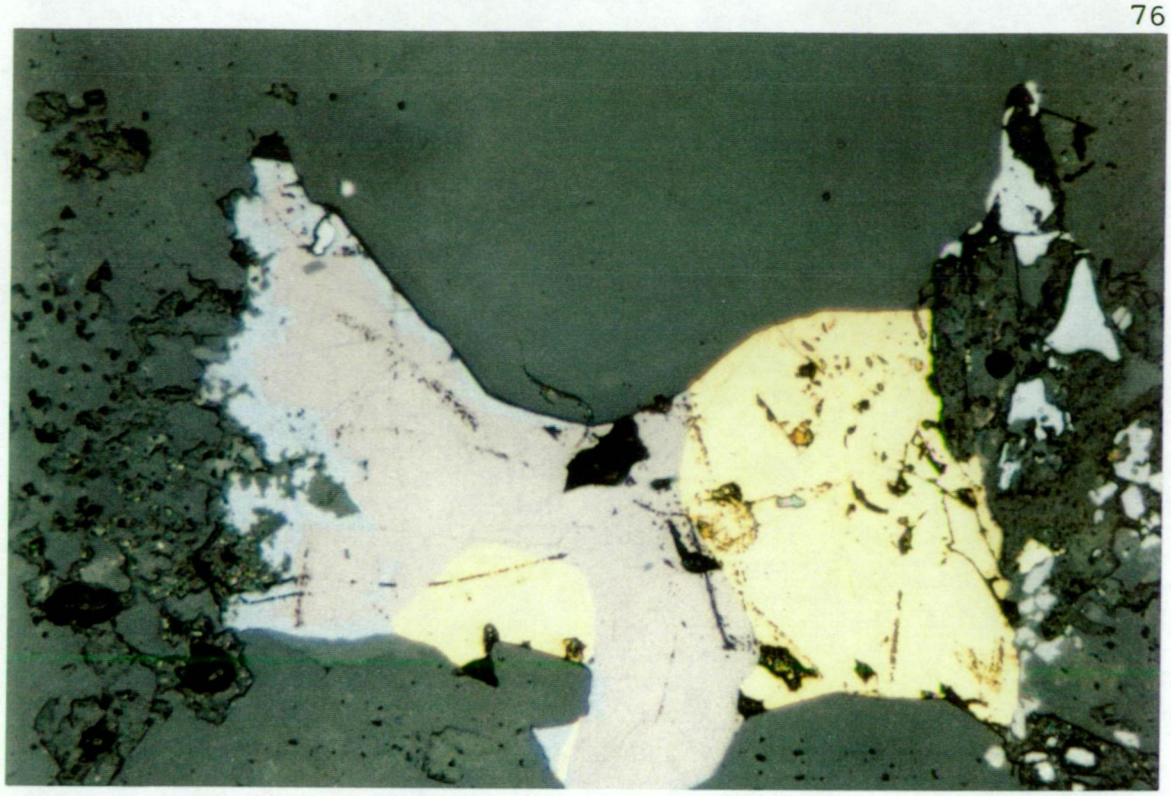

Figure 6.16 Thin rim of chalcocite (blue/grey) after bornite (brown). Hematite (white) and rutile (grey) occur on the right hand side of the sample. The grain occurs as a dissemination in K-feldspar altered groundmass. (Sample 12382.8, reflected light, FOV=0.7mm).

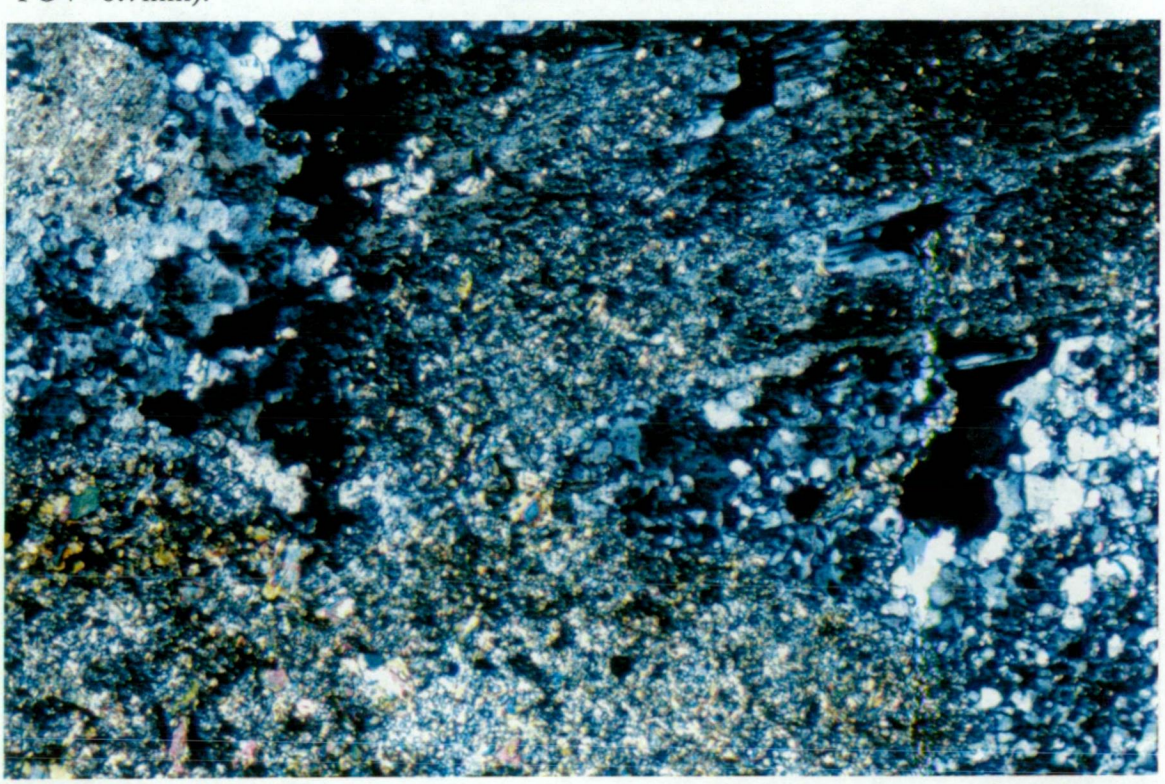

Figure 6.17 Pervasive fine grained biotite alteration (bottom left, stage 3) extending into remnant plagioclase phenocryst (now biotite, sericite, albite). Groundmass to left and immediately below phenocryst is K-feldspar and quartz (stage 4). (Sample 12382.8, Transmitted light, crossed polars, FOV=2.2mm)

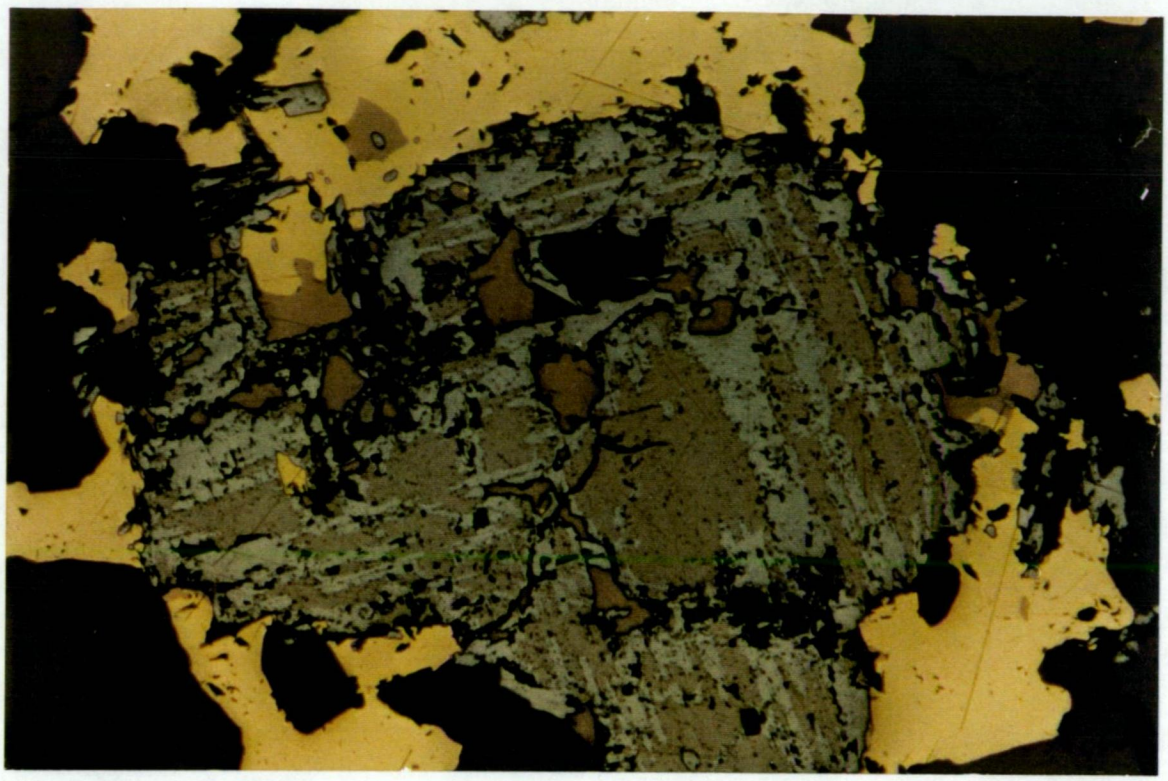

Figure 6.18 Coarse fractured magnetite crystal (brown, stage 3) with crystallographically controlled replacement by hematite (grey) and bornite, which has been partially replaced by chalcopyrite (Sample 126W2596.2, Reflected light, FOV=2.2mm).

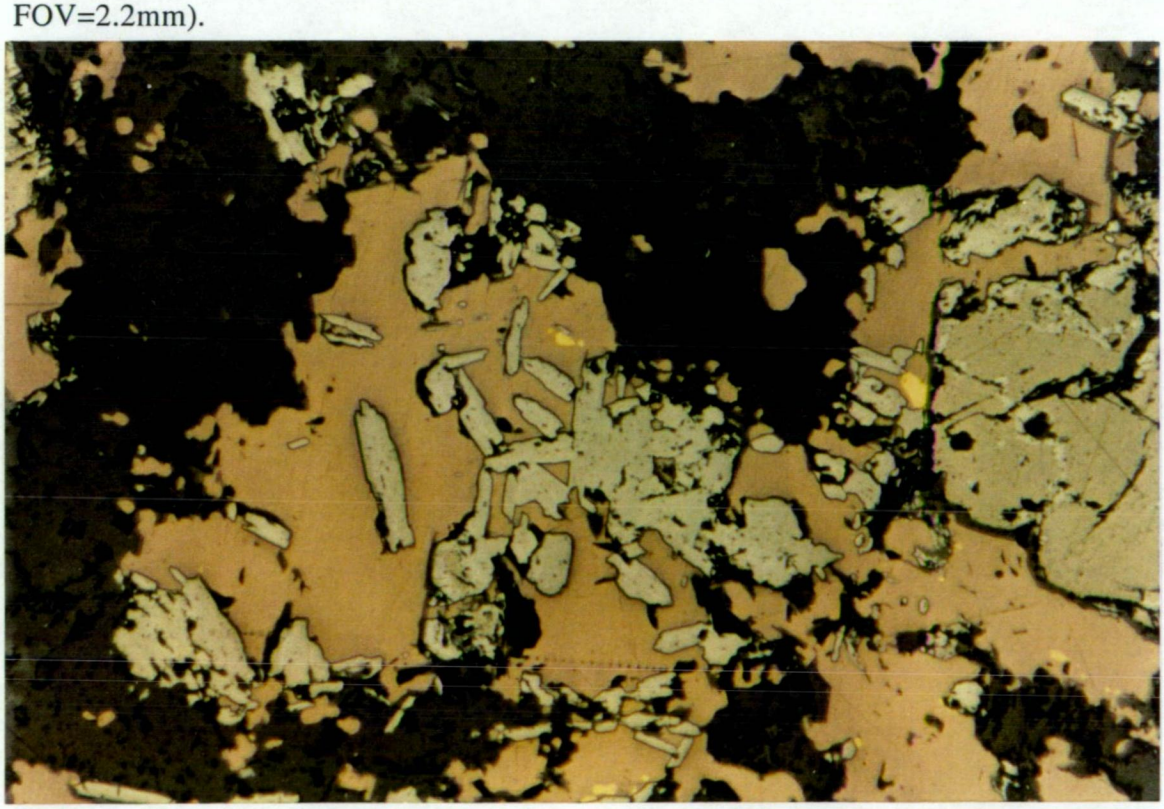

Figure 6.19 Coexisting hematite (grey) and bornite (orange-brown). Magnetite grain (light brown, stage 3) at right (Sample 126W2596.2, Reflected light, FOV=2.2mm).

primary phase with bornite or as a replacement of bornite. Chalcopyrite can be the dominant Cu-sulphide locally, although bornite is typically the most abundant sulphide proximal to magnetite. Hematite-dusted K-feldspar crystals are an accessory phase associated with the magnetite veins. Quartz and carbonate veins crosscut magnetite veins. Thin (10-15 microns thick) halos of sericite enclose aggregates of magnetite crystals in the sample studied.

6.4.2 Stages 4 & 5 Alteration

The overprinting potassic alteration (Stages 4 and 5), which is associated with the bulk of the disseminated mineralisation, is characterised by intense pervasive K-feldspar alteration of the groundmass. K-feldspar is typically dusted by fine hematite which imparts the characteristic pink colouration to the rock. Locally, fine grained quartz occurs with K-feldspar in the groundmass. Sericite, anhydrite and minor albite are also associated with pervasive potassic alteration. Plagioclase phenocrysts and crystals are altered to hematite-dusted K-feldspar and sericite. Coarser biotite associated with Stage 3 alteration is typically altered to sericite and rutile. Anhydrite occurs as irregular grains poikilitically enclosing quartz and K-feldspar. Rutile, apatite, sphene and fluorite are minor secondary phases. Within QMP1, bands of sericitic alteration overprint the Stage 4 potassic alteration but predate the intense quartz veining of Stage 5 (Figure 6.20).

6.4.3 Stage 5 Quartz Veining and Sericitisation

Most of the quartz veining appears to post-date the main K-feldspar alteration. Hematite dusting of the K-feldspar groundmass is most strongly developed adjacent to quartz veins (Figure 6.21). The veins vary in thickness, generally have sharp boundaries with the groundmass, and can contain coarse (up to 1cm) quartz grains that are growth zoned (Figure 6.2) and in some cases show strain lamellae and undulose extinction. Coarse anhydrite grains occupy the centre of some veins (Figure 6.22).

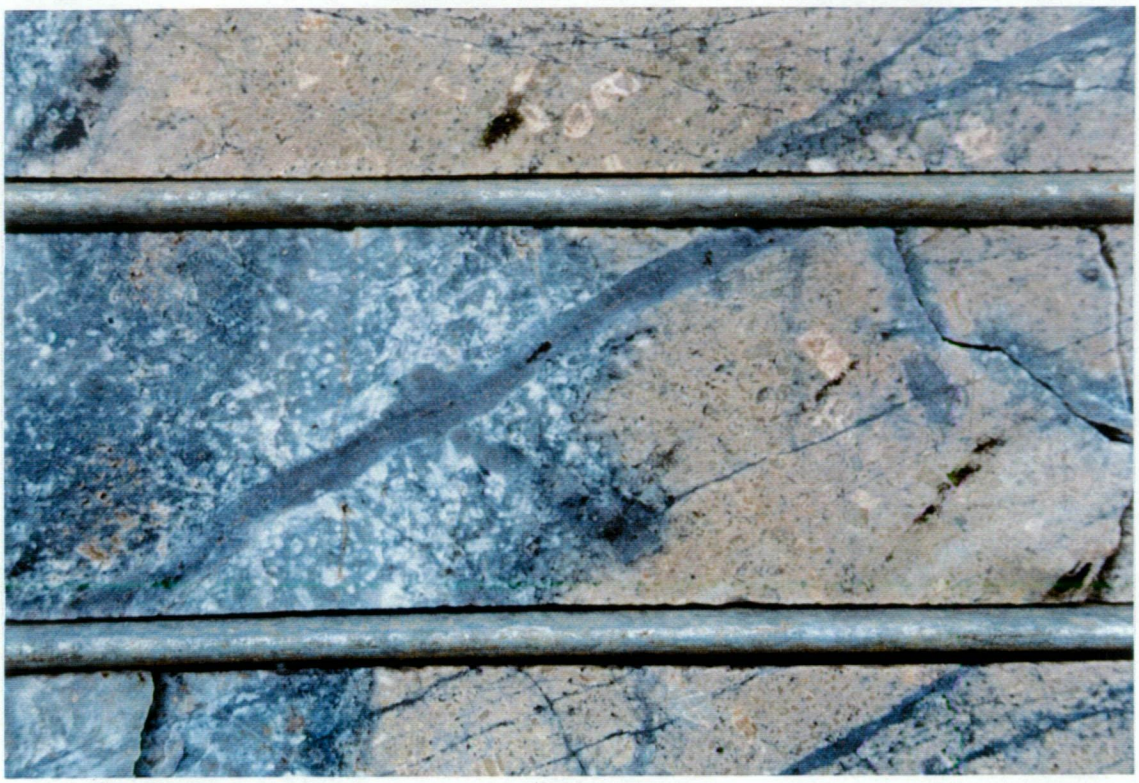

Figure 6.20 Drill core showing stage 5 quartz vein with core of bornite, crosscutting quartz and sericite alteration in QMP1 (Hole E26D126W2, Scale 1:1).

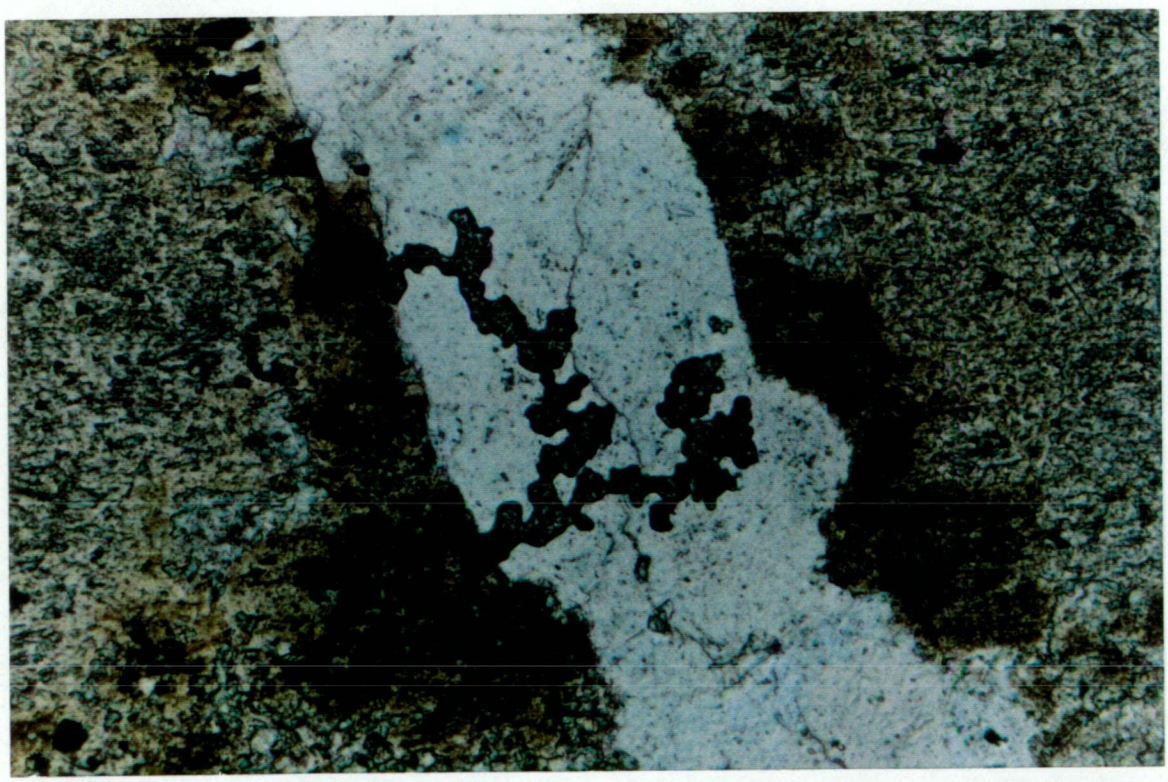

Figure 6.21 Hematite dusting of fine K-feldpsar adjacent to a stage 5 quartz vein (Sample 39503, Transmitted light, FOV=2.2mm).

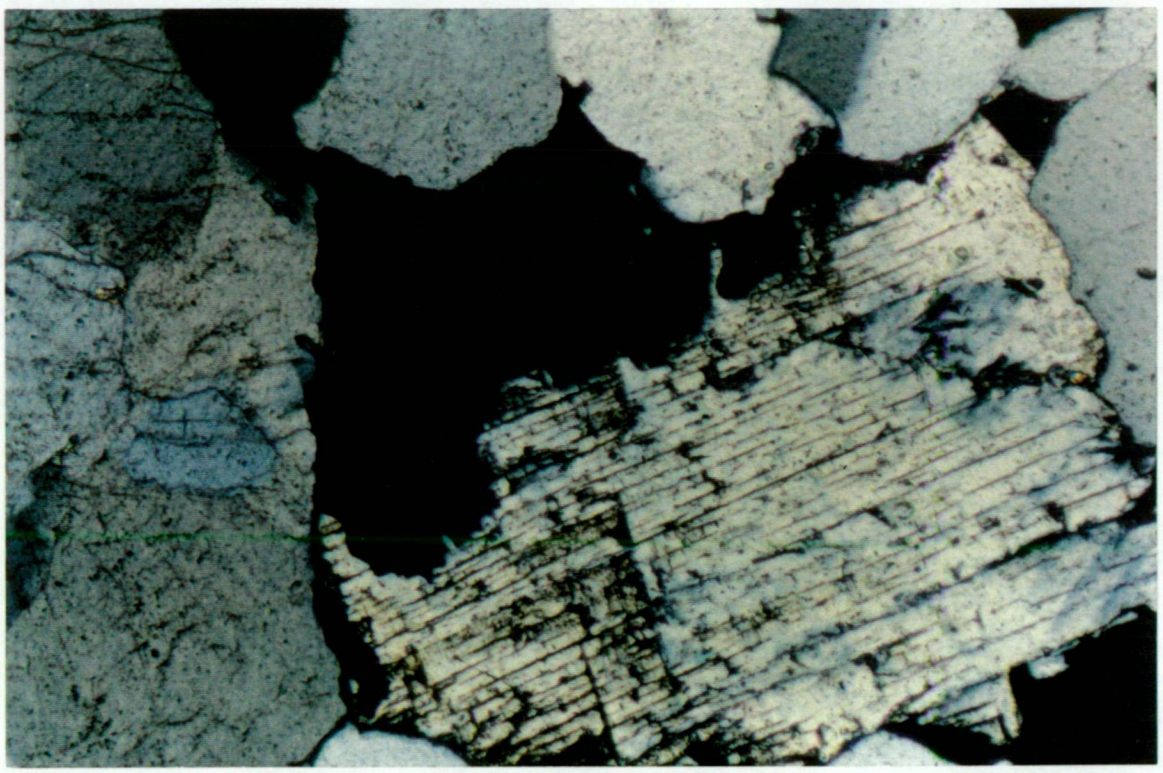

Figure 6.22 Coarse anhydrite in stage 5 quartz vein. Black area is bornite (Sample 67528, Transmitted light, crossed polars FOV=2.2mm).

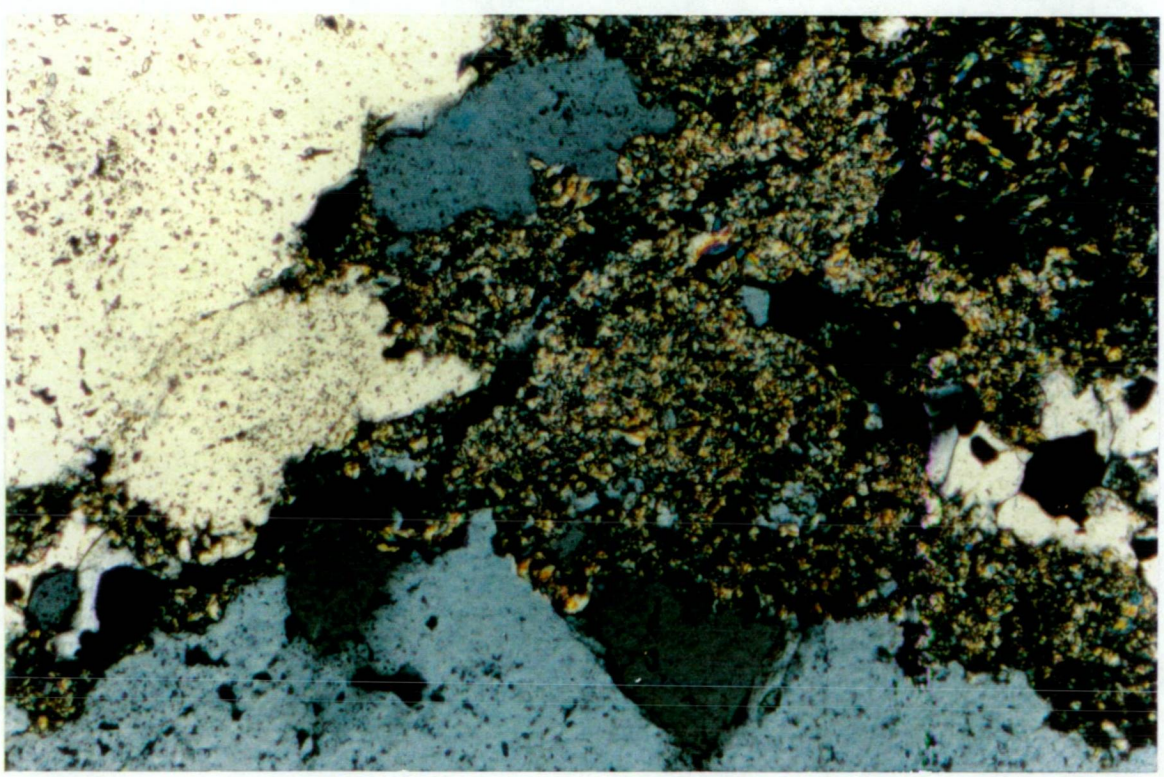

Figure 6.23 Sericitic alteration adjacent to and corroding a stage 5 quartz vein. (Sample 126W2571.4, Transmitted polarised light, FOV=2.2mm).

Many quartz veins are associated with intense sericite alteration. It appears that this sericite at least partly postdates the veins, as it has partly corroded the quartz (Figure 6.23). In the so-called 'silica zone', quartz veins have annealed resulting in poorly defined vein boundaries marked by a change in quartz grainsize. Rock fragments within these zones are totally altered to a pervasive groundmass of quartz and sericite. Even in these zones, it appears that sericite alteration at least partly overprints the silica flooding event. Sericitic alteration may shatter and vein the quartz veins.

6.4.4 *Post Stage 5 Alteration*

Sericite, chlorite, epidote, carbonate, anhydrite and gypsum overprint the potassic alteration and quartz veining of Stages 4 and 5. These occur in varying styles and degrees within the samples examined, including pervasive and selective replacement, and cross-cutting veins. The late alteration minerals usually occur as accessories in the samples studied, but can be locally abundant. Carbonate and anhydrite alteration locally comprises up to 15% of the rock volume. Whereas part of the anhydrite is related to potassic alteration and quartz veining (Stages 4 and 5), the majority is related to overprinting gypsum veining (Stage 11), and vein and pervasive carbonate alteration (Stage 10?).

Late chlorite alteration has in some cases caused partial replacement of bornite grains (Figures 6.24 and 6.25). Shattered grains of bornite in quartz veins have been infilled by late carbonate veinlets, gypsum veins and sericite veins (Figure 6.26).

These late alteration phases best fit into stages 9 and 10 of Heithersay's (1991) paragenesis. Their occurrence within the main mineralised areas indicates that the distribution lines on Stages 9 and 10 in Figure 6.1 need to be extended well into the Potassic Zone.

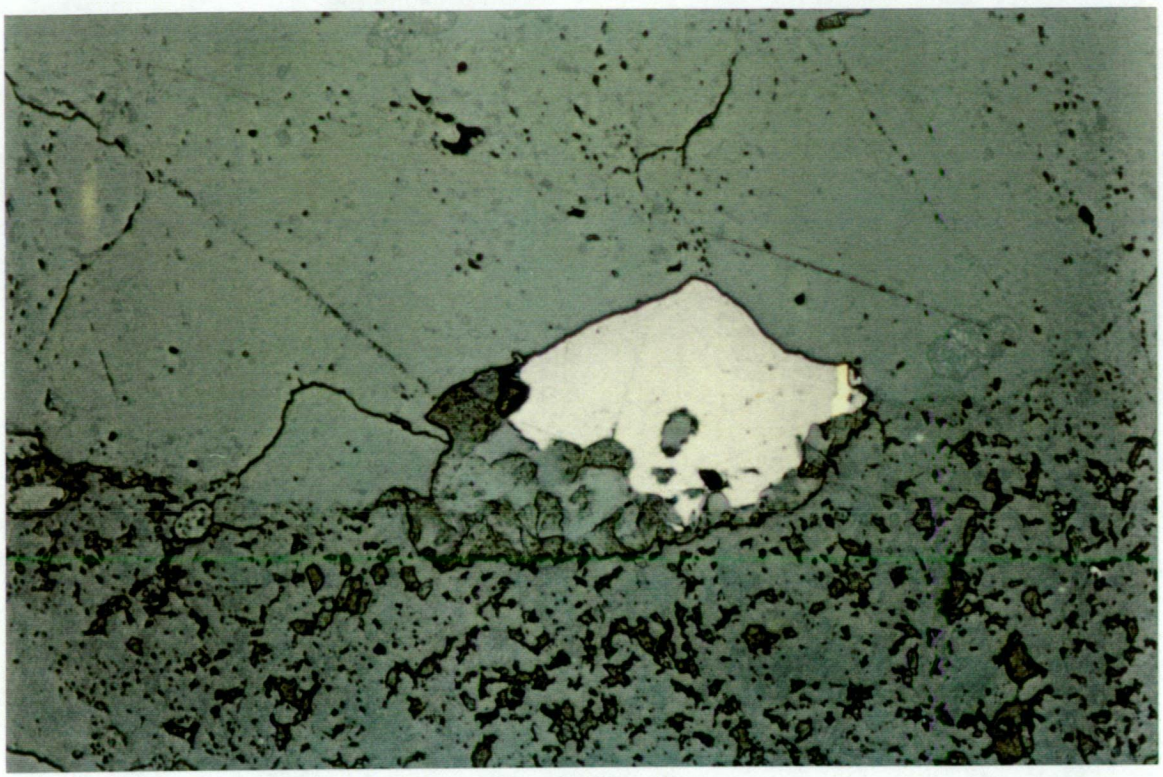

Figure 6.24 Bornite on edge of stage 5 quartz vein replaced by chlorite - bottom left of bornite crystal (Sample 128687.9, Reflected light, FOV=1.2mm)

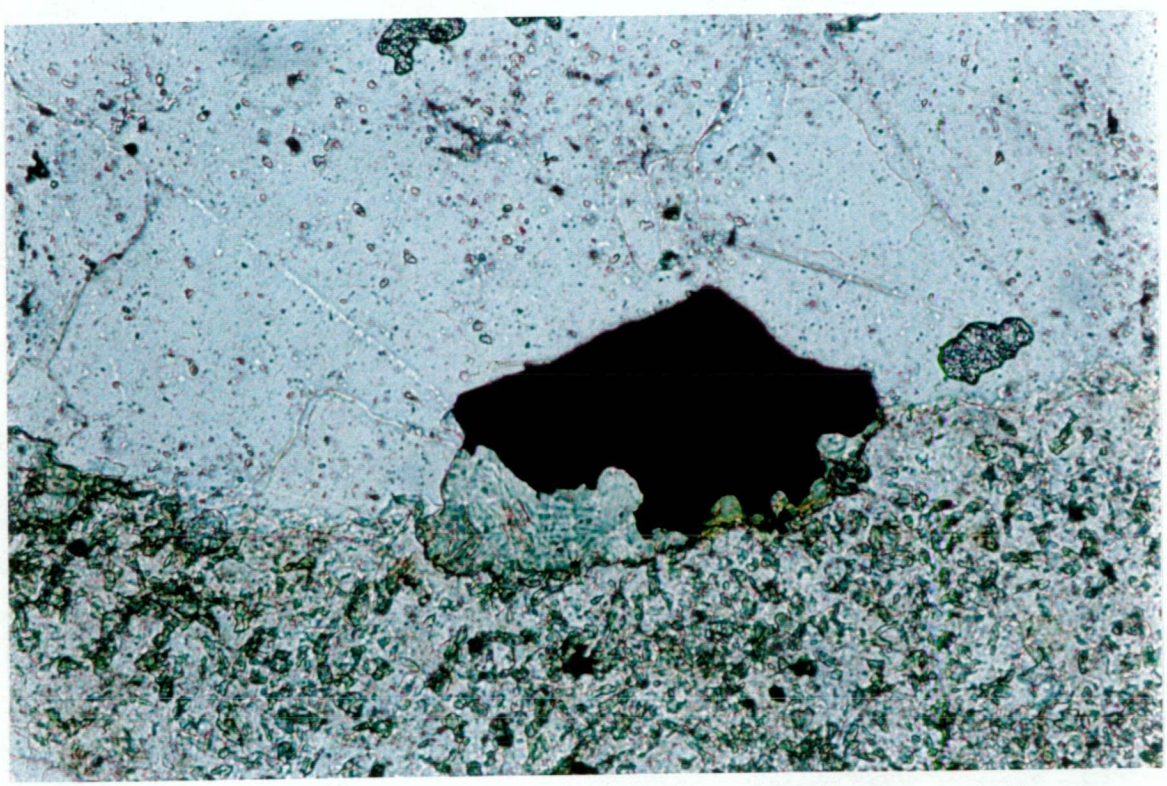

Figure 6.25 Same field of view as Figure 6.24, under transmitted light. Chlorite (pale green) after bornite (Black). (sample 128687.9, transmitted light, FOV=1.2mm)

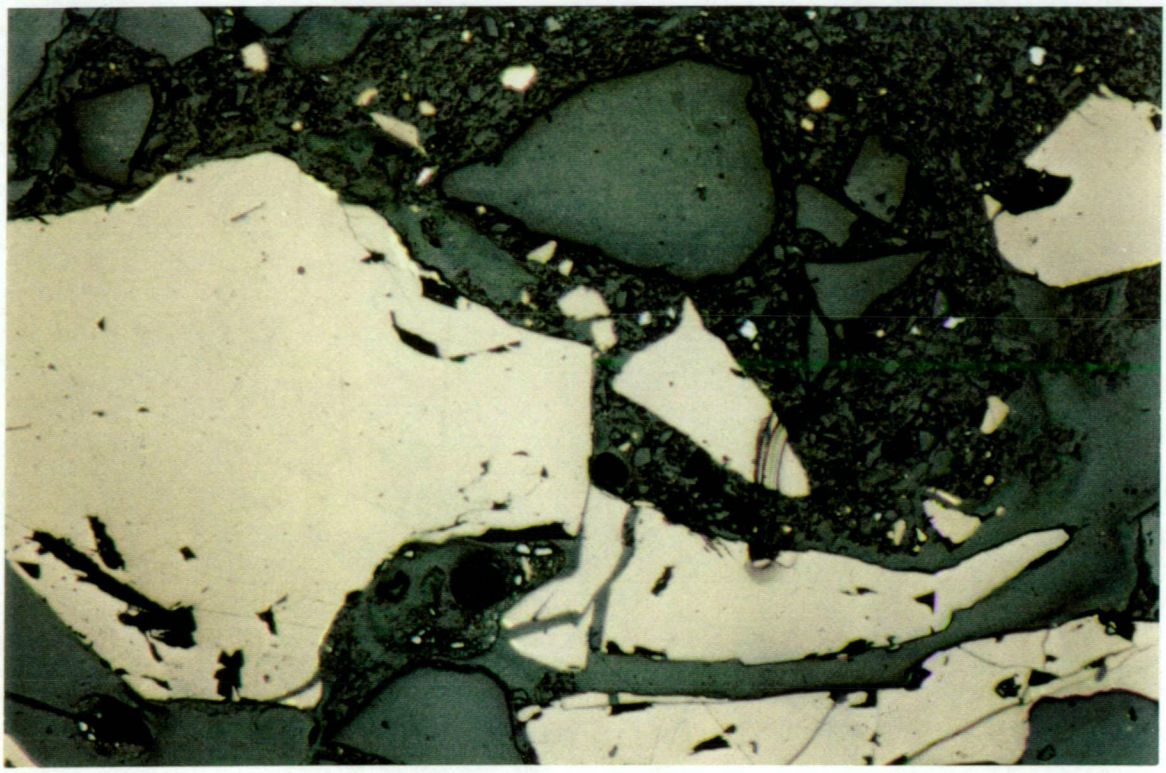

Figure 6.26 Broken bornite and quartz grains infilled by sericite veinlets (Sample 12382.8, Reflected light, FOV=1.2mm)

6.5 ELECTRON MICROPROBE ANALYSES

6.5.1 Introduction

Several samples were sent to the University of Tasmania for electron microprobe analysis. The aim was to determine bornite compositions, particularly looking for any compositional differences between the orange and mauve phase, and map any changes in bornite composition which may help explain the gold distributions described above. The compositions of other copper-sulphide phases and some silicates, were also determined by microprobe analysis.

The samples were analysed using a fully automated, three spectrometers Cameca SX 50 electron microprobe calibrated with natural mineral standards (PAP data reduction). The standards were analysed at least twice during each probe session. Analytical conditions were 15kV accelerating voltage, 20 nA beam current, and 1-2 μm beam size. Approximately 40 grains were analysed for a total of 87 analysis. Totals for some analyses are 2-3 wt% low and appear to have lead to an underestimation of the Cu content of the Cu-sulphide phases.

6.5.2 Results

All electron microprobe analyses are listed in Appendix 2.

6.5.2.1 Cu-Sulphides

The compositions of minerals in the Cu-Fe-S system from E26 are plotted on a ternary phase diagram (Figure 6.27). Both bornite and chalcopyrite show tightly constrained compositions. Chalcocite shows more compositional variations, grading to digenite.

The orange-brown and mauve bornite phases are compositionally identical, and have the stoichiometry $Cu_{4.8\text{-}4.9}Fe_{0.9\text{-}1.0}S_4$. The composition of bornite is constant, even though the four samples were taken from different areas of E26 (Appendix 1) and from Domains 3 and 4 defined in Chapter 5. Trace elements do not vary between the orange-

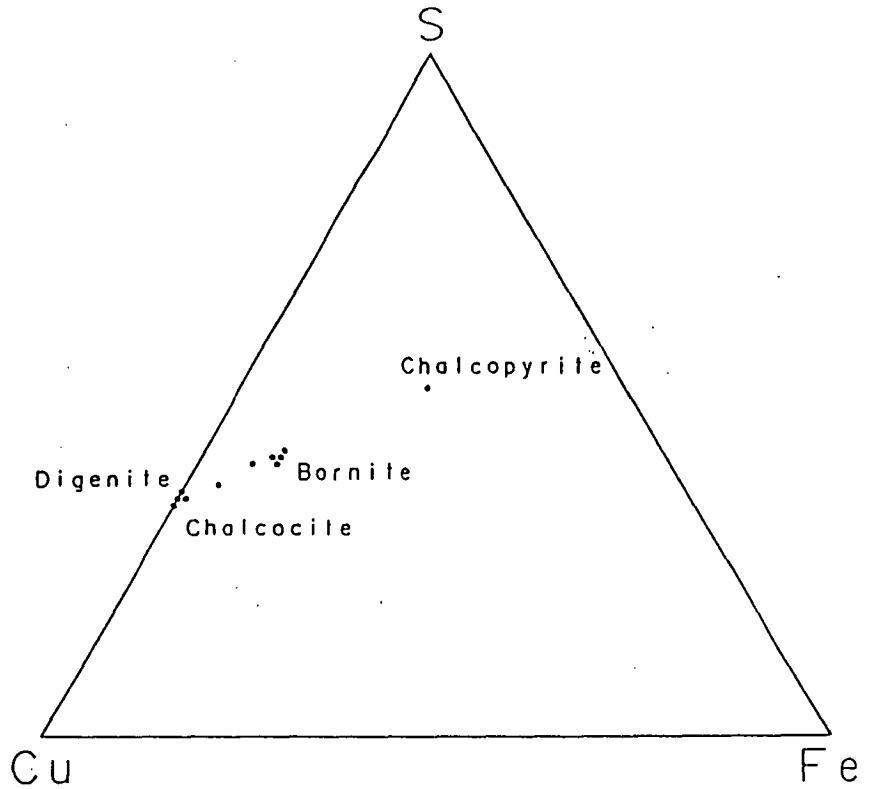

Figure 6.27 Ternary phase diagram for the system Cu-Fe-S, with electron microprobe results (Data provided Appendix 2).

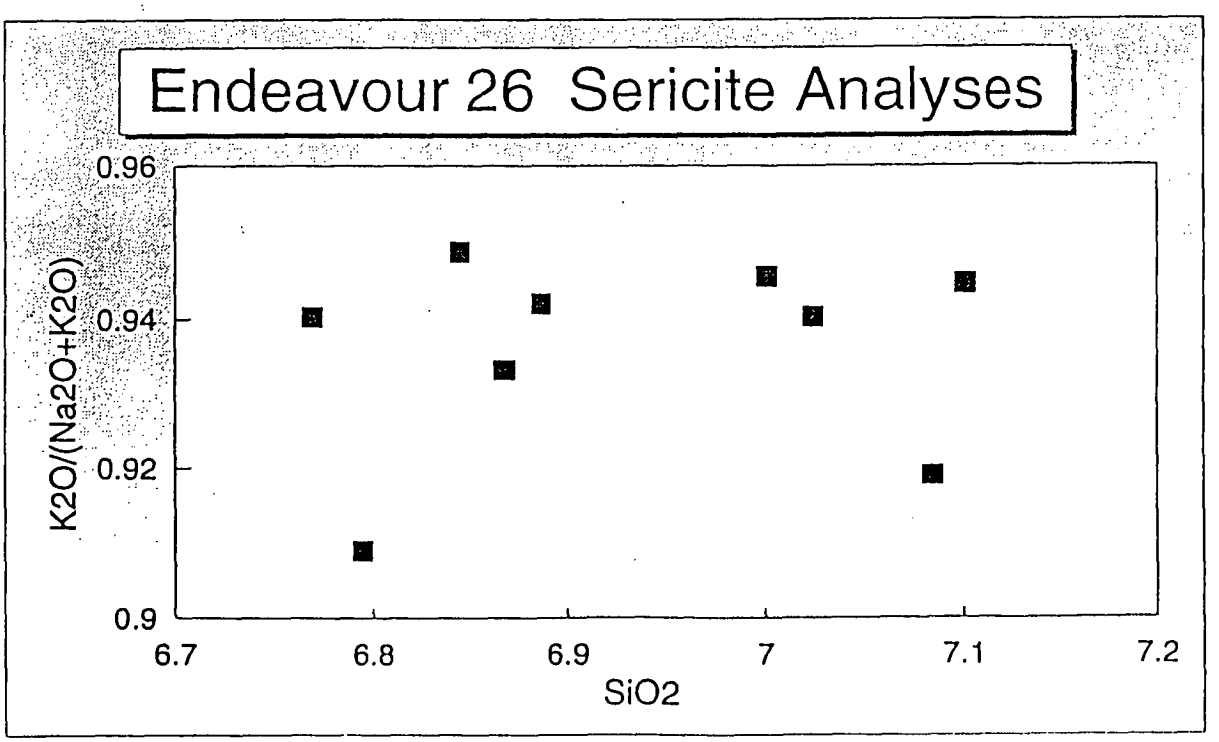

Figure 6.28 K/Na+K ratio versus silica for sericites at E26 (Data provided Appendix 2).

brown and mauve bornites, and remain constant independent of location within the orebody. The silver content within the bornite structure is enough to account for the observed silver grades at the E26 deposit. One chalcopyrite grain was analysed and found to have a constant composition of $Cu_{1.0}Fe_{0.9\text{-}1.0}S_2$. Tetrahedrite (composite grains and myrmekitic intergrowths) from sample 91175.4 (Figure 6.9) is zincian, contains minor As, and has the composition $(Cu_{9.9\text{-}10.0}Zn_{1.8\text{-}1.9})(As_{0.2\text{-}0.7}Sb_{3.4\text{-}3.7})S_{13}$. Ag and Bi contents within tetrahedrite are insignificant (Appendix 2). Chalcocite grains show some compositional variation (Appendix 2), approximating $Cu_{9.4\text{-}9.9}S_5$. This composition is intermediate between chalcocite (Cu_2S) and digenite (Cu_9S_5). Fe contents in chalcocite are generally low, except for one analysis with anomalous Fe and low Cu ($Cu_{7.8}Fe_{0.6}S_5$, Appendix 2).

The phase occurring with bornite in sample 75153.3 (Figure 6.12) was not confidently identified. The probe analysis shows unusual high As with S and a low wt% total. The phase is optically similar to galena, and may be the Pb selenide, clausthalite. As a sphalerite standard was used, the Pb spectra could be mistaken for S, and the Se spectra mistaken for As. A similar high As and S analysis was returned from bornite in sample 91175.4 and is also interpreted to be clausthalite. Gold was confirmed from spectra in sample 128591.5.

6.5.2.2 Sericite

Nine analyses of sericite showed that compositions were close to muscovite, with slightly less K and more Si (Appendix 2). Figure 6.28 is a plot of alkali ratios against silica for sericite. The sericites show only minor substitution of Na for K. The analyses for sample 91175.4 show some substitution of Na for K, in contrast to the other samples (Appendix 2). There is little substitution of Mg or Fe for Al in the octahedral sites.

6.5.2.3 Biotite

Biotites in sample 12382.8 were analysed and found to plot at a relatively low Mg number compared to analysis reported by Heithersay (1991, Figure 6.29). The analyses of Heithersay (1991) showed a clear separation between primary and secondary biotites

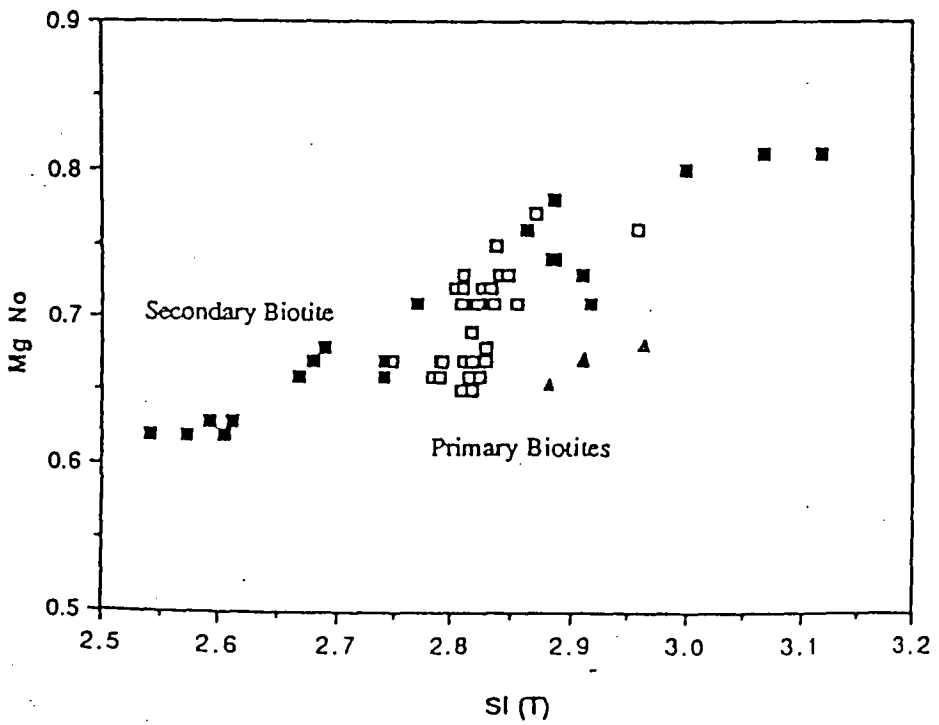

Figure 6.29 Comparison of biotite compositions with those obtained by Heithersay (1991). □ Primary Biotites (Heithersay, 1991), ■ Secondary Biotites (Heithersay, 1991), ▲ Secondary Biotites (this study, Appendix 2)

based on Si (tetrahedral site), Ti (octahedral site) and Mg number. The primary biotites cluster tightly, whereas the secondary biotites show more spread. The biotites analysed in this study are secondary, coming from altered volcanics, but plot closer to the primary biotites of Heithersay (1991).

6.6 DISCUSSION ON SULPHIDE PHASE RELATIONSHIPS

Cabri (1973) and Barnes (1979) noted that both bornite and chalcopyrite exhibit extensive solid solution of Cu, Fe and S at high temperatures (>600^{0}C) and probably also of gold (Cuddy and Kesler, 1982). These solid solution fields shrink with decreasing temperature such that below 547^{0}C, chalcopyrite is ordered (Barnes, 1979; Ramdohr, 1969). If any of these high temperature Cu-sulphide solid solutions contain appreciable amounts of gold, then gold will exsolve with cooling (Cuddy and Kesler, 1982). Bornite forms solid solutions with chalcocite and digenite to lower temperatures (<300^{0}C; Barnes, 1979). Chalcocite forms a solid solution with digenite (Ramdohr, 1969) though digenite is mainly formed at high temperatures (Ramdohr, 1969) and can contain appreciable amounts of Fe (Barnes, 1979). Chalcocite (hexagonal) is stable only below 435^{0}C (Barnes, 1979).

The petrographic and microprobe analysis at E26 (especially the lack of gold in chalcopyrite) suggests that chalcopyrite separated from a high temperature solid solution, leaving an intermediate high temperature bornite solid solution that contained gold. With further cooling, gold exsolved from bornite. The occurrence of gold in coexisting bornite and digenite/chalcocite grains suggests that gold exsolved before or during separation of the bornite-digenite solid solution.

Ramdohr (1969) notes that bornite is usually pinkish-brown to brown in colour, but tarnishes quickly to a violet-blue colour, particularly if intergrown with chalcocite. Cabri (1973) similarly notes that some bornite compositions tarnish quickly, resulting in three distinct colours (purple, blue & brown), two of which show significant compositional differences of the coloured surfaces. One might argue that the two bornite colour phases noted at E26 are simply the result of tarnishing, particularly given no

indication of major compositional differences. However, the following observations suggest that the colour distinction is a primary texture and not due to tarnishing;

i) the colours are constant even after repolishing

ii) the orange bornite/chalcopyrite and mauve bornite/chalcocite associations

iii) the two colour varieties occur together

iv) the varieties are spatially zoned, with the mauve variety occurring in high grade areas (ie. >1.5% Cu) in the deeper and middle parts of the system.

The compositions of the two bornite phases are constant throughout the orebody. This constant stoichiometry is probably achieved by the incorporation of excess Fe and S into chalcopyrite during cooling, and excess Cu into chalcocite.

6.7 SUMMARY

The current study has focused on veining and alteration associated with Stages 4 and 5 of Heithersay (1991) with which most of the copper mineralisation at E26 occurs. The pervasive and fracture-controlled potassic alteration and mineralisation of Stages 4 and 5 has led to the hematisation of Stage 3 magnetite. Stage 5 quartz veining is preceded by local sericitisation of QMP1. The mineralisation associated with Stage 5 veining can be subdivided into an early bornite-chalcopyrite phase (Stage 5A) and a latter bornite-chalcocite phase (Stage 5B). The sulphides of Stage 5A are similar to those associated with Stage 4 veins, however a distinction is made on the basis that the 5A sulphides are clearly associated with stockwork quartz veining and silica flooding.

There is a strong Au-bornite association at E26, with visible gold principally occurring in coarser bornite crystals in Stage 5 quartz veins. However, some areas of bornite mineralisation (e.g. above 9950mRL) contain little Au in comparison to deeper level bornite mineralisation. The bornite-chalcocite association (Stage 5B) which appears to be confined to the core of the mineralising system (i.e. within and immediately adjacent to QMP1) and to the middle and deeper parts of the system, has a similar pattern to the higher Au grades, although Au has been observed in both the orange-brown and mauve bornite phases. Electron microprobe analysis has shown no compositional variation between the bornite phases, or vertical zonation in compositions, which would explain

the distribution of Au at E26. No Au has been observed within chalcopyrite, suggesting Au remained in a high temperature bornite and/or bornite-chalcocite solid solution when chalcopyrite separated, exsolving later with further cooling. The occurrence of tellurides and selenides suggests that locally Te and Se saturation occurred.

Sericite alteration occurring with Stage 5 quartz veining at least partly postdates the veining. Replacement of bornite by chalcopyrite is probably related to the emplacement of QMP2 and slightly higher temperatures. Covellite replacement of bornite postdates the chalcopyrite replacement and indicates cooler, oxidised conditions, possibly related to carbonate, anhydrite/gypsum, sericite, epidote and chlorite associated with Stages 9 and 10 alteration and veining.

7. DISCUSSION ON THE CONTROLS OF GOLD DISTRIBUTION AT E26

7.1 RELATIONSHIP OF GOLD TO QUARTZ VEINING

There is a good correlation with depth between maximum Au assay values and the maximum number of quartz veins per interval (Figure 7.1). There is also a clear decrease in Au assay values with decreasing number of quartz veins out from QMP1 (Figure 7.2). Cu shows a similar lateral correlation with quartz veins abundances, but there are slight discrepancies vertically in the location of the peaks in the maximum Cu assays and the maximum number of quartz veins (Compare Figure 5.6 and Figure 7.2).

Scatterplots of Au versus number of quartz veins per interval are not as well structured. This is thought to be because vein width is not incorporated into the veins per interval data. Unfortunately, vein thickness data is not available to the author. The correlation of the maximum Au peaks and the maximum number of quartz vein peaks (Figure 7.2) suggests that vein intensity (measured in terms of vein number and thickness) is an important consideration. Dense quartz veining in the so called 'silica zone' in the lower and middle levels of the system, is Au-rich with an almost 1:1 Cu/Au ratio (Figure 5.14). However in the upper levels, the 'silica zone' is relatively low in Au (5-10:1 Cu/Au ratio; Figure 5.14) despite no obvious differences in vein density, style or composition.

This study agrees with the findings of Heithersay (1991) who found that Au is closely associated with Stage 5 veins (i.e. quartz stockwork veins). However Heithersay's observation that areas of low Au with high Cu are due to the absence of Stage 5 veins and presence of Stage 4 veins, is contradicted by the current study, which has shown that the zones of high Cu but low Au (Domain 4) do contain Stage 5 veins. The presence of Stage 5 veins may give hope of good Au grades but is not definitive.

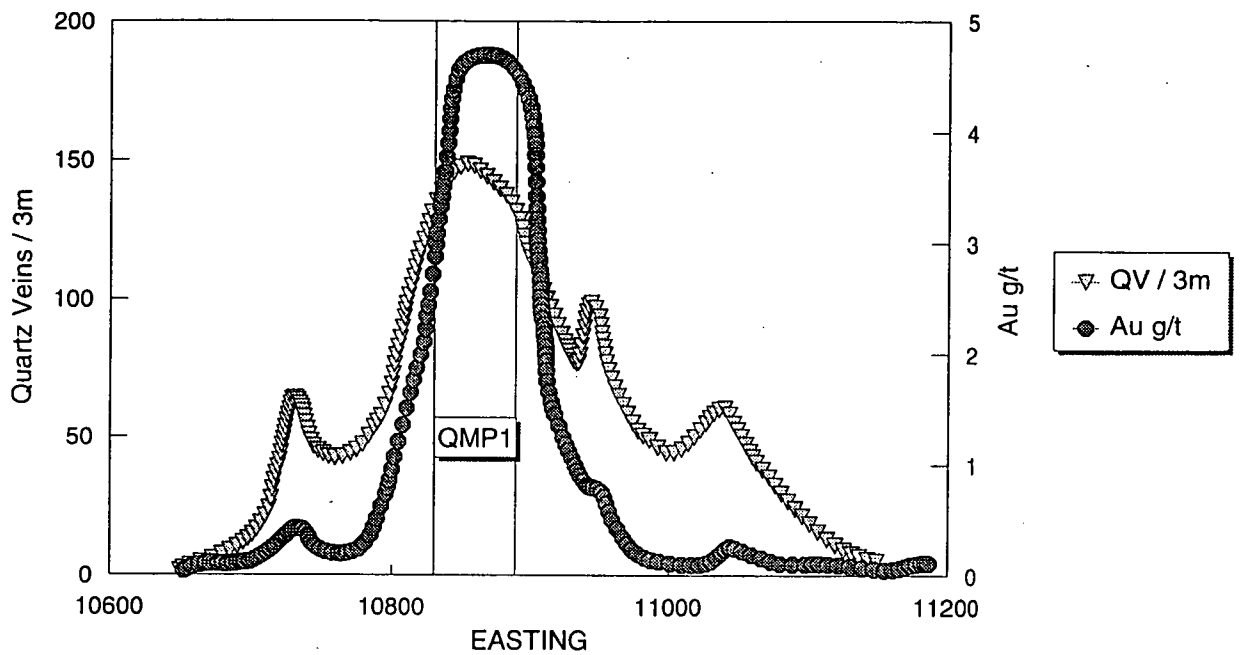

Figure 7.1 Envelope of maximum gold grades and quartz veins/3m showing the lateral variation.

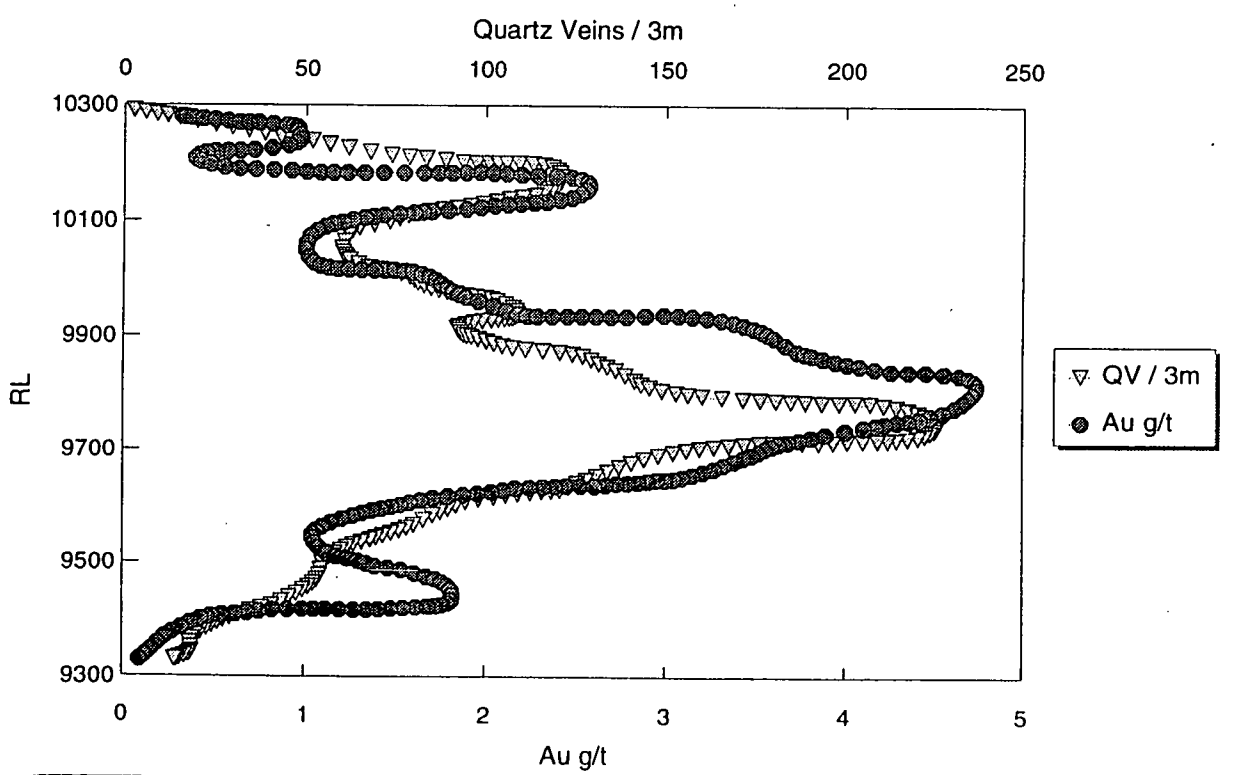

Figure 7.2 Envelope of maximum gold grades and quartz veins/3m showing the vertical variation.

7.2 RELATIONSHIP OF GOLD TO MAGNETITE

One of the characteristics of many Au-rich porphyry Cu deposits from around the world is a Au-magnetite association (Sillitoe and Gappe, 1984; Sillitoe 1990). Magnetite is commonly associated with biotite and forms during potassic alteration (e.g. Sillitoe and Gappe, 1984).

At E26, early potassic alteration is characterised by a biotite-magnetite assemblage (Stage 3). However, the main potassic alteration event (K-feldspar alteration) is magnetite destructive and is associated with most of the Cu and Au mineralisation (Stages 4 and 5). An annular pattern of magnetite occurs at E26, with a magnetic high around the orebody corresponding to Stage 3 alteration, and a magnetic low within the orebody corresponding to Stages 4 and 5 (Figure 7.3). The strongest zone of magnetite development is to the west of E26. Mapping of underground development has shown this magnetite alteration to extend at least 300m west of QMP1 as fracture controlled veinlets and disseminations. In cross-section, the area of greatest magnetite destruction is above 9600mRL (Figure 7.4).

The frequency histogram of magnetite (Figure 7.5) shows a classic bimodal log normal distribution. The higher population is related to Stage 3 biotite-magnetite alteration, while the lower population is related to the overprinting, magnetite-destructive Stages 4 and 5 potassic alteration. This relationship is reflected in the scatterplot of Au versus magnetite, where higher Au grades are associated with low magnetite, and high magnetite content is accompanied by low Au grades (Figure 7.6). Below 9600mRL, however, the scatterplot of magnetite versus Au (Figure 7.7) shows no evidence of this relationship.

7.3 RELATIONSHIP OF GOLD TO OTHER ALTERATION

High grade Au and Cu mineralisation is strongly correlated with K-feldspar alteration. Au contents of 0.2-0.25g/t correspond closely to the limits of the 'Outer K-feldspar Subzone' around QMP1 as defined by Heithersay (1991). In contrast, there is no relationship between Au distribution and the limits of the 'Outer Biotite K-feldspar Subzone'.

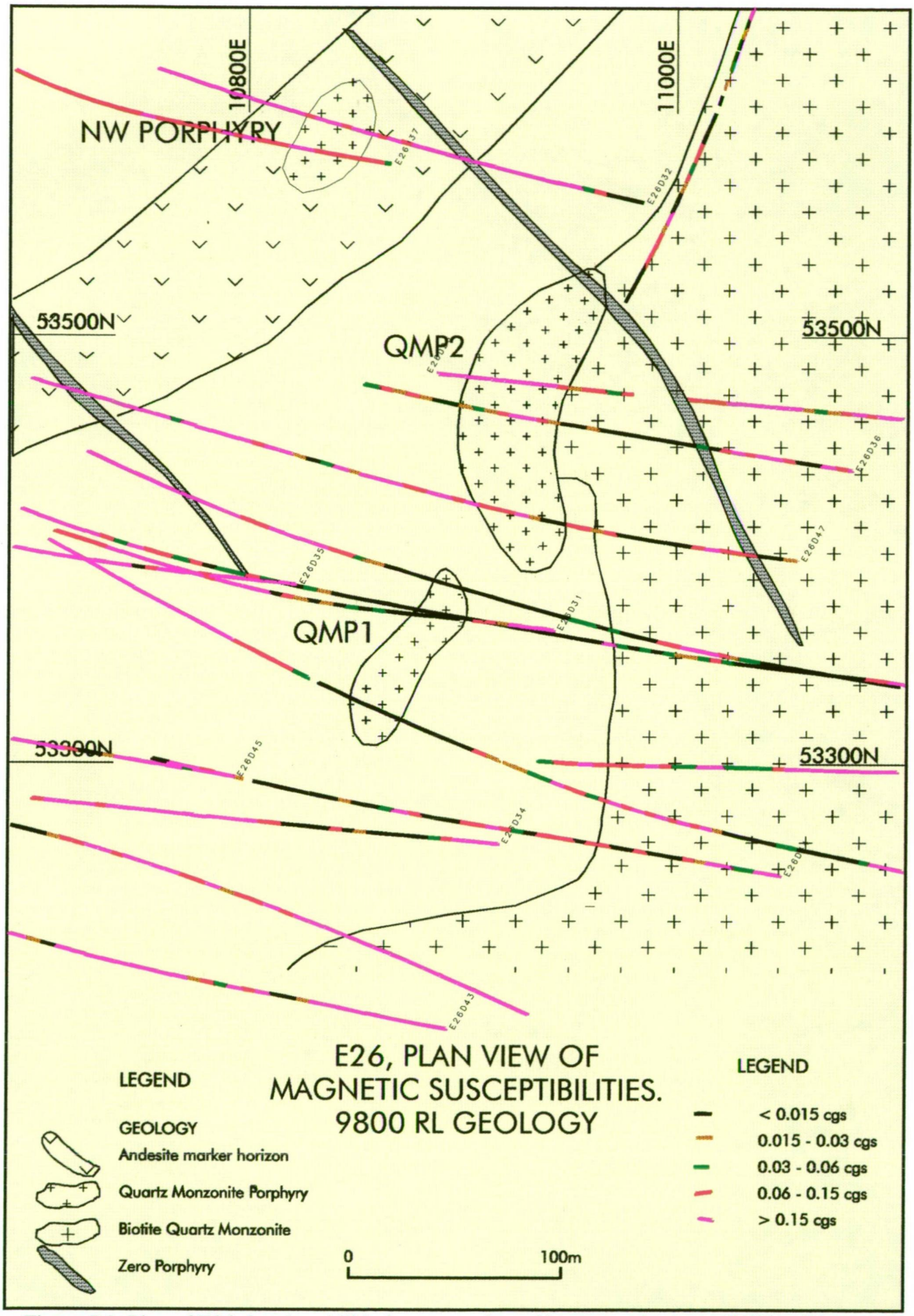

Figure 7.3 Plan of E26 showing drill hole traces coloured by magnetic susceptibilities. Pink traces to the west and south of E26 show magnetite enrichment due to Stage 3 alteration. Black traces around QMP1 reflect magnetite destruction during stage 4 and 5 alteration and veining.

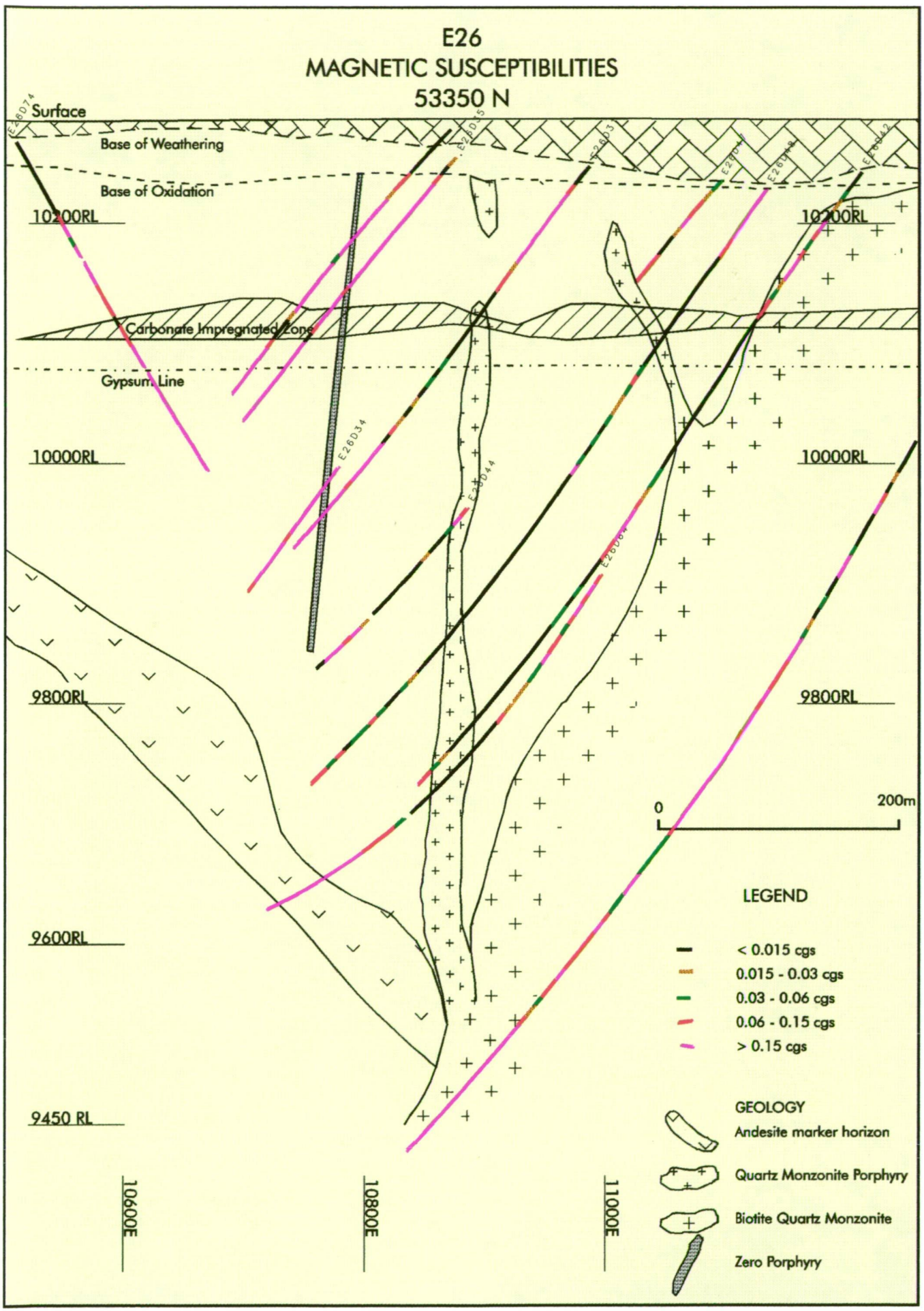

Figure 7.4 Cross section of E26 showing drill hole traces coloured by magnetic susceptibilities. Pink traces to the west of E26 reflect magnetite enrichment due to stage 3 alteration, while black traces near QMP1 reflect magnetite destruction by stage 4 & 5 alteration and veining.

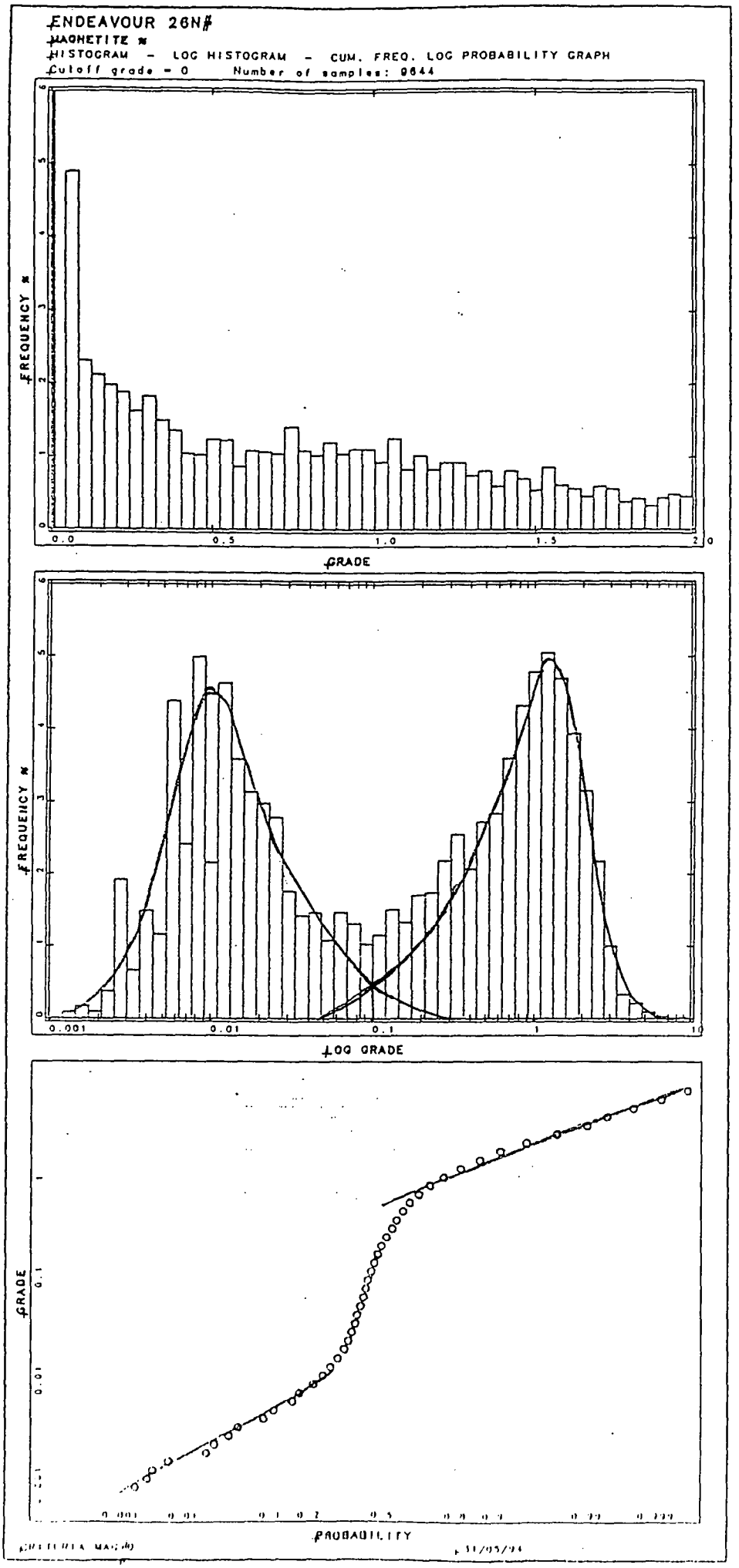

Figure 7.5 Frequency histograms and log probability plot of percentage magnetite in the rock.

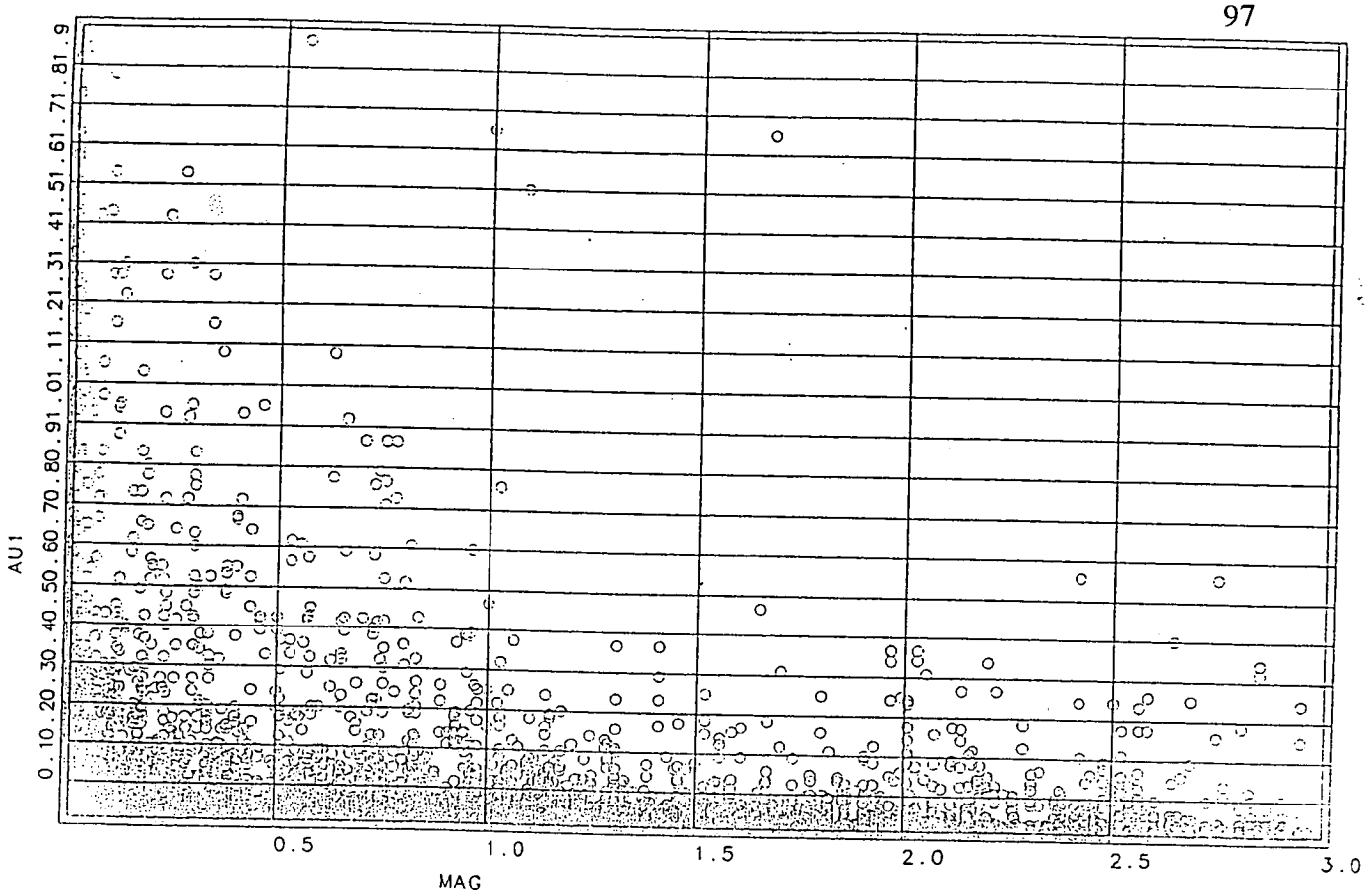

Figure 7.6 Bivariate scatterplot of Au versus percentage magnetite.

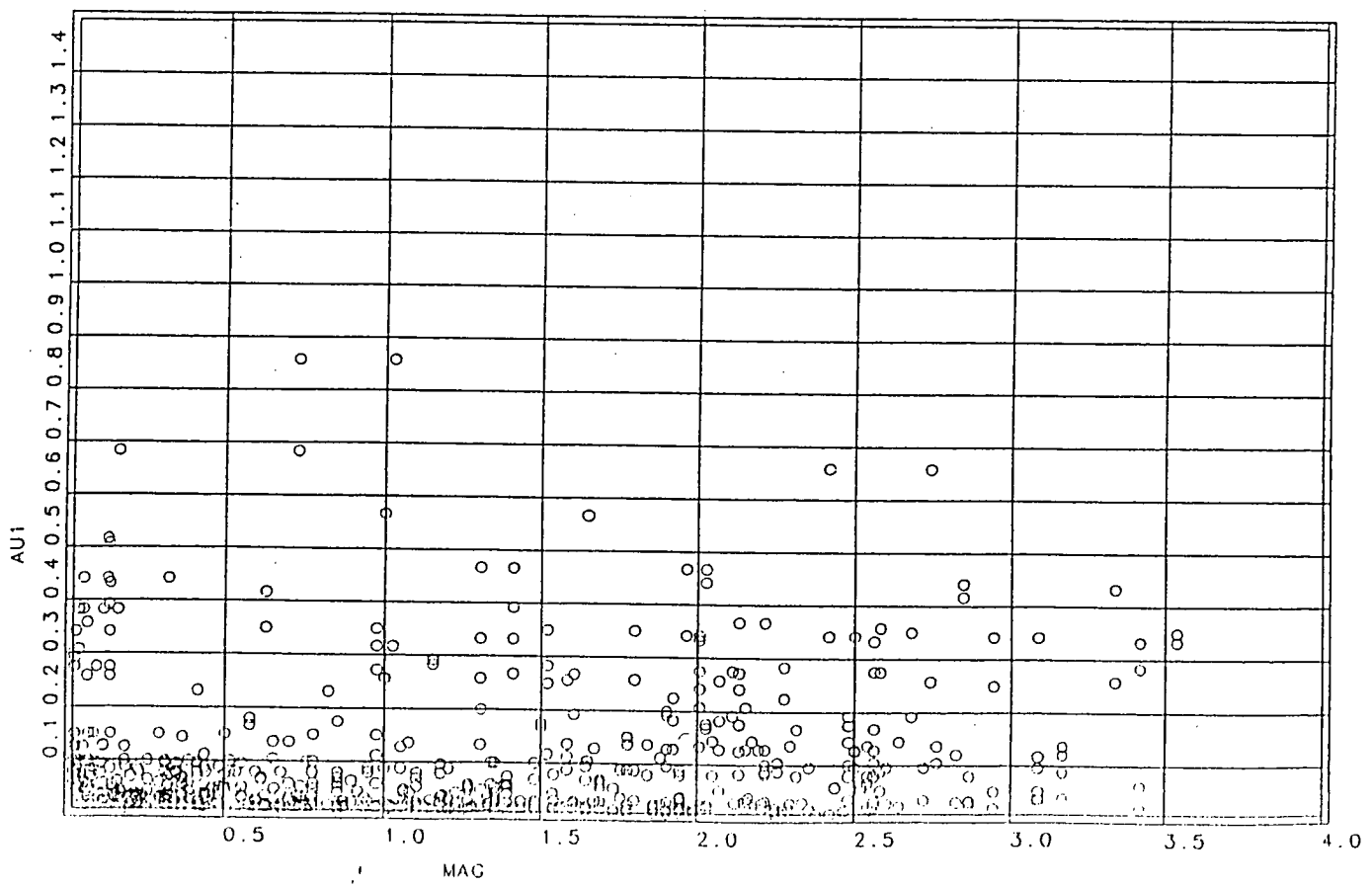

Figure 7.7 Bivariate scatterplot of Au versus percentage magnetite below 9600mRL.

No obvious spatial or petrographic relationship between Au distribution and sericite alteration can be discerned at E26. Sericite alteration is most strongly developed within and adjacent to the 'silica zone', which contains high Au grades (>2g/t) in the middle parts of the system, or low grades in the upper part of the system. In the upper Au-poor zone (Cu/Au Domain 4; Figure 5.15) Au grades are generally highest within the 'silica zone', where sericite alteration is strongly developed.

7.4 SPATIAL DISTRIBUTION OF GOLD AROUND QMP1

Another consideration on the controls of Au distribution at E26 is its spatial distribution about QMP1. This is highlighted particularly by the scatterplots of Au and Cu/Au ratio with easting (Figure 7.1 and 5.13 respectively). In section, Au deposition is seen to have been concentrated immediately above the level at which QMP1 breaks out from the confines of the biotite quartz monzonite (Figure 5.3). In contrast, Cu is not so tightly constrained about QMP1, or within the lower and central parts of the system. It is interesting to note that aspect ratios between zones defined by the same values of Au(g/t) and Cu(%) are similar, suggesting similar lateral and vertical controls on the Cu/Au relationship.

7.5 SUMMARY

The distribution of Au at E26 is tightly confined about QMP1, and the middle and deeper parts of orebody. Gold principally occurs in bornite and shows a strong lateral and vertical correlation with Stage 5 quartz veining. A negative correlation occurs between Au and magnetite, indicating that Au is also associated with the hematisation of Stage 3 magnetite, which occurred during Stages 4 and 5 potassic alteration and veining. A weak Au association occurs with distal, structurally controlled quartz-sericite-pyrite alteration.

8. COMPARISON WITH OTHER DEPOSITS AT GOONUMBLA

8.1 GEOLOGY AND CU/AU RELATIONSHIPS AT E22 AND E27

8.1.1 Summary Geology of E22 and E27

Detailed accounts of the geology, alteration and mineralisation of E22 and E27 are provided in Jones (1985) and Heithersay et al. (1990). Squires (1992) also described E27. E22 is located approximately 4km NW of E26 and 1km west of E27 (Figure 1.2). Mineralisation at E27 is associated with multiple intrusions of quartz monzonite porphyries, which have combined to form a pipe-like intrusive body (Figure 8.1) which is significantly larger in plan dimensions (100m x 250m) than the finger-like intrusions at E22, E26 and E48. At E22, mineralisation clusters around several small finger-like intrusions which are structurally controlled (Figure 8.2).

The volcanic rocks at E27 are interpreted by Squires (1992) to have been andesite-basaltic andesite flows and lesser volcaniclastics prior to K-silicate alteration. At E22 pyroclastics and volcaniclastics are interbedded within the trachyandesitic flows.

Potassic alteration at E22 and E27 is dominantly fracture-controlled and is characterised by K-feldspar and lesser biotite and albite. Pervasive alteration is only developed in spatially restricted zones, in contrast to E26 (Heithersay et al., 1990). Quartz and (in contrast to E26) calcite veins are strongly developed whereas gypsum and anhydrite veins and alteration do not occur. An outer zone of propylitic alteration around E22 and E27 contains carbonate, epidote and chlorite but only minor pyrite (in contrast to E26). A distinct magnetic high encircles E27 in the intermediate mineralised areas (i.e. <1% Cu), with a low 50-70m to the east of the main mineralised area (Figure 8.3). This low corresponds to peripheral low grade mineralisation in one of the monzonite phases. Although magnetite destruction does occur at E27 (fracture-controlled) the location of the magnetic low suggests that it is largely attributable to the intrusion of magnetite-poor QMPs, than destruction of magnetite by hydrothermal fluids.

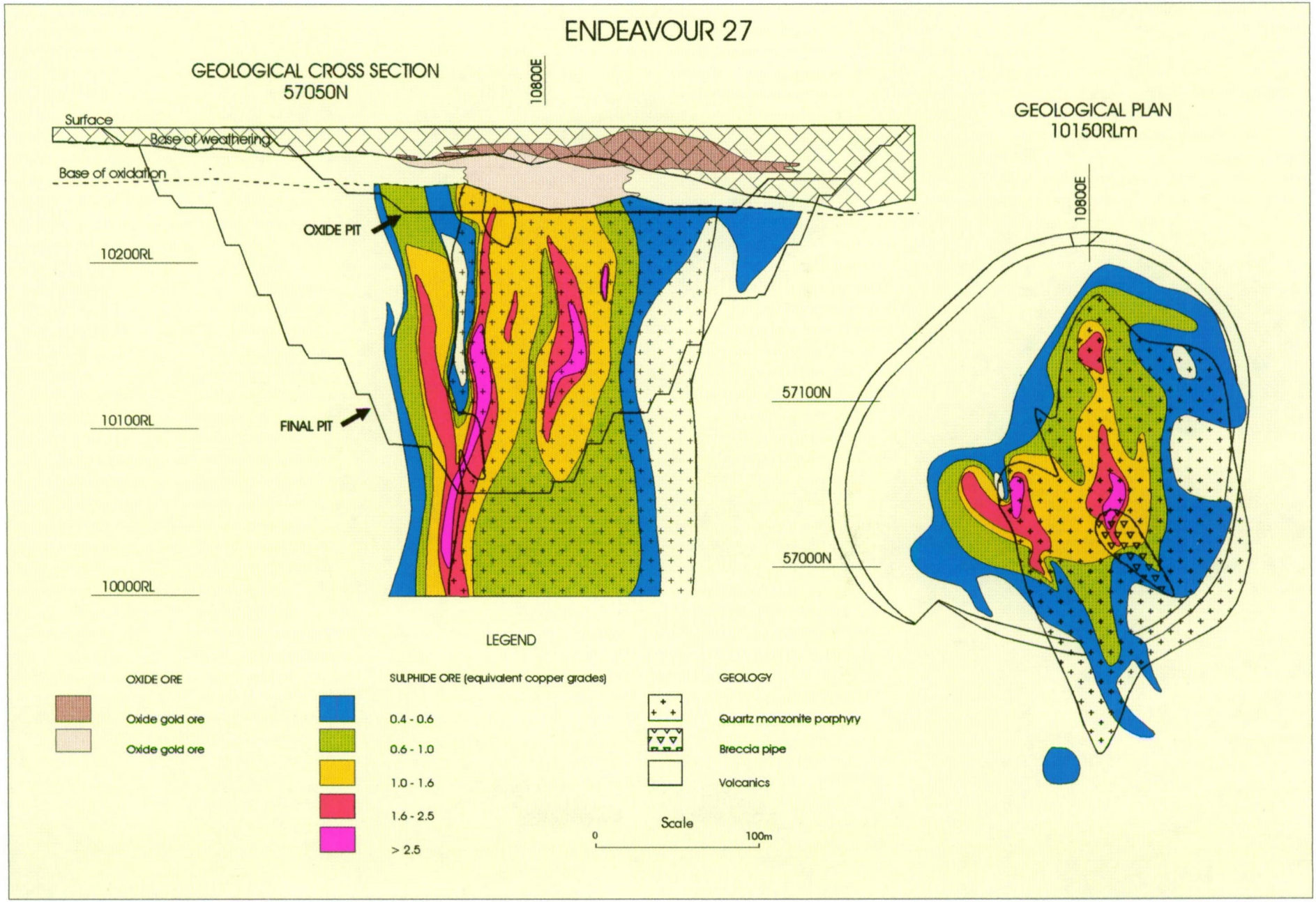

Figure 8.1 Geology and mineralisation distribution at E27 (compiled Northparkes staff, 1994).

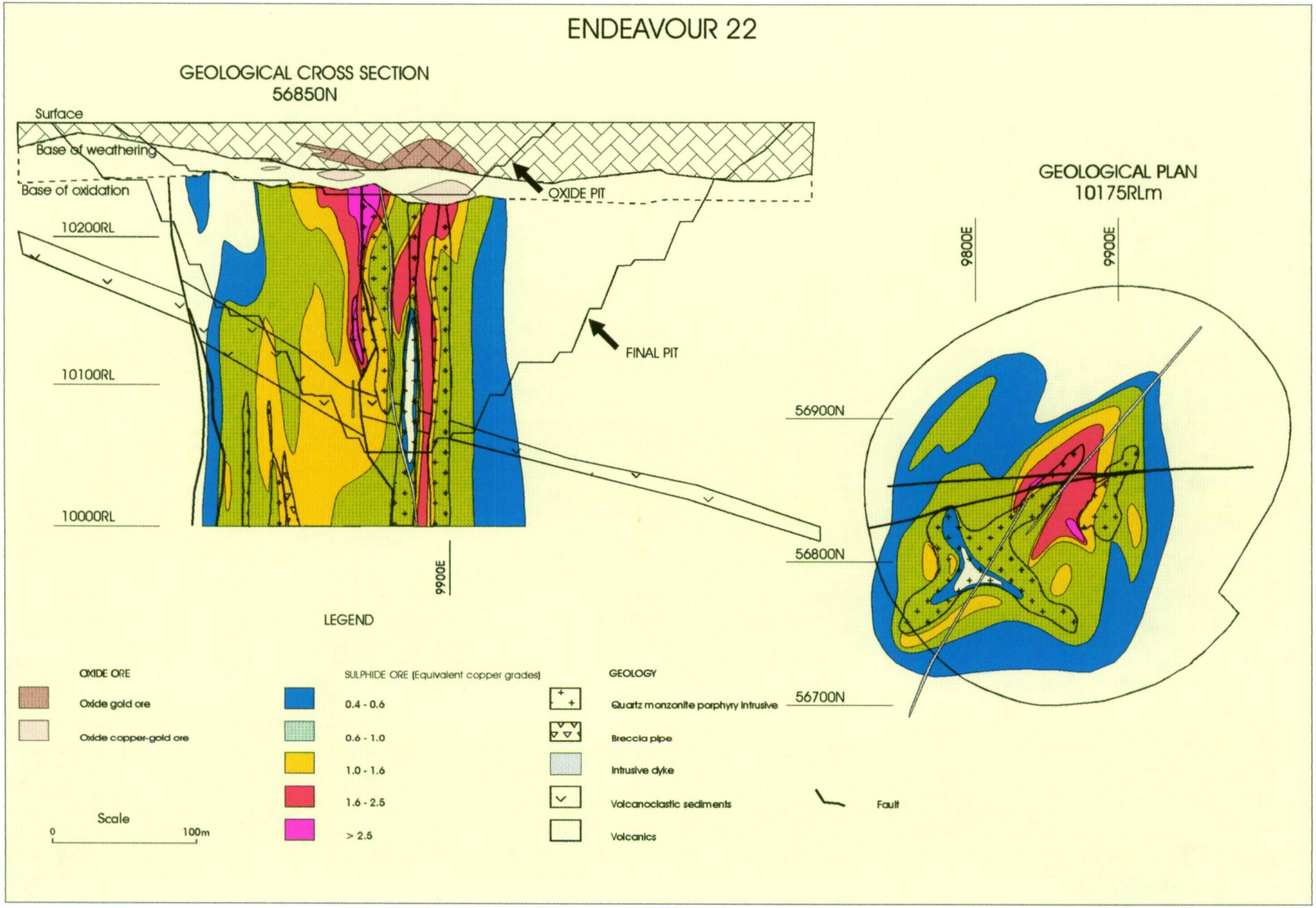

Figure 8.2 Geology and mineralisation distribution at E22 (compiled Northparkes staff, 1994).

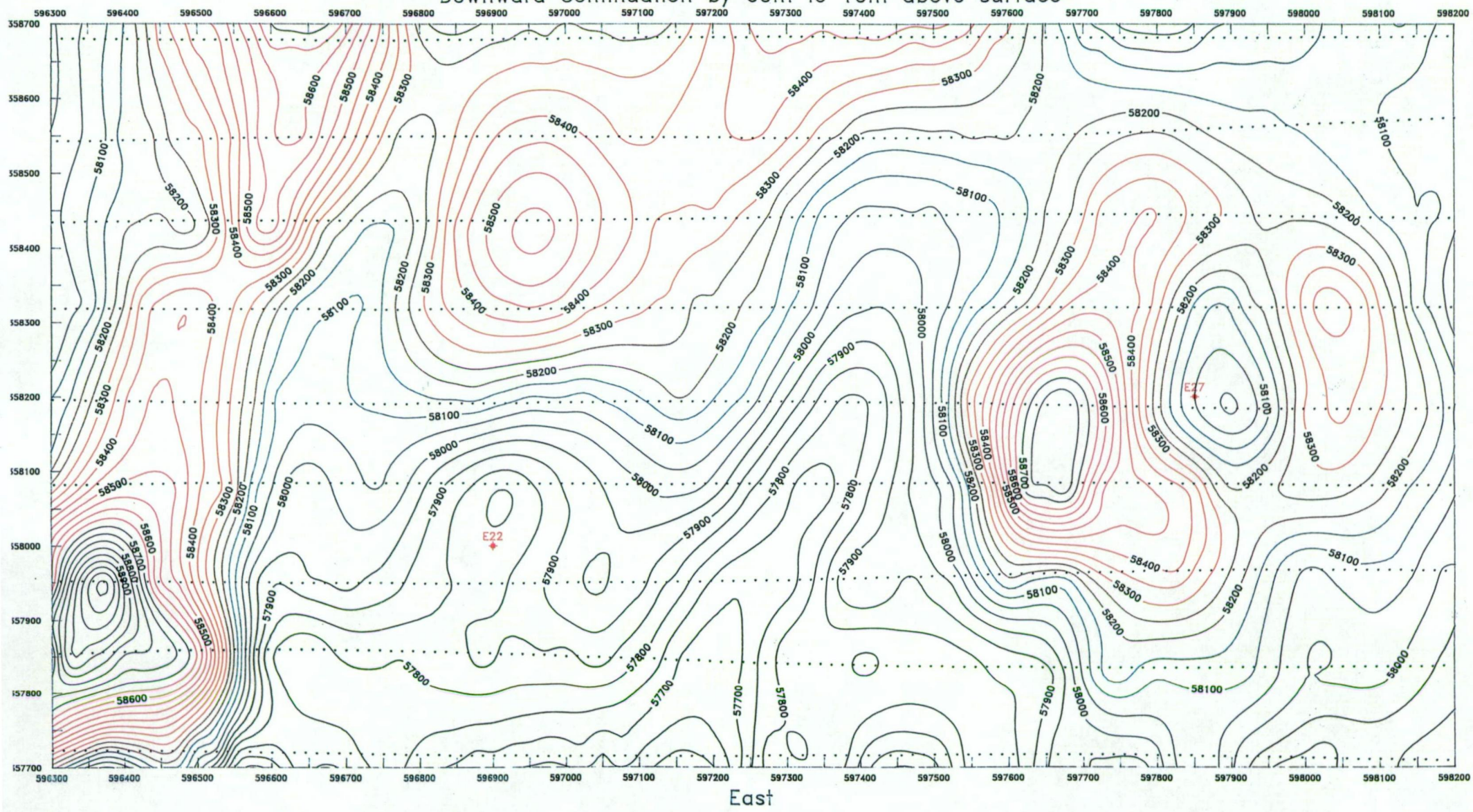

Figure 8.3 E22 and E27 aeromagnetics - downward continuation by 60m - drawn M. Hannington, North Exploration, 1993.

Volumetrically small breccia pipes occur at both E22 and E27. The breccia pipe at E27 contains monzonite fragments healed by quartz, carbonates and accessory minerals including Cu sulphides (Heithersay et al., 1990).

Mineralisation is dominantly vein and fracture controlled with lesser disseminations. Bornite dominates in higher grade areas, while chalcopyrite is dominant in the marginal and lower grade peripheral areas (Heithersay et al., 1990). Two or three varieties of bornite at E22 and E27 have been noted based on colour in unpublished petrological work for Geopeko. As at E26, a purple (mauve) phase is associated with chalcocite and the more-abundant orange-brown phase tends to be associated with chalcopyrite. Both chalcopyrite and chalcocite can occur as exsolution lamellae in bornite. Au occurs as fine blebs <5 microns in size within and rimming bornite grains (Heithersay et al., 1990). There is a strong Au/bornite association, with Au grades decreasing rapidly where chalcopyrite becomes dominant.

Plan dimensions at the 0.4% eCu contour are 270m x 200m at E22 and 240m x 180m at E27. Higher grade zones (i.e. >1.6% eCu) within both deposits are small and poddy in nature.

8.1.2 Cu/Au relationships at E22 and E27

Summary statistics for both Au and Cu in E22 and E27 are given in Table 8.1. Average Au grades for both E22 and E27 are significantly higher (2-3 times) than E26, whereas the average Cu grade is nearly half that at E26.

Bivariate Cu/Au scatterplots for E22 and E27 (Figures 8.4 and 8.5) are similar to each other, but distinct from the scatterplot for E26 (Figure 5.9). The Cu/Au ratio for both E22 and E27 deposits is approximately 1:1. The Cu/Au ratio, however, varies from low Au grade areas (ratio 5-10) to <1 in areas of high Au grades (>2.5g/t). Only a weak spatial zonation of Cu/Au ratios is apparent, with the highest values occurring on the peripheries of the mineralising systems. There is no clear vertical zonation in Cu/Au ratios.

Gold g/t	E26	E22	E27	E31N	E48
Max.	10.5	32.86	34.9	5.63	23.8
Mean	0.16	0.37	0.46	0.46	0.24
Variance	0.41	0.66	0.77	0.63	0.44

Copper %	E26	E22	E27	E31N	E48
Max.	8.1	6.35	13.5	1.55	7.46
Mean	0.71	0.49	0.48	0.19	0.57
Variance	0.81	0.44	0.49	0.18	0.65

Table 8.1 Summary Statistics for the major Goonumbla deposits

Similarities to E26	E27	E22	E48
Intrusions Type	- QMP	- QMP	- QMP
Shape		- Finger-like	- Finger-like
Alteration	- Early biotite/magnetite - Later hematisation of magnetite		- Early biotite/magnetite - Later hematisation of magnetite
Mineralisation	- Bornite dominant - 2 bornite phases - Sulphide zonation	- Bornite dominant - 2 (3) bornite phases - Sulphide Zonation	- Bornite dominant - Sulphide Zonation
Cu/Au ratio			- Decreasing Cu/Au with increasing grade - Vertical zonation.

Differences from E26	E27	E22	E48
Host Lithologies	- Basaltic Andesites	- Basaltic Andesites	- Includes volcanic sandstones
Intrusions	- Multiple, Overprinting		
Alteration/Veining	- K-feldspar alteration weaker and fracture controlled - No gypsum/anhydrite - Carbonate Veining - Breccia Pipe - More magnetite	- K-feldspar alteration weaker and fracture controlled - No Gypsum/Anhydrite - Breccia Pipe	- Strong late sericite-carbonate-albite in QMP's - Little K-feldspar - No gypsum veining - Composite quartz/ carbonate veins
Mineralisation	- Weak Pyrite Halo	- Weak Pyrite Halo	- Late tetrahedrite/tennantite
Cu/Au Ratio	- Approx 1:1 Cu/Au ratio	- Approx 1:1 Cu/Au ratio	- Lacks high copper / low gold association

Table 8.2 Comparison of major Goonumbla deposits with E26

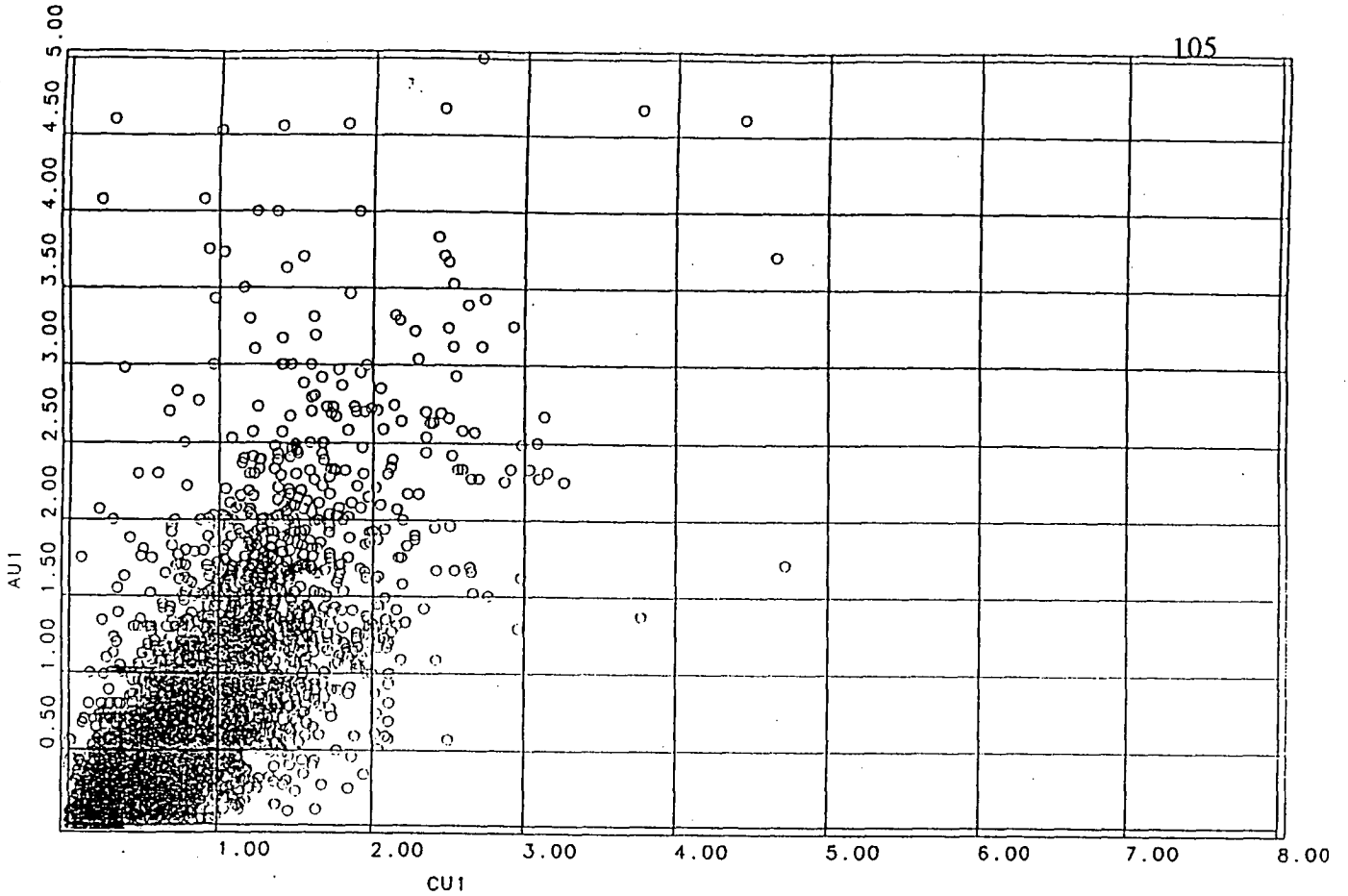

Figure 8.4 Bivariate scatterplot of Au versus Cu at E22.

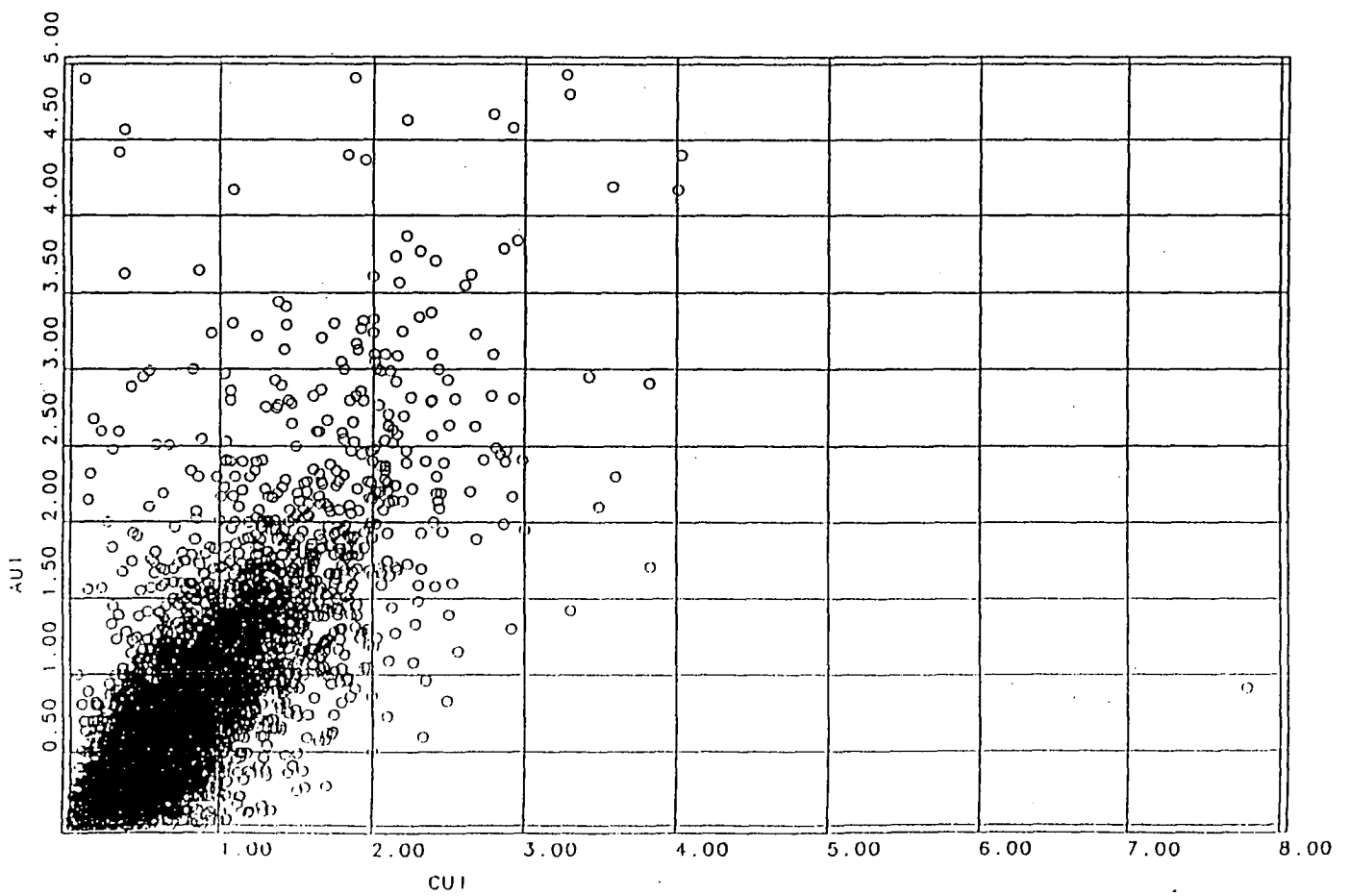

Figure 8.5 Bivariate scatterplot of Au versus Cu at E27.

8.2 GEOLOGY AND CU/AU RELATIONSHIPS AT E48

8.2.1 Summary Geology

The geology of E48 has been updated by Wolfe (1994), but is not available to the author at the time of writing. This geological summary is taken from Hooper et al. (1994). The Endeavour 48 (E48) deposit is located approximately 2km north of E26. The top of the deposit is truncated by a shallow ESE-dipping fault and hence 'blind' at surface. Quartz monzonite porphyries have intruded a mixed sequence of lava flows, breccias and mass flows with interbedded thick (up to 120m) volcanic sandstone units. At least four quartz monzonite porphyry pipes with plan dimensions of 10m x 15m to 20m x 70m have been identified. These are thought to coalesce and broaden with depth (Figure 8.6). The largest QMP pipe is continuous for at least 740m vertically. The deposit is bounded below by a biotite quartz monzonite thought to be equivalent to the E31 stock.

Alteration is centred on the QMP's. An early pervasive biotite-magnetite ± K-feldspar alteration assemblage is overprinted by a patchy biotite-carbonate-sericite-albite-hematite ± K-feldspar assemblage and stockwork quartz veining with which the highest Cu mineralisation occurs. In some areas of the QMPs, this assemblage is overprinted by pervasive sericite-carbonate-albite alteration with associated disseminated Cu mineralisation which is high in arsenic. No intense K-feldspar alteration occurs at E48. Structurally controlled sericite-carbonate-quartz ± pyrite zones are common.

Mineralisation is zoned from an outer pyrite halo through a chalcopyrite zone to a bornite-rich core. Mineralisation associated with quartz veining and fractures is dominantly bornite with lesser chalcopyrite, chalcocite, covellite and digenite. Late disseminated mineralisation related to sericite alteration is dominated by bornite and tennantite/tetrahedrite.

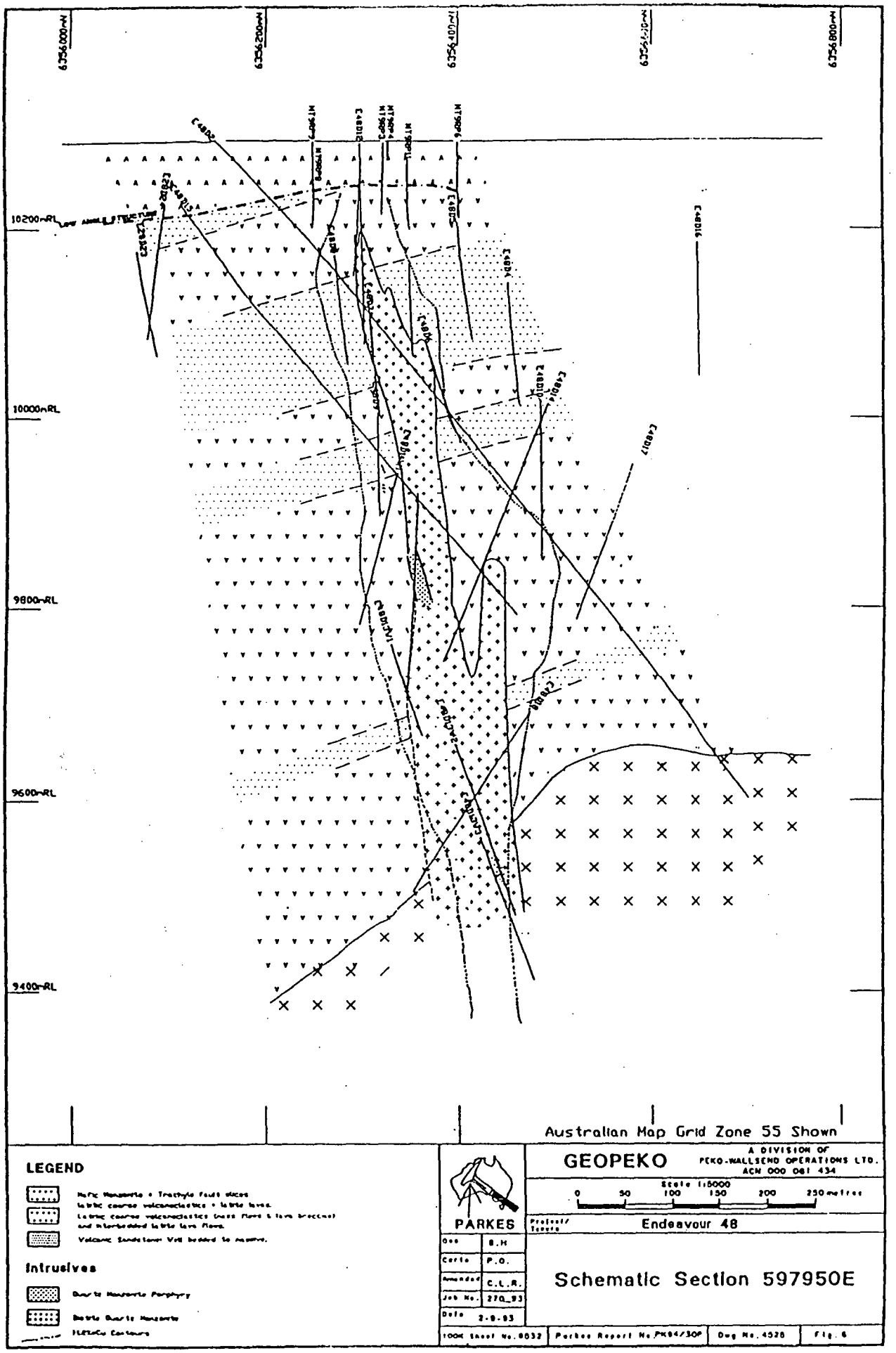

Figure 8.6 Geological cross-section of the E48 deposit (From Hooper et al., 1994).

8.2.2 Cu/Au relationships

Summary statistics for E48 are given in Table 8.1. The means for both Cu and Au are similar to E26. The Cu and Au distributions at E48 are similar to the middle and deeper parts of E26 (Figure 8.7). Cu/Au ratios approach unity with increasing Au grade (Figure 8.8). Unlike E26 however, there is no strong domainality in the Cu/Au ratios.

A clear spatial zonation occurs in the Cu/Au ratio with increasing values laterally away from the orebody (Figure 8.9). Like E26 there is also a clear vertical zonation in Cu/Au ratios, with the lowest Cu/Au ratios below 9900mRL (Figure 8.9).

8.3 GEOLOGY AND CU/AU RELATIONSHIPS AT E31N

The Endeavour 31 North deposit is located on the northern margin of the E31 stock. It is hosted by a sequence of porphyritic lavas which are intruded by narrow quartz monzonite dykes (Harbon and Dunn, 1994). The mineralisation is related to the QMP dykes, and is dominantly chalcopyrite with lesser bornite, occurring on fractures and in fine quartz veins associated with potassic alteration, dominantly biotite. The mineralisation is anomalously Au-rich, with Au grades significantly exceeding Cu grades (Table 8.1). Cu and Au grades do show a positive correlation (Figure 8.10) but the Cu/Au ratios are very low when compared to other deposits in the area.

8.4 DISCUSSION

8.4.1 Comparison with other Goonumbla Deposits

Compared to E22, E27 and E31N, E26 and E48 are copper-enriched, and gold-depleted. The summary comparison of the deposits (Table 8.2) shows that K-feldspar alteration (plus quartz, hematite and sulphides) at E22, E27 and E31N is dominantly fracture controlled, and not pervasive as at E26. Magnetite destruction occurs at E22 and E27, however due to the fracture-controlled nature of the alteration, it is not as strongly developed as at E26 and E48. The magnetic low to the immediate east of E27 is related more to the presence of magnetite-poor QMPs, than magnetite destruction associated with

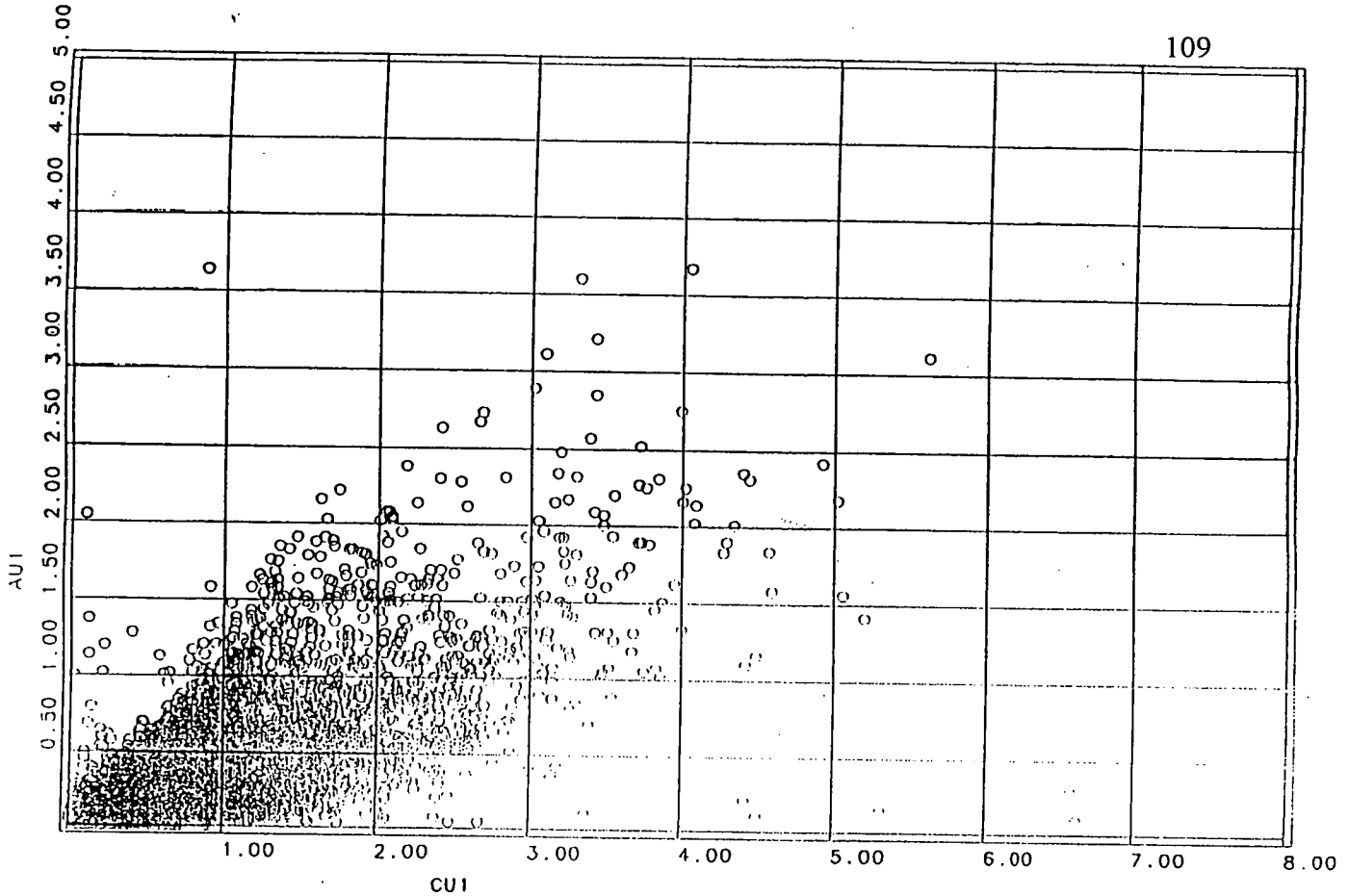

Figure 8.7 Bivariate scatterplot of Au versus Cu at E48.

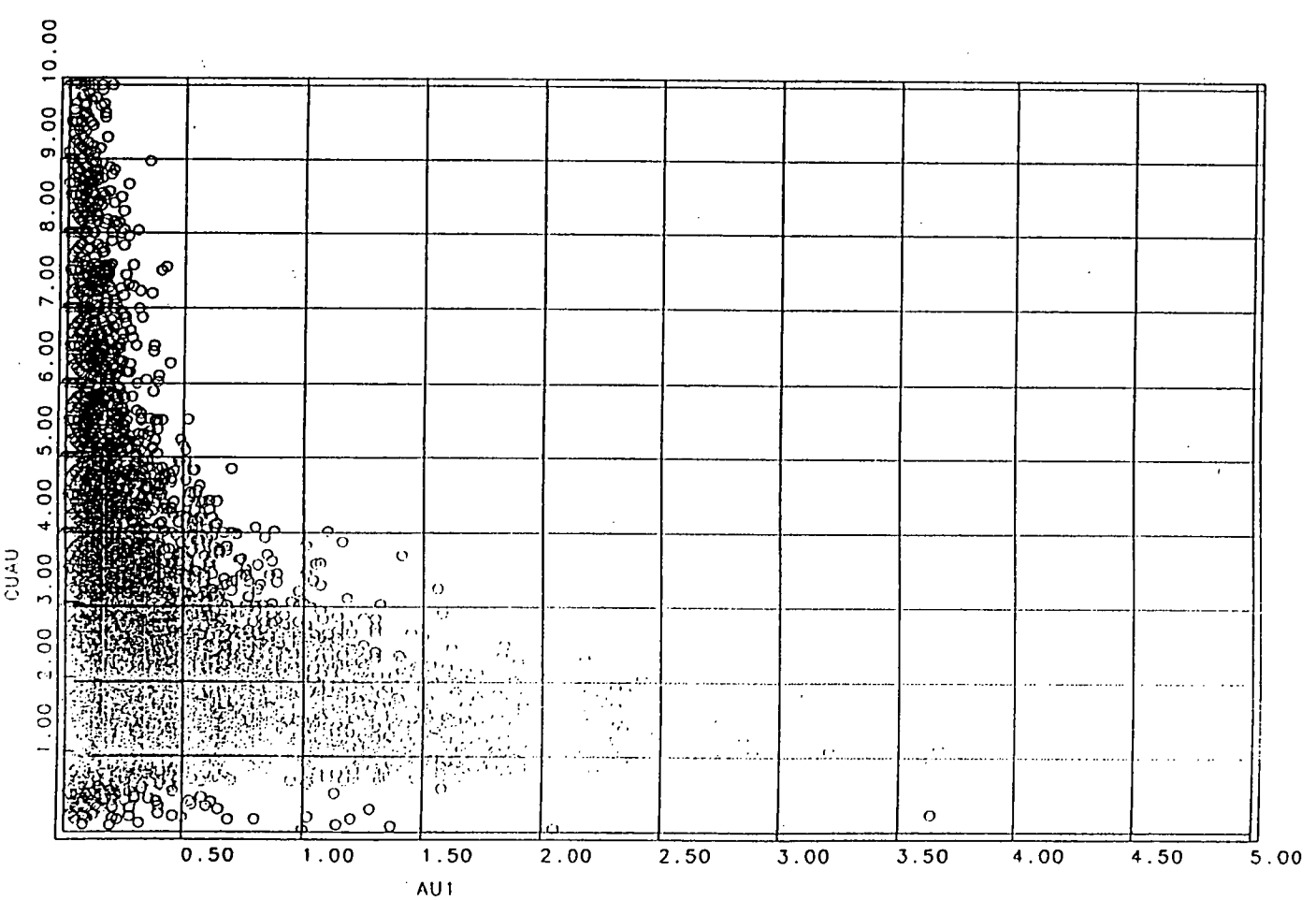

Figure 8.8 Bivariate scatterplot of Cu/Au ratio versus Au at E48.

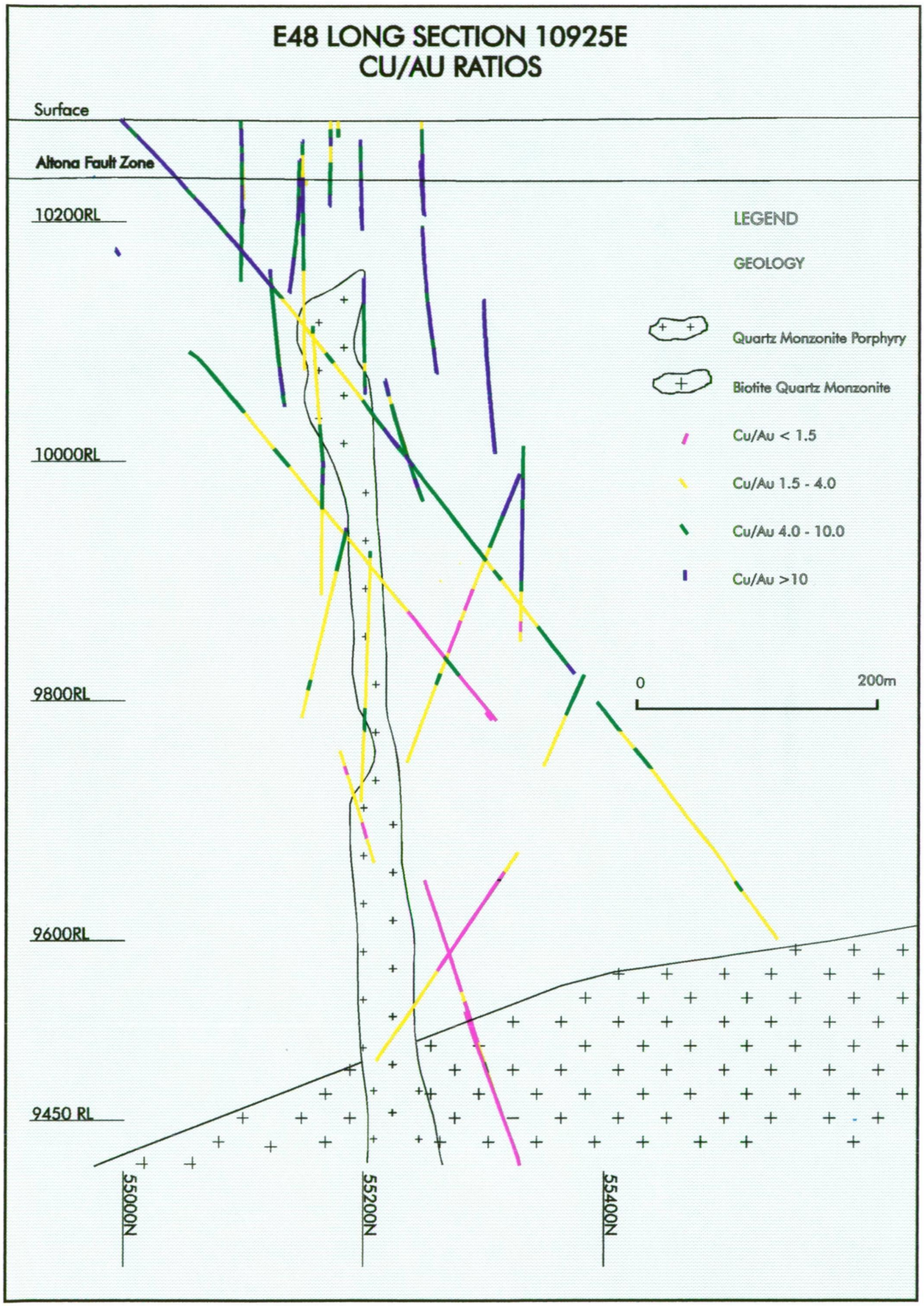

Figure 8.9 Long-section at E48 showing drill hole paths colour coded by Cu/Au ratios. A vertical and lateral zonation in the Cu/Au ratio occurs.

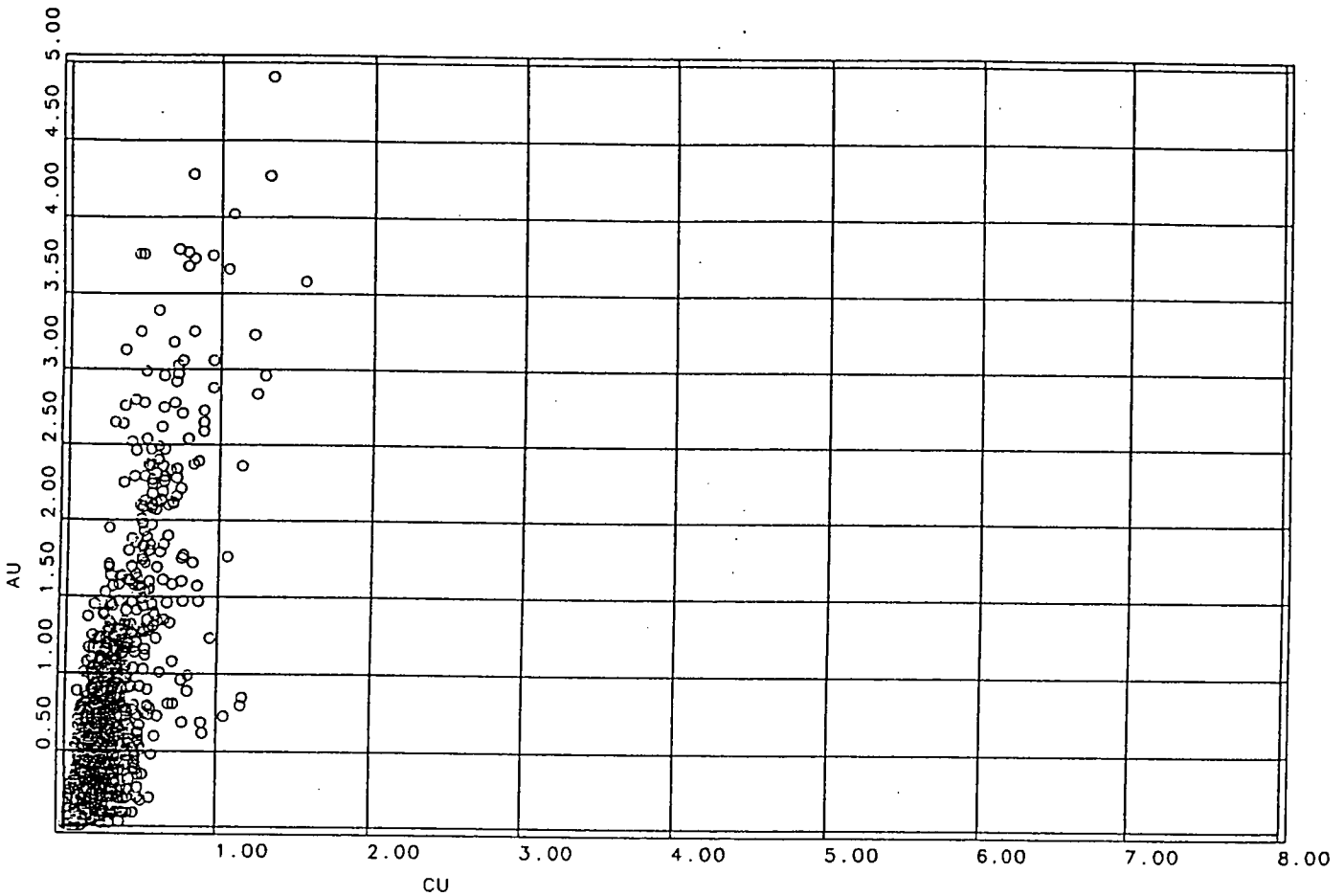

Figure 8.10 Bivariate scatterplot of Au versus Cu at E31N.

hydrothermal alteration. Furthermore, there is no documented magnetite destruction at the Au-rich E31N deposit. The fracture-controlled alteration at E22 and E27 suggests limited interaction between the wall rocks and the fluids. This comparison on the extent of magnetite-destructive potassic alteration suggests that Cu-enrichment within a particular deposit in the Goonumbla region is favoured by hematisation of magnetite. Differing changes in the Au and Cu solubilities may have also contributed to Au-enrichment at E22 and E27.

The exposure levels of the Goonumbla deposits are different. Both E22 and E27 are eroded orebodies, with only the deeper parts of the original mineralised system now preserved. Gold occurrences at E26 and E48 are greatest (and hence Cu/Au ratios lowest) in the middle and deeper parts of the system; while magnetite destruction is weakest in the deeper parts of E26. This is consistent with the magnetite destruction and gold concentrations at E22 and E27, suggesting a correlation with the level of exposure.

Cu/Au ratios of the parent fluids may also have been a controlling factor on the differing metal proportions between the Goonumbla deposits. The Cu/Au ratio in the parental fluids can be changed by sulphur saturation, resulting in the incorporation of Cu into early-formed Mg-Fe silicates, and decreasing the Cu/Au ratios of the remaining fluids. This early removal of copper may also have led to relative gold enrichment in the mineralising fluids responsible for the deposits of E22, E27 and E31N.

8.4.2 Comparison with other Porphyry Cu-Au Deposits

Gold and copper correlate closely in the potassic alteration zones of many porphyry Cu deposits: e.g. Granisle and Bell (Cuddy and Kesler, 1982); Panguna (Clark, 1990); Batu Hijau (Meldrum et al., 1994); and Grasberg (Kavalieris, 1994). Au often occurs in association with bornite (Sillitoe, 1990) and usually in potassic assemblages dominated by biotite and magnetite (Sillitoe, 1979; Sillitoe and Gappe, 1984; Clark, 1990). Cu/Au ratios vary between, and within deposits, but are usually constant within mineralised zones, reflecting coprecipitation (Thompson, 1994). Au and Cu contents decrease with depth at Panguna, but a constant Cu/Au ratio is maintained (Clark, 1990). Of the alkalic porphyry Cu-Au deposits in British Columbia, Galore Creek and 66 Zone at Mount

Milligan, show a strong zonation in Cu/Au ratios, suggested to be the result of variations in physiochemical conditions within a single episode of hydrothermal alteration (Galore Creek), or due to a second Au-enriched episode of hydrothermal alteration (Mount Milligan, Lang et al. in Thompson, 1994). Within the highest grade zones at Grasberg Cu/Au ratios are <1. The 1% Cu limit extends about 100m laterally beyond the 1g/t Au limit (Kavalieris, 1994) suggesting Cu/Au ratios >1 and a lateral zonation in Cu/Au ratios. At Batu Hijau, both metals increase with depth, but Au more markedly than Cu, such that a Cu/Au ratio of 2:1 250m below the surface decreases to 1:2 below 550m depth (Meldrum et al., 1994). A similar increase of bornite content relative to chalcopyrite in the deeper parts of the orebody noted by Meldrum et al. (1994) would appear to mimic the increasing gold content.

In comparison to the deposits mentioned above, E26 is anomalous, as Au and Cu mineralisation is associated with K-feldspar alteration which is destructive of biotite and magnetite associated with earlier potassic alteration. Similarly the strong zonation in Cu/Au ratios at E26 is also anomalous, except possibly in comparison with Batu Hijau. The comparison with other porphyry Cu-Au deposits, shows that Cu and Au deposition usually occurs without hematisation of magnetite. The model presented for E26 does not suggest that hematisation of magnetite is the only mechanism of Cu deposition, but rather causes Cu deposition to be enhanced.

9 FLUID CHEMISTRY AS A CONTROL ON GOLD DISTRIBUTION

9.1 FLUID CHEMISTRY

Fluid inclusion and sulphur isotope studies by Heithersay (1991) have shown that the chemistry of the fluids changed as the E26 system evolved. Fluids associated with Stages 4 and 5 have been shown from fluid inclusion analyses to range from 470-1090°C and 430-610°C respectively, with salinities varying from 50-80wt% NaCl+KCl (Heithersay 1991). At these conditions Au and Cu would be transported as chloride complexes (Seward 1983).

Heithersay (1991) noted a spatial zonation of sulphur isotope values for bornite at E26. $\delta^{34}S$ values for bornite vary from -8‰ to -2.9‰ and generally become more negative laterally away from, and vertically above, the centre of the mineralised system. Temperature determinations from fluid inclusions in the same samples give an approximate linear relationship between $\delta^{34}S$ and temperature, due to isotope fractionation, showing that temperatures decreased away from the centre of the system. The magnitude of the decrease for the Stage 5 veins was from >500°C in the deeper and central parts of the system to near 400°C in the upper and distal regions.

Activity-activity diagrams show that the mineral assemblages at E26 represent an evolving system that in general became more oxidised with time (Figure 9.1) although several exceptions and complications of this general trend exist. The initial biotite-magnetite assemblage formed under relatively reduced conditions. Bornite and hematite are typical of more oxidised conditions (Figure 9.1) and/or lower ΣS concentrations. The coexistence of bornite, chalcopyrite and hematite constrains the fluid conditions to a univariant line representing high sulphur and oxygen fugacities. The bornite+ chalcocite+hematite assemblage indicates more oxidised conditions, lower temperatures and/or lower ΣS concentrations. The replacement of bornite by chalcopyrite suggests higher temperatures, higher ΣS concentrations, or more reduced conditions. The

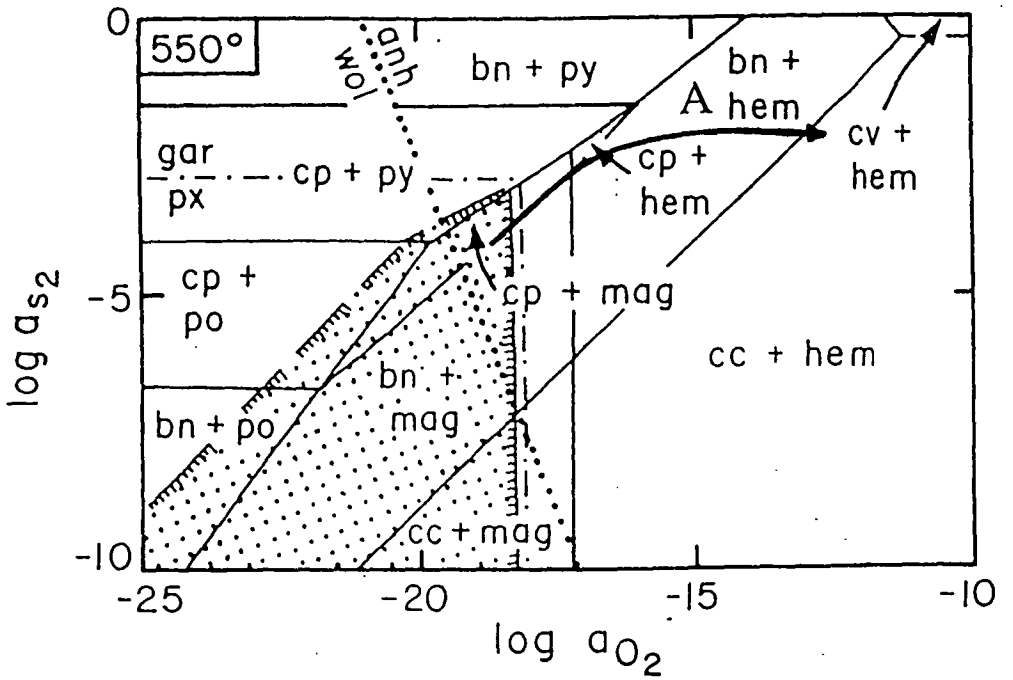

Figure 9.1 Activity diagram for sulphide and silicate phases as a function of $a(S_2)$ and $a(O_2)$ at 550°C (From Beane and Titley, 1981). Path A shows fluid evolution during stages 3 to 5.

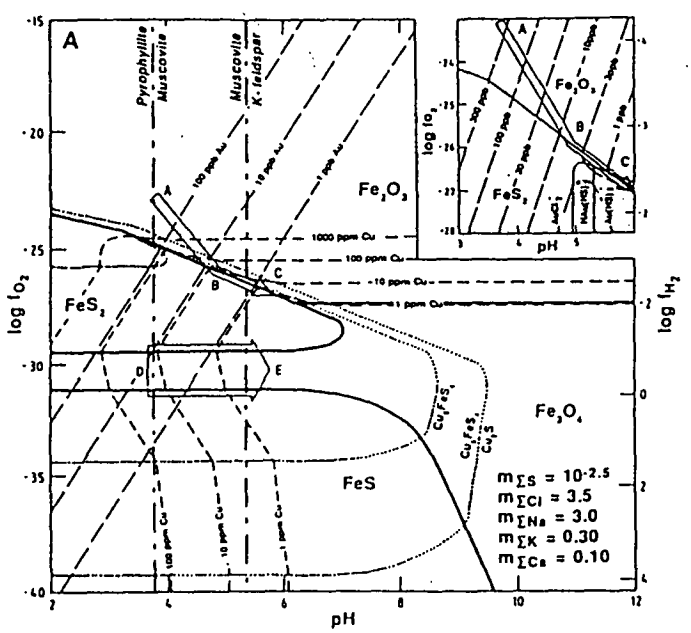

Figure 9.2 fO_2 - pH diagrams constructed at 350°C (From Huston et al., 1993). Fluid evolution similar to path A would lead to a greater rate of change in Au saturation compared to Cu saturation.

replacement of bornite by covellite suggests low temperatures, and/or higher sulphur and oxygen fugacities. The presence of anhydrite in most alteration assemblages indicates oxidised, sulphate-stable conditions throughout much of the lifetime of the system.

9.2 GOLD AND COPPER DEPOSITION

Stage 3 potassic alteration, characterised by biotite and magnetite and precipitated by relatively reduced fluids, was followed by the more oxidised hematite-stable and sulphate-stable, hotter (initially) Stage 4 and 5 fluids responsible for the main pink K-feldspar alteration and sulphide mineralisation at E26. Hematisation of magnetite occurred by the reaction:

$$4Fe_3O_4 + O_2 \Leftrightarrow 6Fe_2O_3 \qquad (1)$$

The consumption of O_2 caused the fluids to become more reduced, resulting in the reduction of sulphate to sulphide by the reaction:

$$SO_4^{2-} + 2HCl \Leftrightarrow H_2S + 2O_2 + 2Cl^- \qquad (2)$$

These reactions led to a decrease in oxygen fugacities, and increase in pH of the fluids, prompting gold deposition by the reaction:

$$4AuCl_2^- + 2H_2O \Leftrightarrow 4Au + 4H^+ + 8Cl^- + O_2 \qquad (3)$$

O_2 is consumed by the hematisation of magnetite (Reaction 1). In response to the increasing H_2S content, copper deposition is promoted, also increasing the consumption of magnetite by the reaction:

$$16H_2S + 4Fe_3O_4 + 20CuCl_2^- + O_2 \Leftrightarrow 4Cu_5FeS_4 + 4Fe_2O_3 + 20H^+ + 40\ Cl^- + 6H_2O \qquad (4)$$

The absence of pyrite from potassic alteration assemblages, indicates that conditions were more oxidised than the pyrite field, and that Fe must come from Fe-oxides (and/or biotite?). According to Reaction 4, the greater the hematisation of magnetite, the more copper is produced. The presence of anhydrite with the copper sulphides would suggest that the fluids remained saturated in SO_4^{2-} despite also being consumed by the reaction above.

Huston et al. (1993) use fO_2 - pH diagrams to explain gold and copper deposition and variances in their relative proportions of distribution at Tennant Creek (Figure 9.2). While Figure 9.2 has been constructed for the Tennant Creek deposits at temperatures

of 350^{0}C and salinities of 20wt% NaCl, compared to temperatures of >500^{0}C and salinities of >50wt% NaCl+KCl at E26 (Heithersay 1991), this diagram does help to illustrate the effects of changes in oxygen fugacity and hydrogen ion activities on the precipitation of gold and copper from chloride complexes. If the Cu/Au ratio in the mineralising fluid is 10:1 (the ratio of the whole mineralising system) then for Cu/Au ratios to be as high as 1:1 in the centre of the orebody, Au deposition has to be enhanced relative to Cu. This relative enrichment can be explained if the fluids evolved obliquely to the copper solubility contours, but at a high angle to the gold solubility contours (Path A; Figure 9.2) in response to decreasing fO_2 and increasing pH. As the fluid rose, copper precipitation remained relatively constant; but by 9950mRL, the gold budget of the fluids had been spent, resulting in a gold-depleted zone (Domain 4) in the upper part of the copper mineralisation.

While the above discussion has focused on changing saturation levels of Au and Cu due to changing fO_2 and pH, the effect of temperature changes on saturation levels is equally, if not more, important. As well as by decreasing fO_2, Au deposition by Reaction 3 is favoured by decreasing temperature and dilution of the chloride complex by water. Decreasing temperatures are indicated by the sulphur isotope zonation. Precipitation of Cu could have occurred at a relatively slower rate than Au, provided a path similar to Path A was followed by the fluid during cooling (Figure 9.2). The greater changes in saturation level for Au promoted rapid deposition of Au relative to Cu in the deeper and central parts of the E26 system. This resulted in Cu deposition being partly decoupled from Au deposition, with Cu precipitating further out from, and above the core of the system. Rapid Cu deposition due to a steeper temperature gradient may have occurred in the carapace of QMP1, where Cu grades are highest. By this stage, the fluids had become spent in Au.

9.3 SUMMARY

It seems likely that throughout the main mineralisation stages of the E26 system, gold and copper were co-precipitated, but at different rates due to variations in physiochemical conditions of the fluids, principally T, fO_2 and pH. The changing fluid conditions resulted in different rates of change of saturation levels for Au and Cu, leading to a lower and middle zone of relative gold-enrichment, and an upper zone of gold-depletion

at E26. Similar changes in fluid conditions and resulting zonation in Cu/Au ratios has occurred at Galore Creek in British Columbia (Thompson 1994). While gold-enrichment occurred locally in the core of the E26 deposit, the continued deposition of Cu laterally away from QMP1, and into the upper levels of the system, was aided by the hematisation of magnetite. Gold was incorporated into high temperature copper sulphide solid solutions, from which chalcopyrite separated at temperatures of approximately 550^0C. Gold remained in the high temperature bornite, and bornite-digenite solid solutions, until exsolving with further cooling.

Gold also occurs in structurally controlled quartz-sericite-pyrite alteration, peripheral to E26. The alteration assemblage and accompanying sulphides (galena and sphalerite) would indicate deposition from bi-sulphide complexes in lower temperature and lower salinity fluids, than those associated with potassic alteration (Jones 1992).

The relative enrichment in Cu at E26 compared to E22, E27 and E31N, may be due to the stronger hematisation of magnetite, favouring Cu-sulphide deposition by Reaction 4. In comparison to E26, the enrichment of Au at E22, E27 and E31N is probably due to more Au-rich hydrothermal fluids, and greater rates of change in Au saturation than Cu saturation. The Cu/Au relationships at E22 and E27 are also consistent with the deep level of exposure at these deposits. If the mineralising systems were fully preserved at E22 and E27, then the Cu/Au relationships of E26 would be expected.

10 CONCLUSIONS

The distribution of gold at E26 is tightly constrained around the central and lower parts of QMP1. By comparison, Cu which is similarly distributed about QMP1, extends laterally beyond, and vertically above the main Au zone. The vertical zonation in the relationship between Cu and Au grades is highlighted in the analysis of Cu/Au ratios, where two distinct vertical domains within the ore grade mineralisation have been defined. Despite the continuity of Cu beyond the main Au zone, the strong structure in the lateral Cu/Au ratios suggests there is still a strong relationship between the two. Gold shows a positive correlation with Stage 5 quartz veins, and a negative correlation with magnetite. The analysis of Ag/Au ratios has shown dispersion of Ag beyond the main Au zone of mineralisation. Gold can also occur in association with Pb and Zn mineralisation in distal, structurally controlled zones of quartz-sericite-pyrite alteration.

The two bornite phases defined on colour and accompanying Cu-sulphide minerals are compositionally similar. The mauve bornite/chalcocite association tends to be restricted to higher grade areas in the middle and lower parts of the system. An orange-brown bornite/chalcopyrite association is the 'normal' association, occurring throughout most of the deposit. The mauve bornite is younger than the orange-brown bornite. Au occurs as small inclusions in both bornite phases and in chalcocite. The petrographic work and microprobe analyses has shown no compositional or timing variation between the sulphide and alteration/veining phases that could explain the zonation in Au observed at E26.

A geochemical model has been presented in which deposition of Au and Cu during Stages 4 and 5 resulted from metal saturation caused by changes in T, fO_2 and pH. Decreasing temperatures, and hematisation of secondary magnetite which formed during early potassic alteration in association with biotite, resulted in deposition of Au and Cu. Gold solubility decreased more quickly than Cu solubility, and as a result, Au deposition occurred relatively more quickly than Cu, resulting in relative gold enrichment in the core of the system. As the fluids moved up, they became spent in Au, resulting in a zone of gold depletion with respect to copper (high Cu/Au ratios) in the top of the system. Continued temperature decreases and hematisation of magnetite favoured Cu

deposition laterally away from QMP1, and to shallower depths. Au remained in high temperature bornite and/or bornite/chalcocite solid solution with chalcopyrite separation. Au exsolved from the intermediate solid solutions with further cooling.

Cu/Au ratios at E22 and E27 are relatively uniform at 1:1; E48 more closely resembles the Cu/Au relationships in the middle parts of E26; while E31N contains relatively high Au with Cu/Au ratios of less than one. The differences in metal contents between the Goonumbla deposits can be explained by differing fluid compositions, differing changes in physiochemical conditions during time of metal deposition, differing degrees of hematisation of magnetite, and level of exposure. Relative Cu-enrichment (E26 and E48) is favoured by hematisation of magnetite. Au-enrichment (E22, E27, E31N) is favoured by greater rates of change in the saturation levels of Au than Cu at the time of metal deposition, and higher Au content of the parental fluids. Higher Au contents and low Cu/Au ratios are also typical of deeper levels in the deposits.

REFERENCES

Barnes, H.L., 1979. Geochemistry of Hydrothermal Ore Deposits. 2nd Edition. Wiley-Interscience Publication. New York.

Cabri, L.J., 1973. New data on phase relations in Cu-Fe-S system. Economic Geology, 68, 443-454.

Cas, R.A.F., Powell, C. McA. and Crook, K.A.W, 1980. Ordovician palaeogeography of the Lachlan Fold Belt: A modern analogue and tectonic constraints. Journal of the Geological Society of Australia, 27, 19-31.

Clark, G.H., 1990. Panguna Copper-Gold Deposit. in Hughes, F.E., (ed) Geology of the Mineral Deposits of Australia and Papua New Guinea. The Australian Institute of Mining and Metallurgy, Melbourne. 1807-1816.

Cuddy, A.S. and Kesler, S.E., 1982. Gold in the Granisle and Bell Copper Porphyry Copper Deposits, British Columbia, in A.A. Levinson (ed.) Precious Metals in the Northern Cordillera. The Association of Exploration Geochemists, 139-155.

Glenn, R.A., 1992. Thrust, extensional and strike-slip tectonics in an evolving Palaeozoic orogen - a structural synthesis of the Lachlan Orogen of southeastern Australia. Tectonophysics, 214.

Hall, M.C., 1993. The stratigraphy and palaeovolcanology of the Late Ordovician Goonumbla Volcanics, Goonumbla, N.S.W. Unpubl. BSc.(Hons) Thesis, Monash University.

Harbon, P. and Dunn, K., 1994. E31N Mineral Resource Report. North Exploration Report No. PK94/55P (unpublished).

Heithersay, P.S., 1986. Endeavour 26 North copper-gold deposit, Goonumbla, N.S.W. - paragenesis and alteration zonation, in *Publications of the 13th CMMI Congress, Vol. 2, Geology and Exploration* (Ed. D.A. Berkman), pp. 181-189 (The 13th Congress of the Council of Mining and Metallurgical Institutions: Melbourne; and The Australasian Institute of Mining and Metallurgy: Melbourne).

Heithersay, P.S., O'Neill, W.J., van der Helder, P., Moore, C.R. and Harbon, P.G., 1990. Goonumbla porphyry copper district - Endeavour 26 North, Endeavour 22 and Endeavour 27 copper-gold deposits. *In* Hughes, F.E. (ed.): Geology of the mineral deposits of Australia and Papua New Guinea. 1385-1398.

Heithersay, P.S., 1991. The shoshonite-associated, Endeavour 26 North porphyry copper-gold deposit, Goonumbla, N.S.W. Unpubl. PhD. Thesis, Australian National University.

Heithersay, P.S., 1994. The Central West New South Wales Copper-Gold Province. in Ore Deposit Studies and Exploration Models. Master of Economic Geology Course Manual 1. Centre for Ore Deposit and Exploration Studies. Part 1.

Hooper, B.G.D., Mills, M., Hannington, M., 1994. 2nd Annual Exploration Report for ML 1247 Period December 1992 to November 1993. North Exploration Report No. PK94/52S (unpublished).

House, M.J. and Bischoff, K., 1994. Report on the E26 Mineral Resource and the Lift 1 Block Cave Ore Reserve Options. Northparkes Mines Report.

Jones, B.K., 1992. Application of metal zoning to gold exploration in porphyry copper systems. Journal of Geochemical Exploration, 43, 127-155.

Jones, B.K., and Thompson, J.F.H., 1991. Application of Empirical Models to Porphyry Copper-Gold Exploration. Gangue, MDD-GAC.

Jones, G.J., 1985. The Goonumbla Porphyry Copper Deposits, New South Wales. Economic Geology Vol 80, 591-613.

Kavalieris, I., 1994. The Grasberg Superporphyry, in Ore Deposit Studies and Exploration Models - Porphyry copper-gold deposits Ch 3 CODES: Short Course Manual 5.1.

Lowell, J.D. and Guilbert, J.M., 1970. Lateral and Vertical Alteration-Mineralisation Zoning in Porphyry Ore Deposits. Economic Geology 65, 373-408.

MacDonald, G.D. and Arnold, L.C., 1994. Geological and geochemical zoning of the Grasberg Igneous Complex, Irian Jaya, Indonesia. Journal of Geochemical Exploration 50, 143-178.

Meldrum, S.J., Aquino, R.S., Gonzales, R.I., Burke, R.J., Suyadi, A., Irianto, B. and Clarke, D.S., 1994. The Batu Hijau porphyry copper-gold deposit, Sumbawa Island, Indonesia. Journal of Geochemical Exploration 50, 203-220.

Oversby, B., 1971. Palaeozoic Plate Tectonics in the Southern Tasman Geosyncline. Nature Physical Science Vol 234, 45-48.

Packham, G.H., 1987. The eastern Lachlan Fold Belt of southeastern Australia: a possible Late Ordovician to Early Devonian sinistral strike-slip regime. In: E.C. Leitch and E. Scheibner (Eds.), Terrane Accretion and Orogenic Belts. Am. Geophys. Union Geodyn. Ser., 19: 67-82.

Perkins, C., McDougall, I., Claoue-Long, J. and Heithersay, P.S., 1990. $^{40}Ar/^{39}Ar$ and U-Pb geochronology of the Goonumbla Porphyry Cu-Au deposits, NSW, Australia. Econ. Geol. 85, 1808-1824.

Ramdahr, P., 1969. The Ore Minerals and their Intergrowths. Permagon Press.

Scheibner, E., 1973. A Plate Tectonic Model of the Palaeozoic Tectonic History of New South Wales. Journal of the Geological Society of Australia, 20, 405-426.

Seward, T.M., 1983. The transport and deposition of gold in hydrothermal systems, in Foster, R.P. (ed) Gold 82: The geology, geochemistry and genesis of gold deposits. A.A. Balkema: Rotterdam. 165-181.

Sillitoe, R.H., 1979. Some thoughts on gold-rich porphyry copper deposits. Mineral. Deposita. 14, 161-174.

Sillitoe, R.H., 1989. Gold Deposits in Western Pacific Island Arcs: The Magmatic Connection. Econ. Geol. Monograph 6 266-283.

Sillitoe, R.H., 1990. Gold-rich porphyry copper deposits of the Circum-Pacific region - an updated overview. The Australasian Institute of Mining and Metallurgy Pacific Rim Congress 90, Vol 2, 119-126.

Sillitoe, R.H. and Gappe, I.M., 1984. Philippine Porphyry Copper Deposits: Geologic setting and characteristics. United Nations ESCAP, CCOP Tech. Pub. 14.

Solomon, M., 1990. Subduction, arc reversal, and origin of porphyry copper-gold deposits in island arcs. Geology 18, 630-633.

Squires, V.E., 1992. The Mineralization and Alteration of the Endeavour 27 Porphyry Copper-Gold Deposit, Goonumbla, New South Wales. Unpubl. B.Sc. Hons Thesis, University of Sydney.

Thompson, J., 1994. Porphyry copper-gold deposits of Canada and the eastern Pacific. in Ore Deposit Studies and Exploration Models. Master of Economic Geology Course Manual 1. Centre for Ore Deposit and Exploration Studies. Part 4.

Titley, S.R., 1990. Contrasting metallogenesis and regional settings of circumpacific Cu-Au porphyry systems. The Australasian Institute of Mining and Metallurgy Pacific Rim Congress 90, Vol 2, 127-133.

Wolfe, R.C., 1994. The Geology, Paragenesis and Alteration Geochemistry of the Endeavour 48 Cu-Au Porphyry, Goonumbla, N.S.W. Unpubl. B.Sc. Thesis. University of Tasmania.

Wyborn, D., 1992. The tectonic significance of Ordovician magmatism in the eastern Lachlan Fold Belt. Tectonophysics, 214.

Wyborn, D., 1994. Mantle Magmatism and Large Gold-Copper Deposits. in Ore Deposit Studies and Exploration Models. Master of Economic Geology Course Manual 1. Centre for Ore Deposit and Exploration Studies. Part 5.

APPENDICES

APPENDIX 1

POLISHED SECTION

DESCRIPTIONS

Sample No.	Hole No.	Depth	Cu %	Au g/t	Cu/Au domain	Rocktype	Alteration	Veining	Sulphides
39503	E26D39	503	2.20	0.09	4	Volcanic NE Ext.	Biot. (Stage 3) variably altered to ser. & rut. K-spar altered groundmass and plag phenocrysts, minor anhy. Weak overprinting ser./carb. & chlor.	Stage 5 Qtz veins	Bn Some cpy replacing bn Cov. replacing bn.
67528	E26D67	528	2.57	0.43	4	Volcanic NE Ext.	Biot. (stage 3) altered to K-spar & Ser. (stage 4) K-spar altered groundmass and plag. phenocrysts, anhy. Minor alb. (stage 4), Rut. Late Gyp. (stage 10)	Stage 5 Qtz veins	Bn Most Cpy. replacing Bn. Covellite replacing bn.
75150	E26D75	150	4.10	0.83	4	Volcanic	Relict Plag. phenocrysts. K-spar & alb. (stage 4) altered groundmass Rut. common in bn.	Stage 5 Qtz Veins	Bn, Cpy. Some Bn. replaced by cpy and cov.
75153.3	E26D75	153.3	5.30	0.38	4	QMP1 Silica Flooded	Strong silic., and ser. alteration adjacent to qtz. veins Groundmass of K-spar, Qtz., and Ser.	Stage 5 Qtz veins Silica Flooding	Bn., Clausthalite Cpy. and Cov. after Bn. Cpy veinlet (stage7 or 8) with py.
91175.4	E26D91	175.4	5.80	1.27	4	Volcanic	Stage 4 & 5 K-spar, qtz., ser. and anhy. altered groundmass Rut.	Stage 5 qtz veins	Bn./cpy./tetra. intergrown Some cpy. after Bn. Cov. after Bn.
12382.8	E26D123	82.8	0.85	0.04	2	Volcanic	Pervasive biot., + magn., + apatite (stage3), altered to ser. & hem. Plag. phenocrysts altered to K-spar./alb./hem. Very fine groundmass of K-spar., qtz., alb., and ser. & monir anhy.	Stage 5 qtz veins	Bn./Hem. association Later Cpy./hem. association Cc. after Bn. in one grain
123138.3	E26D123	138.3	4.40	0.67	4	Volcanic	Strong Silic. and ser. alteration. Minor alb. and K-spar.	Stockwork stage 5 qtz veins	Bn. Cpy. and cov. after bn.
126W2513.4	E26D126W2	513.4	4.60	5.17	3	Volcanic	Qtz. vein, minor carb., anhy. and ser.	Stage 5 Qtz vein Stage 10/11 gypsum	2 bn. colour phases Minor cpy. after Bn. Au in bn.
126W2571.4	E26D126W2	571.4	2.65	2.54	3	Volcanic Silica Flooded	Qtz. veined & sericitised Minor rutile	Stage 5 qtz vein Silica flooded	2 bn. phases, Au Cc. with mauve Bn. minor Cov. after Bn.
126W2596.2	E26D126W2	596.2	4.64	3.40	3	Volcanic	Stage 3 magn. partly replaced by hem. and bn. Stage 4 K-spar in groundmass. Stage 5 qtz & ser. Late carb./ anhy./ser./chlor.	Stage 3 magn. vein Stage 5 qtz. vein Late Carb. vein	Bn.(orange)/ cpy. Bn. dominant near magn. Cpy. dominant away
128591.5	E26D128	591.5	4.80	5.10	3	Volcanic	Plag. phenocrysts now K-spar. & ser. Bn. & hem. after Magn. K-spar., qtz.,?biot. and minor alb. alteration of groundmass Minor late epidote	Stage 5 qtz. vein	2 bn. phases, Au mauve bn./cc., orange bn./cpy. some cpy./cov. after bn.
128657.9	E26D128	657.9	2.03	1.64	3	Volcanic	Stage 3 Biot. and Magn. (replaced by hem.) Pervasive K-spar./alb./hem. (minor rut.) alteration (stage 4). Ser. overprint. Minor late chlor.,carb.,anhy.	Stage 5 qtz vein	Bn./cc., Minor cpy. coexisting with bn.

List of abbreviations: K-spar= K-feldspar; alb.=albite; biot.=biotite; magn.=magnetite; anhy.=anhydrite; qtz.=quartz; ser.=sericite; carb.=carbonate; chlor=chlorite; epi=epidote; gyp=gypsum; plag=plagioclase; silic=silicification
hem.=hematite; bn=bornite; cpy.=chalcopyrite; cc.=chalcocite; tetra=tetrahedrite; cov=covellite; rut=rulile; Au=gold; py=pyrite

Appendix 1 - polished section descriptions

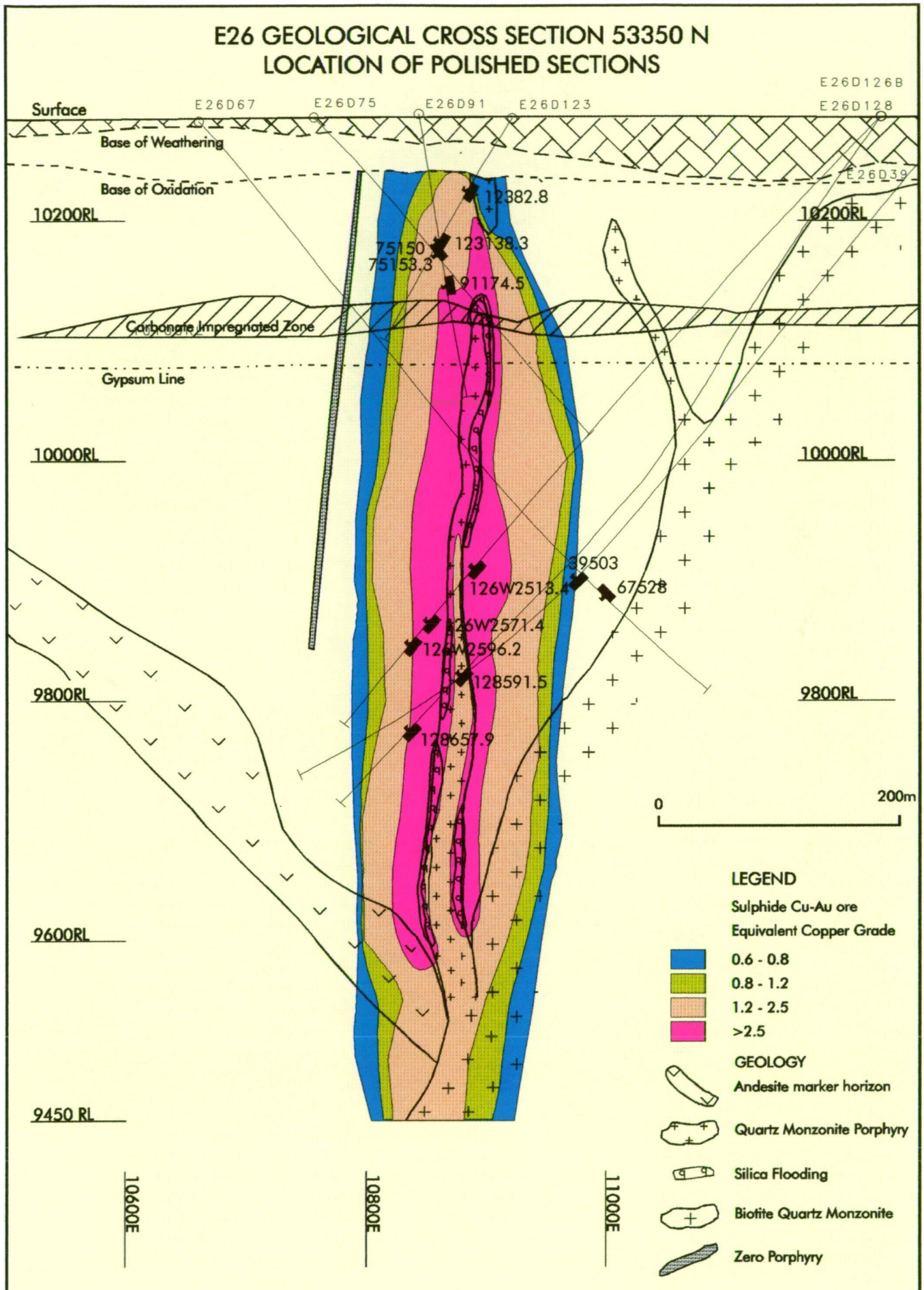
E26 GEOLOGICAL CROSS SECTION 53350 N
LOCATION OF POLISHED SECTIONS
E26D126B
Surface
E26D67
E26D75
E26D91
E26D123
E26D128
Base of Weathering
Base of Oxidation
E26D39
10200RL
12382.8
75150
123138.3
75153.3
91174.5
Carbonate Impregnated Zone
Gypsum Line
10000RL
9503
126W2513.4
67528
126W2571.4
126W2596.2
128591.5
9800RL
128657.9
0
200m
LEGEND
Sulphide Cu-Au ore
Equivalent Copper Grade
0.6 - 0.8
0.8 - 1.2
1.2 - 2.5
>2.5
GEOLOGY
Andesite marker horizon
Quartz Monzonite Porphyry
Silica Flooding
Biotite Quartz Monzonite
Zero Porphyry
9600RL
9450 RL
10600E
10800E
11000E

APPENDIX 2

ELECTRON MICROPROBE ANALYSES

The samples were analysed using a fully automated, three spectrometers Cameca SX 50 electron microprobe callibrated with natural mineral standards (PAP data reduction). The standards were analysed at least twice during each probe session. Analytical conditions were 15kV accelerating voltage, 20 nA beam current, and 1-2 μm beam size. Approximately 40 grains were analysed for a total of 87 analyses. Totals for some analyses are 2-3 wt% low and appear to have lead to an under estimation of the Cu content of the Cu-sulphide phases.

TABLE 1: ELECTRON MICROPROBE ANALYSES - SULPHIDE MINERALS

Sample No	Ring No.	Point No.	Mineral	S	Fe	Cu	Zn	As	Ag	Sb	Bi	Wt % Total
75153.3	1	1	Bornite	40.46	9.78	49.71	0	0.01	0.01	0	0.05	98.217
75153.3	1	2	Bornite	40.98	9.33	49.61	0	0.05	0.01	0.01	0.02	95.109
75153.3	1	3	Bornite	41.14	9.32	49.51	0	0	0	0.02	0.01	97.631
12382.8	3	1	Bornite	40.54	9.79	49.64	0	0	0.01	0	0.02	98.227
12382.8	3	2	Bornite	40.72	9.88	49.33	0	0	0	0.02	0.05	97.895
75153.3	1	3	?Claushalite	39.15 (Se?)	0	0.51	0.03	60.29 (Pb?)	0.02	0	0	57.537
91175.4	1	1	Bornite	40.54	9.82	49.63	0	0	0	0	0.01	97.905
91175.4	1	2	?Claushalite	37.32 (Se?)	0.21	0.53	0	61.93 (Pb?)	0	0.01	0	56.495
91175.4	1	3	Bornite	40.47	9.76	49.75	0	0.02	0	0	0	98.804
91175.4	1	4	Bornite	40.81	9.21	49.81	0	0.13	0.02	0.01	0	97.41
91175.4	1	5	Chalcopyrite	50.9	23.86	25.18	0.01	0.04	0	0	0	95.381
91175.4	1	6	Chalcopyrite	50.8	24.08	25.06	0	0.05	0	0	0	97.205
91175.4	2	1	Tetrahedrite	44.99	0.09	34.4	6.43	2.3	0	11.78	0	99.271
91175.4	2	2	Tetrahedrite	44.78	0.12	34.4	6.36	0.54	0.05	13.75	0	100.221
91175.4	2	3	Tetrahedrite	45.06	0.08	34.36	6.33	1.15	0.04	12.98	0	99.248
91175.4	2	4	Bornite	40.7	9.6	49.64	0.02	0.01	0.02	0	0	97.961
91175.4	2	5	Bornite	40.47	9.72	49.79	0	0	0	0.01	0.02	98.377
91175.4	2	6	Chalcopyrite	50.72	24.16	25.09	0	0.02	0	0	0	96.994
91175.4	2	7	Chalcopyrite	50.64	24.13	25.23	0	0	0	0	0	97.37
128591.5	2	1	Purple Bornite	40.53	9.64	49.82	0	0	0	0.01	0	98.052
128591.5	2	2	Chalcocite	37.35	4.24	58.38	0	0	0.02	0	0.01	98.558
128591.5	2	3	Chalcocite	34.76	1.27	63.93	0	0	0.03	0.01	0	98.736
128591.5	2	4	Orange Bornite	40.52	9.61	49.85	0	0	0.02	0	0	98.282
128591.5	2	5	Orange Bornite	40.68	9.59	49.72	0	0	0	0.01	0	98.108
128591.5	1	1	Chalcocite	34.16	0.05	65.74	0.01	0	0.05	0	0	99.24
128591.5	1	2	Chalcocite	34.58	0.13	65.23	0	0	0.01	0	0.06	98.754
128591.5	1	3	Purple Bornite	40.87	9.36	49.75	0	0	0.01	0	0	96.34
128591.5	3	1	Orange Bornite	40.45	9.78	49.71	0.01	0	0.01	0.01	0.04	98.157
128591.5	3	2	Orange Bornite	40.4	9.66	49.93	0	0	0.02	0	0	98.663
128591.5	3	3	Chalcocite	34.61	0.13	65.25	0	0	0	0	0.01	97.275
128591.5	3	4	Chalcocite	34.67	0.17	65.12	0	0	0.01	0	0.03	98.567
128591.5	3	5	Purple Bornite	40.46	9.52	49.93	0	0	0.04	0	0.05	98.171
128591.5	3	6	Purple Bornite	40.56	9.63	49.75	0	0	0.02	0	0.04	97.093
128591.5	4	1	Chalcocite	33.57	0.1	66.32	0	0	0.02	0	0	99.144
128591.5	4	1?	Chalcocite	33.68	0.11	66.17	0	0	0.01	0	0.03	99.157
128591.5	4	2	Chalcocite	34.33	0.17	65.41	0.01	0	0.02	0	0.05	98.675
128591.5	4	3	Purple Bornite	40.3	9.7	49.87	0	0.09	0.04	0	0	98.112
128591.5	4	4	Purple Bornite	40.43	9.68	49.86	0	0	0.03	0	0	97.484
128591.5	4	5	Chalcocite	33.96	0.12	65.89	0	0	0.02	0	0.01	98.605
128591.5	4	6	Orange Bornite	40.81	9.45	49.67	0	0.03	0.03	0	0.02	97.541
128591.5	4	7	Orange Bornite	40.21	9.65	50.1	0	0.01	0.01	0.01	0	98.972
128591.5	4	8	Chalcocite	33.78	0.12	66.01	0	0.05	0	0.01	0.03	98.734
128591.5	1	1	Orange Bornite	41.32	9.78	48.86	0	0	0.04	0	0	96.106
128591.5	1	2	Orange Bornite	39.86	6.65	53.44	0	0	0.05	0	0.01	93.451
128591.5	1	3	Purple Bornite	41.2	9.8	48.97	0	0	0.01	0.01	0.02	96.421
128591.5	1	4	Chalcocite	34.95	0.11	64.82	0	0	0.03	0.03	0.06	94.757
128591.5	1	5	Purple Bornite	41.17	9.89	48.86	0	0	0.02	0.01	0.05	96.459
128591.5	1	6	Chalcocite	34.95	0.02	64.91	0	0	0.01	0	0.11	96.106
128591.5	1	7	Chalcocite	34.94	0.09	64.94	0	0	0.04	0	0	95.781
128591.5	1	8	Purple Bornite	41.36	9.59	48.99	0	0	0.02	0	0.03	95.918
128591.5	1	9	Orange Bornite	41.55	9.67	48.6	0	0.06	0.04	0.01	0.07	95.888
128591.5	1	10	Purple Bornite	41.11	9.19	49.69	0	0	0.01	0	0	96.678
128591.5	2	1	Purple Bornite	41.28	9.68	49.01	0	0	0.03	0	0	96.923
128591.5	2	2	Chalcocite	35.89	0.47	63.4	0	0	0.03	0.01	0.19	96.264
128591.5	2	3	Chalcocite	35.88	0.1	63.96	0	0	0.03	0	0.02	95.665
128591.5	2	4	Bornite	41.83	9.75	48.37	0	0	0.03	0	0.03	95.815
128591.5	2	5	Orange Bornite	42.01	9.84	48.04	0	0	0	0.02	0.09	96.532
128591.5	2	6	Orange Bornite	41.89	9.69	48.33	0	0.06	0.03	0.01	0	96.043
128591.5	3	1A	Bornite	40.96	9.73	49.31	0	0	0	0	0	97.426
128591.5	3	1	Purple Bornite	41.02	9.73	49.23	0	0	0.01	0	0.01	96.761
128591.5	3	2	Chalcocite	35.11	0.26	64.62	0	0	0.02	0	0	98.369
128591.5	3	3	Purple Bornite	41.93	9.75	48.23	0	0.01	0	0.01	0.06	95.218
128591.5	3	4	Chalcocite	35.85	0.24	63.9	0	0	0.02	0	0	95.996
128591.5	3	5	Orange Bornite	41.64	9.84	48.5	0.01	0	0	0.02	0	96.61
128591.5	3	6	Orange Bornite	41.41	9.95	48.55	0	0.02	0.04	0	0.03	96.45
128591.5	4	1	Purple Bornite	41.87	9.69	48.4	0	0	0.03	0	0	96.261
128591.5	4	2	Purple Bornite	41.34	9.98	48.64	0	0	0.03	0.01	0	96.541
128591.5	4	3	Chalcocite	34.58	0.24	65.07	0	0.04	0.03	0	0.04	96.458
128591.5	4	4	Chalcocite	35.02	0.76	64.17	0	0	0.03	0.01	0.01	95.222
128591.5	4	5	Orange Bornite	41.27	9.85	48.76	0	0	0	0	0.11	97.043
128591.5	4	6	Orange Bornite	41.47	9.85	48.63	0.01	0	0	0	0.04	96.417
91175.4	1	1	Tetrahedrite	46.3	0.11	33.1	6.48	0.96	0.01	13.04	0	96.887
91175.4	1	2	Tetrahedrite	46.05	0.1	33.18	6.57	1.16	0.01	12.94	0	96.869
91175.4	1	3	Bornite	41.69	9.88	48.35	0	0	0.03	0	0.04	96.458
91175.4	1	4	Tetrahedrite	46.05	0.36	32.92	6.48	1.44	0.03	12.71	0.01	97.13

TABLE 2: ELECTRON MICROPROBE ANALYSES - SILICATE MINERALS

Sample No	Ring No.	Point No.	Mineral	SO3	P2O5	SiO2	TiO2	Al2O3	Cr2O3	MgO	CaO	MnO	FeO	NiO	Na2O	K2O
75153.3	1	1	Sericite	0	0.0045	7.0239	0.0287	5.607	0.0013	0.345	0.0047	0.0003	0.1715	0	0.1131	1.7795
75153.3	1	2	Sericite	0.0045	0.0013	6.8671	0.0203	5.9629	0.0033	0.1515	0	0	0.1378	0	0.1259	1.7571
75153.3	1	3	Sericite	0.0023	0.0008	6.8865	0.0408	5.6289	0.0018	0.4881	0	0	0.2102	0.0011	0.1148	1.8655
12382.8	1	1	Sericite	0.0023	0.0072	7.101	0	5.3643	0	0.542	0.0027	0	0.3134	0.0032	0.0959	1.6351
12382.8	1	2	Sericite	0	0.0108	7.0008	0	5.3576	0.0049	0.6488	0	0.0007	0.3732	0.0008	0.0984	1.7077
128591.5	4	1	Sericite	0	0.0019	6.7692	0.0459	5.537	0.0005	0.6596	0	0	0.4027	0.0011	0.1186	1.8657
128591.5	4	2	Sericite	0	0.0024	6.8443	0.0502	5.6211	0.0008	0.424	0	0	0.3614	0	0.1008	1.8641
91175.4	1	1	Sericite	0	0.0066	7.0848	0.0119	5.542	0	0.3483	0	0.001	0.1862	0.0023	0.1521	1.7266
91175.4	1	2	Sericite	0.0201	0.0023	6.7944	0.0144	5.9187	0.0013	0.3043	0.0003	0	0.1913	0.0027	0.1709	1.705
12382.8	2	1	Biotite	0	0	5.7553	0.3326	3.4201	0	3.672	0	0.0448	1.9956	0	0.0946	1.838
12382.8	2	2	Biotite	0.0074	0.0042	5.9211	0.3649	3.1162	0.0057	3.83	0	0.0497	1.8323	0	0.1113	1.8501
12382.8	2	3	Biotite	0	0.0013	5.8289	0.3629	3.2759	0	3.7817	0	0.0367	1.8791	0.0005	0.1096	1.8714